National Library
of Canada

Acquisitions and
Bibliographic Services Branch

395 Wellington Street
Ottawa, Ontario
K1A 0N4

Bibliothèque nationale
du Canada

Direction des acquisitions et
des services bibliographiques

395, rue Wellington
Ottawa (Ontario)
K1A 0N4

Your file Votre référence

Our file Notre référence

NOTICE

The quality of this microform is heavily dependent upon the quality of the original thesis submitted for microfilming. Every effort has been made to ensure the highest quality of reproduction possible.

If pages are missing, contact the university which granted the degree.

Some pages may have indistinct print especially if the original pages were typed with a poor typewriter ribbon or if the university sent us an inferior photocopy.

AVIS

La qualité de cette microforme dépend grandement de la qualité de la thèse soumise au microfilmage. Nous avons tout fait pour assurer une qualité supérieure de reproduction.

S'il manque des pages, veuillez communiquer avec l'université qui a conféré le grade.

La qualité d'impression de certaines pages peut laisser à désirer, surtout si les pages originales ont été dactylographiées à l'aide d'un ruban usé ou si l'université nous a fait parvenir une photocopie de qualité inférieure.

Canada

STUDIES OF TRACE METAL SPECIATION BY CONVENTIONAL AND LASER THERMAL LENSING SPECTROMETRY: THE CASE OF COPPER IN IRON HYDROUS OXIDES

Donald William Gutzman

A Thesis

in

The Department

of

Chemistry and Biochemistry

Presented in Partial Fulfilment of the Requirements
for the Degree of Doctor of Philosophy at
Concordia University
Montreal, Quebec, Canada

March 1992

ISBN 0-315 80999 X

ABSTRACT

Studies of trace metal speciation
by conventional and laser thermal lensing spectrometry:
The case of copper in iron hydrous oxides

Donald William Gutzman, Ph.D.
Concordia University, 1992

Of importance to understanding and predicting the toxicity of metal ions in aquatic systems is a knowledge of their "speciation" or distribution among various forms. There are indications that risk to aquatic organisms increases with the concentration of free metal. The large majority of studies performed have evaluated speciation on the basis of equilibrium considerations. This approach may not be the most effective one in the evaluation of dynamic systems. The kinetic approach employed here determines speciation on the basis of relative labilities of species. The method is described and its prior applications to several chemical systems is reviewed. This kinetic approach is applied to the study of copper binding to iron(III) hydrous oxide. A minimum of four species are identified including one with extremely high kinetic lability, at least two of intermediate labilities and a final fraction which is fairly inert.

Due to analytical restrictions speciation studies are usually carried out using high analyte concentrations. The assumption is made that the distribution of ligand sites binding the metal is unaffected by dilution to the much lower concentrations of environmental relevance. The sensitive photothermal technique of laser thermal lensing is used here to monitor solutions of low analyte concentration. These results are compared to those obtained using conventional spectrophotometry. In a variety of studies

using iron(III) hydrous oxide it is observed that the characteristics of this colloidal material are in fact quite sensitive to its concentration. Results obtained at high concentrations may not be extrapolated to a more dilute system. This stresses the importance of "modelling" under conditions of environmental significance.

Thermal lensing was evaluated for application to the analysis of natural samples. One problem with these substances is the presence of light scattering material. In theory thermal lensing is insensitive to a small degree of light scatter. This was observed using purely scattering polystyrene latex particles. Difficulty was encountered, however, when particles which both absorbed and scattered light at the wavelength of analysis were present. In this case noise levels were found to increase drastically and with a non-random component.

Acknowledgements

There are a great many fine individuals with whom I have had the privilege of interacting during my time at Concordia. It would be difficult to mention them all within this limited space. Each of them has influenced me in one way or another. They will all be remembered.

Special thanks are due to Dr. C.H. Langford. His extraordinary patience and devotion are admirable. I would also like to thank the members of the Langford group who have aided in innumerable ways, the departmental secretaries for always managing to find a way to get it done, the staff (and particularly the reference librarians) of SEL for enthusiastically giving the extra effort and the guys in the Science Technical Centre for always getting it to work...just one more time.

For moral support I never had to look too far. For this I offer special thanks to my parents and family for their encouragement over the years, to M. and MME. Poissant and especially to Lyne. They never lost hope...

Finally I would like to acknowledge a figure from my youth who showed me that there is always a way. Without my realizing it at the time he taught me how to think. Thanks Mr. Suess.

Table of Content

Index of figures

Index of tables

Chapter 1

INTRODUCTION

1.1 SPECIATION OF METALS

It has long been recognized that water quality in natural systems is influenced by the presence of various trace metals. Many metals which are essential nutrients at natural levels behave as toxicants at elevated concentrations [1,2,3]. But from a toxicological perspective, risk to aquatic organisms by toxic species such as metals is a function of *both* the toxicity of the substance and its bioavailability [4,5,6,7]. The latter term is as yet ill defined. While any metal capable of being involved in a biological reaction is "bioavailable", this term is generally taken to relate to potential reactions at the cellular level via penetration of a biological membrane [8].

A major finding in recent years is that the risk to aquatic organisms may be more closely related to the concentration of free metal than to that of total metal. This has lead to the so called "free metal ion hypothesis" [9]. Naturally occurring metal buffers limit the concentration of free metal species. Among the major contributors are organic and inorganic ligands, especially colloidal ones. These species reduce trace metal lability through complexation or adsorption. The most thoroughly studied of these are organic polyelectrolytes such as humic and fulvic substances. Also of importance are the hydrous oxides of various metals. Generally these are of somewhat less importance than the organic fraction. In some freshwater systems, however, the hydrous oxides of iron and manganese may be the main substrates of metal complexation and adsorption [10].

Complexation by humic coated colloidal particles has also been proposed [11,12,13]. The distribution of a metal among its possible forms such as free, adsorbed or complexed is termed its "speciation".

The importance of being able to predict metal buffering capacities and determine speciation is obvious. Analysis of the speciation of trace metals is performed in an attempt to ascertain which species are likely to have adverse effects on aquatic biota. These physicochemical parameters must be related to bioassay toxicity data of many members of the aquatic food chain in order to understand the full impact of a chemical species [14]. Speciation also has profound effects on the efficiency of various methods of waste water treatment such as those based on flocculation or biological activity.

The free metal ion hypothesis was introduced to account for reduced metal ion toxicity observed in natural waters in the presence of complexing agents. Results of Borg have suggested that the term "labile metal" should replace "free metal ion" in this context [15]. It is rarely noted that there are, in fact, three possible origins of the protective effect of complexing agents. The obvious one is a simple "free metal ion" effect related to preferred uptake of the aqua metal ion $[M(H_2O)_n]^{m+}$. A related thermodynamic effect is uptake governed by the metal ion activity. Both of these may be related to equilibrium speciation. A third aspect involves the kinetics of uptake. Since life processes are dynamic, this cannot be overlooked. The relevance of equilibrium speciation will, in fact be limited to those cases where the equilibria are established rapidly with respect to the time scale of uptake. This issue has been analyzed by Buffle [16].

Unfortunately, almost all of the large literature on metal ion speciation in natural systems is based on equilibrium studies. There is good reason for this. Methods for

examination of kinetic speciation with high resolution and high sensitivity are extremely hard to design. What follows will describe an approach which has evolved over the past dozen years which provides a compromise between equilibrium and kinetic speciation and which is now being extended from laboratory models toward "real samples".

In order to understand the basis of the method, consider a classical colorimetric (or fluorometric) determination. A sample containing a metal ion is treated with excess colour forming reagent. Ideally, 100% of the metal ion enters the detection species and is estimated. All that we now do is to add monitoring of the time course of the formation of the detection species. If the time course can be resolved into contributions from the competing reaction of the various species present in the sample, the various species can be identified and quantified. In order to maintain reproducible and analyzable kinetics, it is necessary to control the kinetically crucial parameters of temperature, pH, and ionic strength. Thus, the reagent solution must be designed to buffer pH and ionic strength. This means that the speciation is controlled by the history of the sample prior to the initiation of the metal ion transfer reaction, but that the rate constants are specific to the conditions of the run. This experimental limitation is not as serious for metal complexes as it might be in other circumstances since 6-coordinate metal complexes tend to have reaction rates controlled by the rate of ligand dissociation, and extrapolation from one condition to another is fairly simple and reliable. In particular, relative rates tend to remain the same.

It should be evident that the same factors which govern equilibrium colorimetric analysis are important in choosing a chromophore for use in kinetic speciation. The equilibrium of analyte with chromophore should lie far to the product side. Sensitivity

is maximized by use of an absorbing complex with a large absorptivity. There is one factor which is more critical in kinetic study than in equilibrium analysis. Since the samples are monitored for an extended time (sometimes in the region of hours) it is necessary that the chromophore remain stable over this period.

In order to be able to develop theories of these methods, it is useful to clarify the nature of the complexing agents involved. Figure 1-1 outlines several possible distributions of metal complexing sites. S-sites refer to the functional group of the ligand directly involved in binding, the Lewis base atom itself. L-sites encompass both the coordinating group and those features of its environment which can influence complex stability. Such secondary effects have been divided by Buffle [17] into three types denoted (a)-(c) in the figure. *Polyfunctional* (a-effects) are related to the multifunctionality of the complexing agent. These arise from diversity of S-sites as well as their electronic and steric environments. *Conformation* (b-effects) of the overall complexant is largely dependent on the degree of hydration and the extent of hydrogen bonding and bridging metal groups. These factors can cause the material to appear as distinctly different phases such as simple solutes, hydrated surface layers on particles or aggregated gels and may condition the steric requirements for metal ion binding. The third effect (c) is that due to the *polyelectrolyte* properties of the complexant. Where ions are involved, these will be electrostatic terms depending on total polymer charge. The importance of any of these effects is dependent on the extent of occupation of binding sites.

Scheme A in the figure shows binding of a metal by two simple ligands. A readily quantifiable complexation constant for each is evident. In scheme B binding by

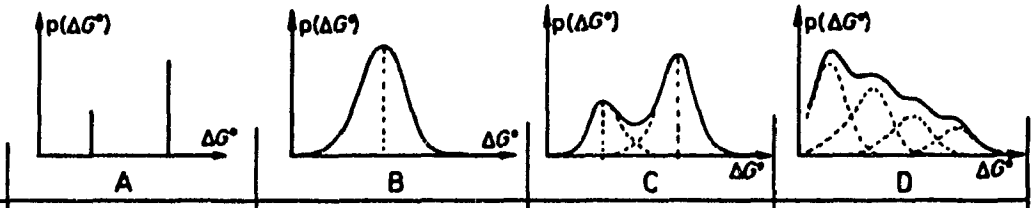

	A	B	C	D
Property	2 different sites S zero (*a*)–(*c*) effects → 2 sites L	Unimodal distribution 1 single site S non-zero (*a*)–(*c*) effects → large number of sites L	Bimodal distribution 2 sites S non-zero (*a*)–(*c*) effects → large number of sites L	large number of sites S non-zero (*a*)–(*c*) effects → infinity of sites L
Typical examples	mixture of simple ligands (e.g. CO_3^{2-}, amino-acids) or simple ligand with 2 independent sites	homopolysaccharides (site = –COOH) Δ*G* variation is mostly due to effects (*b*) and (*c*)	peptides (e.g. sites are –COOH and $-NH_2$)	PROM AND AROM (sites = –COOH, Ø–OH, $-NH_2$, –SH, etc . . .) Δ*G* variation is mostly due to effects (*a*) and (*c*)

Figure 1-1: Possible distributions of sites forming metal-ligand complexes. $p(\Delta G^0)$ is the probability of a site being present which will complex a metal with a free energy of formation of ΔG^0. PROM and AROM refer to pedogenic and aquagenic refractory organic matter, respectively. See text for definitions of S-sites, L-sites and (a)-(c) effects. (Taken from Buffle [17].)

a single S-site is distributed over a range of ΔG° values as a result of secondary effects. More complex distributions of stabilities are seen in cases C and D.

While considerable advances have been made in speciation study by aquatic chemists and biologists, the work is far from complete. Of particular importance is the task of identifying and quantifying those substances which are major contributors to metal buffering, the nature of their interaction and their cycling and equilibrium within the environment.

1.2 CONTEXT OF KINETIC SPECIATION

1.2.1 Kinetics

The kinetic methods of speciation described above require analysis of a common product originating from several closely associated sources, such as multiple binding sites on a single complexant molecule. In this case the signal may be "separated" into different time scales for each species using differential kinetic methods. Unlike traditional kinetic methods which require only a few data points, differential methods take advantage of the full kinetic profile. These techniques employ nonlinear or multilinear regression to fit the kinetic data.

Nonlinear regression analysis (NLR) may be performed in one of two ways. The more rigorous of these examines the entire multi-dimensional solution "surface" to obtain the rate constants and pre-exponential terms which yield the least sum of square deviations. As might be expected, analysis of this sort is exceedingly time consuming

and still requires knowledge as to the number of components which must be fit. The second approach employs not only knowledge of the number of components but also estimates of rate constants and initial concentrations for each component. Given these estimates, the method is able to approach the optimal solution with much greater rapidity. Poor initial estimates may, however, allow convergence to an incorrect solution.

The latter approach is chosen for use here. This leaves the problem of finding reasonable values for estimates. One solution to this is the application of an approximate Laplace transform [18]. This method evaluates the number of kinetic components as well as providing estimates of rate constants and initial concentration of each component species. Derivation of the Laplace transform applicable to multicomponent kinetic analysis may be found in the theory section.

1.2.2 Speciation

The critical factor in determining toxicity is the rate of metal ion uptake by organisms. Most research to date has relied on the measurement of equilibria to model and quantify species distributions. Several of these models are discussed in references [19,20]. Each has its advantages and limitations. However, it is reiterated at this point that even an "ideal" speciation model based on thermodynamic considerations alone cannot provide a complete picture of the parameters of relevance to metal availability and uptake.

Kinetic considerations reveal factors which are not within the realms of equilibria. In dealing with biological problems it is of importance to have information associated with rates which might control uptake as well as with equilibrium distributions. In some

situations not uncommon to natural systems equilibration periods are sufficiently long that organisms sample the system in a non-equilibrium state. Allowing for the difficulty in extrapolation from kinetic conditions to sample conditions, kinetic information provides hints as to the appropriate labilities which are related to problems associated with uptake rates by organisms.

1.3 PROBLEM OF SPECIES DETECTION

As will be pointed out on several occasions in this thesis, a major limitation in applying kinetic speciation at environmentally significant concentrations is insufficient analytical resolution. Indeed, this problem plagues all trace metal (TM) speciation methods. Natural concentrations of TM's are often so low that extreme difficulty may be encountered even in determining total concentrations. The present problem goes beyond one of detection limits to one of *resolving* component species at low concentrations. Table 1-1 shows concentration ranges which have been reported for some metals in a selection of natural systems (summarized by Buffle [21]). Note that many of these important metals are typically present at nano-M to pico-M concentrations.

Some metal complexes are sufficiently non-labile to allow speciation based on separation followed by species non-specific analysis. For this to be accomplished the metals must be present at sufficiently high concentrations. The use of preconcentration has also been frequently reported. The case often arises, however, where this is "harsh" treatment of the sample suggesting possible changes in TM species distribution. Further, problems of adsorption or analytical restrictions on solution conditions can influence

TABLE 1-1
Ranges reported for the total concentration of some inorganic elements in natural waters as summarized by Buffle [21][a].

	Log concentration (M) of total metal					
	Fresh waters		Soil pore waters[b]		Pelagic sea water	
Fe	-6.8	-4.7	-5.8	-4.8	-10.0	-8.7
Al	-6.5	-4.0			-8.3	-7.5
Mn	-9.5	-5.6	-6.4	-4.4	-9.7	-8.5
Ni	-9.5	-6.3	-7.0		-8.7	-7.8
Cu	-8.5	-6.2	-6.8	-6.0	-9.2	-8.2
Zn	-8.5	-5.8	-6.0	-5.2	-10.5	-8.0
Cd	-10.0	-7.6	-9.0		-12.0	-9.0
Pb	-9.5	-6.2			-11.4	-9.7
Cr	-8.8	-6.9			-8.7	-8.2
Hg	<-10.5	-7.8	-9.5		-11.7	-11.0

[a]Data from [22] fresh waters; [23,24] soil pore waters; [25] sea water.
[b]In some cases only single values were reported.

speciation results. Lund [9] has recently discussed many of these cases and the various combinations of analytical methods employed. The vast majority of speciation studies have been carried out under conditions of thermodynamic equilibrium. Equilibrium studies may not always provide the most relevant information about the "free metal ion". This will be hinted at in studies of the Cu(II)/HA system (chapter 3) and clearly shown in the case of Cu(II) binding by Fehox.

Figure 1-2 uses copper to define some of these concerns. Natural concentrations of Cu^{2+} in fresh waters and salt waters are shown on the left side of the scale. At somewhat higher concentrations but still of great importance in environmental studies are measures common to aquatic toxicology such as the LC_{50} (lethal concentration for 50% of the population). This value varies considerably with carbonate and pH but generally falls in the range shown, with perch being quite resistant and salmon quite sensitive [26]. From the analytical perspective, anodic stripping voltammetry (ASV) is one of the most sensitive techniques and is, to a degree, species selective. It suffers from problems of adsorption and the potential to shift equilibria. Flameless atomic absorbtion and inductively coupled plasma have evolved into very sensitive methods but only provide information of total metal concentrations. Ion selective electrodes (ISE) for Cu^{2+} are reported to have detection limits of 10^{-8} M under only the most ideal conditions and are prone to interference from other ions as well as the chemical matrix. Judicious choice of chromophore reagents make spectrophotometric determinations quite metal specific. With the copper specific chromophore used in this work (ϵ = 13100 M^{-1} cm^{-1}) conventional absorbance measurements are of only moderate sensitivity (shown as ABS

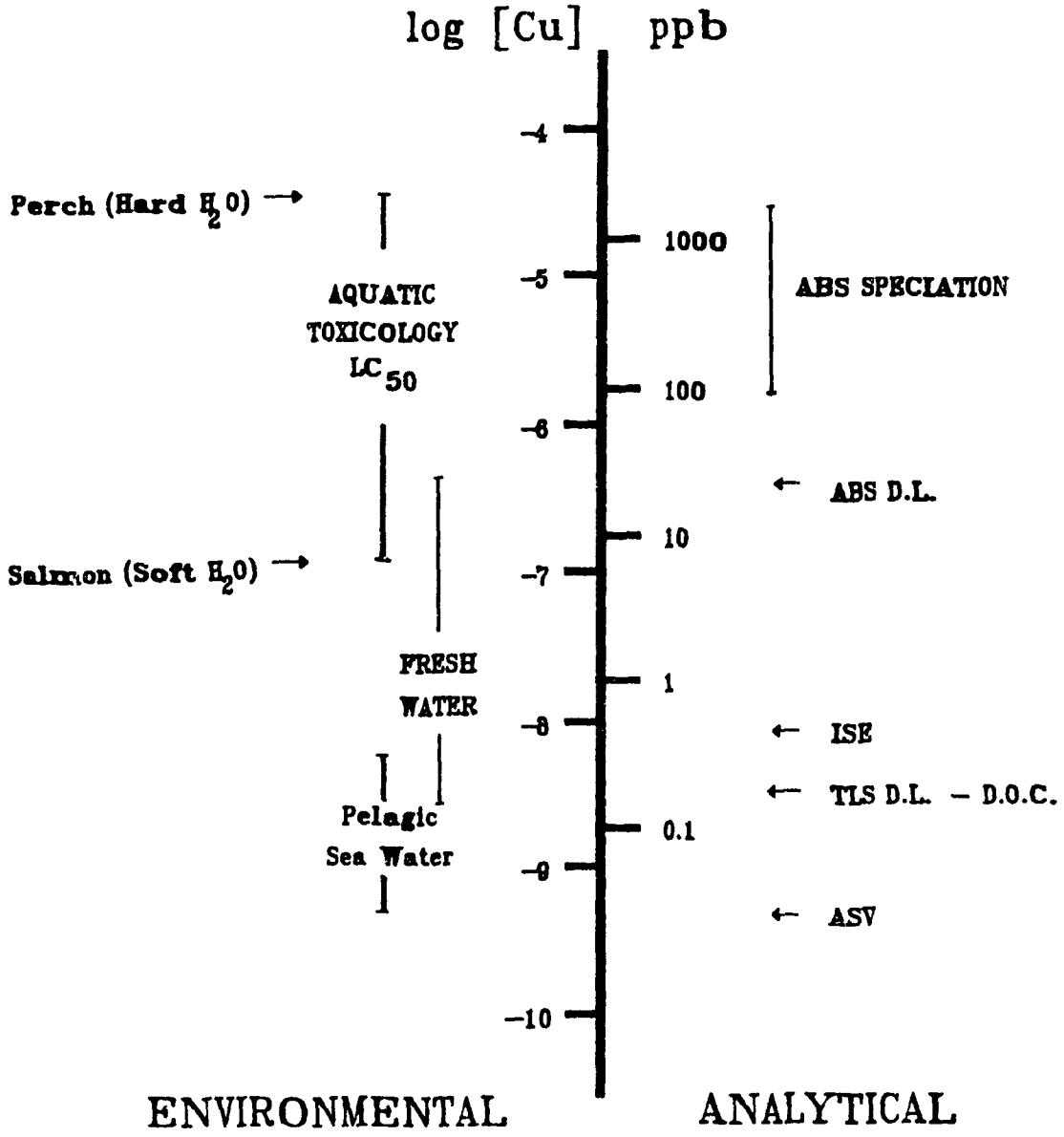

Figure 1-2: Schematic representation of copper concentrations relevant to environmental studies and detection limits (DL) of several analytical techniques. The DL by conventional spectrophotometry is shown with an arrow. The bar above it denotes a range convenient to analyze speciation. For speciation studies, similar bars could be placed over anodic stripping voltammetry (ASV) and ion-selective electrode (ISE). The capacity to study speciation requires that the least significant species be present at concentrations greater that the detection limit of the method. See text for further explanation of terms.

in figure 1-2). Even at current sensitivity the method is applicable to some toxicological studies, but improved sensitivity is a priority.

1.4 LASER THERMAL LENSING SPECTROMETRY

The relatively new technique of laser thermal lensing spectrometry (TLS) enjoys both the selectivity of the spectrophotometric methods and the sensitivity of fluorescence. A beam from a laser having a radial Gaussian intensity profile ($TEM_{0,0}$ mode) is focused into a cell containing the absorbing analyte. Nonradiative relaxation of the electronically excited complex leads to heating of the solvent in the vicinity of the (pump) beam. Since the refractive index of the solvent is a function of density, local heating results in the formation of a transverse refractive index gradient. This gradient reflects the Gaussian character of the incident beam and is, in effect, a thermal lens [27,28]. A second beam tuned to a wavelength not absorbed by the analyte (probe) is directed through the sample coaxially to the pump beam. After passing through the sample, the pump beam is filtered and the intensity at the centre of the probe is monitored with a pinhole/photodiode combination. The change in peak intensity is a sensitive indicator of *absorbed energy*, hence of the analyte concentration. This affords two advantages. First, sensitivity may be increased by use of higher pump power. Second, since the signal is directly dependent on energy absorbed and converted to heat, it is less sensitive to scattering by small particles in the sample. This offers a significant advantage in terms of sample treatment over normal spectrophotometry which measures energy transmitted (where absorbance and scattering both contribute). Larger particles which may block a

significant fraction of the focused laser beam present some problem. As well, particle absorbers can introduce inhomogeneous heating.

1.4.1 Factors affecting analytical application

It is important at this point to discuss some of the factors affecting the TLS signal and how the signal may provide quantitative information. Of greatest importance for analytical studies is the relationship:

$$\frac{I_o - I_\infty}{I_\infty} = \frac{\Delta I}{I_\infty} = \frac{2.303\ P\ (dn/dt)}{\lambda\ k} A = 2.303\ E\ A \qquad (1.1)$$

I_o is the intensity of the centre of the probe beam at the detector in the absence of a pump source. Upon irradiation by the pump beam the lens begins to form. Steady state is obtained when the rate of energy input is equal to the rate of its loss by thermal diffusion. The intensity of the probe at the detector after passing through this steady state lens is I_∞. The magnitude of the thermal lens effect is dependent on the power of the pump beam at the cell (P), the absorbance (A) of the sample at the pump wavelength (λ), thermal conductivity of the sample solvent (k) and the change in refractive index of the solvent with temperature (dn/dt). As shown in Eqn. 1.1, several of these parameters are bulked into an enhancement factor (E) which expresses the gain in signal intensity of TLS over conventional spectrophotometry.

Other things held constant, $\Delta I/I_\infty$ is linearly related to absorbance and hence solute concentration. Linearity is maintained up to a value of $\Delta I/I_\infty$ of about 0.15. For more highly absorbing samples, the focal length of the thermal lens is significantly shorter and the thin lens approximation used in deriving the relationship no longer holds. The higher

order term, $(2.303EA)^2/2$ becomes non-negligible with the consequence that the relationship between $\Delta I/I_o$ and A becomes parabolic. There are many parameters related to the optical configuration affecting the intensity of the TLS signal. As such, its application is most safely and easily handled by calibration versus a purely absorbing standard.

It is clear from the terms in Eqn. 1.1 that while the absorbing solute is responsible for energy input to the solution, the magnitude of the signal is also very dependent on the solvent. Several studies have considered the effect of solvents [29,30] on TLS signal intensity and the thermo-optical constants for various gases, liquids and solids have been summarized [31]. Unfortunate for the studies of aquatic systems is the fact that water is one of the poorest solvents, having both a high thermal conductivity (5.95 mW cm^{-1} $°C^{-1}$ at 20 °C) which prevents build up of a large thermal gradient and a small dn/dT (-8.1×10^{-5} $°C^{-1}$ at 20 °C) [31]. In spite of this, enhancement factors of 10 or greater are frequently observed for water. Less polar solvents (such as CCl_4) offer significantly greater enhancement.

Thermal lenses having two different types of optical characteristics are possible. In one case the lens will result in thermal defocusing. Here the probe beam is broadened and the peak intensity reduced by traversing the thermal lens. The alternative case, thermal focusing, results in a narrowing of the probe and an increase in peak intensity. The source of this difference is the sign of the solvents characteristic dn/dT. For most liquids and gases dn/dT is negative. This leads to the equivalent of a biconcave lens. In some media, such as many solids, refractive index increases with increasing temperature (ie. dn/dT is positive). The resulting lens in this situation has the optical properties of a

biconvex lens. In liquids this latter situation is rare.

Since this work has involved the analysis of aqueous solutions, it is important to comment on the refractive index of water as a function of temperature. Figure 1-3 shows this relationship [32]. Note that near 0°C the refractive index is nearly independent of temperature. In fact, figure 1-4 using data from Dovichi [31] shows that dn/dT for water actually changes from negative to positive values as temperature declines in this region. This process has been studied in detail by Franko and Tran [33] who determined that this transition actually occurs at -0.01 ± 0.04 °C (point shown in figure 1-4). That this change does not occur at 4 °C shows that it is not simply a function of density. Besides thermal expansion, molecular polarizability may also be dependent on temperature [29].

Irrespective of the type of thermal lens created, it is possible to observe both thermal focusing and defocusing for any solvent based on the optical properties of the thermal lens. Focusing or defocusing of the probe beam as it passes through a lens results from an increase in the rate of change of the beam phase fronts. If the probe is focused to a waist before the cell then the phase fronts are expanding at the cell position. Encounter with a "biconcave" thermal lens causes accelerated phase front expansion which appears as defocusing. If the probe is focused at some position past the cell, thermal focusing is observed. In a single beam system the maximum TLS effect is seen when the beam waist is located one confocal length on either side of the cell. At the beam waist, the phase fronts are planar. When the probe is focused at the cell it is unaffected by the presence of a thermal lens.

The final salient feature of TLS is that related to mode-matching. In a mode-

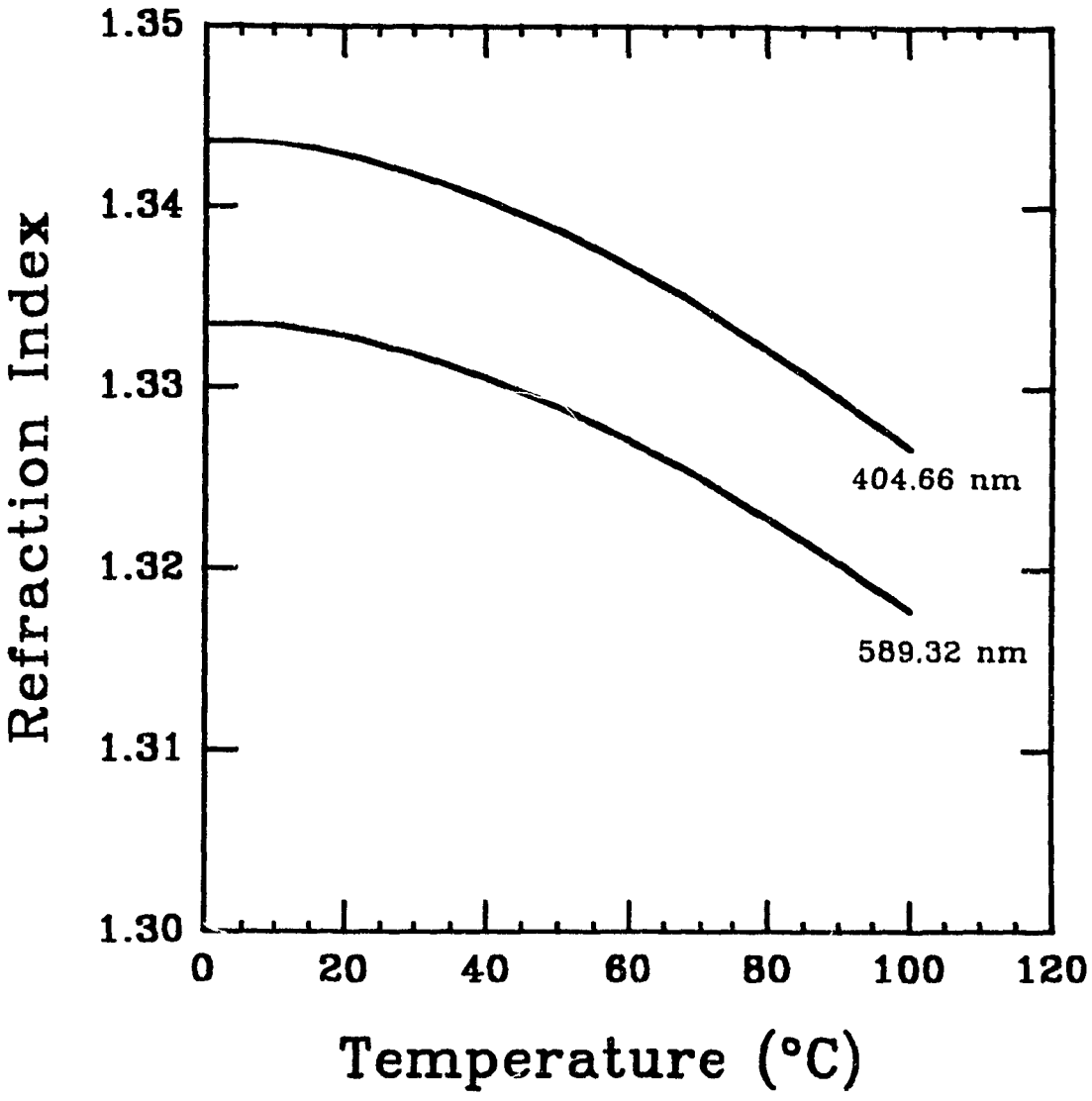

Figure 1-3: Refractive index of water as a function of temperature at atmospheric pressure. Note the greater temperature sensitivity at higher temperatures.

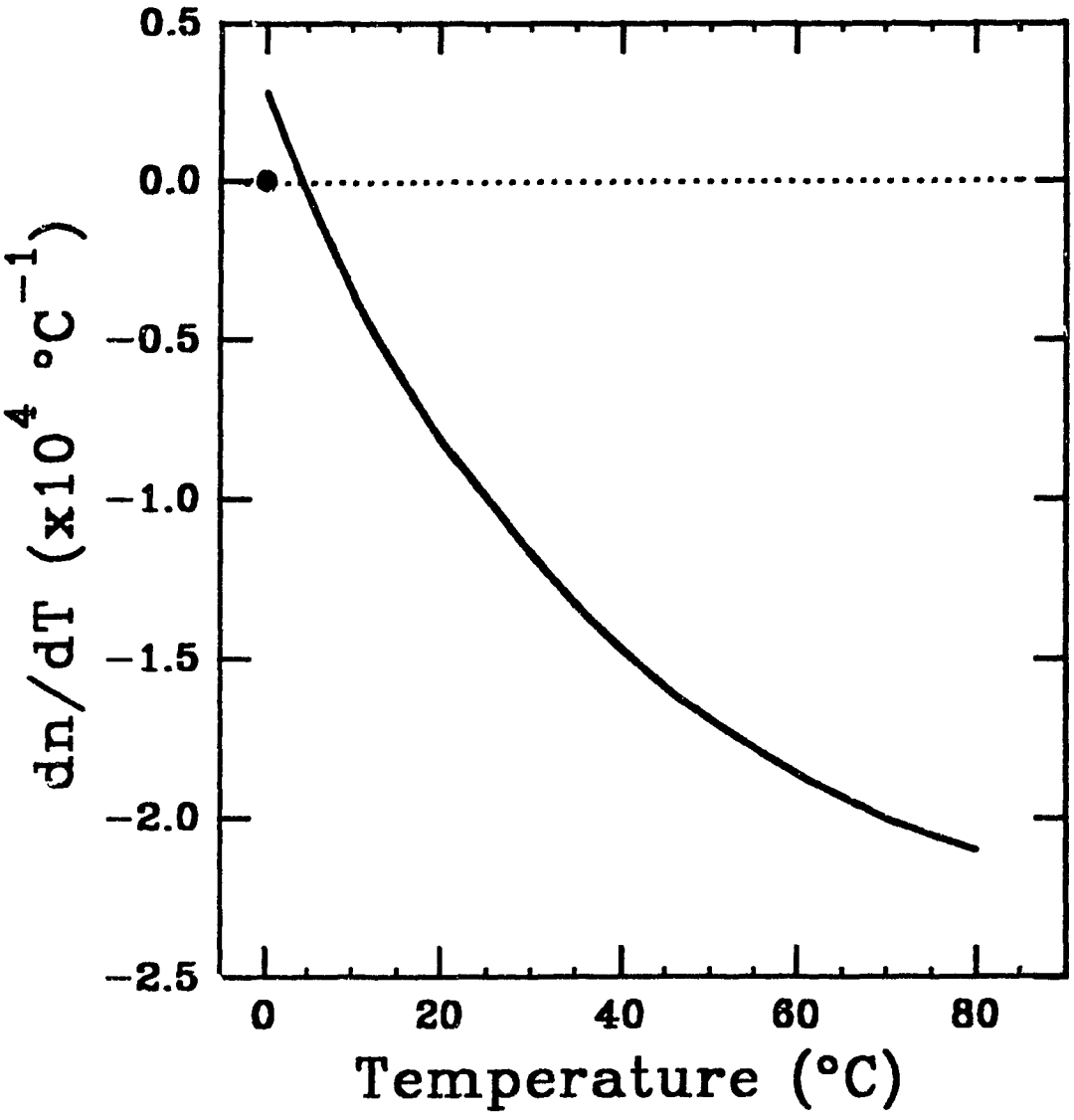

Figure 1-4: Temperature sensitivity of the refractive index of pure water as a function of temperature. dn/dT is generally calculated for liquids, gases and supercritical fluids using the Lorentz-Lorenz formula which relates refractive index to density.

matched configuration the pump and probe beams are focused (frequently with a single lens) to some point either before or after the cell. As a result, the diameters of the two beams in the cell are approximately equal. Since all changes in the probe beam are due to refraction, its intensity profile and width change as it traverses the thermal lens but its Gaussian character remains intact. This optical configuration and the resultant probe beam intensity profile for thermal defocusing are shown in figure 1-5. It is obvious that this is the only possible phenomenon for single beam systems. Greater sensitivity may be obtained by independently focusing the pump and probe beams. The "strength" of the thermal lens (quantified as the reciprocal of the focal length) may be maximized by placing the cell at the focal point (beam waist) of the pump beam. The effect on the probe beam may be independently maximized by focusing the beam $3^{1/2}$ confocal lengths on either side of the sample. This causes an odd effect. At the cell the pump beam diameter is now narrower than that of the probe. Hence, only the centre portion of the probe interacts with the pump generated thermal lens. This optical configuration (figure 1-6A) results in the doughnut-like I_- intensity profile shown in figure 1-6B. The Gaussian character in this case is lost.

1.4.2 The evolution of thermal lensing spectrometry

Thermal lensing (or thermal "blooming" as it was initially called) was first noted in 1965 by Gordon *et al.* [34] while studying the Raman spectra of organic liquids inside a laser resonator cavity. They observed build up and decay transients, mode changes and relaxation oscillations upon introduction of slightly absorbing materials. More highly absorbing samples inhibited lasing completely. Time constants for all

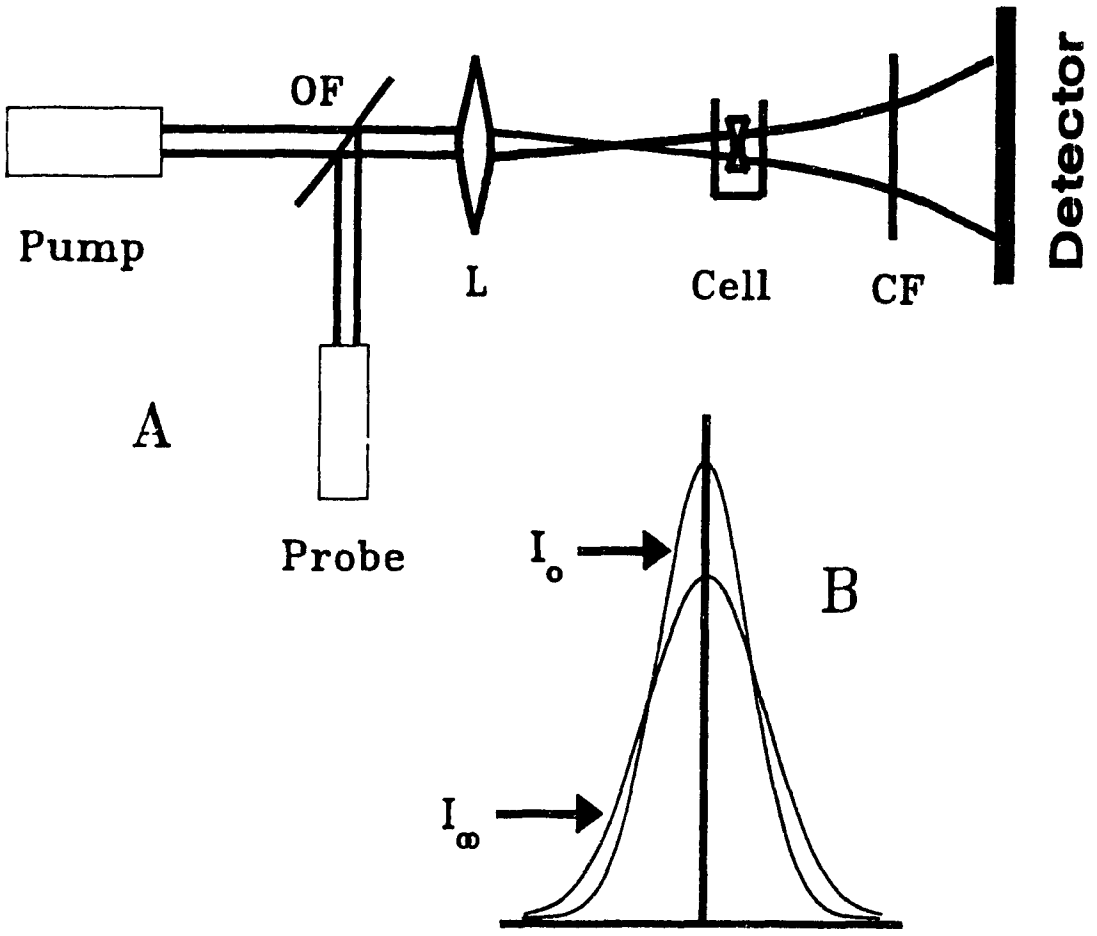

Figure 1-5: A) Optical configuration for mode-matched thermal defocusing with a dual-beam system. OF is an optical flat or partially transmitting mirror. L is a converging lens and CF a cut-off filter for removal of the pump beam. B) Transverse intensity profile of the probe beam with the pump beam off (I_0) and on (I_∞).

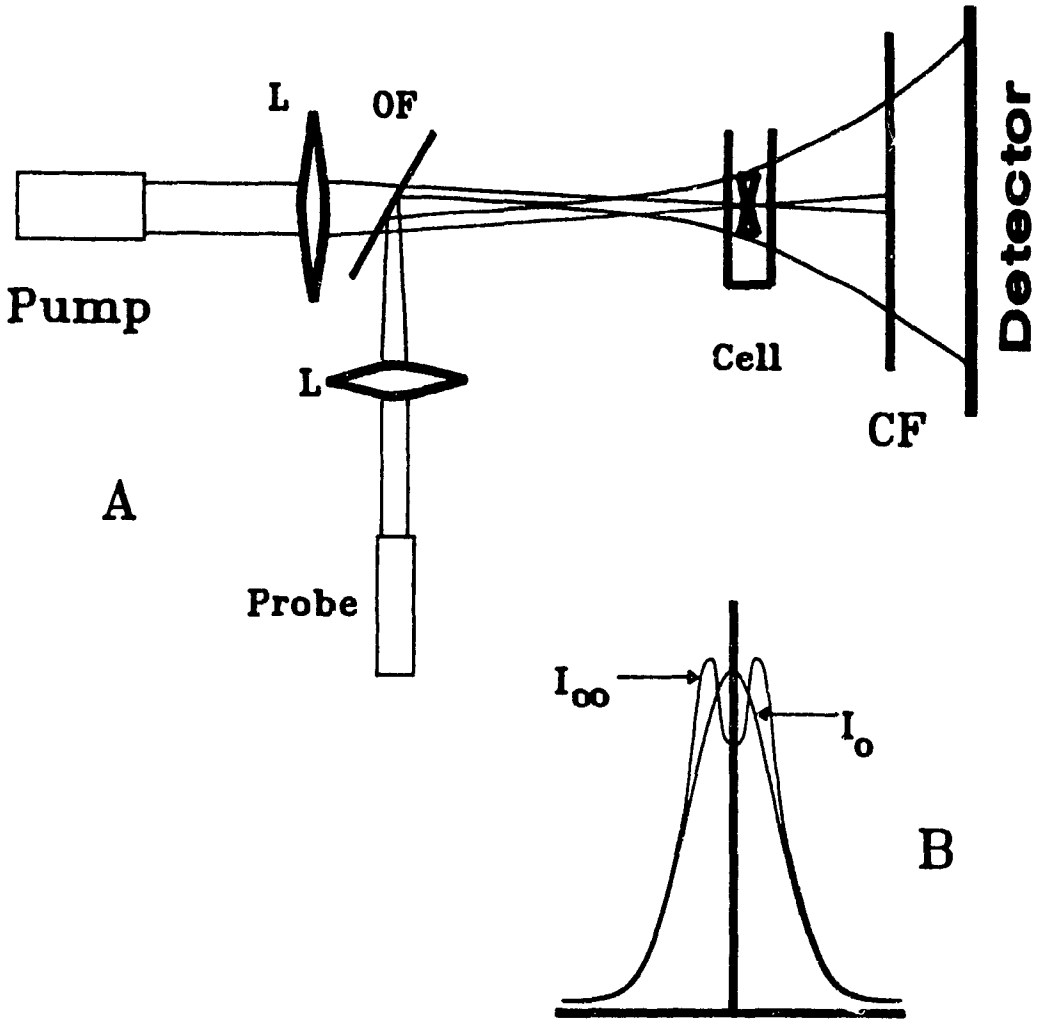

Figure 1-6: A) Optical configuration for mode-mismatched thermal defocusing. Components are explained in the caption of figure 1-5. B) Probe beam intensity profile in the absence (I_0) and presence (I_∞) of a thermal lens. Note that in this configuration only the centre of the probe beam is affected by the thermal lens due to the smaller diameter of the pump beam at the cell.

phenomena were of the order of seconds indicating a thermal process. Detailed analysis confirmed the presence of thermally induced refractive index changes.

The first TLS study done outside of a laser cavity was performed by Hu and Whinnery [35] in 1973. Their simple configuration employed a single continuous wave laser which served as both pump and probe and was focused by a converging lens. Their pinhole/photodiode detector assembly was located 4.5 m beyond the sample to allow for sufficient beam expansion.

In later work (originally by Swofford *et al.* [36]) separate lasers have been used for pumping and probing the sample [37,38]. The potential for noise reduction was now found in the ability to use very stable, low power lasers for probing without any loss of spectral range which was now solely dependent on the pump beam. Moderately noisy, high power lasers could be used as pumps. Because lens formation is slow (ms to seconds) it is insensitive to the fairly high frequency optical noise of the pumping laser. Further, synchronous detection using a pulsed pump beam and lock-in amplification was also possible leading to a further reduction in noise.

With a pump-probe configuration, greater sensitivity and compactness was possible using mode-mismatching [39,40]. Because of the enhanced TLS effect, the path length following the cell could be significantly reduced.

While dual beam has remained the standard configuration, virtually every component of the thermal lensing spectrometer has been "probed" in an effort to improve the method's sensitivity. Many of these modifications are quite innovative and worthy of mention.

Although it has been found that dual beam operation offers greater sensitivity than

single beam, noise due to mechanical vibration is a greater problem. Vibration causes movement in the relative position of sources, optical components and detectors. This is exacerbated in pump-probe systems where vibration leads to misalignment of the two colinearly propagating beams. Pointing stability of the laser sources can also contribute significantly to this misalignment. A number of researchers have attempted to minimize this problem. One method has been to use a single laser source but in a pump-probe configuration. In one case [41] a He/Ne laser was split using a simple beam splitter. The geometry of the apparatus was such that although the pump and probe beams were nearly colinear at the sample, they were counter propagating and thereby separable. The same author also created another apparatus where the laser optics were modified such that two beams of different wavelength were emitted, one from each end of the laser. These were then both used in the system.

Two groups have made use of the polarization of light. Pang and Morris [42] split the beam from an argon ion laser then rotated one of the beams to be orthogonally polarized to the other. A polarization sensitive prism was used after the sample in place of the usual cut-off filter.

Yang [43] took this approach one step further. Light emerging from the source was focused then reflected toward the sample by a polarizing beam splitter. This served to generate the thermal lens. After having passed the cell, the beam encountered a quarter-wave retarder followed by a mirror. Light reflected back toward the cell passed twice through the quarter-wave retarder causing its polarization to rotate by 90°. The rotated beam passed the cell in the opposite direction, this time acting as a probe. The beam was then transmitted through the polarizing splitter to the detector assembly.

Ishibashi and co-workers [44] tried an approach which could help to improve beam alignment. In their system they used an optical fiber to guide the laser light to the sample cell and a second fibre in the detector plane in place of a pinhole. In spite of some problems related to the character of fibre optics, this arrangement offers significant potential.

As mentioned, the intensity profile of a beam emitted from a laser is Gaussian. Before reaching the detector the probe beam encounters a number of optical components. Minor imperfections present in even high quality components lead to inhomogeneity in the quality of the Gaussian profile. This can make the system more sensitive to vibrational noise and to detector alignment. One means of reducing this problem is to monitor the entire profile rather than simply peak intensity. Some early work on beam imaging was done by using a motor-driven micropositioner to move a pinhole/photodiode assembly across the probe beam [45]. More recently, self-scanning linear photodiode arrays have been used [28,46] enabling high speed imaging for real time monitoring and data acquisition. Fitting and spatial averaging of the mode-matched TLS signals allowed reduction of noise levels. Analysis of the I_- profile resulting from a mode-mismatched configuration may be done based on diffraction theory [46]. However, the complexity of the procedure precludes application to routine analysis. Alternatively, fitting of the I_- profile in the "spatial frequency domain" using Fourier analysis has been used [47].

Thermal lensing analysis of flowing samples has also been performed. Cells where flow is axial [48,49,50] or perpendicular [50,51,52] to the beam axis

have been used. Sample flow affects a number of parameters including lens formation time, signal intensity and noise levels. There is a reduced dependence of sensitivity on the sample matrix. The transport of heat is now controlled by both bulk flow and thermal conductivity of the solvent. Theory of flowing TLS may be found in references 51 and 53.

Liquid chromatography using a TLS detector has been applied to the analysis of nitroanalines [42,54,55,56] and other compounds [49] using cell volumes as low as 0.5μL. TLS has also been used as an HPLC detector for the measurement of circular dichroism [57]. Enantiomers of $Co(en)_3^{3+}$ were analyzed using an electrooptic modulator which alternately allowed left and right hand polarized light of the pump beam to pass.

The thermal lensing apparatus has been successfully used in these laboratories for the determination of Fe(II) (and indirectly SO_2) [58], formaldehyde [59] and dissolved organic carbon [60].

1.5 STATEMENT OF THE RESEARCH PROBLEM

This work investigates the speciation of copper(II) in the presence of iron(III) hydrous oxides. This system is of interest due to the binding and diffusion limitations controlling the availability of free Cu(II). Components are determined on the basis of their relative kinetic lability. Data analysis involves the use of a Laplace transform to provide estimates of rate constants and initial component concentrations and nonlinear regression for final parameter fitting.

Prior application of kinetic speciation has been limited to the relatively high concentrations of reagents which may be detected by conventional analysis methods. Therefore, a particular aim of this work is to perform speciation at low metal concentrations comparable with those found in natural environments. To this end the sensitive method of laser thermal lensing is used to detect the very small absorbance changes which occur during kinetic analysis. The study of some other chemical systems is also performed as a means of establishing a relationship between speciation determined at high and at low concentrations.

Chapter 2

GENERAL THEORY OF KINETIC SPECIATION

The chemical system of Ni(II) binding by fulvic acid (FA) will be used here to describe the method of data analysis which has been employed in this work. This is done for two reasons. First, it recognizes that this combination of methodologies flows from the Ni/FA work of J.A. Lavigne [61]. Second, the speciation of Cu(II) binding by Fehox involves an extra complication which could obscure the basic simplicity of the methodology. To maintain consistency, the Ni/FA system will also be used in chapter 3 to show the application of the mathematical techniques.

2.1 BASIC CONCEPTS

Consider the complexes of Ni^{2+} with the acid soluble soil humic fraction called fulvic acid (FA) as they react with a reagent R to form a spectrophotometrically detectable product NiR. We have a set of competing reactions:

$$Ni^{2+}(aq) + R \rightarrow NiR \qquad (2.1)$$

$$FA_1\text{-}Ni + R \rightarrow FA_1 + NiR$$

$$FA_2\text{-}Ni + R \rightarrow FA_2 + NiR$$

.....

$$FA_i\text{-}Ni + R \rightarrow FA_i + NiR$$

The subscripted FA_i represent the different binding sites for Ni(II) on the FA. The first reaction with free Ni^{2+} is the fastest. As long as a large excess of R is used, all reactions

will reduce to pseudo first order kinetics. More fundamentally, the rates of all reactions after the first will often but not always be described mechanistically as:

$$FA_i\text{-}Ni \xrightarrow{\text{(slow)}} FA_i + Ni^{2+}(aq) \qquad (2.2)$$

$$Ni^{2+}(aq) + R \xrightarrow{\text{(fast)}} NiR \qquad (2.3)$$

In this favourable case, the rate constant measured for each component will be the dissociation rate constant of the corresponding complexing site. With all reactions reduced to pseudo-first order, the experimental rate law with excess R takes the form:

$$d[NiR]/dt = \Sigma_i A_{o,i}[1-\exp(-k_i t)] + X \qquad (2.4)$$

In equation 2.4, $A_{o,i}$ represents the initial (time zero) concentration of the i-th species expressed in units consistent with the product NiR, k_i is the rate constant for reaction with the i-th species and X is a time independent term which contains the spectrophotometric blank plus contributions made by any species which react fast on the time scale of the measurements and therefore appear to be time independent. The task is to fit the observed time course to a set of rate constant and concentration parameters; k_i and C(o,i) (related stoichiometrically to $A_{o,i}$). Since the equation is non-linear, this is a difficult task.

The approach just described was stimulated by an interesting series of papers on kinetic analysis from the laboratories of D.W. Margerum [62]. In a typical paper of this series, a mixture of aminopolycarboxylates was analyzed by forming their complexes with Ni(II) then reacting the mixture with excess cyanide, monitoring formation of $[Ni(CN)_4^{2-}]$. The number of components is known in this case and a rate constant for each can be independently estimated by study of the aminopolycarboxylates individually.

The fitting problem is only the linear problem of finding the concentrations. Unfortunately, in the case of natural mixture colloidal polymeric ligands such as humic substances (e.g. FA) there is no way to study the individual binding sites separately, or even to know *a priori* how many distinct sites to assume - the actual situation may be a nearly continuous distribution. Thus, the first task is to develop an appropriately objective procedure to assign a number of components. Then, non-linear fitting must be used to yield the parameters.

Equations (2.2) and (2.3) describe the release of a metal from a complexant and its reaction with a reagent where the first step is rate limiting. It is of importance to point out the possible exceptions to this rule. In some cases ligand exchange reactions are of the type where the rate limiting step is dissociation of an intermediate ternary complex. Reactions of this type have been extensively characterized by Margerum et al. [63]. Borrowing an example from them, consider the exchange of EDTA from Ni^{2+} to Cu^{2+}. This reaction may demonstrate two distinct $[Cu^{2+}]$ dependent second order rate constants and three different ($[Cu^{2+}]$ independent) first order rate constants. Further, there are two possible ternary reaction intermediates. Which reaction pathway will be followed and which step will be rate determining is found to be a function of $[Cu^{2+}]$ and pH. A series of equilibria determine the concentration of the complex involved in the rate limiting step. It is apparent that extrapolation of rate data to different species concentrations in such a circumstance would be highly uncertain. The variation of reaction pathway with species concentration under such conditions has also been addressed by Hering and Morel [64] who raise the significance of its importance for natural waters.

The structural information available on complexation sites of hydrous oxides and humic substances have normally been interpretable in terms of mono and bidentate binding [65,66]. These simple one and two coordinate complexes are expected to dominate in natural systems. The occurrence of higher polydentate chelation is relatively rare in the environment. The simplicity of these one and two coordinate complexes precludes the intricate dissociation mechanisms observed for polydentate complexes. This circumstance is fortuitous to the type of study discussed here as numerical fitting based on complex mechanisms would not be possible. It is pointed out that one need be wary of being mislead by studies of analogues of limited environmental significance such as EDTA.

In circumstances such as the conditions used in experiments described here, pseudo first order reactions are guaranteed. Variation of ligand and metal concentrations would reveal if the simple mechanistic assumption was incorrect. The observation of consistent rate data allowing a chemically significant interpretation over a range of conditions reinforces confidence in the simple complex assumption. Further, structural knowledge of the ligand species employed does not imply the formation of higher coordinate complexes. It is, however, realized that extrapolation of the rate constants based on a mechanistic assumption is uncertain.

2.2 EVALUATION OF KINETIC PARAMETERS

Two procedures have been used to establish an initial approximation to the number of components and the rate constants. In the first, the concentration-time data can be

plotted using the Guggenheim method for obtaining first order rate constants when the final concentration is unknown. This plots differences of log concentration for a fixed time interval *vs* time. In the present context, the plot is searched for linear regions where each component dominates and the slopes of those linear regions provide the initial estimates of rate constants [67]. Intercepts provide approximations of component quantities.

A better procedure was introduced by Mark Shuman and his associates [18,68]. It is a kinetic analog of the affinity spectrum method of analysis of the distribution of equilibrium constants for a multi-site complexant [68]. It uses a numerical approximation of a Laplace transform. The starting point is analogous to an integrated form of equation (2.4).

$$C(t) = \Sigma_i C(o,i)\exp(-k_i t) \qquad (2.5)$$

In this expression, C(t) represents the decrease over time of the overall concentration of the complexes (e.g. FA complexes) which is mirrored by the formation of the product (e.g. NiR). The summation in equation 2.5 may be replaced by an integral either as an approximation to a finite sum or as the representation of the essentially continuous distribution of binding sites which may arise with the heterogeneous mixture polymeric ligand systems.

$$C(t) = S \int H(k)\exp(-kt)d[\ln(k)] \qquad (2.6)$$

In equation 2.6, the new quantity H(k)d[ln(k)] is the probability of finding a site with a rate constant in the range from ln(k) to ln(k)+d[ln(k)] in molar concentration units. Second order approximate solutions can be obtained using the first and second derivative of C(t)and the approximate inversion of a Laplace transform expression equivalent to 2.6 where the integral is taken with respect to ln(k) in place of k. The resulting expressions are:

$$\mathbf{H}(k) = d^2\mathbf{C}(t)/d(\ln t)^2 - d\mathbf{C}(t)/d(\ln t) \qquad (2.7)$$

$$\mathbf{S} = 4\mathbf{C}(t)/\Sigma\mathbf{C}(0,i) \qquad (2.8)$$

H(k) and S originate from the approximate Laplace transform and the value of S depends upon whether the first, second, or n-th derivative is taken in the approximation. When H(k) is plotted *vs* ln(k) [= ln(2/t)] it gives the distribution of rate constants about a peak value of ln(k) with an area under the peak proportional to the concentration of complexes, since the constraint applies that the integral over the entire range of H(k) adds to the sum of all C(o,i)s.

Typical absorbance versus time results obtained under pseudo first order conditions are shown in figure 2-1. The data refer to nickel(II) bound to an organic polymer (FA) at different ligand to metal ratios. Although the curves appear rather featureless they are comprised of at least four kinetically distinguishable components. Results for the Laplace analysis of the curve at a ratio of 1:1 appear in figure 2-2. This system will be described fully in chapter 3.

This Laplace transform approach appears at first sight to provide a solution to the

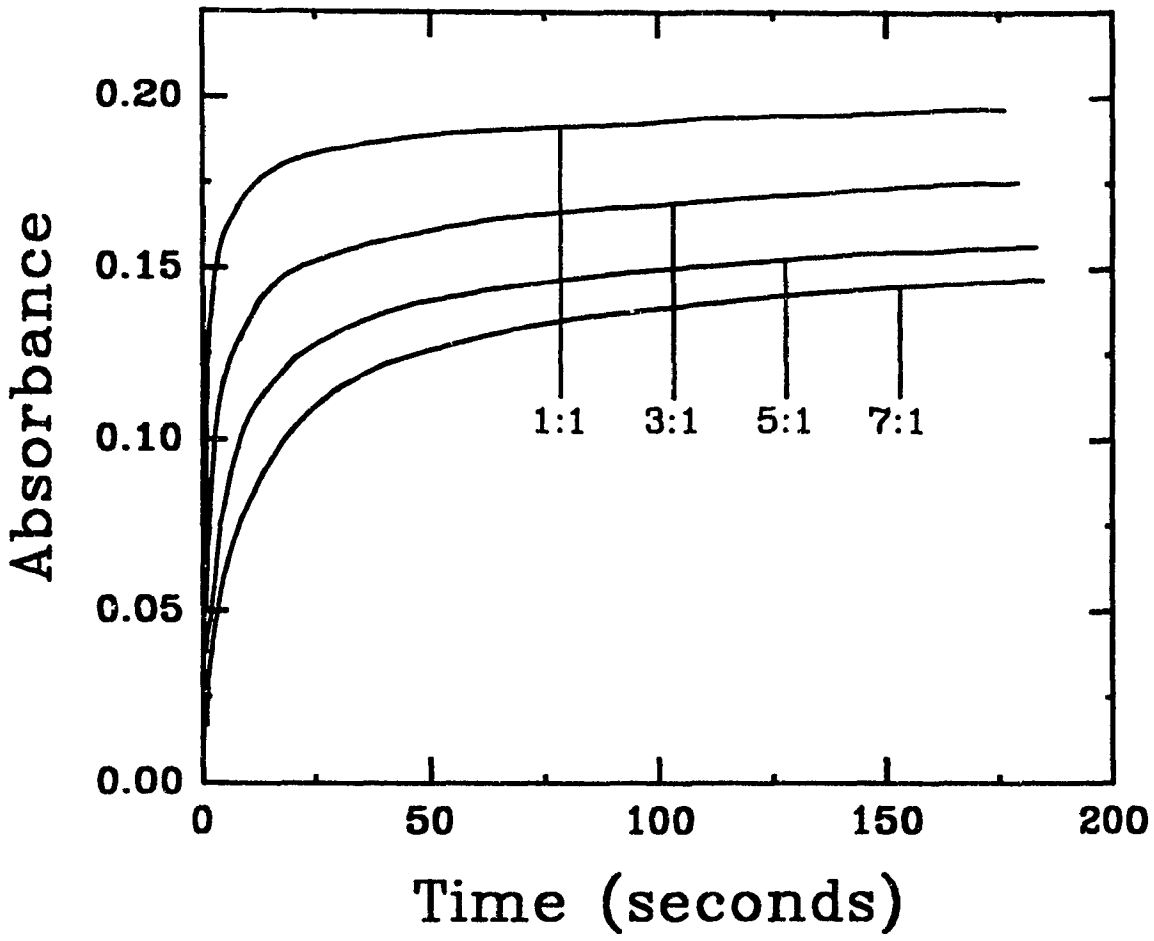

Figure 2-1: Kinetic results for the reaction of an excess of chromophore with nickel(II). The metal was pre-equilibrated at pH 6.4 at several ratios of fulvic acid to Ni(II). Background X components have been removed.

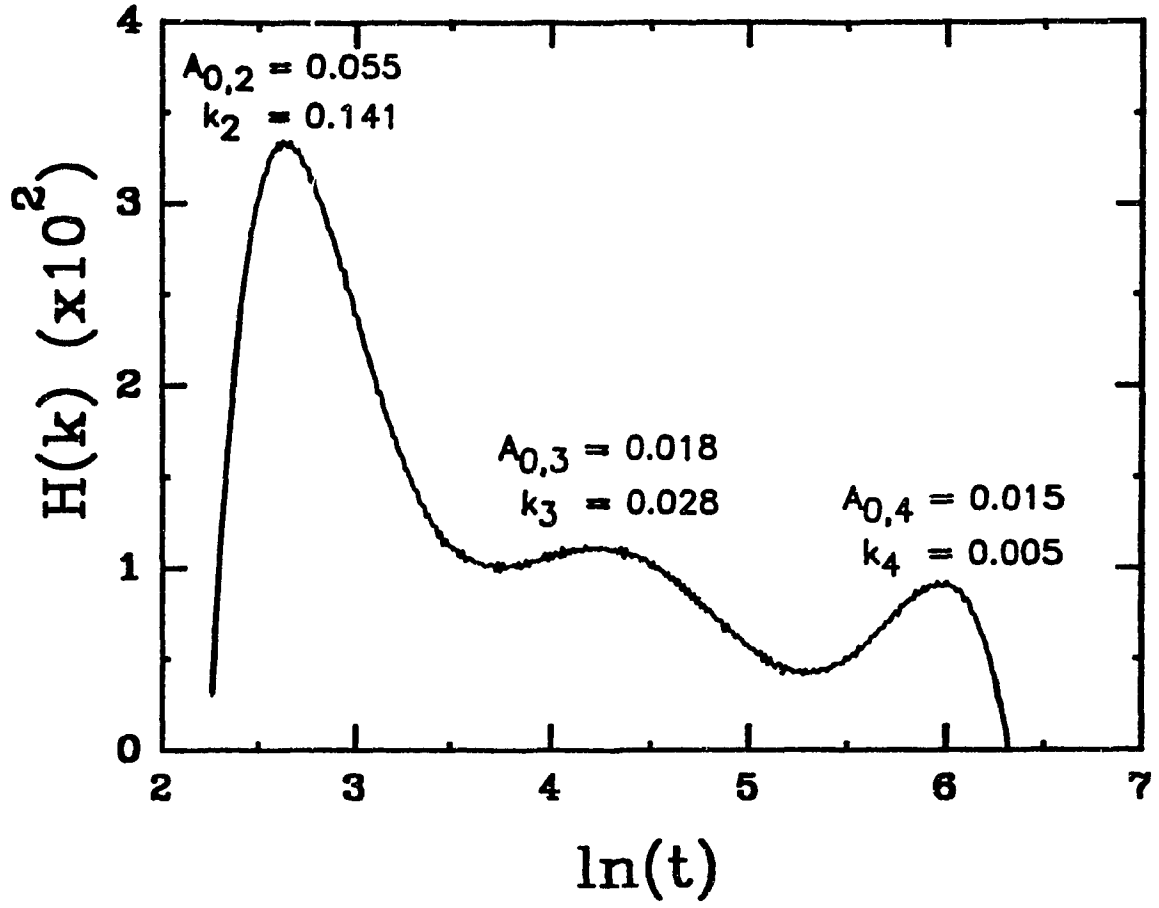

Figure 2-2: Laplace spectrum of the 1:1 fulvic acid-Ni(II) curve seen in the previous figure. The three slowest components are shown. Data corresponding to the fastest component were truncated prior to Laplace analysis. The units of H(k) are the appropriate transform of concentrations expressed in units of absorbance change. Rate constants are in s^{-1}.

whole problem. The integrated **H**(k) and peak values of ln(2/t) provide concentrations and rate constants. However, the numerical differentiation required by equation 2.7 makes the treatment extremely sensitive to artifacts. A number of examples are in the literature which show the dangers. In consequence, it is wise to go beyond the Laplace transform treatment before accepting a model of the kinetic data. There is a further reason for such caution.

The second order approximation to the Laplace transform introduces broadening to a peak in the **H**(k) *vs* ln(2/t). Thus, two cases cannot be directly distinguished. In one case, a set of well defined and distinct components will give broad peaks because of mathematical approximation. In the other case, a distribution of differentiated sites groups about an average value to give broad peaks in the ln(k) spectrum. It is not a simple matter to distinguish the two cases. In what follows, we outline a method to address this complex issue. At present, the immediate point is that the Laplace transform is used to obtain initial objective estimates of the number of components and the rate constants which can be used as input parameters to a non-linear regression (NLR) fitting of equation 2.4. The first condition which must be satisfied is that the regression converge and that the output parameters are sensibly related to the input parameters.

The iterative nonlinear regression routine used in this work (EXPFIT) is one which was written specifically for application to multicomponent kinetic analysis [69]. This affords it the advantage of *a priori* knowledge of some parameter characteristics (associated with the sums of exponentials and increasing signal observed in this type of

kinetics) and allows "streamlining" of the algorithm. Such "streamlining" improves the accuracy of the results and limits the chance of convergence of the results to incorrect minima.

Nonlinear regression may be easily conceptualized by considering a surface defined by two adjustable parameters (x and y-axes). Wells in the surface (z-axis) represent the quality of fit to the data, the deepest well being the lowest value of the sum of the squares of the deviations. In more complex systems such as the ones investigated here the "surface" is multi-dimensional. In all cases, however, the least squares criterion is optimally met when the partial derivatives of the sum of squares with each adjustable parameter equal zero.

In EXPFIT two different techniques are combined in adjustment of the fitting parameters. The first involves expansion of the first-order function into a Taylor series linear about the correction terms. A linear least squares analysis of the partial differentials may then be solved for new values of the correction terms. This procedure is repeated until the correction terms become negligible. Although convergence using this technique is rapid, poorer estimates cause divergence. The second method is that of "steepest-descent". This algorithm determines which direction results in the fastest decrease in the sum of squares. Initial convergence is rapid. As the minimum is approached, the steepest-descent vector becomes almost perpendicular to the least squares "axis". This causes final approach to the least sum of squares to become excessively slow.

In both of these approaches the direction of the correction vector is determined

prior to its magnitude. A modification devised by Marquardt [70] determines both of these simultaneously. It incorporates features of both the Taylor series and steepest-descent methods. By gradually switching from one method to the other, this algorithm reduces the chance of diverging during initial iterations where the magnitude of the correction factors are large while not becoming excessively slow as the minimum is approached.

EXPFIT accepts time-signal data in a [$S(t_1)$, t_1, $S(t_2)$, t_2...$S(t_n)$, t_n] format to a maximum of 250 data pairs. Independent estimates of rate constants and initial concentrations for each component as well as a background term must be supplied. These parameters are considered to have converged when the sum of squares of the deviations is less than or equal to 10^{-8}. More thorough explanation of the concepts incorporated into the program may be found in [69].

Cabaniss [71] has evaluated transform and statistical methods for analysis of kinetic data based on equation 2.4. These included continuous distribution (Laplace transform), nonlinear regression of k_i and C_i and linear regression on either k_i or C_i. He concluded that methods based on regression of both parameters were the best suited of these for kinetic modelling.

Mak and Langford [67] used artificial data to evaluate the effectiveness of the NLR method in resolving kinetic parameters in two and three component systems. The Laplace transform method has also been tested in detail with synthetic data plus added noise [72].

The approach just sketched describes the transform techniques which have been exploited so far in this area. Other related mathematical techniques may well merit evaluation (see for example [73] and [74]).

2.3 SIGNIFICANCE OF RESULTS

A very serious question must now be faced. If a polymeric colloidal complexant mixture may have a distribution of binding sites, how may we be assured that fitting of a small number of kinetic components has chemical significance? Are the rate constants and concentrations which emerge from the combination of the Laplace transform and non-linear regression more than a way of archiving the concentration time function? There is a direct way to answer this key question.

A *chemically significant* partition into a few kinetically defined components will have two characteristics. First, the rate constants will be fairly stable and only the concentrations of components will vary significantly as pH and concentration ratios vary. Second, the changes in concentrations of components will follow trends required by mass action law considerations. As will be seen in the cases discussed below, these two tests are commonly satisfied. The reported partitioning into two to four kinetic components does appear to reflect definite features of the chemistry of the systems. This does not mean that the two to four rate constants given refer to specific molecular species. There may still be some diversity of the individual sites, but they group into recognizable sets which may be adequately approximated by a small set of stable rate constants. This behaviour is found for Cu(II) and Ni(II) complexes of humics, Cu(II) complexes of

hydrous ferric oxide*, and for the Fe(III) humic and hydrous oxide (hox) species. That such a simple speciation is by no means required is shown by data for Al(III) hydrous oxides and humics. Here the rate constants are not stable and the kinetic analysis recommended here shows that there is a very complex species distribution for which no small set of rate constants provides chemical insight.

One more preliminary problem deserves comment. The test of significance just proposed requires that a study be conducted over a range of pH and total concentration. Such a range can be studied in laboratory modelling, but is not possible if analysis of a specific natural sample is desired. This problem has recently been addressed by a former member of the Concordia group, Luis Sojo, collaborating with Henk deHaan in the Netherlands [75]. In order to validate a study of iron speciation in a lake, they extracted the humics from soils surrounding the lake and prepared models of the humic - hydrous oxide system over a pH and concentration range. Rate constants obtained from and validated by the modelling effort could be associated with the rate constants found for the components in the lake samples.

* The term "hydrous ferric oxide" is chosen to imply the material which is formed on polymerization of Fe(III) in aerated systems. It is not designated "hydrous iron(III) oxide" because there is evidence for the presence of some Fe(II) in several circumstances. To the best of our knowledge, there is no satisfactory nomenclature.

Chapter 3

HISTORICAL PERSPECTIVE OF KINETIC SPECIATION

3.1 "TIMED REACTION" SPECIATION STUDIES

Two methods of metal speciation have evolved which quantify components on the basis of their extent of "reaction" within a fixed period of time. The first of these involves contacting the analyte solution with an ion exchange resin. Metals which are exchanged within a short fixed interval (typically seconds to minutes) are termed "labile". Those which are exchanged after longer periods (hours to days) are "moderately labile". These studies have in some cases used schemes including electrochemical monitoring to determine "very labile" components, sample digestion to determine an "inert" fraction and photooxidation to measure metals associated with colloidal organic material. Applications have included speciation of Cu, Cd, Pb and Zn [76] and Al [77] in freshwaters and of Cd and Zn in seawater [78].

Speciation of aluminum(III) has frequently been carried out by timed reaction with oxine (8-hydroxyquinoline), ferron (8-hydroxy-7-iodo-5-quinoline-sulphonic acid) or more recently pyrocatechol violet. The reactions are monitored spectrophotometrically. Hexaaqua and the other mononuclear Al(III) species are assumed to react very rapidly while reactive polynuclear species are determined after a longer time. Absorbance is typically measured about 15 seconds and 60 minutes after initiation of reaction. The evolution of these methods has been reviewed by Bertsch [79]. They have been widely applied to studies of aluminum [see for example references 80,81,82] and as

procedures in other speciation work [83,84].

The (contact or reaction) times used in these types of work are initially selected on the basis of studies of model or well characterized systems where the speciation is known or determined by other methods. This allows times to be chosen which will provide significant results. The "selectivity" of these times may be reduced when the methods are applied outside of the model system. Under these less restricted conditions, the method related times become operational definitions which do not allow the technique to recognize changes in the chemical system such as the presence of complexes not accounted for in the model. In spite of this fault it is recognized that methods of this type serve a useful purpose in allowing simple monitoring well suited to routine application. These methods may be particularly useful in measurement of Al(III) where (as will be seen) the complex chemistry of the metal impedes more detailed kinetic speciation.

3.2 STUDIES OF SIMPLER SYSTEMS

3.2.1 Nickel(II)-fulvic acid

We begin with a discussion of the Ni(II)-fulvic acid (FA) system [72]. The reason is that the lability of Ni(II) complexes is at a favourable intermediate value. This allows the most complete analysis. Nickel(II) complexes have been important paradigm systems in the study of complex formation kinetics in general.

The ligand system was a well characterized FA [85] extracted from a Bh horizon soil from Armadale, Prince Edward Island. This organic polyelectrolyte has 7.7 meq g^{-1} carboxylate groups of which 3.3 meq g^{-1} are salicylate like. Total bidentate

chelating sites number at least 5.5 meq g^{-1}.

The nickel concentration was held constant ($1x10^{-5}$ M) and kinetics were measured at FA:Ni ratios between 1:1 and 9:1. Solution pH was adjusted to 4.0, 5.0 or 6.4 followed by an equilibration period of at least 24 hours at room temperature in the dark. The low pH is slightly above the unadjusted pH of the FA solutions while 6.4 is just beyond the pK_a's of the FA carboxylates.

The colourimetric reagent solution included the chromophore 4-(2-pyridylazo)resorcinol (PAR), $NaNO_3$ for ionic strength (I, mol L^{-1}) control and $NaHCO_3$ for pH buffering. After mixing equal volumes of sample and reagent solution, the mixture had I = 0.125 and pH = 7.8. A general purpose least-squares polynomial routine was applied to the data. Conversion to ln(A) and ln(t) optimized the data for polynomial fitting. Choice of the lowest degree polynomial which would faithfully follow the curves prevented reproduction of noise or the creation of irregular artifacts in the Laplace analysis. A smoothed discrete data set was generated with equal spacings of ln(t). The latter procedure was an essential prerequisite to successful Laplace calculations.

Laplace transform analysis of kinetic curves revealed the presence of four kinetically distinguishable components. The two fastest components have rate constants separated by only a factor of about 4 making them difficult to distinguish. This complication led to a standard procedure as follows.

Step 1. Ni(II) has sufficiently low lability that reaction of the "free" hexaaqua species is readily measured. $Ni(OH_2)_6^{2+}$ (component 1) is certainly the most labile of the Ni(II) species present. Kinetic analysis in the absence of FA yielded a rate constant of 0.62 s^{-1}. This rate constant for Ni(aq) indicates that almost 99% of this component has

reacted within the first 7 seconds and its contribution to absorbance changes beyond this time are negligible. The second fastest component had a rate constant of about 0.14 s^{-1}. Therefore, about 40% of this component reacts at times longer than 7 seconds. For these reasons, the first 7 seconds of data were truncated and handled separately. Since the time dependence of hexaaqua nickel may be determined, it does not contribute to the time independent X component (eqn. 1). This is "background" due entirely to absorbance by FA and PAR. The value of X was estimated by fitting the first few data points to a low degree polynomial and extrapolating to the absorbance at time zero. These results were verified by comparison to measurements of blank solutions.

Step 2. At sufficiently long times only the slowest component contributes to absorbance changes (component 4). The linear section in a plot of $\ln(A_\infty - A_t)$ versus time reliably estimates k_4 and C_4 from the slope and intercept. Based on these estimates, component 4 is numerically stripped from the data. The resulting absorbance-time data contains only contributions from components 2 and 3 whose parameters are estimated by Laplace analysis.

Step 3. The estimates and raw data (saved prior to the stripping of component 4 and smoothed to equal spacing of time) are passed through a nonlinear regression routine written expressly for sums of exponentials with positive values of parameters. NLR results for components 2, 3 and 4 are sequentially stripped from the data at less than 7 seconds. Component 1 parameters are determined by NLR and k_1 verified for agreement with that measured in the absence of FA.

Table 3-1 shows rate constants obtained at the three different pH's used. The standard deviations are somewhat larger than those obtained using simulated data with

TABLE 3-1
Mean and standard deviations of rate constants determined by Lavigne *et al.* [72] for nickel(II) binding to a fulvic acid at several values of pH[a].

		k_1	k_2	k_3	k_4
pH 4	m	0.61	0.153	0.0208	0.0021
	SD	0.17	0.036	0.0080	0.0009
pH 5	m	0.70	0.139	0.0203	0.0032
	SD	0.13	0.031	0.0078	0.0015
pH 6.4	m	0.533	0.132	0.0197	0.0018
	SD	0.096	0.026	0.0064	0.0009
pooled results	n	40	39	40	24
	m	0.67	0.147	0.0205	0.0026
	SD	0.16	0.038	0.0082	0.0010

[a]m and SD are the mean and standard deviation of the rate constants in s^{-1}.
n refers to the number of kinetic runs for which the rate constant was resolved.

white noise added slightly in excess of that estimated to apply to the experimental data. This suggests that in the Ni-FA system the kinetically identified components are not discrete. While component 1 is the "free" nickel, each of the other three k's probably represent the mean of a distribution of similar kinetic behaviour. The fact that observed rate constants do not vary systematically with equilibration pH, FA concentration or FA:Ni ratio is important.

It is important to realize that the four components found represent the minimum number needed to model the Ni(II)-FA equilibrium. Component distributions as a function of FA:Ni ratio are shown in figures 3-1 and 3-2 for equilibration pH's of 4.0 and 6.4, respectively. Results similar to those at pH 4.0 were found at pH 5.0. It may be seen that the decreased proton competition at pH 6.4 results in a reduction of the aqua-Ni(II) and an increase in the relative contributions of the bound species. Further, variation of component contributions with FA:Ni ratio follow expected mass action laws. It must be noted that while complete Ni(II) recovery was obtained at pH 4.0 and 5.0 only 60% was recovered within 24 hours at pH 6.4. The remaining 40% required up to 10 days to be completely recovered corresponding to a rate constant of the order 10^{-5} s^{-1}. Even though this very slowly labile component became apparent at pH 6.4, the rate parameters identifying the other 3 bound species were unaffected. Only their relative quantities were reduced.

More recently Cabaniss has studied speciation of Ni(II) complexes of water derived FA from a somewhat different perspective [71]. He observed variations in component k_i and C_i parameters with changes in kinetic reaction conditions. Ionic

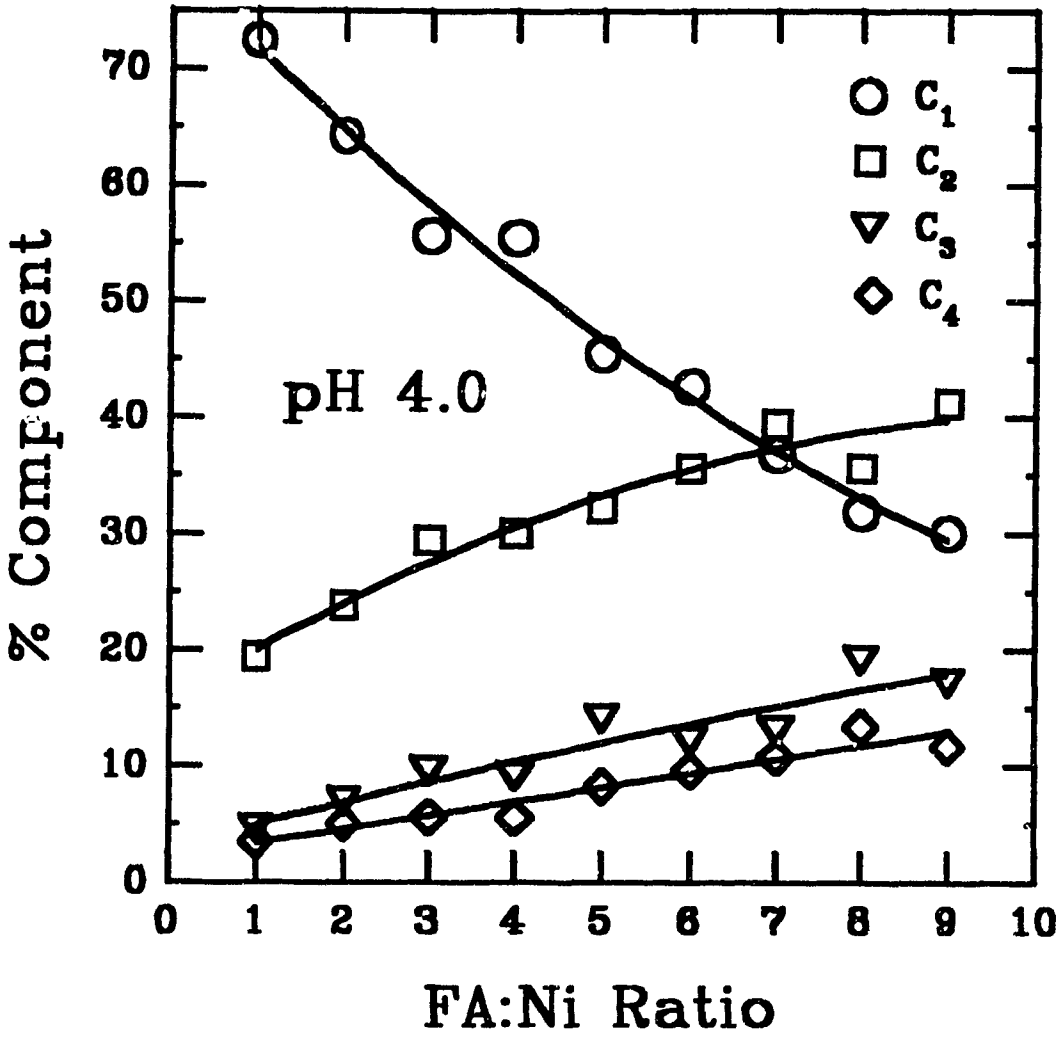

Figure 3-1: Changes in relative contribution of initial component concentrations (C_i) as a function of ligand to metal ratio following equilibration of Ni(II) with fulvic acid at pH 4.0.

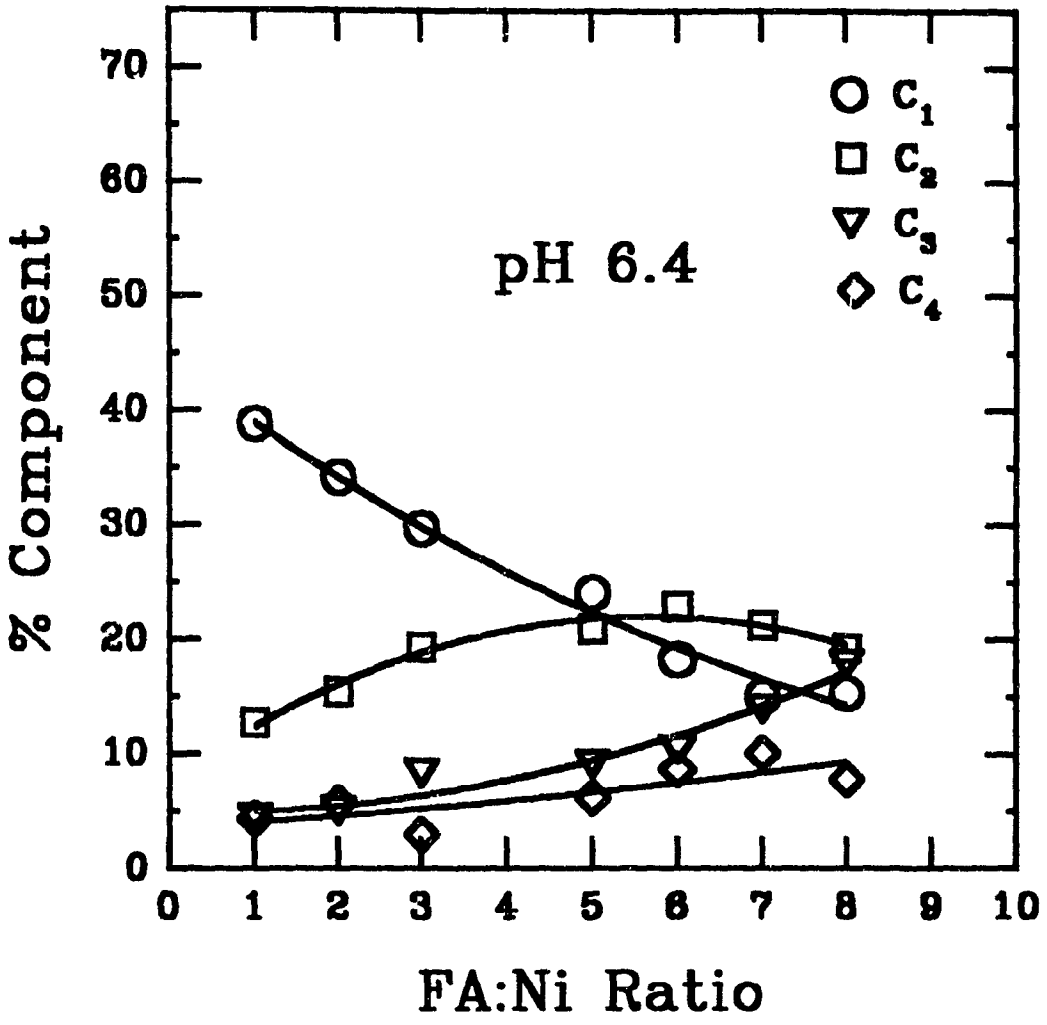

Figure 3-2: Initial component contributions in the Ni(II)-FA system after equilibration at pH 6.4. Note that the sum of components is only about 60%, showing the presence of a very slowly reactive component. (Recalculated from Fig. 6 of Lavigne et al. [72].)

strength, pH and FA:Ni ratios were adjusted followed by the equilibration period. Kinetics were determined by the introduction of *only* the chromophore, PAR. It was observed that dissociation rate constants increased with increasing I, decreasing pH and decreasing FA:Ni ratio. The effect of pH and I were quite marked.

Rate constants of the more labile species showed greater sensitivity to pH change. Ionic strength effects were comparable in magnitude to those of pH. As expected increased ionic strength caused C_1 to increase. The rate constant of the kinetically slowest component was relatively insensitive to a change in I from 0.002 to 0.100 whereas k_2 for the fastest of the bound components increased five fold. These extremes suggest a difference in the relative importance of electrostatic contribution to the binding although the author did not consider the effect of ionic strength on aggregation of the fulvic acid.

An interesting observation of environmental importance is that at the FA:Ni ratios found in nature, metal binding is expected to be predominantly to the least labile sites. Since these sites are least sensitive to pH and ionic strength changes, a "buffering" effect exists. It was pointed out, however, that measurements are needed at environmentally significant metal and colloid concentrations to confirm this effect. Of course, the interpretation of these experiments is uncertain because the analysis depends on specific mechanistic assumptions which may not be valid.

3.2.2 Copper(II)-Humic Acid

A study of the binding of copper to humic acid (HA) has recently been completed by Bonifazi [86]. The HA was extracted from a podzol soil of the Laurentian Forest

Preserve of Laval University and has been characterized by Wang *et al.* [87,88]. Samples were prepared at either pH 6.0 or 7.0 and had HA:Cu ratios between 2 and 5. Copper concentration was 8.3×10^{-5} M. Samples were equilibrated in the dark for 24 hours prior to kinetic analysis. Reaction was with a chromophore specific to copper present at a 30-fold equivalent excess. The combined sample-reagent mixture had a pH buffered at 6.0, an ionic strength of 0.100, and was maintained at 24.5 °C.

The water exchange rate of $Cu(OH_2)_6^{2+}$ ($10^{8.4} s^{-1}$) is more than 4 orders of magnitude greater than that of hexaaquanickel(II) [89,90]. Free Cu(II) and labile components react on time scales inaccessible by even stop-flow techniques. As a result, these components appear as part of the X time independent component and must be determined by blank subtraction. In this system over 80% of the total copper appeared as this fast "component 1". Laplace/NLR analysis revealed the presence of two less labile components having rate constants of 0.093 ± 0.013 s^{-1} (component 2) and 0.0078 ± 0.0008 s^{-1} (component 3).

Figure 3-3 shows component contributions as functions of pH and HA:Cu ratio. A decrease in component 1 and an increase in components 2 and 3 is observed with increasing ratio. As expected there is little difference between results obtained at equilibrium pH 6.0 or 7.0. These pH's fall in a relatively "quiet" region between the pKa of carboxyl groups and that of the phenols (pKa near 9). Copper speciation could not be studied at higher pH due to the precipitation of $Cu(OH)_2$. Much below pH 6 too little copper is bound by the humic acid in suitably non-labile forms.

Again the stability of the rate constants and the rational behaviour of the component contributions indicates that a chemically significant model of speciation is

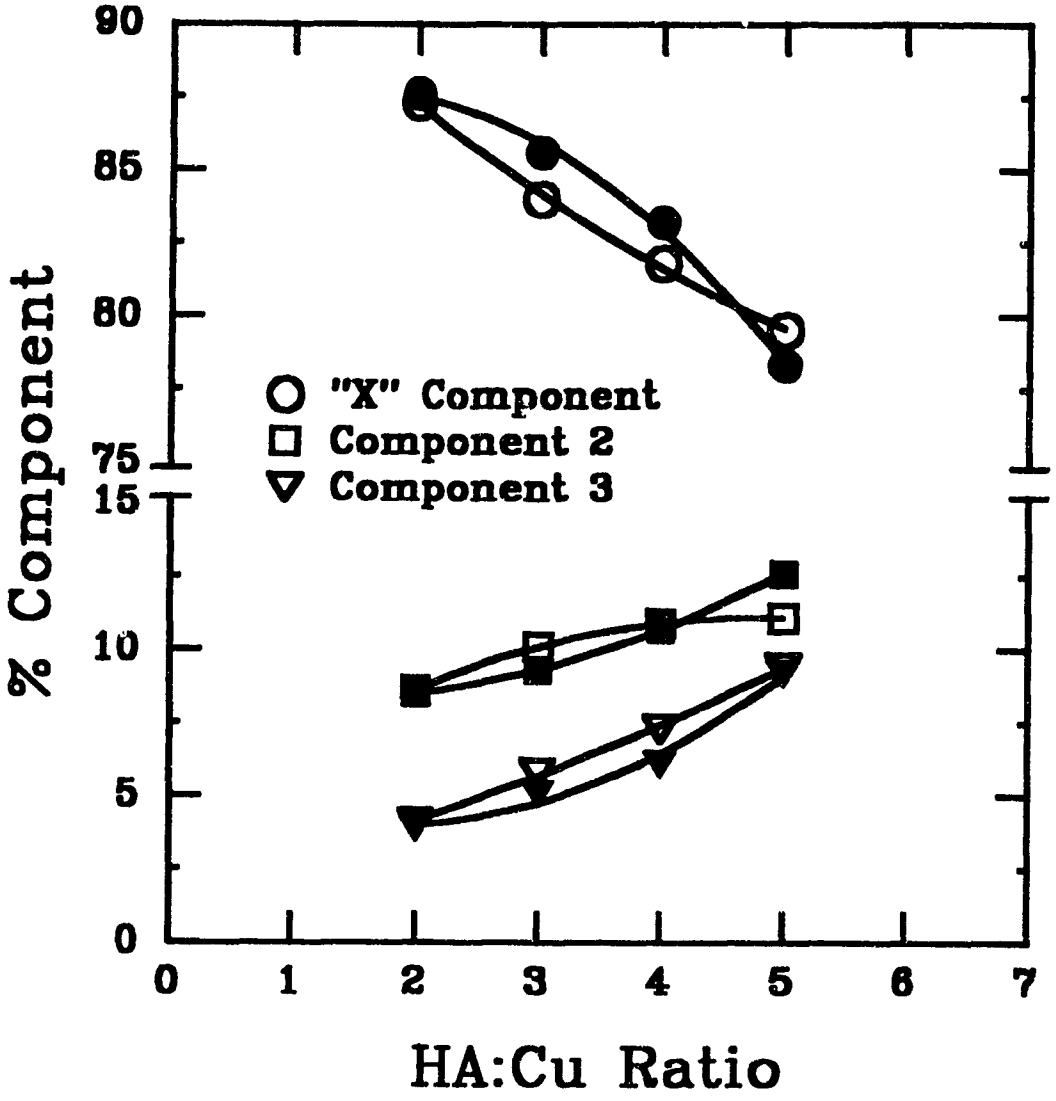

Figure 3-3: Relative initial contributions of components in the Cu(II)-humic acid system. The majority of Cu(II) appears in the highly labile X component. Results are for solutions equilibrated at pH 6.0 (open symbols) and at pH 7.0 (solid symbols).

obtained. As in the case of Ni-FA, the components should probably be considered as averages of a range of related sites of similar lability.

Typically, simple complexes of copper have stability constants of the order $K=10^3$. If formation rate constants lie near 10^8 $M^{-1}s^{-1}$, pseudo first order dissociation rate constants are about 10^5 s^{-1}. It is important to note that labilities of some humic bound copper species were measured to be many orders of magnitude below such values. In fact the range of labilities from simple complexes to those with complex polyelectrolyte ligands spans more than 8 orders of magnitude!

Shuman and coworkers [68] applied Laplace analysis to kinetic speciation of copper. Their ligand consisted of an organic material extracted from estuarine waters on the basis of colloid size using diafiltration/ultrafiltration. Reaction with the chromophore PAR was carried out at pH 7.5 and ionic strength 0.100 using stop-flow mixing. For $7.1x10^{-6}$ M copper equilibrated with 21 mg L^{-1} dissolved organic carbon, three components were identified. Measurable rate constants ranged from 10^{18} to 10^{12} s^{-1}. Some instability of rate constants with changes in total copper concentration was seen at the two extremes. Again, over 75% of the copper was too labile to be measured. Although a different organic fraction was used, these values are comparable to those found by Bonifazi for fulvic acid associated copper.

Shuman *et al.* [68] also performed an equilibrium study. Potentiometric titration with copper indicated stabilities distributed over three regions with centres at log K = 4.5, 5.3 and 6.2. These values are close to those expected for simple complexes. Similarly narrow ranges of stability constants for Cu(II)-FA complexes were determined by Turner

et al. [91] and are summarized by Buffle [92]. If the range of 3 or 4 orders of magnitude of stability constants encompasses both simple species and polymer bound complexes, it is surprisingly narrow in comparison to that of the labilities. Similar "ranges" might be expected.

The discrepancy between ranges of complex stability and lability suggests the consideration of additional factors. Humic substances are large porous gels. Diffusion through the gel is a slow process which can be kinetically limiting. Diffusion has a comparable effect on both rates of association and dissociation. Olson and Shuman [93] studied three operationally defined size ranges of organic matter extracted from the river estuary. They observed a shift toward less labile species with increasing size fraction but offered no explanation of its origins. In the study discussed previously, Cabaniss [71] started with FA extracted from two different rivers. Although the materials differed somewhat in carbon content (53.8% vs. 44.5%), the two displayed very similar equilibrium binding of copper. Cabaniss discontinued use of the higher carbon sample when it was noticed that rates of Ni(II) dissociation from it were somewhat faster. A difference in particle size was postulated to be the cause.

3.3 STUDIES OF MORE COMPLEX SYSTEMS

Systems involving colloidal metal oxides interacting with colloidal organic matter are more complex. The metal ions Al(III), Fe(III), Cr(III) and Mn(IV) have inherently lower lability and can exist as colloidal hydrous oxides in the pH 4 to 9 range. Recovery of the former two metals from colloids has been studied. Iron(III) was initially chosen

because simple complex formation rates for $Fe(OH_2)_6^{2+}$ and $Fe(OH_2)_5OH^{2+}$ are convenient for stopped flow analysis.

3.3.1 Hydrous ferric oxide

The kinetically simplest of the systems to be discussed is the acid hydrolysis of hydrous ferric oxide [94]. Acidic solutions of Fe(III) were adjusted to pH 4.00 with sodium acetate. Colloids formed by this base hydrolysis were equilibrated for 24 hours. The total iron concentration of the equilibrium solutions was $1x10^{-4}$ M. The reaction was initiated by the addition of a solution of sulphosalicylic acid (SSA) in $HClO_4$. Both conventional and stopped flow techniques were used to monitor the Fe-SSA complex formation following acid hydrolysis at pH 1. Components were identified by the Guggenheim method and fitted by non-linear regression using the Marquardt algorithm.

Three kinetic components were observed. The fastest had a rate constant near 0.89 s^{-1} identifying it as monomeric Fe(III) [95]. A rate constant of $7.0x10^{-4}$ s^{-1} was found for component 2. This value is very close to that of $10x10^{-4}$ s^{-1} determined by Sommer *et al.* [96] with the same aging period for a colloid prepared at higher iron concentration and having about 90 Fe atoms per polymer. Quantities of the third and slowest component correlated with that amount of iron which could be removed from solution by a 0.45 μm filter. These larger particles may represent incipient crystalline goethite formation [97]. However no particle settling occurred even after several months.

3.3.2 Hydrous ferric oxide-Fulvic acid

The same procedure was applied to hydrous ferric oxide equilibrated with Armadale fulvic acid. Two quantities of FA were used corresponding to mole ratios of FA-phenolic sites to iron of 1:1 and 2:1. Rate constants extracted were k_1=0.13 s^{-1} and k_2=5.7x10^{-3} s^{-1} at ratio 1:1 and k_1=0.26 s^{-1} and k_2=6.4x10^{-3} s^{-1} at ratio 2:1. The sum of the component quantities account for 72% and 61% of the total iron present.

The values of k_2 are very close to that of 7x10^{-3} s^{-1} estimated from the rate of equilibration of Fe(III) with strong complexing sites of this fulvic acid at pH=1.65 [95]. The rate constants of the more labile components may vary a little with FA:Fe ratio. They are, however, clearly distinguishable from the well established constant for reaction of hexaaquairon(III) with SSA. The most striking fact is that reactions in the presence of FA are faster than acid hydrolysis of Fehox polymers. This is not simple solubilization of Fe(III) by an organic complexing agent. The particle size is larger in the presence of FA as will be described below.

The incomplete recovery of iron is not due to the presence of an unreactive Fe(III) component. The "component" was found to be available to the ferrous ion specific chromophore 1,10-phenanthroline (analog of the nickel-fulvic acid system).

The evolution of the experiments led to a new approach in the analytical procedure. Hydroxylamine hydrochloride was introduced to the acidic chromophore solution as a reducing agent allowing detection by the sensitive reagent for Fe(II), ferrozine [98]. Kinetic studies were performed at pH 2 and 25 °C on samples which had been equilibrated at pH 6. The reactions were pseudo first order in both ferrozine and NH_2OH HCl.

A 1:1 mixture of Fe(II) and Fe(III) was analyzed kinetically to determine the discriminating ability of the chromophore solution. Two rate constants were observed. The first, a fairly rapid component, was attributed to the reaction of free ferrous ion. The second had a value of 4.3 ($\pm$ 0.5) $x10^{-3}$ s^{-1} and was attributed to reduction of hydrous ferric oxide.

Analysis of a hydrous ferric oxide solution showed that 96% of the iron was present in colloidal form. The corresponding rate constant of 4.8 ($\pm$ 0.2) $x10^{3}$ s^{1} is in good agreement with the value above. The remaining 4% of iron had a constant of 0.15 s^{-1} for reduction of free Fe(III).

A fulvic acid iron mixture of 1:1 FA to Fe(III) was analyzed. A fast component ($k>5$ s^{-1}) accounted for 10% of iron. A second rate constant of 1.49 s^{-1} was also extracted. Note that both of these values are larger than those observed for reaction of Fehox in the absence of FA. This greater lability suggests that at least some of the iron is present at equilibrium in the +2 oxidation state. In this context, reaction of the Fe(III)-FA solution with ferrozine in the absence of NH_2OH HCl gave complete recovery with rate constants of 0.113 s^{-1} and $8.6x10^{-3}$ s^{-1}. There is negligible recovery of Fe(II) from hydrous ferric oxides prepared without FA. Although these rates are considerably slower than in the presence of the reducing agent, they show that fulvic acid can reduce and labilize Fe(III).

In the course of performing these experiments, an interesting observation was made. More iron from Fehox equilibrated in the presence of FA was retained on micropore filters than from Fehox alone. Rayleigh scattering at 90° was measured as a function of the amount of Fe(III) added to solutions of constant FA concentration. A

large increase in scattering is seen in the region of a 1:1 ratio of FA phenol carboxylate sites to Fe(III). Although the iron-fulvic acid complexes are larger, the fulvate bound iron is more labile.

3.3.3 Hydrous aluminum(III) oxide and aluminum fulvates

A major concern in development of these methods is improvement of sensitivity so as to permit studies at concentrations near natural water levels. A gain in sensitivity was achieved by use of fluorescence detection. The fluorophore calcein blue (CB) was applied to kinetic study of the hydrous oxides of aluminum (Alhox) and Alhox with FA [99]. For fluorescence a diamagnetic metal was needed.

Hydrolysis of Al(III) was carried out in the presence of FA by slow addition of $NaHCO_3$ until the desired pH was attained. Once again the "equilibrium period" was 24 hours. The ionic strength and pH of the kinetic mixture were established by a 0.100 M acetate buffer and measurements taken at 19.5 °C. The pH was 5.0 in kinetic runs. Higher acidity, favouring hydrolysis of the colloidal complexes, would have been detrimental to the intensity of the fluorescence. Reactions were routinely followed for 24 hours. Beyond this period, instrument instability became significant. Detection of components present at as low as $5x10^{-7}$ M shows the potential for application to natural waters.

In the introduction it was insisted that variation of concentrations and pH values should leave the rate constants fairly stable in order to engender confidence that the kinetic speciation model had identified meaningful components (either unique or a cluster of closely related species). This test was satisfied for Ni(II), Cu(II) and Fe(III) systems.

It is well known that a large range of distinct polycations arise in the hydrolytic polymerization of Al(III). Thus, we might expect Al(III) results to be the exception that "proves the rule" and shows that in some cases the kinetic model is little more than a numerical method for constructing a convenient archive of the signal versus time data. All of the curves obtained in this study were fitted well by one or two components. Under any specific set of chemical conditions, rate constants were reproducible to within 10% and the sum of component concentrations achieved mass balance within 5%. The good quality of the fits does not objectively justify use of more parameters.

Rows A and F in Table 3-2 correspond to Alhox analyzed in the absence of FA at two different concentrations of total aluminum. Both were equilibrated at pH 5. The rate constant measured for $2x10^{-5}$ M Al is similar to that determined for reaction of unhydrolyzed Al(III) with CB at pH 3. A lower rate constant is found for $2x10^{-6}$ M aluminum. This implies that the species formed at lower total aluminum concentration is more extensively hydrolyzed. This is supported by the larger quantity of aluminum falling into an unrecoverable fraction at lower concentration. These unreactive oxides could not be labilized even by boiling with excess perchloric acid. Some light is shed on this oddity by results reported by Matijevic *et al.* [100,101]. They observed a maximum in turbidity curves occurring at 10^{-5} M Al(III). Sol stability at lower concentrations was ascribed to adsorption of Al(III) polyhydroxo cations. At higher concentration anion adsorption stabilizes the colloid.

The bulk of the data in Table 3-2 describes Alhox associated with FA. Fulvic acid concentrations were varied over a fairly wide range as reflected by the FA:Al ratios. The range of 0.9-45 mg L^{-1} is appropriate to fresh water modelling. Note that in all cases

TABLE 3-2
Kinetic results obtained by Mak and Langford [99] for the hydrolysis of aluminum(III) with fulvic acid present.

	[Al] total (10^{-6} M)	FA:Al ratio[a]	pH of sample	k_{Al} (s^{-1})	"k_1" (10^{-2} s^{-1})	"k_2" (10^{-3} s^{-1})	"k_3" (10^{-4} s^{-1})	Kinetic recovery C_1 (%)	C_2 (%)	C_3 (%)	Equilibrium: very slowly recovered[b] (%)	Equilibrium: not recovered (%)
A	20.0	0	5.0	0.562							7.8	13.7
B	20.0	3	5.0		2.71	3.36		29.5	31.9		3.8	34.8
C	20.0	7.5	5.0		2.62	3.30		14.5	20.7		(-1.8)	66.7
D	20.0	3	6.0		2.35	1.98		18.2	29.8		8.5	43.5
E	20.0	7.5	6.0		2.64	3.54		12.7	18.6		2.0	66.7
F	2.00	0	5.0	0.0125							10.2	48.9
G	2.00	1.5	6.0		2.34	3.57		10.7	5.2		1.5	82.6
H	2.00	3	6.0		1.85	1.92		12.5	13.6		13.8	60.0
I	2.00	7.5	6.0		1.66	1.76		16.8	22.6		12.5	48.2
J	2.00	30	6.0		1.35	1.53		16.1	40.8		19.0	24.1
K	2.00	75	6.0				5.51			35.1	2.0	62.9
L	2.00	75	5.0				7.77			42.0	(-3.6)	61.5
M	2.00	3	8.0		16.6	30.9		11.8	19.9		3.4	64.9
N	2.00	30	8.0				18.7			20.3	9.5	70.2

[a]Based on approximately 3 equivalents of phenol-carboxylate per mole FA.
[b]Difference between recovery at 24 hours and at 2 hours.

there is a nonrecoverable aluminum fraction.

It is seen that at pH 5 to 6 data are fit well by two rate constants falling into fairly well defined regions. These are referred to as k_1 and k_2. Study of the reaction of aluminum citrate with CB under the same conditions [67] yielded a rate constant of 4.8×10^{-3} s^{-1}. At 25 °C a value of 7.9×10^{-3} s^{-1} was found for dissociation of aluminum salicylate [102]. The proximity of these values for dissociation of simple chelates to k_1 and k_2 is interesting. It may be inferred that these components represent distributions of sites of similar binding strength on the fulvic acid approximating simple Al(III) complexes.

It is clear that in this system the number of chemically distinct "binding sites" is larger than the number of components required to model the kinetic data. This does not preclude the recovery of some practical information from application of this method. Recognition of the subtle phenomenon of dependence of Al(III) hydrolysis on the total aluminum concentration is of significance to aquatic toxicology. Aluminum availability may have a complex dependence on both pH and concentration. Having recognized the largely "mathematical" nature of the k's and C's in the Alhox/FA system, assignment of greater chemical significance to their values would be imprudent.

3.4 APPLICATION TO NATURAL SYSTEMS

To date the majority of studies based on kinetic speciation have employed either synthesized colloidal compounds or those chemically extracted from natural systems and purified. Two investigations have, however, extrapolated this technique to the study of iron speciation in its native aquatic matrix.

3.4.1 Lake "Esthwaite Water"

Tipping *et al.* [103] included the method of acidification and reaction with SSA in a study of iron redox cycling in the water column of a natural system. Flow centrifugation was used to separate iron particles from "Esthwaite Water" (a small lake in the UK). Iron species larger than about 70 nm were collected as sediment (fraction A). The supernatant (fraction B) was generally concentrated by ultrafiltration (UF) with 10 nm nominal pore size filters prior to analysis. Throughout most of the year iron is about equally split between the two fractions. The annual overturn leads to a large increase in particulate iron.

For comparison of kinetic results, two types of standards were employed. A synthetic hydrous oxide was prepared by base hydrolysis of a ferric salt and aged for several days. Sampling from the oxic/anoxic boundary during the early period of thermal stratification allowed the collection of larger quantities of particulate iron which were also used as "standards". Samples were collected from a well oxygenated zone 5 m below the surface in the months prior to the start of overturn. Absorbance changes in kinetic runs corresponded to within 5% of total iron as determined by the ferrozine method. Ferrozine tests revealed no Fe(II) in the samples, although polarography indicated 5-10% ferrous iron following ultrafiltration.

As shown in Table 3-3, both of the standards yielded single rate constants. The value for the synthetic hydrous ferric oxide is similar to both those of Sommer *et al.* [96] (5.5×10^{-4} s^{-1}) determined after 3 days of colloid aging and by Langford *et al.* [94] (7×10^{-4} s^{-1}) after aging for 24 hours. A single component is also observed for material collected from the oxic/anoxic boundary. Values similar to this are seen as the slower component

TABLE 3-3
Kinetic speciation of iron in Esthwaite Water, UK performed by Tipping et al. [103].

			Relative Distribution of Reactive Species	
	"k_1" ($10^{-3}s^{-1}$)	"k_2" ($10^{-4}s^{-1}$)	C_1 (%)	C_2 (%)
Synthetic Fe-hox		6.7		100
Fraction A from oxic/anoxic boundary		1.3		100
Samples from oxygenated zone (-5m):				
Fraction A	a	1.7	<5	>95
Fraction B:				
-unconcentrated[b]	7	2	30	70
-UF concentrated	5.7	2.5	52	48
-2[y] fraction B[c]	2.2	1.8	52	48

[a]Small contribution of this component prevented estimation of a rate constant.
[b]Values were estimated due to the very small total absorbance change observed.
[c]Supernatant from further centrifugation of the "UF concentrated" fraction.

(k_2) in samples collected from surface waters. These rate coefficients are significantly smaller than that determined for the synthetic colloid. Tipping *et al.*[103] ascribe this difference to the presence of organic matter adsorbed to the acid sensitive surface Fe-OH or Fe-OH^+ groups. Sommer *et al.* [96] showed that decomposition rates of Fehox decrease with aging of the polymer as oxolation proceeds. This decrease was drastic during the first two days under their chemical conditions but became more uniform after a few days. The effect is highly temperature dependent. Also bearing on polymer "age" are the effects of pH and total iron concentration.

A second, faster component is observed for surface water samples having k_1 averaging about $5x10^{-3}$ s^{-1}. This component appears mostly in fraction B. These rate coefficients are also very close to those near $6x10^{-3}$ s^{-1} observed by Langford *et al.* [94,95] for iron associated with fulvic acid. Tipping and coworkers could not confirm the presence of such iron-organic complexes. Ultrafiltration of their samples showed that a little over half of the humic material present was able to pass through the filter but only about 10% of the iron appeared in the filtrate. Tipping *et al.* assigned the kinetically faster component to freshly formed Fehox which aged little between collection and kinetic analysis.

Iron occurs in Esthwaite Water at about $3x10^{-5}$ M. The pre-concentration techniques required in this study limit a clearer understanding of the chemical processes occurring. The possibility of equilibrium shifts during such manipulation cannot be ignored. Clearly the study of such natural systems would benefit from greater analytical sensitivity.

3.4.2 Lake Tjeukemeer

Recently Sojo and DeHaan have studied iron speciation in Lake Tjeukemeer, The Netherlands [75]. Previous investigation using ultrafiltration had implied that about 10% of fulvic acid is involved in Fe-FA complexes. A sensitive Fe(II) specific chromophore was used in conjunction with hydrazine hydrochloride as reducing agent. Kinetics were run at about pH 4.5 using an acetate buffer. Data analysis involved Guggenheim estimation of input parameters followed by nonlinear regression. Equilibrium pH of some of the standards and samples are shown in Table 3-4.

A key concern in natural system studies is how to obtain validation of a kinetic model by pH and concentration ratio variation. Sojo and DeHaan solve this problem by calibration in advance of study of the lake water. Calibration was accomplished with laboratory models prepared from components extracted from the environment of interest. Aquatic fulvic acid was isolated from the lake and soil fulvic acid from its drainage basin.

The soil FA was found to contain 5.7 meq g^{-1} carboxyl sites. This is slightly less than the 7 meq g^{-1} determined for the Armadale FA. Solutions of Fe(III) or Fe(III)-FA were pH adjusted and equilibrated at 22 °C for 48 hours in the dark. No precipitation occurred. Total iron was determined following acid hydrolysis and corresponded to infinity absorbance of the kinetic curves in all cases.

Analysis of iron in the absence of FA yielded two components. Samples equilibrated at pH 3 showed the majority of iron to be present in the "X" component. It should be pointed out that kinetic measurement was only started 15 seconds after mixing with the chromophore solution. Any component with a rate constant greater than about 0.1 s^{-1} would be expected to appear in the time independent term. With the equilibration

TABLE 3-4
Summary of results obtained by Sojo and DeHaan [75] for speciation of iron in Lake Tjeukemeer, The Netherlands.

Sample	Equilibration pH	"k_1" ($10^{-3}s^{-1}$)	"k_2" ($10^{-4}s^{-1}$)	Relative Distribution "X" (%)	C_1 (%)	C_2 (%)
Lab solutions:						
Fe^{3+}	3.00		3	74.1		25.9
	6.23		2	26.0		74.0
Fe^{3+} - WFA[a]	6.23	3.3	8	3.3	81.1	15.6
Fe^{3+} - SFA[b]	3.00	14	10	79.4	17.9	2.8
	6.02	3.7	7	13.2	66.5	20.2
Lake water:						
- natural	6.4	16	5		62	38
- acidified	3.13		2	44		56

[a]Water derived fulvic acid.
[b]Soil derived fulvic acid (drainage basin sediment).

pH raised to 6.23 most of the iron now appears as time dependent components. It is therefore likely that a large part of the X component corresponds to hexaaqua Fe(III) for which Langford *et al.* [94] measured a dissociation rate coefficient of 0.89 s^{-1}. The measurable rate constants in these solutions are about half those determined by Langford [94], Sommer [96], Tipping [103], and their coworkers. Sojo and DeHaan attribute this deviation to possible differences in experimental conditions such as pH and temperature. The slower component corresponding to 450 nm filterable iron particles observed by Langford *et al.* was not seen in this case. Filtration of the colloids showed that little of the material was larger than 200 nm.

In the presence of either soil or water derived fulvic acid a third species becomes apparent. The dissociation rate constant of this component (k_1) is intermediate between fast monomeric Fe(III) and its hydrous oxide. This component is most reasonably assigned to simple iron-fulvate complexes. The rate coefficient of this complex is somewhat unstable with equilibration pH as was seen in the case of Fe(III) associated with soil fulvic acid. Rate constants for component 2 (Fehox) in these systems are much more in line with those observed by other authors previously discussed.

Averaged results for kinetic analysis of lake water are also shown in Table 3-4. In its natural state, the iron speciation may be modeled by two kinetic components. No "time independent" Fe(III) is detected. Analysis of lake water which had been ultrafiltered showed the presence of an "X" component. This indicates a change during the filtration. Measured rate constants of component 1 are somewhat larger than those determined for the model solutions. This could be a result of differences in composition between lake water and laboratory models. Natural samples had about a ten times larger

ratio of dissolved organic carbon to iron. Also lake samples ultimately contain other metals which could compete for strong binding sites on the FA thereby increasing the average lability of Fe(III). Acidification of lake water resulted in the disappearance of the terms associated with Fe-FA complexes and the appearance of a large amount of labile species.

It may be concluded that iron in Lake Tjeukemeer is largely distributed between two kinetically distinct species. The magnitude of their dissociation rate constants and the manner in which their component contributions vary with equilibrium chemical conditions indicates that they are most likely Fehox and Fe(III) associated with humic matter. Rate constants for the former are reasonably well behaved with varying equilibrium conditions. The variation of rate coefficients for iron fulvate dissociation indicates an adsorbate with a more complex species distribution.

Chapter 4

EXPERIMENTAL

A great deal of the work involved in this study may be classified under the heading of "trouble-shooting". Some of the problems encountered are of a general nature and warrant discussion. Most of these will be considered in the experimental section. This has been done to prevent the topics of greater chemical significance, discussed in chapter 5, from being clouded by experimental detail.

Most of the research to be discussed has been performed using one of two types of instrumentation. As will be seen in the next chapter, the majority of results were collected by conventional spectrophotometry (CS). This method is widely understood and experimental details of its use will receive limited attention. Laser thermal lensing spectrophotometry is a less conventional technique. Although only a moderate portion of the results were obtained using TLS, the nature of this method requires a more detailed presentation both experimentally and in the interpretation and discussion of results.

The thermal lensing apparatus will be discussed prior to describing other experimental procedures. This will allow the reader greater insight into some of the more subtle characteristics of TLS which will arise in the kinetic analysis section of this chapter.

4.1 THERMAL LENSING

4.1.1 Instrumentation

A schematic of the thermal lensing apparatus employed is shown in figure 4-1. Sample excitation (pumping) is by means of an argon ion laser (Ar^+). Several lasers have been used at different times in the course of this research. The majority of data was collected using a Spectra-Physics model 165 chassis with a model 265 exciter. The chassis was fitted with a Coherent Innova ionpure metal-ceramic tube (model 160-196-00). The combination of the Spectra-Physics chassis and the Coherent tube (SPICE upgrade kit) provides a beam which is stable in both pointing and output power. As shown in the figure the output of the Ar^+ may be used to excite a dye laser (Coherent model CR-590) allowing a wider range of pumping wavelengths. For all experiments reported here one of the Ar^+ lines was used directly. Two mirrors (not shown in the figure) are used to raise the pump beam. The upper mirror is fixed on an adjustable mount (Newport) having X and Y 200 turn-per-inch thumb screws facilitating alignment to the optical axis. On/off cycling of the pump beam is effected by the use of a shutter (Ledex) connected to a transducer allowing automated control. The pump beam is then focused by a lens (L) to the position of sample cell after passing through an optical flat (OF). After exciting the sample the pump beam is removed by a colour filter (CF; Oriel 630 nm cut-off). The sensitivity of the thermal lens signal to position of the pump beam lens is clearly seen in figure 4-2.

The 632.8 nm line of a He-Ne laser (Siemens LGK 7623) is used as a probe beam. After being elevated to the correct height by a pair of mirrors (not shown) it is reflected off a third mirror fixed on the same type of adjustable mount as previously described.

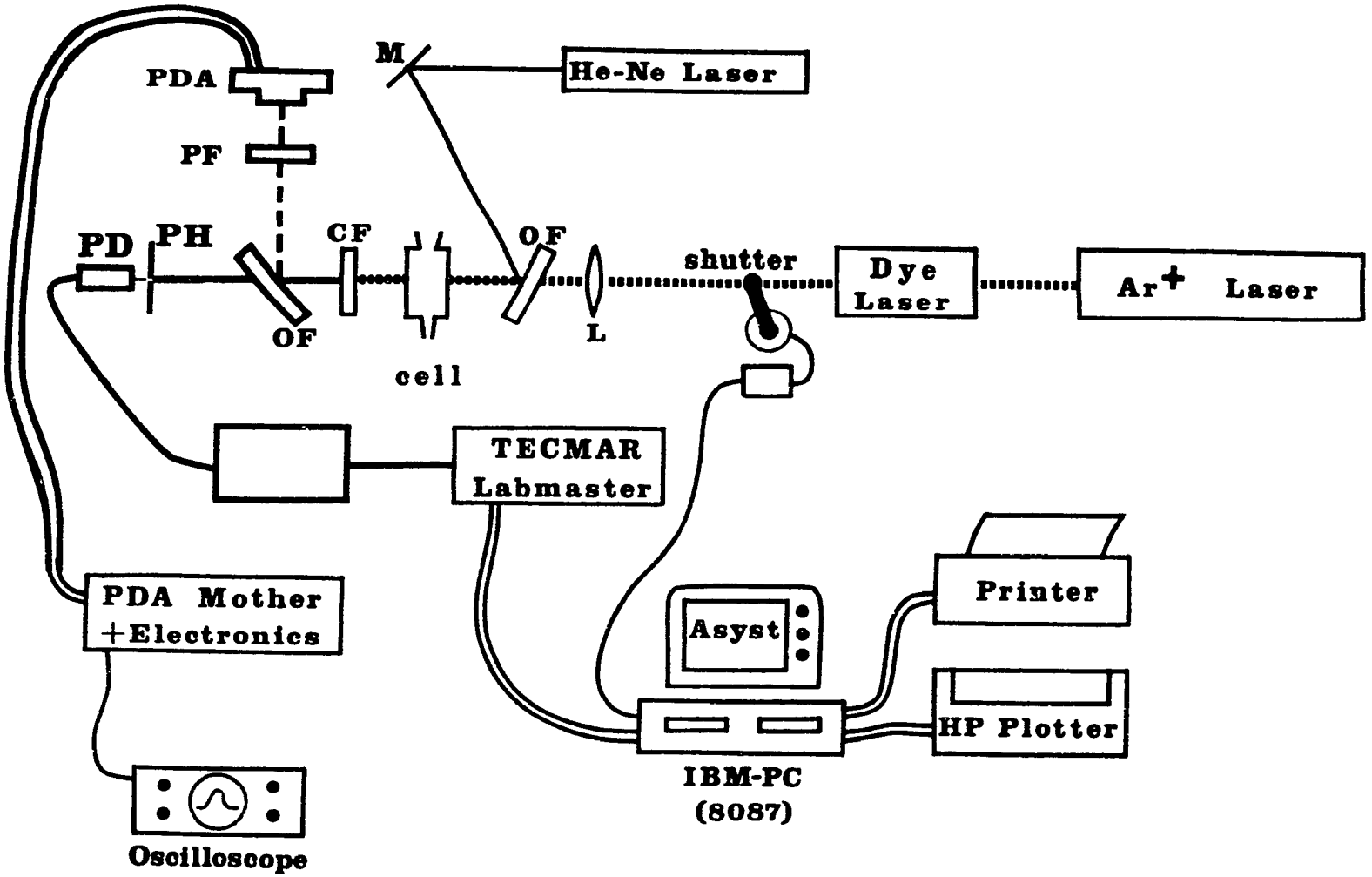

Figure 4-1: Diagram of the dual-beam mode mismatched laser thermal lensing apparatus used in this work.

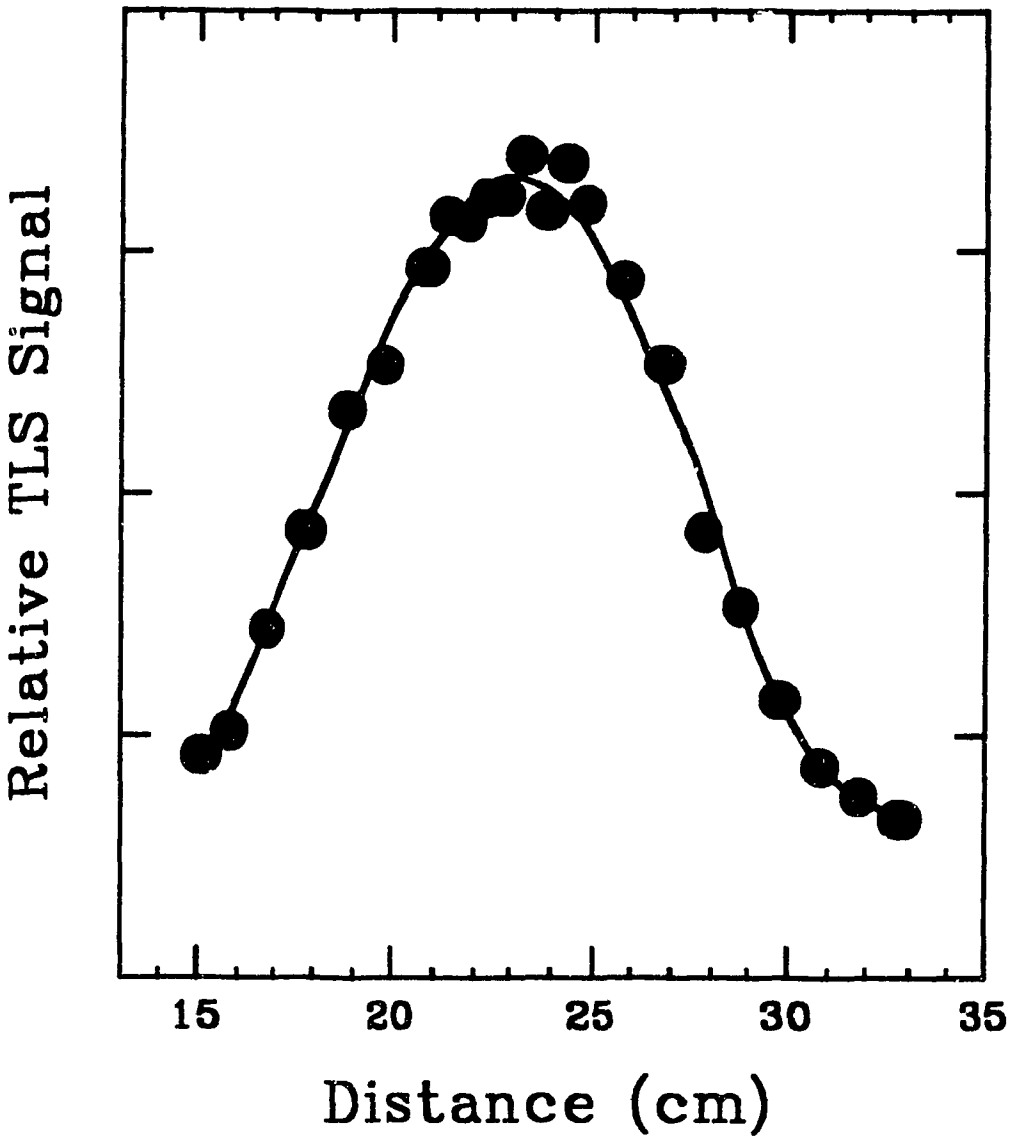

Figure 4-2: Variation of thermal lensing signal with distance from the pump beam lens to the centre of the sample cell. The signal was maximized after each movement of the lens along the optical axis. The maximum sensitivity occurs at c. 23.5 cm at which point the principal focus of the lens is at the cell centre.

The probe beam is "mixed" with the pump beam by reflection off the front face of the optical flat. It then passes through the sample and the colour filter to the detector system. Several sample cell types were evaluated. Problems associated with their configurations are discussed further on in the chapter. For all of the data reported here a cylindrical cell of 10.0 mm path length and 18 mm diameter was used (hereafter known as the "fill-drain" cell). The cell was glued to an optical mount to avoid problems of cell positioning such as changes in beam intensity profiles resulting from small imperfections in the glass. At the top of the cell is a female standard taper connection. A clamped piece of tubing connected to a nipple at the bottom of the cell allows drainage.

Earlier work was done using a self scanning linear photo-diode array (PDA) detector (Reticon RL256G with an RC301 current amplifier). Operation of this detector is thoroughly described in reference [46]. Use of a PDA allows imaging of a cross section of the probe beam intensity. This configuration offers some advantages such as beam profile analysis and correction for pointing instability in one dimension. However it also leads to the collection of a large amount of data (256 array elements for each scan). Data analysis of mode mismatched TLS by profile fitting [46] is overly complex for routine analysis. Due to the number of points corresponding to each sampling, fewer repetitions may be collected within a reasonable period (c. 100 ms per array scan). This precludes efficient noise reduction by signal averaging. Thus when technical difficulties with the PDA created problems in data acquisition, its use as a detector was discontinued. The PDA continues to be a component of the optical set-up as it is very useful as an alignment aid and in the monitoring of the probe beam profile "purity". A second optical flat is used to direct a portion of the beam to the PDA. A rotatable polarizing filter is

used for attenuation of the probe beam which is vertically polarized. The PDA signal may be monitored in real time using an oscilloscope (Tektronix). Figure 4-3 shows the thermal lens effect as observed with the PDA.

The present detector is comprised of a pinhole/photodiode (PH/PD) combination. The pinhole has a diameter of 100 μm allowing only the centre of the beam to pass. The photodiode (Silonex NSL-810) has an active surface area of 0.036 cm^2. The short circuit current of this photovoltaic cell is extremely linear over a wide range of irradiance. The cell was placed at the end of a bore in a cylindrical piece of plastic (3.8 cm long by 2.5 cm diameter). This both reduced sensitivity to stray radiation and facilitated mounting of the detector. Only about 1 μW of light passes the pinhole and impinges on the photodiode. The circuit diagram of the PD amplifier appears in appendix A (figure A-1).

The detector and shutter were interfaced to an IBM-PC using an A/D D/A (Tecmar Labmaster; Scientific Solutions). This device consists of a mother board in an expansion slot of the computer and an external daughter board. The amplified detector signal is read by an A/D convertor of the daughter board. The probe beam shutter is driven by a D/A channel on the mother board. A description of the hardware settings of the Labmaster are contained in appendix A (table A-1).

While analyzing sources of spatial noise it was observed that air currents directed toward the He/Ne laser resulted in extremely high noise levels at the detector. This is most probably due to vibration of the laser tube caused by air passing through the cooling vents of the case. This problem was rectified by placing a transparent polystyrene case over the laser. A hole was made in one end to allow the beam to exit undistorted. To prevent heat build up in the enclosed space, a water cooled copper tube was clamped over

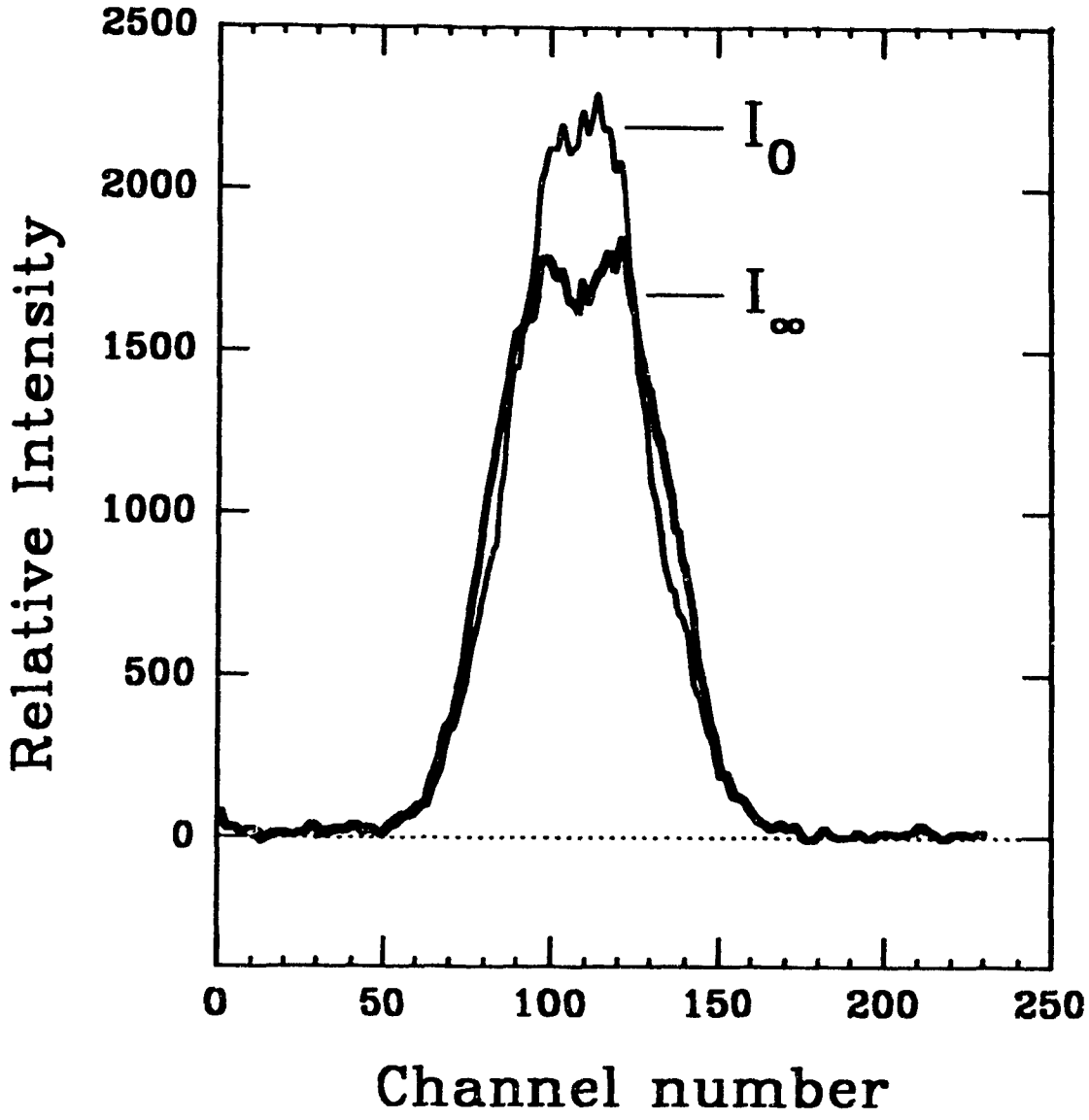

Figure 4-3: Typical probe beam intensity profiles observed under mode mismatched conditions. Profiles were measured with a 256 channel linear photodiode array. Diodes have a centre-to-centre spacing of 25 μm. A highly absorbing sample was used to enhance the effect. Note the lower, broader profile upon excitation with the pump beam (thick line) and the development of a "well" near beam centre.

the chassis.

A second case was placed over the components on the optical axis (starting from the pump lens). This prevents the accumulation of dust on components and possibly reduces spatial noise caused by dust particles in the beam path. A section of the case around the PH/PD was closed off and lined with aluminum foil which had been painted black. The foil was grounded, effectively creating a Faraday cage. This enclosed area also ensures a low stray background light level at the detector.

Of crucial importance to good optical alignment of the thermal lensing apparatus is the optical flat. It is a simple flat piece of glass. As shown in figure 4-4 several processes occur at the OF. It permits coaxial alignment of the pump and probe beams. It is also a simple attenuator of the probe beam intensity. Only about 5% of the beam is reflected off the face and toward the sample. The angle of contact of the probe beam with the face (22.5°) was kept fairly small to minimize perturbation of its Gaussian intensity profile. As shown in the figure there is also reflection off the back interface (glass to air). The OF used was 9.00 mm thick. Due to its thickness the front and rear reflections are well spaced (4.32 mm) allowing the rear reflection to be removed. A thinner piece of glass could result in overlap of the two reflections leading to an interference pattern.

About 90% of the pump beam is transmitted through the OF the rest being lost by reflection. Of importance to notice in aligning the beams in this manner is that the pump beam does not pass along the optical axis until encountering the OF. The necessary displacement of the pump from the optical axis was calculated to be 1.30 mm for the

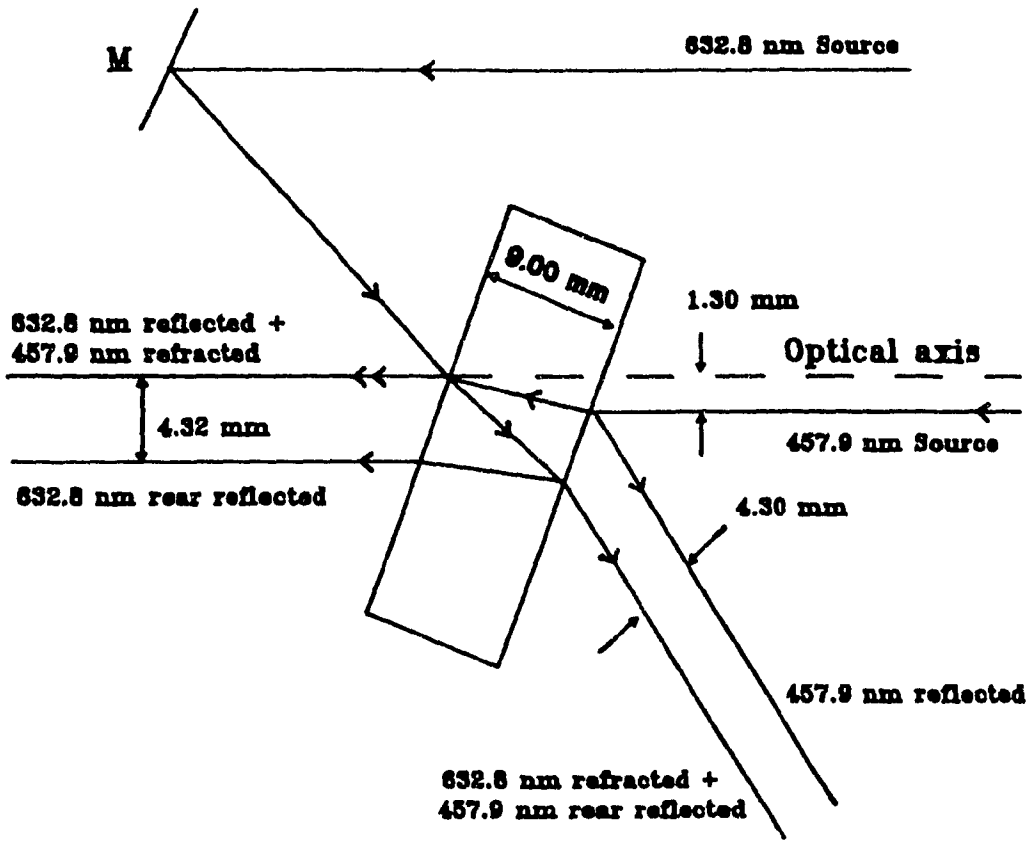

Figure 4-4: Diagram of the "optical flat" used for coaxial alignment of the pump and probe beams in the thermal lensing apparatus. The flat also attenuates the probe beam as only about 5% is reflected. The face and rear reflections of the He/Ne beam are well spaced simplifying their separation. Note that the pump beam travels about 1.3 mm off the optical axis until encountering the optical flat.

457.9 nm Ar^+ line. This assumes the refractive index of the OF medium (borosilicate crown glass) to be 1.52 [104].

4.1.2 Operation of TLS acquisition software

4.1.2.1 *Timing of data acquisition*

Data acquisition and control of the thermal lensing apparatus was performed using programs written in the Asyst language (ASYST: A Scientific System V 1.02; Asyst Software Technologies). The program source code and an explanation of its operation may be found in appendix B.

Figure 4-5 diagramatically shows the steps performed during data acquisition using this program. There are a number of user adjustable parameters. Some of these are indicated in the figure by capital lettering. The number of photodiode readings averaged during each acquisition is defined by the parameter SCANS/ACQ (scans per acquisition; not indicated in figure 4-5). The program currently allows a maximum of 1000 scans for any acquisition of background, I_0 or I_∞.

The READY DELAY allows the user to delay continuation of the program for a fixed period of time. During this time reagents may be readied for mixing. A bell is sounded to provide a warning that 5 seconds remain to "kinetic time zero". A second bell sounds at time zero at which point the reagents are mixed. Timing within the program is relative to this time zero.

The MIXING DELAY serves three purposes. 1) It provides the user with time to perform the mechanical operations of mixing and placing the solution in the sample cell. 2) The sensitivity of TLS to turbulence in the sample necessitates allowance of a

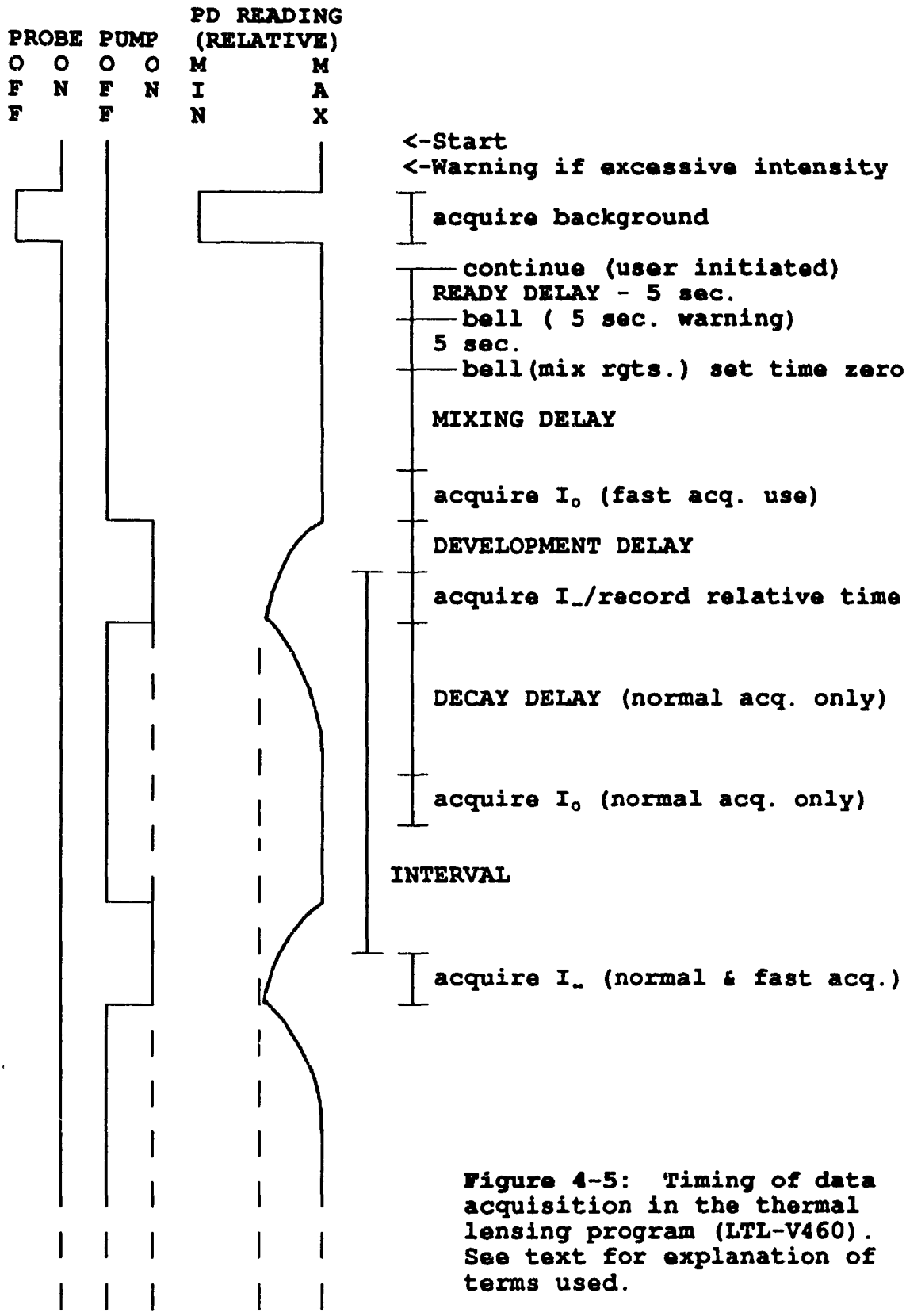

Figure 4-5: Timing of data acquisition in the thermal lensing program (LTL-V460). See text for explanation of terms used.

period of time for the solution to become tranquil. This may take several minutes. It appears that pulsing the sample with the pump beam (such as during data acquisition) during this calming stage serves to stimulate further turbulence. Samples have been observed to remain turbulent for more that 30 minutes when continuously pulsed. 3) When analyzing non-kinetic samples (such as standards) it is optimal to use a long mixing delay to allow the turbulence to completely subside prior to acquiring data. The MIXING DELAY allows this to be automated.

Thermal lens formation is a fairly slow process. Depending on the solvent parameters and optical configuration it may require as long as 2-3 seconds. The DEVELOPMENT DELAY allows a period of time to pass between initiation of lens formation and the start of I_∞ data acquisition. Similarly the DECAY DELAY allows the lens to dissipate prior to I_0 acquisition.

The INTERVAL is defined as the period from the start of one I_∞ acquisition to the start of the next one. Intervals in the program are defined in "windows". Each of up to 5 windows may have different intervals. This allows shorter intervals to be used during the initial part of a kinetic run where the signal is changing most rapidly and longer intervals as the reaction slows. Each window is defined by the user by entering a start time, stop time and number of points to be acquired in that window.

Related to acquiring data more rapidly is a parameter called MINIMUM TIME. When a window is defined to have an interval below a certain threshold (approximately defined by MINIMUM TIME) the window operates in the "fast acquisition" mode. In this mode the shutter initially opens to allow lens formation then remains open. The effect of this is shown by the dotted lines in figure 4-5. No DEVELOPMENT DELAY

is necessary for subsequent I_∞ acquisitions. This allows data to be collected at much shorter intervals. A consequence is that corresponding I_0 values may not be collected. To rectify this, I_0 is acquired before initial lens development. This I_0 value is then paired with all I_∞ values collected while in "fast acquisition" mode. This makes the signal very susceptible to low frequency variation in beam power, however. When a subsequent window has an INTERVAL longer than the threshold, the mode is reset to "normal" and the pump beam shutter becomes operational.

4.1.2.2 *Optimization of program parameters*

As may be surmised from the previous description, there is some interaction of the timing parameters. This is particularly important with respect to lens development. It would appear desirable to employ a long DEVELOPMENT DELAY to monitor the steady state thermal lens and maximize the TLS signal. However, thermally induced turbulence in the cell results in significant noise levels for total development times longer than about 1 second. The total development time is a combination of the user defined DEVELOPMENT DELAY and the time required to acquire data. Therefore it is also dependent on the SCANS/ACQ parameter. Each scan requires 591 μs. While noise may be reduced by increasing SCANS/ACQ ($N^{-1/2}$ white noise reduction) doing so also increases the total development time. This interrelationship was studied by evaluating signal-to-noise ratios using SCANS/ACQ ranging from 10 to 1000 at each of 8 DEVELOPMENT DELAY's. The results appear in figure 4-6.

At each of the DEVELOPMENT DELAYs, signal-to-noise ratios are generally seen to improve with the number of SCANS/ACQ. (In a separate experiment using a

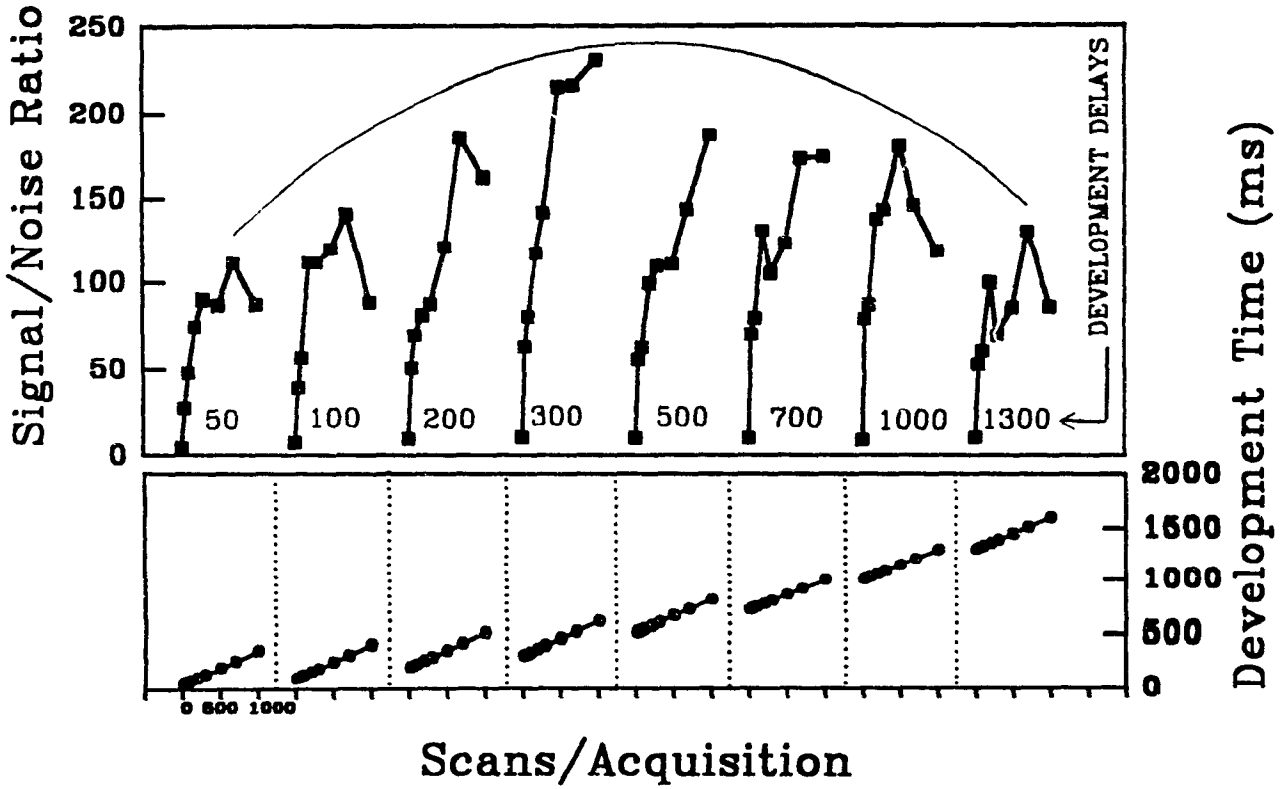

Figure 4-6: Sensitivity of signal-to-noise ratio to DEVELOPMENT DELAY and number of readings averaged (SCANS/ACQ). The lower part of the plot shows the actual development time calculated as DEVELOPMENT DELAY + 1/2 of the acquisition period [Development time = DEVELOPMENT DELAY + (0.591/2 X SCANS/ACQ). Tick marks on the x-axis correspond to 0, 500 and 1000 SCANS/ACQ at each of the 8 DEVELOPMENT DELAY's. Values of SCANS/ACQ used were 10, 50, 100, 200, 300, 500, 700 and 1000. It is clear that signal averaging of scans is the major factor in improving signal-to-noise ratios. Each point is the average of 50 acquisitions.

very short development delay, signal-to-noise ratio was observed to adhere to $N^{1/2}$ noise reduction for 1 to 1000 SCANS/ACQ.) The best signal-to-noise ratios are obtained using a DEVELOPMENT DELAY of 300 to 500 ms. Longer delays lead to poorer ratios as acquisition occurs after the onset of thermally induced turbulence in the sample. This is exemplified in figure 4-7 which clearly shows that a minimum in noise level near 400 ms DEVELOPMENT DELAY is largely responsible for the maximum in signal-to-noise ratio. Noise then increases at longer DEVELOPMENT DELAYs. In this figure all data was collected at 1000 SCANS/ACQ. It is unlikely that noise levels would improve by averaging a larger number of scans.

Concentrated samples were used in obtaining the data shown in figures 4-6 and 4-7 as is apparent from the very large values of $\Delta I/I_\infty$. This was largely done to make the effect more obvious. To ensure that these optimal conditions were independent of concentration, the data for SCANS/ACQ = 1000 were repeated for a more dilut ` sample where $\Delta I/I_\infty$ did not exceed 0.22. The results were the same with two minor differences. First, the noise level remained at a constant value up to 500 ms DEVELOPMENT DELAY above which it increased. Second, the maximum signal-to-noise ratio was observed for a DEVELOPMENT DELAY of 400-600 ms. It may be expected therefore that these optimal parameters will also hold for typical analysis conditions where $\Delta I/I_\infty \leq 0.15$.

Although data acquisition from the photodiode only requires 591 μs per scan, the pump beam shutter remains open for a period calculated as 911 μs x SCANS/ACQ. This is due to software overhead resulting from background subtraction which necessarily had to be performed immediately following acquisition. (For clarity this factor was not

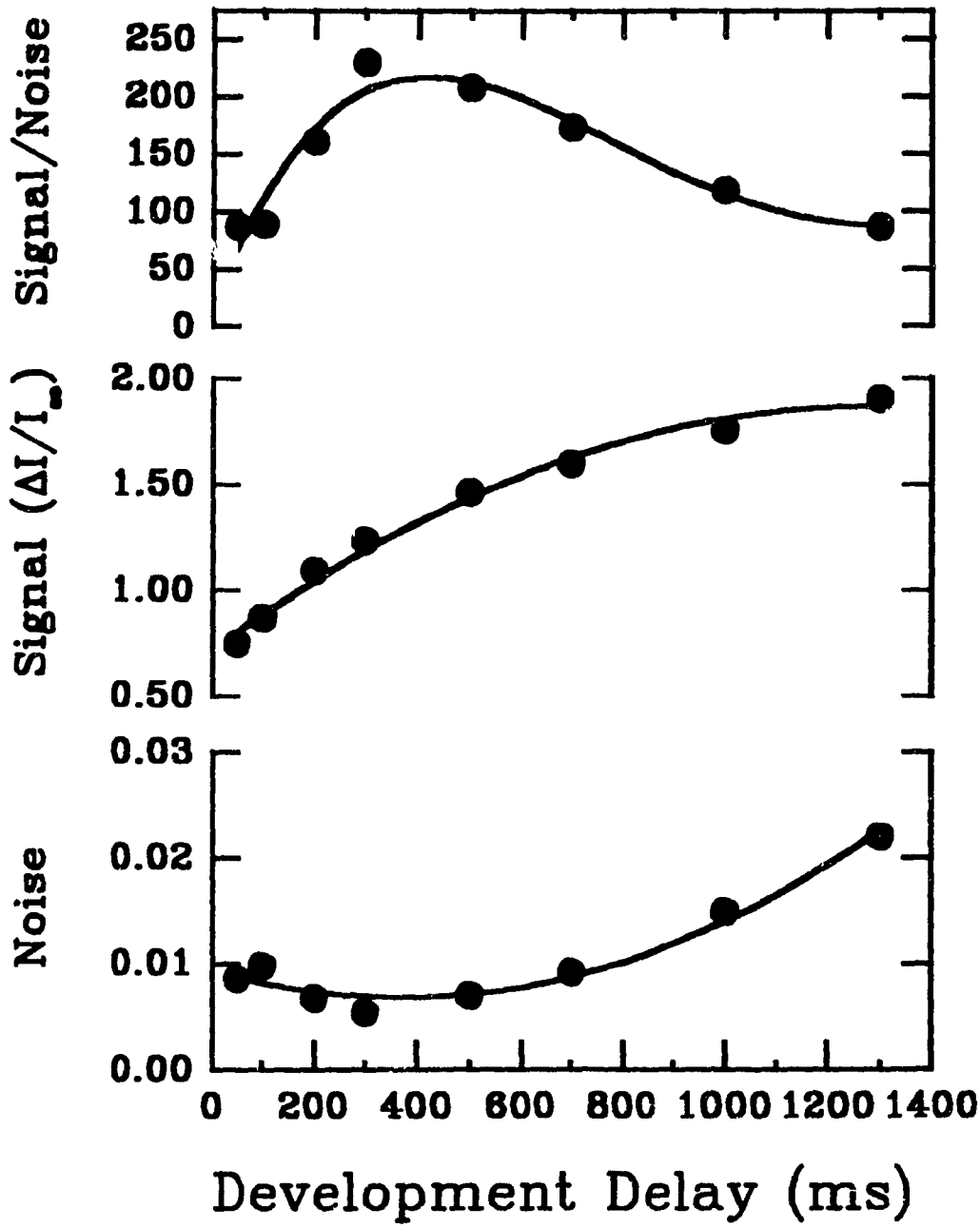

Figure 4-7: Effect of DEVELOPMENT DELAY on signal-to-noise ratio. Data is the same as that in figure 4-6 where SCANS/ACQ = 1000. The noise level is minimal in the region of 300-500 ms DEVELOPMENT DELAY. Including the full acquisition time this region corresponds to sample development for 900-1100 ms. With longer development thermally induced turbulence leads to higher noise.

represented in figure 4-5.) The result is a greater extent of thermal lens development. To ensure complete dissipation of the thermal lens a longer DECAY DELAY is needed. Using the optimal values of SCANS/ACQ and DEVELOPMENT DELAY defined above, a DECAY DELAY of 2000 ms was found to be sufficient to completely restore the I_0 intensity. Longer times could be used with a resultant increase in sensitivity to low frequency fluctuations in beam power.

Unfortunately it has been observed that the interrelationship of the parameters dictates that sensitivity of the instrument be calibrated under each of the sets of conditions used. If multiple windows are defined, a calibration curve must be prepared corresponding to each of them. Thus although the software allows multiple windows, routine use of TLS is best done using one set of conditions.

4.1.3 "Peculiarities" of TLS

4.1.3.1 *Negative values of $\Delta I/I_\infty$*

It has been previously mentioned that the thermal lens effect may occur in gases, liquids or solids. The vast majority of TLS studies (including this work) have been concerned with liquid phase samples. This "preoccupation" tends to cause one to ignore the other possibilities. The realization that thermal lensing does occur in other phases was vividly impressed upon the author.

It was observed on several occasions that I_∞ values were slightly larger than I_0 values when analyzing blanks or very dilute solutions. This phenomenon was attributed to scattered radiation entering the detector area once the pump beam was unblocked. A variety of steps were taken to minimize this scattering. One of these included placing the

colour filter immediately following the cell in the hope of increasing the effective angle of light interception. The result was quite the opposite of that expected...large negative values of $\Delta I/I_{-}$. The cause of this effect became clear as it was observed that $\Delta I/I_{-}$ became less negative as the filter was moved away from the cell. Thermal lensing was occurring in the filter medium. Although the filter was displaced somewhat from the pump beam focus (optimal thermal lensing sample position) its utility as an optical component is its effectiveness at absorbing light of the pump beam wavelength. It is apparent that dn/dT of this medium is positive as thermal focusing is observed. Although this phenomenon could not be eliminated without loss of instrument sensitivity, it was minimized by placing the colour filter as far from the sample cell as possible. Assuming that the filter remains stationary and that only a small fraction of the pump beam power is absorbed by the (liquid) sample, this effect results in a constant offset of $\Delta I/I_{-}$. This is demonstrated in figure 4-8 which shows a calibration curve for bromine. Although negative values of $\Delta I/I_{-}$ are observed at low concentrations, linearity is maintained.

In the name of probity it must be clarified at this point that the detrimental effects of thermal lensing were noted even before advantage was taken of this phenomenon as an analytical tool. Indeed, thermal lensing was first observed as an obstacle to focusing in Raman spectrometers either through its occurrence in samples or in absorbing optical elements such as filters.

4.1.3.2 *"Spikes" in I_{-} intensities*

With some regularity large "spikes" in $\Delta I/I_{-}$ occur. Increases in $\Delta I/I_{-}$ of greater than 0.2 have been observed for individual acquisitions. Closer examination reveals that

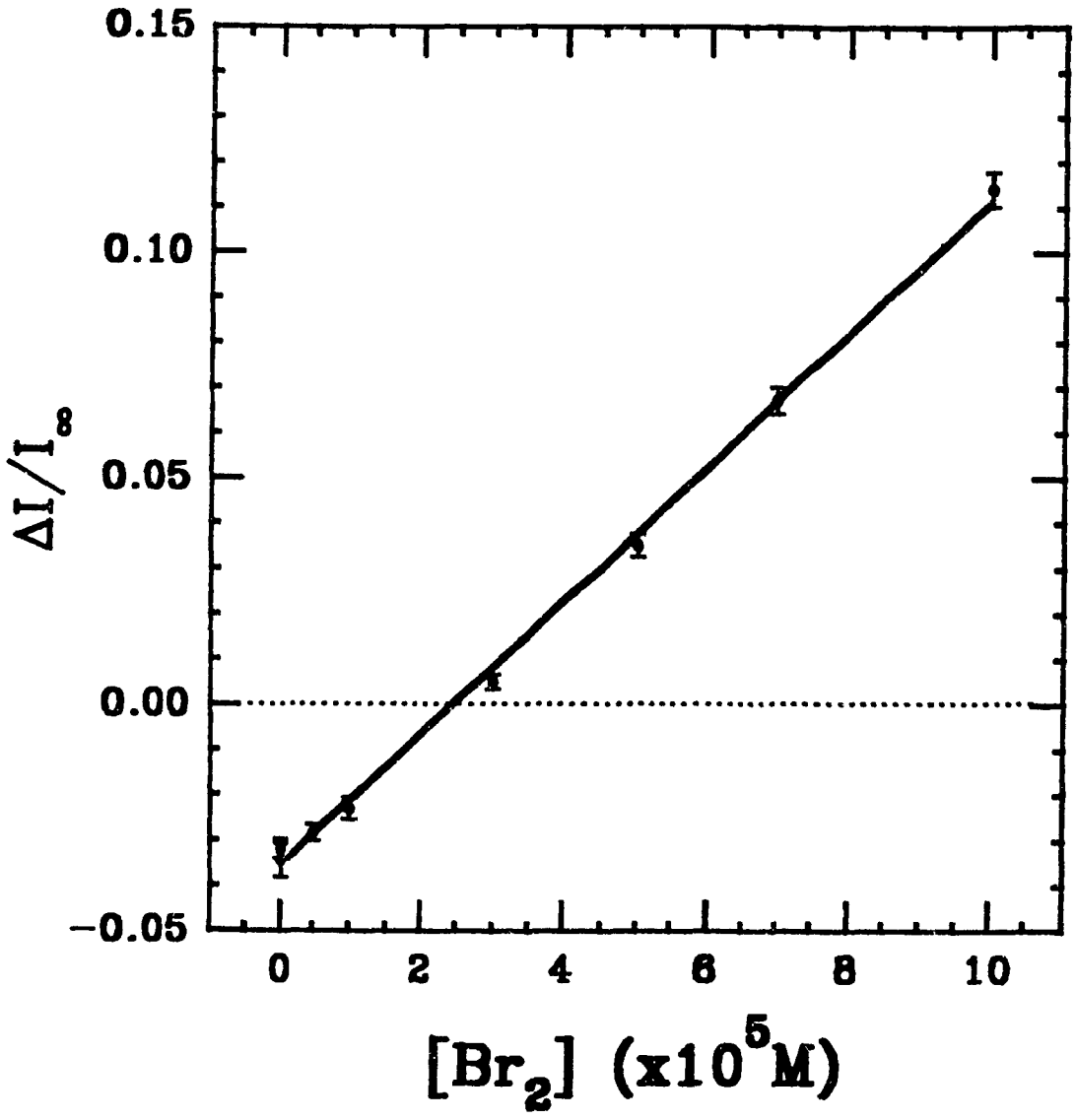

Figure 4-8: Thermal lensing standard curve for bromine in a matrix of 0.2 N H_2SO_4. Note the negative intercept. This is a result of thermal lensing which occurs in the colour filter used for removal of the pump beam. dn/dT of the filter medium is positive resulting in thermal focusing.

these are due uniquely to very low values of individual I_- acquisitions. The occurrence of these spikes is random and independent of concentration or analyte species. An example is shown in figure 4-9.

As yet the origin of this phenomenon is uncertain. It may be associated with bursts of scattered radiation which have been observed on a few occasions. These episodes begin shortly after the start of irradiation by the pump beam. The scattered light intensity climbs to a maximum and begins to subside after a period of approximately one second. The randomness of this occurrence has made it difficult to unambiguously relate the two events. It is proposed that pump beam irradiation causes thermally induced formation of air bubbles in the sample. Such bubbles travelling through the optical axis would result in both a varying scatter of laser light and a reduction in the intensity of the probe beam at the detector. The magnitude of these spikes in detector signal necessitates that they be removed by numerical procedures prior to further data analysis.

4.1.3.3 *Aperiodic signal oscillation*

On numerous occasions I_0 and I_- signals monitored over a period of time have been observed to oscillate. When the two are in phase $\Delta I/I_-$ is unaffected. On occasion I_- is found to oscillate more slowly than I_0. As shown in figure 4-10 this leads to oscillation in the analytical signal, $\Delta I/I_-$. This phase shift is not always so pronounced. Subtle effects such as that shown in figure 4-11 can result if the shift is very minor. Here the value of $\Delta I/I_-$ is seen to slowly decrease at times below c. 1800 seconds. Only at longer times does $\Delta I/I_-$ begin to reflect the steady state character of the sample. Use of this data would necessitate ignoring values at times shorter that 1800 seconds.

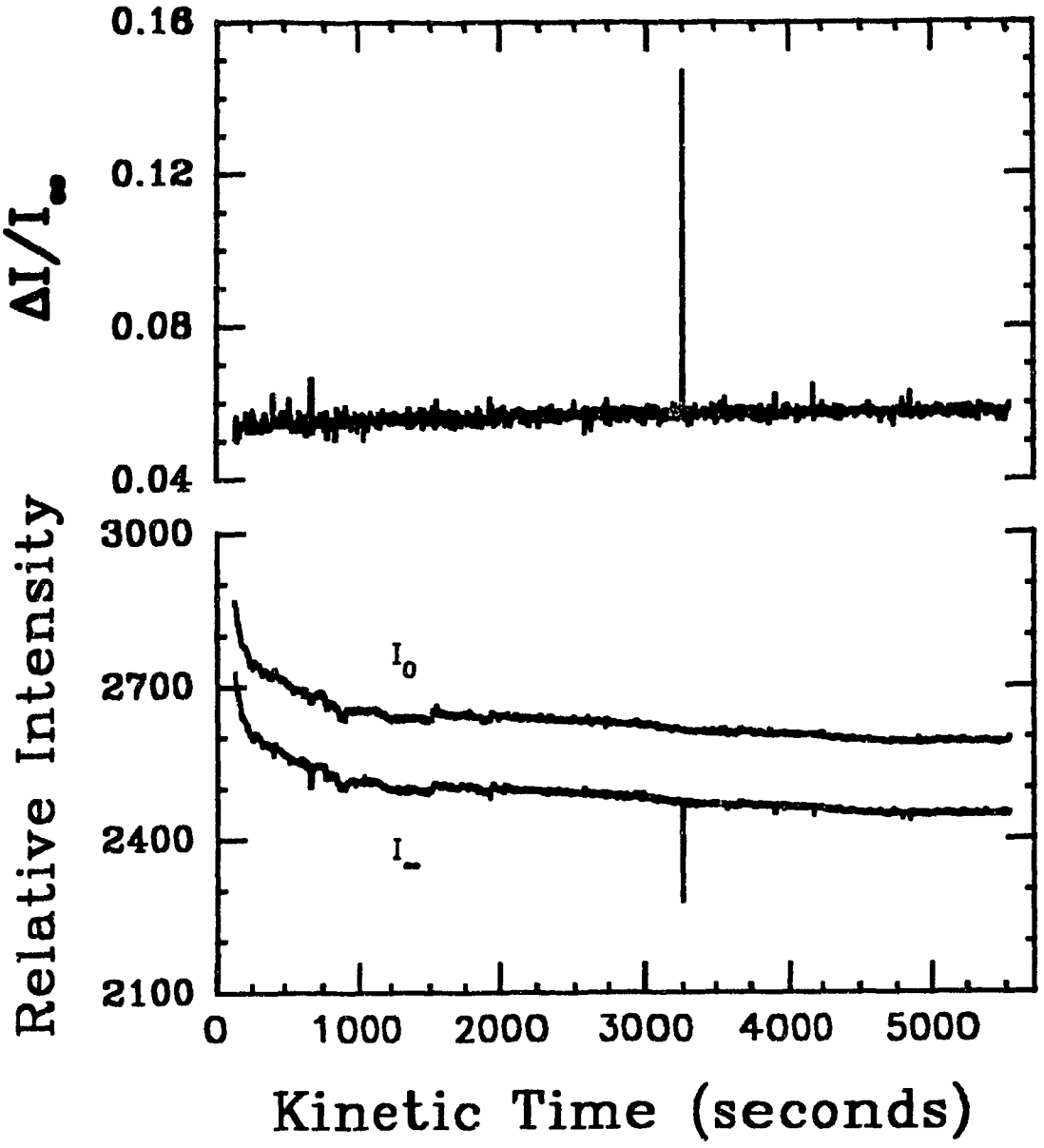

Figure 4-9: Kinetics of the acid hydrolysis of c. 6×10^{-5} M cis-$[Co(en)_2Cl_2]^+$ monitored by thermal lensing. Note the spike which occurs near 3200 seconds. As shown in the lower curves, this is the result of a low I_- value possibly resulting from a bubble passing through the optical path.

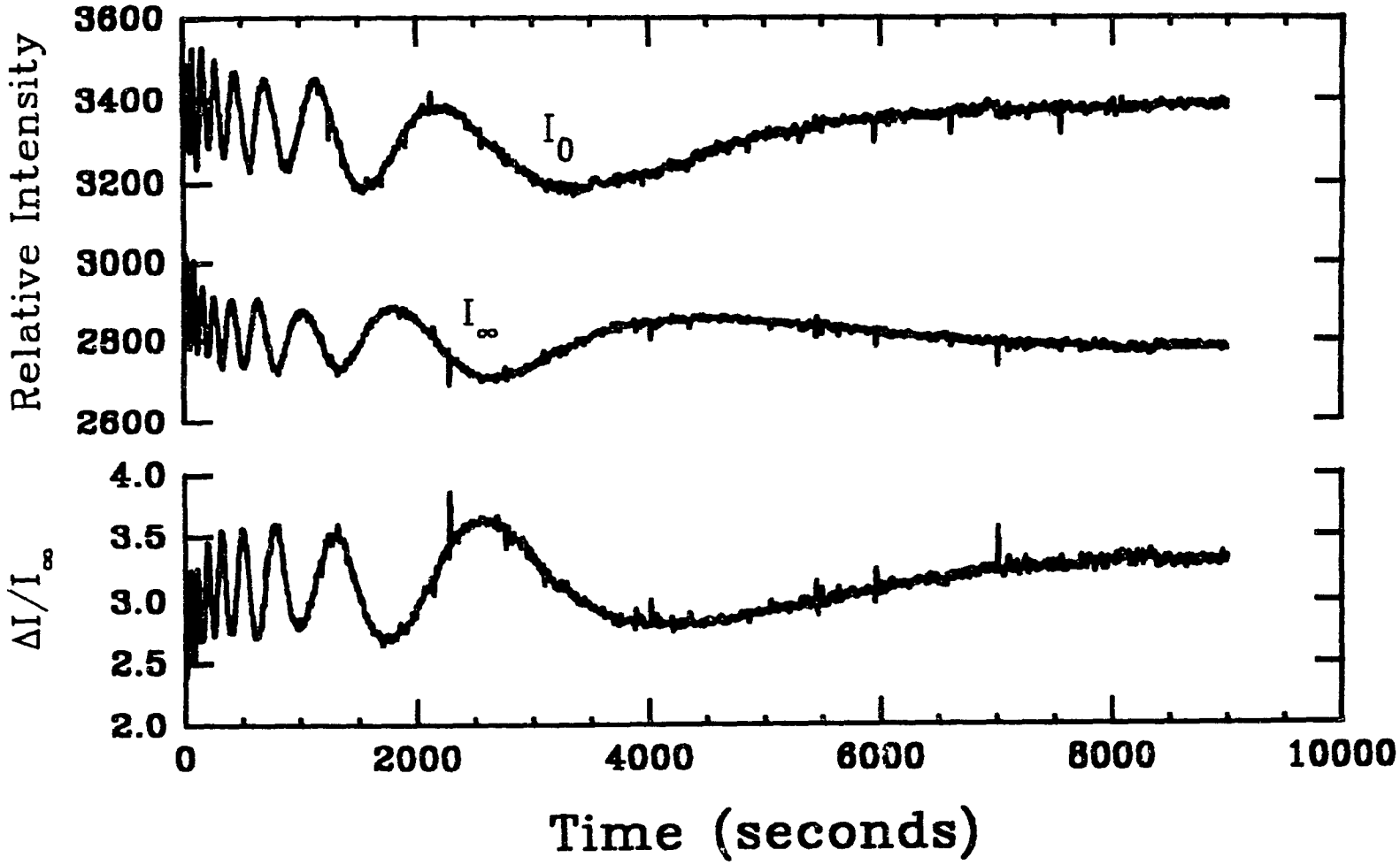

Figure 4-10: Out of phase oscillation of I_0 and I_∞ impedes analysis of the kinetics of reaction of the chromophore PHTTT with Cu(II) equilibrated with a humic acid. I_∞ intensities have been raised by 2000 units for graphing purposes. Analysis conditions were: DEVELOPMENT DELAY = 1000 ms; DECAY DELAY = 3000 ms; INTERVAL = 9000 ms; SCANS/ACQ = 900; P_0 = 68 mW at 457.9 nm.

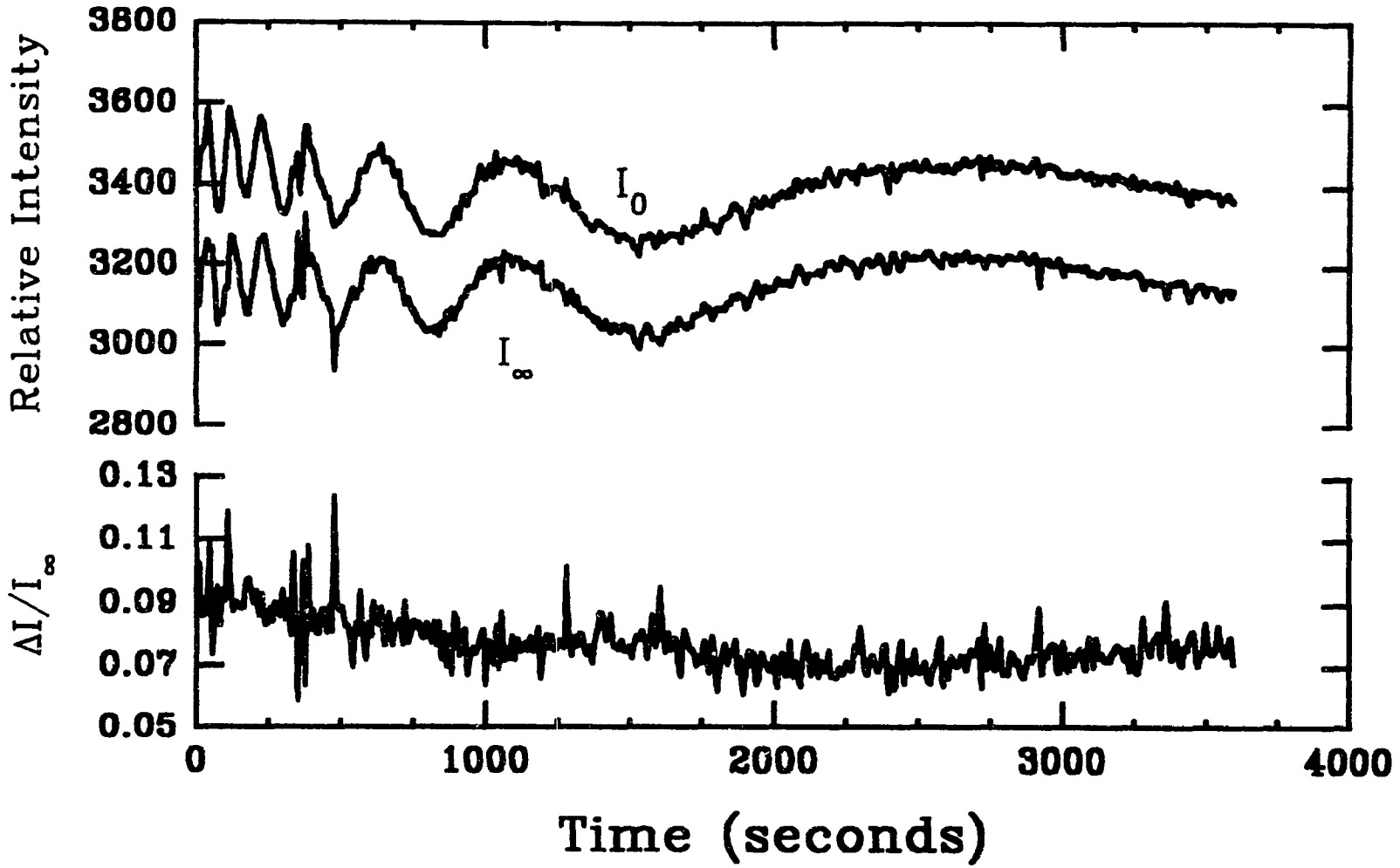

Figure 4-11: Slight out of phase oscillation of I_0 and I_∞ intensities causes a slow drift in $\Delta I/I_\infty$ at short times. The steady state sample analyzed is a humic acid with no copper present (blank). Analysis conditions are as indicated in figure 4-10.

Oscillation, whether in or out of phase, has been observed over a wide range of concentrations (including pure water) and both in the presence and absence of light scattering particles such as humic acid. The dependence of the effect on these parameters has not been quantified.

The time scale of these oscillations indicates a convection related phenomenon. In several instances thermally induced oscillations in liquid samples have been discussed in the literature. Anthore *et al.* [105] focused a continuous wave laser into a sample then took advantage of its divergence to observe a pattern as the beam was projected onto a screen. A shape consisting of concentric rings initially formed and endured for about 1 second. The pattern then changed to a steady collection of concentric "$\cup$" shapes in the form of a side-up half moon. This shape has been associated with free convection [106] and is observed to rotate as the beam approaches a cell wall. The exact shape was a function of beam power, path length and concentration of absorbing or particulate species. If the beam was aimed just below the solution surface the shape oscillated between the concentric ring pattern and the half moon with a period of the order 1 second. An increase in beam power resulted in a more complex double-beat oscillation. In all cases the development of a pulsing pattern was sensitive to beam power and particle concentration. Anthore *et al.* [105] suggest that the presence of particles may be necessary for oscillation to occur.

Convective effects occurring on a longer time scale were observed by Buffett and Morris [107]. Using a standard 1.00 cm square cuvette they noted a periodic component in their signal. This component varied in magnitude and "regularity" with minor changes in sample volume and cell position. Upon initial excitation the TLS signal

started at its maximum value. Oscillation began after several minutes. Periodicity was preserved over the tested pump beam chopping frequency range of 10 to 150 Hz. When the beams were focused near the centre of the cell, oscillation was approximately sinusoidal with a period of about 22 minutes. The waveform changed to a sawtooth when the beams passed in close proximity to the cell wall. Amplitudes of 10% of the total signal were common. Using a dye they observed convective flow in a cylindrical cell to originate at the optical axis, rise vertically then split and move back down the walls. The observations were made using a solution of iodine in CCl_4. As pointed out by the authors, the different thermooptical properties of water should lead to more localized convection with oscillation frequencies about 2 orders of magnitude higher than in CCl_4.

Low frequency noise was also observed by Alfonso *et al.* [108] in analyzing 0.22 μm filtered acidified solutions of methyl red in 50% water/ethanol matrix. Oscillations were approximately sinusoidal with periods of 1-5 minutes. Measurements were made in a standard 1.00 cm square cuvette. The convective pattern was found to take the form of a whirling "∪" shape in the region above the beam axis and a "∩" shape in the region below the axis. Regions to either side of the beam remained calm. Amplitude of the noise was extremely sensitive to alignment. For measurements made over several weeks neither the frequency nor amplitude were reproducible. Oddly, the convective patterns were found to cause lateral displacement of the thermal lens of more than 2 mm. This was particularly prominent when the beams were passed near a wall of the cell in which case the lens moved away from the interface. Vertical lens movement was noted when the optical axis approached the bottom of the cell or the solution surface.

All of these previously noted oscillations were periodic. Those observed here are

clearly aperiodic. The damping of both amplitude and frequency indicates that something occurs before or near the start of analysis which requires a long period of time to diminish. It is strongly suspected, however, that the origin is the same.

In an attempt to better understand the origins of this phenomenon, I_0 and I_- signals were analyzed in the frequency domain. The intensities were first adjusted to oscillate about a zero axis by subtraction of the mean intensity. Imaginary components were set to zero by creating an array of the form; I_1, 0, I_2, 0, ... I_{512}, 0. In some cases every second intensity reading was used. When necessary, data was padded with zero's to complete 512 points. The values were then normalized to $\pm$ 1. Following Fourier transformation relative intensities of frequencies were regenerated from the real (r) and imaginary (i) components as $(I_r^2 + I_i^2)$.

Figure 4-12 shows an example of the frequency domain spectrum of I_0 and I_-. The converted data correspond to the results shown in figure 4-10 where I_0 and I_- are oscillating out of phase. It is apparent that very low frequencies make the largest contribution to the time domain result. Power spectra for I_0 and I_- which oscillate in phase are not significantly different from those shown. Broad band noise is apparent in many of the power spectra. (This is quite prevalent in the I_- spectrum of figure 4-12.) These resemble the power spectra shown in figure 5 of reference [109] corresponding to chaotic flow. Removal of the oscillation "noise" by frequency domain filtering would be very difficult as kinetic changes also occur at low frequency. This is exemplified in figure 4-13 where the zero order decay of the bromine signal as it reacts with acetone clearly shows a dampened oscillation embedded in it resulting from a slight phase shift of I_0 and I_-.

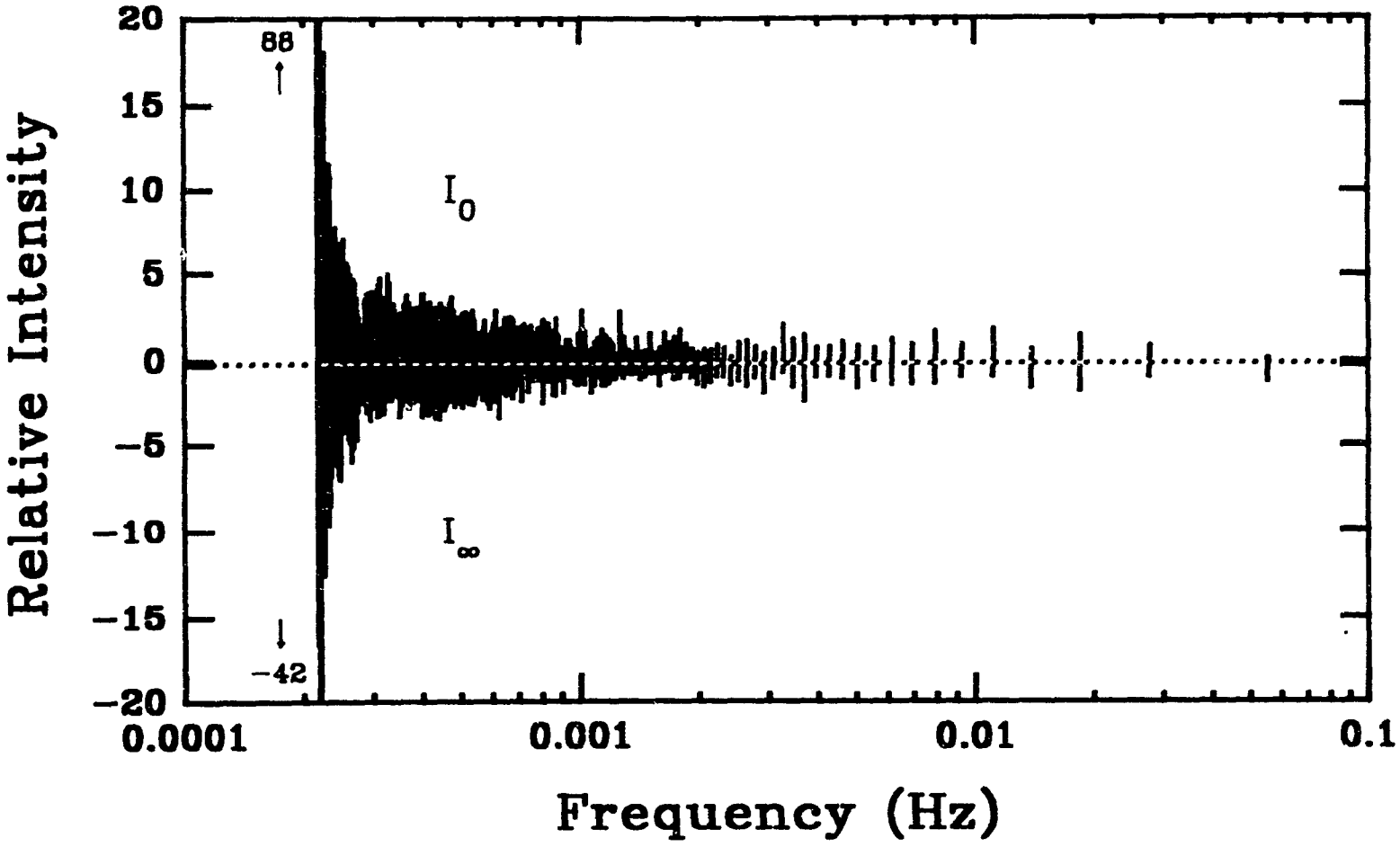

Figure 4-12: Power spectrum of I_0 and I_∞ time profiles obtained by Fourier transform. Every second intensity of the raw data was used. Values for I_∞ have been inverted for clarity. Oscillation in the time domain is composed of a series of low frequencies whose contribution decrease with increasing frequency.

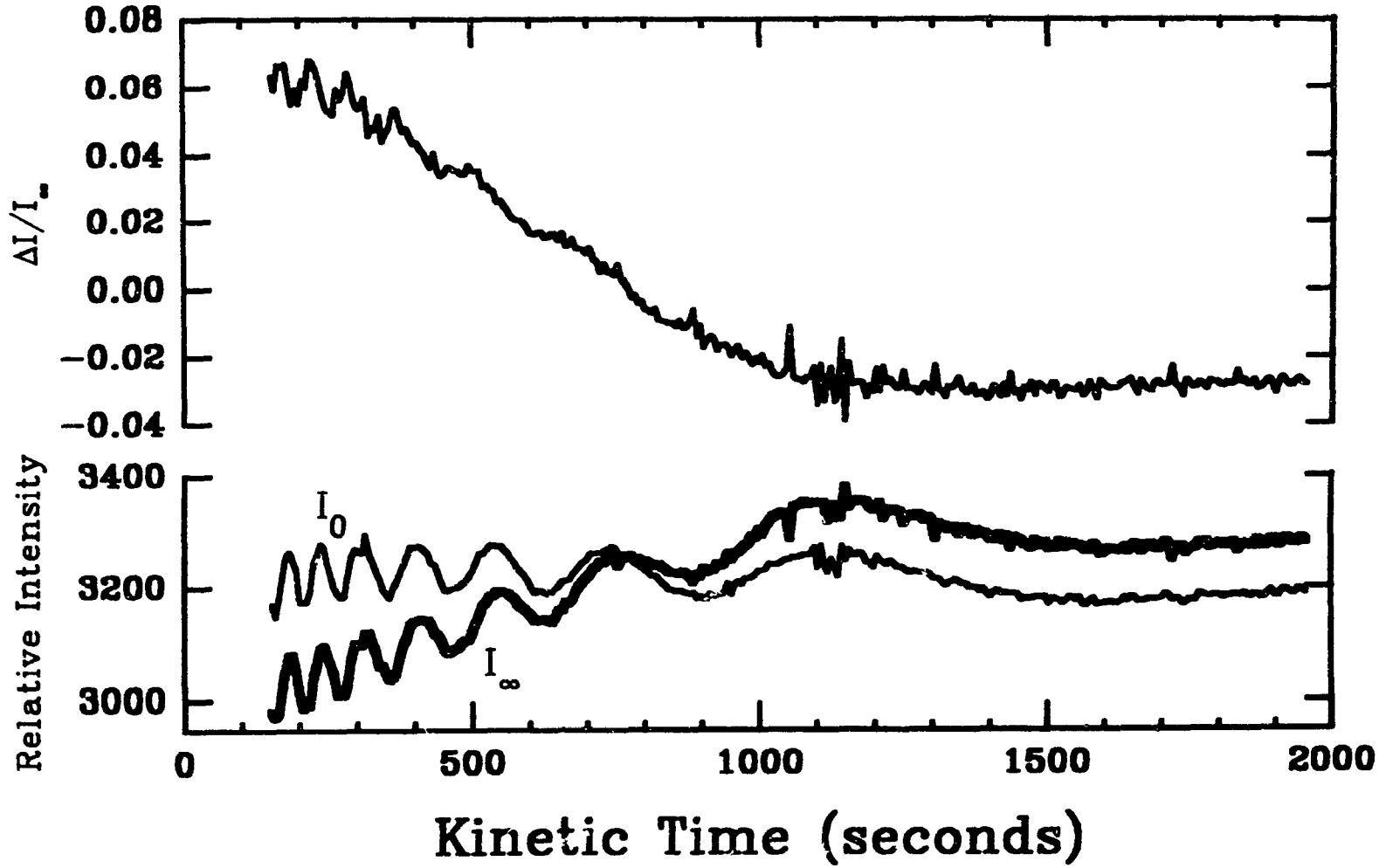

Figure 4-13: Thermal lensing result for the acid catalyzed bromination of acetone. The undulations superimposed on $\Delta I/I_\infty$ are a result of out of phase oscillation of I_0 and I_∞. Thermal lensing conditions were: DEVELOPMENT DELAY = 600 ms; DECAY DELAY = 2000 ms; INTERVAL = 6000 ms; SCANS/ACQ = 1000 and P_0 = 65 mW at 457.9 nm.

The possible origins of this phenomenon indicate that oscillation of I_0 and I_- may be sensitive to the type of sample cell used. Particularly, a continuous flow cell should remove any "memory" of events which occurred at the start of analysis. Three cell geometries were evaluated in an effort to minimize this effect. These included a standard 1.00 cm square cuvette, the cylindrical fill-drain cell previously described and a continuous flow cell (Hellma; model 178.710-OS). The latter has a 1.00 cm path by 0.30 cm diameter cylindrical bore with an inlet at one optical face and an exit at the other. Cell volume is 71 μL. The inlet was connected by a FEP tube to a liquid chromatography solvent delivery system (Pye Unicam LC3) which provided pulsation free pumping. The cell exit was connected to a small flask holding the bulk of the sample which was continuously stirred. This cell was found to have optimal (albeit poor) signal-to-noise ratios at zero flow. Signal-to-noise rapidly diminishes with increasing flow rate as seen in figure 4-14. Sensitivity was also observed to be very dependent on cell location. Further, the optimal cell position was affected by flow rate. Results in figure 4-14 were obtained by reoptimizing cell position at each flow rate. Higher frequency chopping or pulsing of the pump beam is better suited to the analysis of flowing samples. At sufficiently high frequencies flow rate becomes less important. Buffett and Morris [107] report a decrease in signal but a constant signal-to-noise ratio using chopper frequencies from 5-20 Hz in their analysis of flowing samples.

The results of the comparison of the three cells appear in table 4-1. They were evaluated by analyzing a steady state solution of $Cu(PHTTT)_3$. Means and sample standard deviations of I_0, I_- and $\Delta I/I_-$ were calculated for 300 acquisitions. "Spikes" were removed manually. Other analysis conditions were equal for the 3 cells. Values

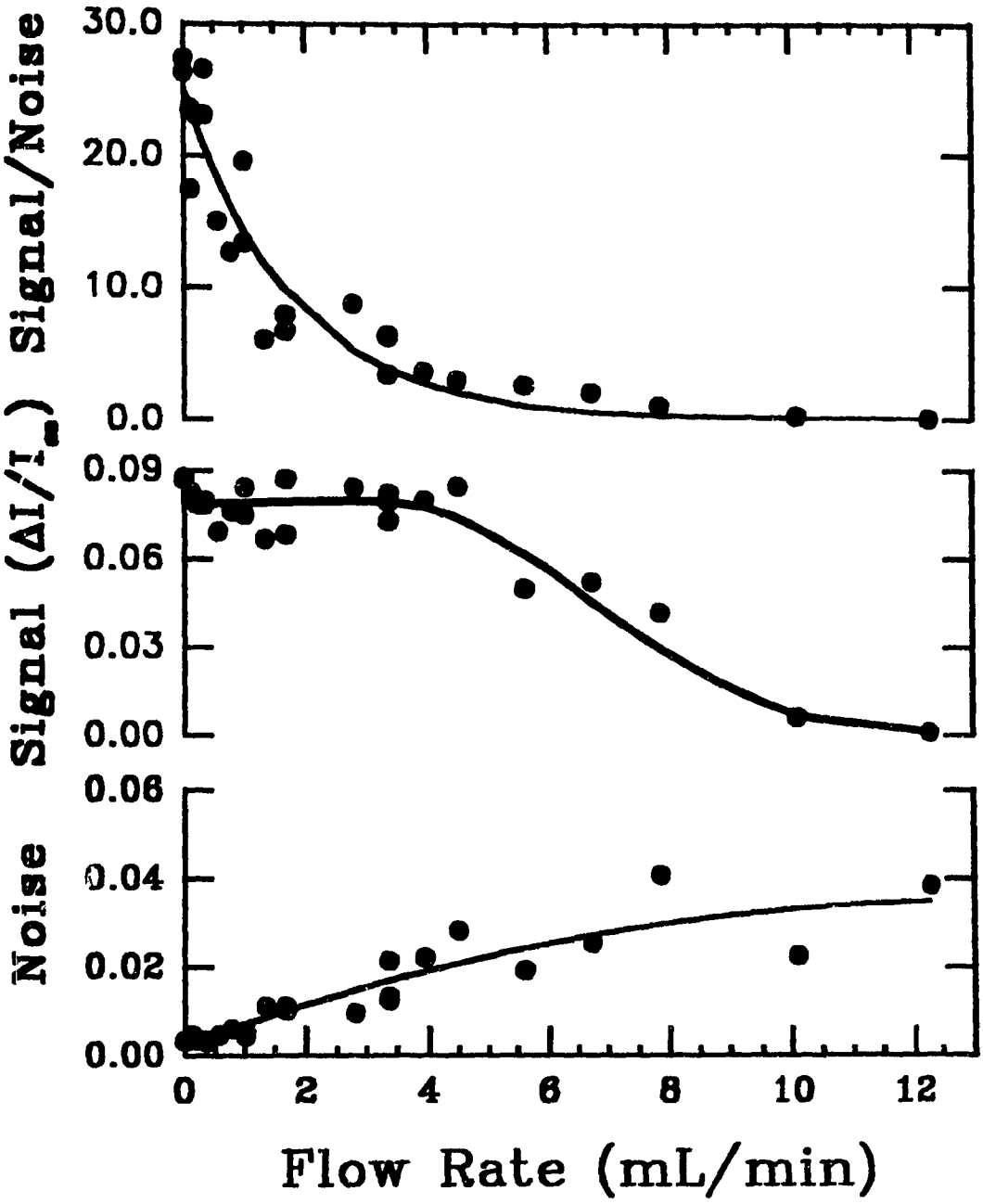

Figure 4-14: Effect of flow rate on TLS signal-to-noise ratio. Sample volume in the continuous flow cell is 71 µL. The signal rapidly diminishes as the development time begins to exceed the solution residence time in the cell (corresponding to c. 4 mL/min.). Analysis parameters were DEVELOPMENT DELAY = 500 ms; DECAY DELAY = 5000 ms; INTERVAL = 9000 ms and SCANS/ACQ = 1000. Each point is the average of 20 acquisitions.

Table 4-1:

Results obtained for the analysis of 6.0×10^{-7} M $Cu(PHTTT)_3$ (A_{458}~0.006). The noise levels of three cell geometries are compared at several values of MIXING DELAY. Oscillation of I_0 and I_∞ are reflected in their standard deviations. Out of phase oscillation elevates the standard deviation of $\Delta I/I_\infty$. Analysis conditions were DEVELOPMENT DELAY = 500 ms; DECAY DELAY = 1200 ms; INTERVAL = 6000 ms; SCANS/ACQ. = 1000; P_0 = 65 mW at 457.9 nm.

Cell geometry	MIX DELAY (minutes)	Flow rate (mL min^{-1})	Standard deviation I_0	I_∞	$\Delta I/I_\infty$
standard square cuvette	1	--	44	44	0.0070
	5	--	34	40	0.0064
	60	--	20	18	0.0034
"fill-drain" cell	1	--	8	11	0.0070
	5	--	5	5	0.0025
	60	--	6	6	0.0016
continuous flow	60	0.00	19	23	0.0046
	—	0.20	102	99	0.0055

of averaged I_0, I_∞ and $\Delta I/I_\infty$ were then normalized to 2600, 2400 and 0.0833, respectively. The normalization factors were then used to correct the standard deviations. This was necessary due to adjustments in alignment which were made after changing sample cells.

Oscillation of I_0 and I_∞ increases their standard deviations. Out of phase oscillation increases the standard deviation of $\Delta I/I_\infty$. Turbulence from placing the sample in the cell is also at least partially responsible for elevated standard deviations at short mixing delays. The standard cuvette suffers much more that the fill-drain cell from I_0 and I_∞ oscillation although this is largely in phase. Amplitudes of oscillation are observed to decrease with increasing MIXING DELAY for both of these cells. Approximately the same degree of oscillation is observed in the flow cell (with zero flow) and in the standard cuvette using a MIXING DELAY of 60 minutes. Even at a low flow rate, in phase oscillation of I_0 and I_∞ significantly increases in the continuous flow cell.

At a flow rate of 0.2 mL min^{-1}, the continuous flow cell has an overturn time of 21 seconds. The presence of oscillation in this cell with periods on the order of tens of minutes is unexpected. This allows three possible conclusions as to the source of oscillation. First, the origins of oscillation are external to the cell. This is improbable as oscillation is observed to be sensitive to the MIXING DELAY. Second, the "source" of oscillation is travelling upstream in the flow cell. Given the low flow rates and the short path length in the cell this may not be precluded. Third, turbulence has a mechanical origin (mixing) rather than a thermal one, or possibly a combination of the two.

The last of these is the most probable explanation. The frequency of oscillation was found to be significantly higher in kinetic samples (mixed seconds to minutes prior

to analysis) than in steady state ones (mixed tens of minutes to hours earlier and only lightly agitated prior to analysis). As an example, all the results in table 4-1 (steady state samples) were observed to have oscillation periods in the range 15-30 minutes. There is also limited evidence that the origin is a combination of mechanically and thermally induced turbulence. It was observed that starting acquisition immediately after sample introduction to the cell led to high noise levels which endured for very long periods of time. It is possible that thermally induced turbulence perpetuates that which results from mixing.

As pointed out, the phenomenon of aperiodic oscillation is difficult to handle using mathematical tools. Its origin is not entirely certain and is possibly rather complex. However oscillation does not present an overwhelming problem. First, it is clearly visible when it does occur. Second, its magnitude may be minimized or eliminated by proper choice of sample cell, analysis conditions and optical alignment.

4.2 COLLOIDAL SOLUTIONS

All glassware was cleaned by soaking for at least 24 hours in 10% nitric acid followed by thorough rinsing with doubly deionized, distilled water. A higher grade of water having resistivity of $\geq$ 18 MΩ-cm was used for the last two rinsings and for the preparation of all solutions (NANOpure-A system, Sybron/Barnstead). Unless otherwise specified, all chemicals were of reagent grade and were used without further purification. Several of the stock solutions whose preparations are described in section 4.2 are also used in other procedures.

Stock HCl (1.00 M) was prepared from Acculute® (Anachemia). On several

occasions HCl concentrations were verified by titration with NaOH which had been previously standardized against potassium hydrogen phthalate. Approximately $1x10^{-2}$ M copper(II) solutions in $1.00x10^{-2}$ M HCl were made using $CuSO_4 5H_2O$ (Fisher) which had been recrystallized from water and dried at 170 °C (The compound should dehydrate at 150 °C). Iron(III) solutions of (1 or 2)$x10^{-2}$ M were prepared by dissolving $FeCl_3$ (Fisher) in $1.00x10^{-2}$ M HCl. Exact concentrations of Fe(III) and Cu(II) stock solutions were determined by flame atomic absorption [110]. The weak base "tris" [tris[hydroxymethyl)aminomethane] was prepared in stocks of 0.500 M (Trizma® base; Sigma; oven dried).

Iron hydrous oxide colloids were prepared by the continuous dropwise addition of dilute tris to stirred 50.0 mL mixtures of Fe(III) and Cu(II) in $1.00x10^{2}$ M HCl. The output from a peristaltic pump (LKB) was split to deliver tris to four solutions in erlenmeyer flasks simultaneously. All four solutions were prepared at a single iron concentration while the amount of copper was varied. The concentration of tris added was calculated assuming the release of 3 protons for each Fe(III) as the hydrous oxide forms. All samples were at room temperature (insulated from heating by the stirrer) and open to the atmosphere. Addition continued for approximately 4 or 6 hours until the total volume was about 98 mL. The presence of Fehox was apparent from its yellow colour. The samples were adjusted to the desired pH by manual addition of further tris. The volume was adjusted to 100.0 mL with water and the pH verified. One blank colloid containing no copper was always prepared.

The pH of the colloids were measured with a general use combination electrode and a meter made by the Science Technical Centre of Concordia University. The meter

was calibrated at pH 4.01 and 7.00 using Anachemia or Canlab buffer solutions. Determination of pH of colloid containing solutions is hampered by a slow continuous drift toward lower values. This appears to be due to the adsorption of Fehox onto the glass electrode surface. To reduce inaccuracies, contact time between colloids and the electrode were minimized. No clear distinction between equilibration of the electrode and drift due to colloid interference could be determined. Resultantly, values of colloid pH should not be considered accurate to better than ±0.1 pH units. Precision may be somewhat better. Colloids were removed from the electrode surface periodically by immersing in standard buffer solution for a short time.

For some colloids Cu(II) was added after the Fehox had been formed (hereafter called "post" addition colloids). Suitable quantities of stock copper solution were added to 25.0 mL of the blank colloid. Due to the low volume of copper solution added, there is negligible dilution of the Fehox.

All colloids were aged sealed, in the dark and at room temperature for approximately 24 hours prior to study. An attempt was made to perform all analysis as closely as possible to 24 hours after preparation of the colloids. Due to the long duration of the experiments and the number of samples to be analyzed, the "aging" periods do very somewhat. An alternative approach would have been to prepare colloids individually allowing them to be analyzed after 24 hours. Experience indicated, however, that variation in kinetic parameters between "batches" of colloids was probably of greater significance than changes resulting from different ages. The problem of batch-to-batch reproducibility has also been noted by Swallow *et al.* [111]. They resolved this difficulty by preparing large volumes of stock colloid to which they added desired

quantities of adsorbate metals and pH equilibrated. This approach is unacceptable for the study discussed here for two reasons. First, it does not easily allow measurements to be made at an approximately constant colloid age. Second, it does not allow adsorbate metals to be present during the formation of the Fehox.

Homodisperse colloidal hematite samples (α-Fe_2O_3) were provided by L.K. Koopal, Wageningen, Netherlands. Particles having mean diameters of 107, 212 and 404 nm were used. Stock solutions contained about 0.028 g Fe mL^{-1}. These hematite particles had been prepared by a method of heterogeneous nucleation [112]. Strict control of experimental conditions suppressed further formation of particle nuclei beyond the initial seed sol preparation. Larger diameter sols were obtained in a step-wise manner using grown sols as the seeds for further growth. The result is nearly spherical particles of homogeneous diameter which may be varied over a wide range.

The final colloidal substances used in this study were spherical polystyrene latex particles (Marivac, Halifax, Nova Scotia). These particles are homodisperse having mean diameters of 176±2, 481±3 and 1090±8 nm. As received, their concentrations were $3.35x10^{11}$, $1.64x10^{10}$ and $1.36x10^{9}$ particles mL^{-1}, respectively corresponding to c. 0.1% (w/v).

Binding of Cu(II) to the 212 nm hematite particles was studied by adjusting a solution containing aliquots of hematite and Cu(II) to pH 6.00 with tris. The solution was left to equilibrate for 24 hours before analysis.

For thermal lensing scattering studies, hematite and latex solutions were repeptized prior to dilution by sonicating small volumes for 5-7 minutes (Sonic 3000 dismembrator, Artek systems, Farmingdale, N.Y.). Samples were diluted with water as required to obtain an absorbance of 0.050 at 458 nm. Solutions were then diluted a further 10-fold with water for thermal lensing analysis.

4.3 NON-KINETIC ANALYSES

4.3.1 Scanning electron microscopy

Both the hematite samples and a series of iron hydrous oxide colloids were studied by electron microscopy. Solutions were evaporated onto aluminum stubs under a vacuum bell over a period of 1 to 2 hours. Stubs had been prewashed with spectra grade acetone. The samples were coated with a 240 Å layer of Au/Pd in the case of hematite and 140 Å of Au for Fehox samples (SEM coating unit E5100, Polaron Equipment Ltd.). Fehox samples were coated 24 hours after preparation. Micrographs were run on an Hitachi S-520 SEM. A second series of micrographs of the Fehox samples were taken using a Jeol JSM-840A scanning microscope. Hematite was studied at magnifications of up to 35000 with 20 kV accelerating voltage. Fehox samples were compared at magnifications up to 15000 and 10kV accelerating voltage. No thermal decomposition resulting from the electron beam was apparent for any of the materials run on the Hitachi. Some decomposition of the Fehox samples using the Jeol SEM was evident and will be discussed in chapter 5.

4.3.2 Filtration/elemental analysis

In earlier studies "free" copper was determined by filtration of colloidal solutions followed by atomic absorption analysis. Free metal analysis for the preparation of equilibrium isotherms involved passing 20.00 mL of the colloidal samples through 0.45 μm polycarbonate filters (Millipore type HA) under a slight vacuum. Iron and copper were determined by flame atomic absorption (Perkin-Elmer model 503 atomic absorption spectrophotometer) in comparison to Fisher standards. No iron was detected in the filtrates indicating complete retention of the colloidal suspension by the membrane filters. The absence of free copper loss by adsorption on the membranes was demonstrated by filtering copper solutions between 2.50×10^{-6} M and 5.00×10^{-5} M at both pH 2.0 and pH 6.0. Quantitative recovery of copper, as determined by AAS, was observed in all cases demonstrating that any loss was less than the detection limit of the analysis method.

A possible source of error in the filtration procedure should be addressed. As filtration of the colloid samples proceeds, the concentration of Fehox at the membrane surface becomes greater than that in the bulk solution. This elevated concentration can result in excess adsorbate being retained on the filter leading to low values of free metal concentration. The result of such an error would be low estimates of the free-to-bound copper ratio in the Langmuir isotherm particularly at higher sorbent/sorbate ratios. Since linearity of Langmuir plots was observed it appears that such a deviation was minimal, possibly due to the fairly high filtration rates used.

Data were tested for adherence to the Langmuir isotherm based on the expression:

$$\Gamma = \Gamma_{max} [KC/1+KC]$$

where $\Gamma = x/m$ (x being absorbed Cu^{2+} and m the concentration of iron colloid). C is the equilibrium concentration of free copper. Units of mol L^{-1} were used for x, m and C.

4.4 KINETIC ANALYSES

4.4.1 Sample handling

4.4.1.1 *Conventional spectrophotometry*

Kinetics of higher concentration samples were run on a Hewlett-Packard model 8452A photodiode array UV/VIS spectrophotometer interfaced to an IBM PC or an XT compatible. This instrument operates from 190 to 820 nm with a spectral resolution of 2 nm. Absorbance was typically measured at intervals of 3 seconds with an integration period of 1 second. Mixing was normally performed by adding 1.00 mL of reagent "A" (usually chromophore/buffer solution) with a micropipette to 1.00 mL of reagent "B" (usually colloid) in the cell at time zero. Solutions were mixed twice with a pasteur pipette. Both solutions were pre-equilibrated and the reaction maintained at 25.0 ± 0.01°C by a thermostatted circulating water bath (MGW-Lauda model K2R or model RMT-6). The cells used were standard 1.00 cm path length (Hellma type OS or QS) equipped with a tapered stopper. A background of the cells containing water was recorded and automatically subtracted from all spectra by the HP8452. Time base data which was to be treated by Laplace/NLR analysis was converted to a suitable format using the program which appears in Appendix C.

4.4.1.2 *Thermal Lensing*

The thermal lensing signal is extremely sensitive to turbulence in the sample cell. Such a disturbance disrupts the thermal gradient induced by irradiating the sample with the pump beam. Efficient mixing of reagents requires the introduction of turbulent action. To limit this problem, reagents for kinetic analysis were mixed in a separate vessel at time zero. The mixture was then slowly transferred to the cell using a pasteur pipette. Passage through the narrow tip of the pasteur leads to a laminar flow which significantly reduces the turbulence. The solution is then left for a further period of time to become tranquil before commencing TLS analysis. For non-kinetic samples, where signal is time independent, a long period is used to minimize noise levels. Unless otherwise stated, analyses were carried out in the 1.00 cm path length cylindrical "fill-drain" cell. The cell was always filled to the same level with solution.

4.4.2 Chemical systems and data handling

4.4.2.1 *Bromination of acetone*

Experiments for the bromination of acetone employed spectra grade acetone (J.T. Baker) and dilutions of bromine (Anachemia) prepared from a saturated solution. Sulphuric acid (J.T. Baker) was used as the catalyst. The concentration of stock H_2SO_4 was determined by titration with previously standardized NaOH.

A number of factors of importance to thermal lensing analysis were considered in determining optimal reagent conditions to be used. Both H_2SO_4 and acetone alter the thermo-optical properties of the solvent. Two approaches may be used to prevent problems resulting from this. Concentrations may be maintained sufficiently low so as

to have negligible contribution to the solvent properties. Alternatively, higher concentrations may be used provided they remain constant through the course of the kinetic reaction. The former approach was necessary for the acetone as calibration standards must be prepared in a matrix having the same thermo-optical properties as those of the kinetic solutions. An acetone containing matrix was unfeasible for preparation of the standards. This required the use of a somewhat higher concentration of H_2SO_4 to allow reactions to proceed at rates viable for kinetic monitoring. Sulphuric acid was used at 0.0516 M (0.0602 M H^+) in the kinetic mixtures and in the standards. This concentration has only a limited effect on the solvent matrix.

For kinetic study bromine was added at time zero to a solution containing acetone and H_2SO_4. By conventional spectrophotometry the reaction was followed at both 394 nm (absorption maximum of Br_2) and 458 nm (TLS pump beam wavelength).

Sulphuric acid was maintained at 0.0516 M in kinetic mixtures and standards for both CS and TLS analyses. The change in reaction rate with variation of acetone concentration was monitored over the range 0.200 to 1.00 M acetone by CS. Concentrations of acetone and Br_2 were reduced by two orders of magnitude for TLS study.

Due to its volatility, some difficulty was encountered in maintaining the Br_2 concentration in solutions. This was particularly problematic during mixing and for stock solutions having higher concentrations. Bromination of acetone is zero-order in bromine. As a result the amount of Br_2 initially introduced to kinetic mixtures is of only limited importance. Knowledge of accurate concentrations was, however, of greater importance in the preparation of standard curves for TLS. The ability to relate the sensitivities of CS

and TLS is prerequisite in comparing rate constants obtained by the two methods.

For CS analyses molar absorptivities were calculated on the basis of work done by Pink [113] who determined absorptivities for Br_2 and Br_3^- over the range 250 to 390 nm. Values of $\varepsilon(Br_2)=174$ and $\varepsilon(Br_3^-)=250$ were calculated for 394 nm by extrapolation. Comparison of the absorption spectrum of a stock solution with the results of Pink indicated the presence of a small amount of Br_3^-. Simultaneous equations based on:

$$\varepsilon_\lambda(Br_2)\,[Br_2] + \varepsilon_\lambda(Br_3^-)\,[Br_3^-] = A_\lambda$$

were solved for 7 pairs of wavelengths. The averaged results showed the stock solution composition to be 4.99 (±0.05) x 10^{-3} M Br_2 and 6.4 (±0.7) x 10^{-6} M Br_3^-. Based on these results $\varepsilon(Br_2)$ = 90 was calculated for 458 nm. The effect of Br_3^- was assumed to be negligible at this longer wavelength.

The standard curve for determination of thermal lensing sensitivity was prepared using dilutions of a freshly prepared Br_2 stock solution. TLS analyses were run very soon after preparation of the standards. A standard curve for CS was prepared in the same manner. Comparison of the CS curve with the known molar absorptivities allowed calculation of the actual concentration of the stock solution. The same correction factor was then applied to both the CS and TLS results. Figure 4-15 shows some results obtained by TLS for Br_2 "standards". Curve A was measured with dilutions of a Br_2 stock solution (c. 0.07 M) which had been prepared 3 days earlier. The following day curve B was measured using the same stock solution. Curve C was determined from fresh Br_2 stock and corresponds to a TLS sensitivity of 2080 M^{-1}. After application of

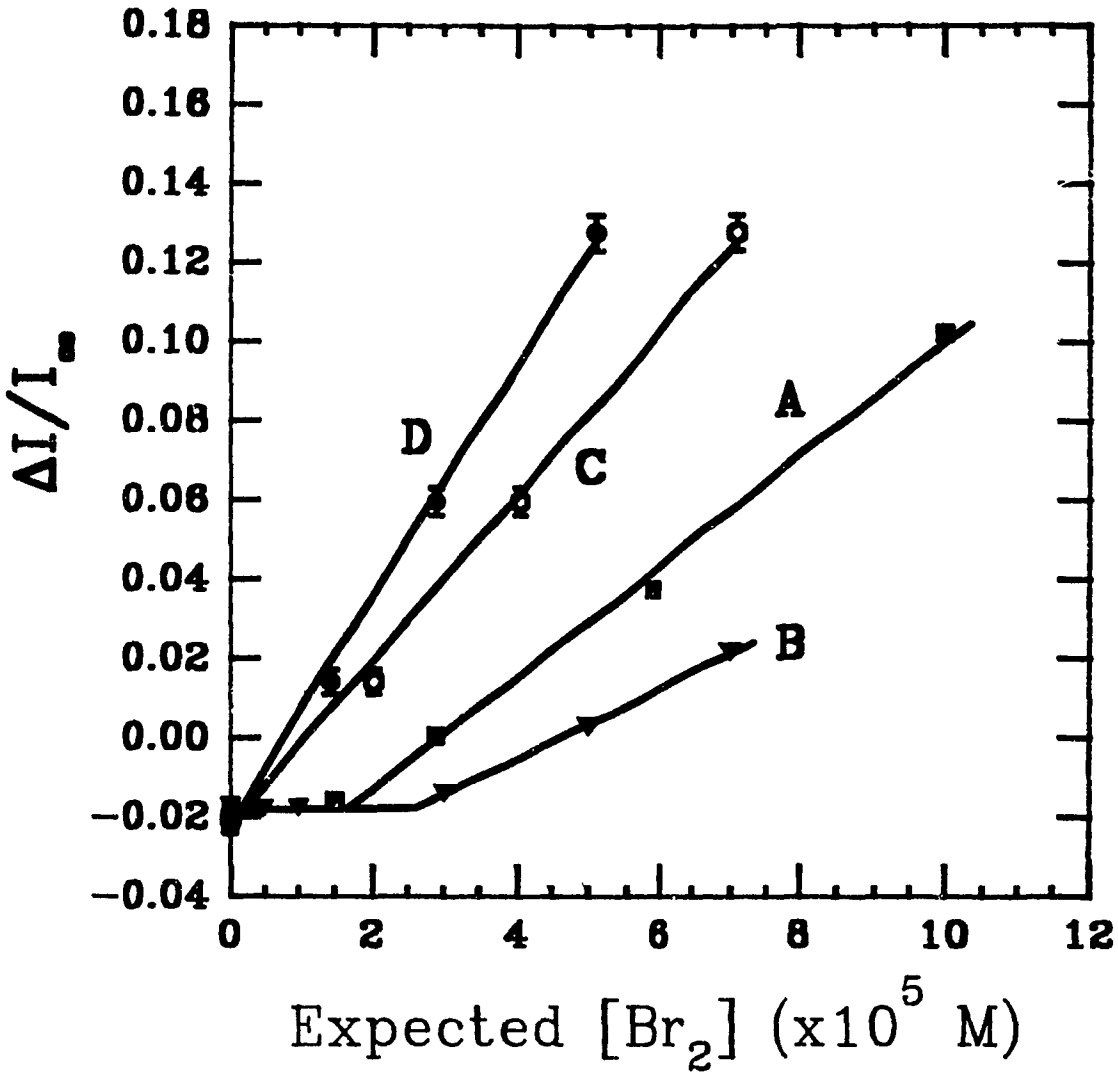

Figure 4-15: Some of the "standard curves" for bromine obtained by thermal lensing. Curves A and B were determined for some of the preliminary results and demonstrate problems associated with the volatility of bromine. Curve C was used for calibration of TLS sensitivity for kinetic results reported here after having cross-calibrated with CS to correct for the actual bromine concentrations (resulting in curve D). TLS conditions were: DEVELOPMENT = 600 ms (500 ms for A and B); DECAY = 2000 ms (1200 ms for A and B); INTERVAL = 6 s; SCANS/ACQ = 1000; P_0 = 65 mW at 458 nm. Points were averaged over 100 acquisitions.

the correction factor determined by CS (0.719) the sensitivity was found to be 2900 M^{-1} corresponding to an enhancement factor of 14.

Second order rate constants for the bromination of acetone were calculated based on:

$$\text{rate} = k\,[H^+]\,[\text{acetone}]$$

Rates of bromine consumption (zero-order) for both TLS and CS kinetic analyses were determined by linear regression of the signal vs. time data. TLS data at short times were truncated prior to regression. "Spikes", although few, were also removed.

4.4.2.2 *Hydrous ferric oxide*

Colloids were prepared at pH's 5.5, 6.0 and 6.7 by the base hydrolysis method described earlier. No copper was present. Iron concentration of all colloidal solutions was 1.56×10^{-4} M. Colloids were used at this concentration for kinetic analysis by conventional spectrophotometry. For TLS analysis, Fehox solutions were diluted to 1.25 or 1.56×10^{-5} M. Dilution was done using solutions of HCl which had been adjusted with tris to match the matrix of the colloid.

The chromophore solution for CS analysis contained 0.0150 M SSA (sulphosalicylic acid, Fisher) and 0.100 M HCl. The SSA concentration was reduced 10-fold for measurements by TLS. Kinetics were initiated by mixing equal volumes of chromophore solution and colloid. Standards were prepared from iron solutions which had been maintained at pH 2.0 or lower to prevent colloid formation. Figure 4-16 shows a visible absorption spectrum of the Fe/SSA complex and a standard curve obtained by

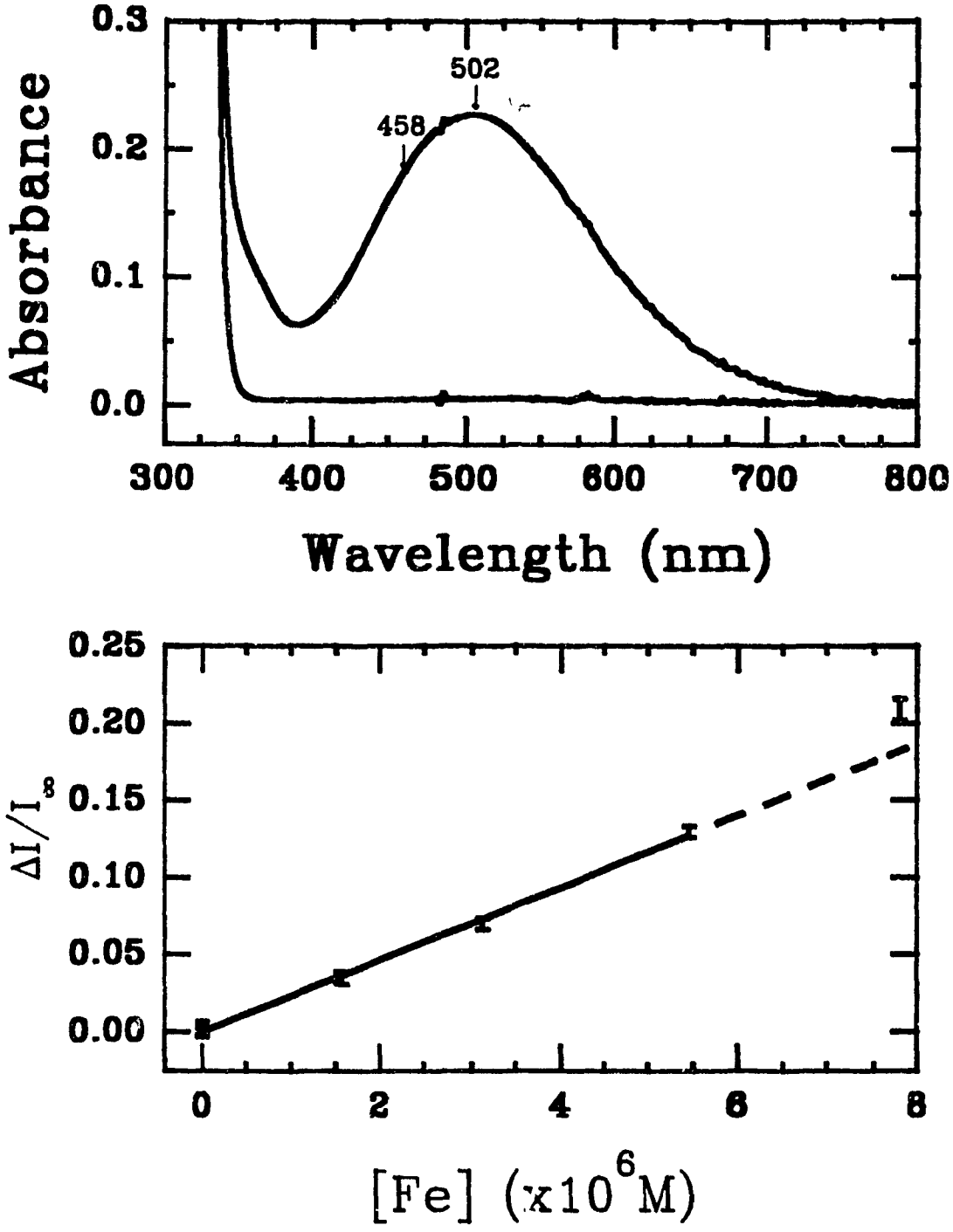

Figure 4-16: Upper) Absorption spectrum for a 1.25×10^{-4} M $Fe(SSA)_3$ solution and a blank containing no iron. Lower) TLS standard curve for $Fe(SSA)_3$. Note that the point at 7.8×10^{-6} M Fe is in the nonlinear region for TLS. Sensitivity is 2.33×10^4 M^{-1} corresponding to a modest enhancement factor of 7.3. The matrix for all solutions is 0.05 M HCl. TLS conditions were: DEVELOPMENT DELAY = 600 ms; DECAY DELAY = 2000 ms; INTERVAL = 6 s and P_0 = 65 mW at 457.9 nm. Points are the average of 100 acquisitions.

TLS. The complex between Fe(III) and SSA has an absorption maximum at 502 nm. Absorptivity at 458 nm (1390 ± 20 M^{-1} cm^{-1}) is about 78% that of the maximum (1790 ± 20 M^{-1} cm^{-1}). Kinetics were followed at both wavelengths by CS.

Kinetic data were treated by first-order analysis methods. As discussed in section 3.3.1, reaction of SSA with Fehox in an acidic medium is expected to yield three kinetic components. Within the time scale used in these experiments the fastest component has reached completion and the slowest component has a negligible contribution to signal change.

Kinetic curves obtained by TLS show significantly higher noise levels than are generally observed in non-scattering media. As such, smoothing of the raw data was necessary. A variety of methods were compared. The greatest success was obtained by first manually correcting spurious spikes in the kinetic curve. The data analysis routines used could not easily handle discontinuities in the time spacing of successive points. Therefore any points removed were replaced by interpolated values of $\Delta I/I_{\infty}$.

The data were then smoothed in the frequency domain using the Blackman "lucky guess" window [114] as convolution weights [115]. The data spectrum is multiplied by the square modulus ($|W|^2$) of the window function, W:

$$W(f) = 0.42 + 0.5 \cos(\pi f/f_o) + 0.08 \cos(2\pi f/f_o)$$

where f is frequency and f_o is the low pass frequency limit. This process may also be thought of as convoluting the data with the inverse Fourier transform of the window function. This low pass frequency response window results in extremely small side lobes

in its convolution weights. Since W slowly decreases as f_o is approached, minimal "Gibbs ripple" is introduced into the smoothed data. This smoothing operation was carried out using ASYST software [116]. The default value of $f_o = 0.25$ was used.

Smoothing with the Blackman window can lead to reductions in signal intensity. No such effect was observed in the curves analyzed possibly due to the very low frequency of the signal component. This method was not entirely effective in removing large "spikes" in the data. While it reduced their intensities considerably, it also led to significant broadening of the peaks. Hence the initial "manual" removal of these spurious points.

TLS data were analyzed by first-order methods following Blackman smoothing as well as after further smoothing by polynomial fitting as described in section 3.2.1. When polynomial fitting was used, "spikes" in the raw data were removed (as opposed to replaced by interpolated values) as data sets could be regenerated with equal time spacing. The progression of this smoothing is shown in figure 4-17. It should be noted that the results shown in this figure are among the least noisy of the TLS data recorded for the Fehox/SSA system. CS data were analyzed without smoothing.

Data were first analyzed using the Kezdy-Swinbourne method:

$$S_t = S_{t=\infty} (1-e^{k\Delta t}) + S_{t+\Delta t} e^{k\Delta t}$$

where S refers to signal (either A or $\Delta I/I_\infty$). An increment of 1500 s was used as Δt. Rate constants and estimates of $S_{t=\infty}$ were calculated from plots of $S_{t+\Delta t}$ vs. S_t as:

$$k = -(\ln m / \Delta t)$$

$$\text{and } S_{t=\infty} = b / (1-m)$$

where the slopes (m) and intercepts (b) were determined by linear regression.

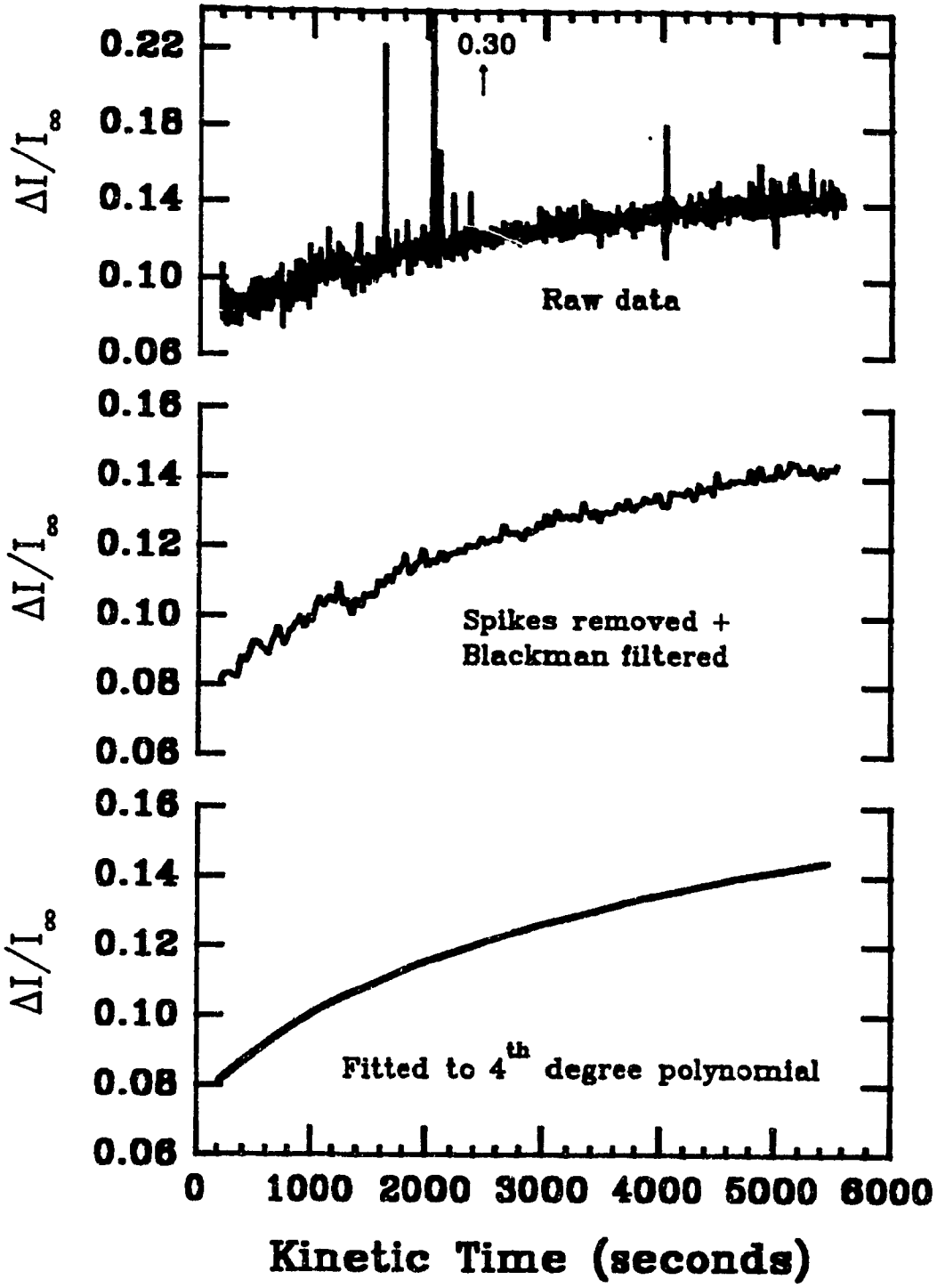

Figure 4-17: Smoothing applied to data obtained by TLS monitoring of the reaction of 1.0×10^{-5} M Fehox (equilibrated at pH 5.5) with the chromophore SSA in a matrix of 0.05 M HCl at 25.0 °C. First order analysis was performed both before and after least squares fitting of the data. TLS conditions were: DEVELOPMENT DELAY = 600 ms; DECAY DELAY = 2000 ms; INTERVAL = 6000 ms; MIXING DELAY = 200 seconds and P_0 = 65 mW at 457.9 nm.

Both measured values of $S_{t=\infty}$ and those obtained from the Kezdy-Swinbourne results were used to prepare first-order plots based on:

$$\ln(S_{t=\infty} - S_t) = -kt + \ln(S_{t=\infty} - S_{t=0})$$

When using $S_{t=\infty}$ estimates from the Kezdy-Swinbourne method the calculated k's were (not unexpectedly) nearly identical. This plot does,however, allow estimates of $S_{t=0}$ to be calculated which are useful in validating the quality of the rate constants by comparison with the raw data.

Data were also fit using the method of Guggenheim:

$$\ln(S_{t+\Delta t} - S_t) = -kt + \text{constant}$$

In accordance with Swinbourne [117] Δt was chosen to be 1500 s, of the same order as the expected $t_{1/2}$.

4.4.2.3 *Copper(II)-hydrous ferric oxide*

The chromophore used for the kinetic speciation of copper (II) was a homologue of 3-alkyl-5-hydroxy-5-(D-arabino-tetrahydroxybutyl)-thiazolidine-2-thione. This is a class of compounds first synthesized and characterized by Dalton in 1966 [118]. The general structure is shown in figure 4-18. The methyl homologue was used later that year [119] as a selective chromophore for the determination of copper in steels and aluminium alloys due to its insensitivity to large excesses of other metals. Stiff [120] used the propyl compound to determine copper species by timed spectrophotometric reactions as part of a scheme to speciate copper in river water and sewage effluents. Chow *et al.* [121] have shown that copper complexes with the homologues from methyl to butyl all have absorption maxima at c. 434 nm with molar absorptivities

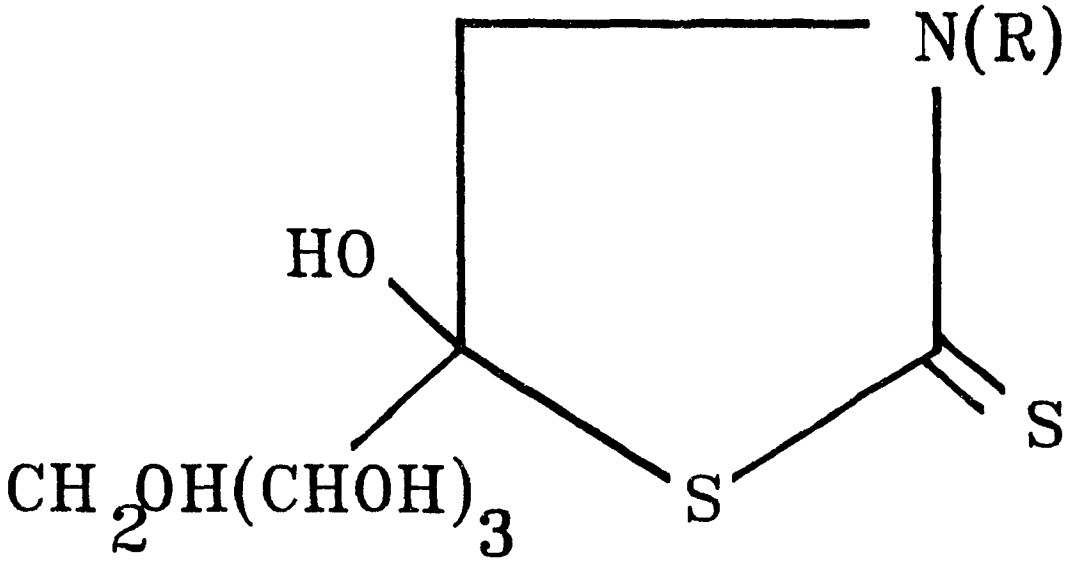

(R)HTTT

Figure 4-18: General structure of the thiazolidine-2-thione class of copper selective chromophores. The use of alkyl groups (R) from methyl to butyl have been discussed in the literature. This work employed the propyl homologue.

increasing slightly with chain length. They also showed that complexation occurs at a ligand to metal ratio of 3:1.

For this work the propyl homologue (PHTTT) was prepared and purified by the method of Chow *et al.* [121]. The absorption spectra of PHTTT and $Cu(PHTTT)_3$ are shown in figure 4-19. Note that the ligand has nominal absorbance at 434 nm. The complex was found to have a molar absorptivity at 434 nm of 13100 ± 300 M^{-1} cm^{-1}. This is based on the analysis of two concentrations of standard prepared on 9 separate occasions. This value is somewhat lower than those of 13900 M^{-1} cm^{-1} [122] and 14500 M^{-1} cm^{-1} [121] found in the literature. There are two possible reasons for this. First, chromophore solutions were buffered at the lower end of the PHTTT stability region (pH 6-8) [121,122]. Second, the mixed chromophore solutions have a high ionic strength. Electrostatic interaction between the absorbing species and ions in solution could change the absorptivity of the complex [123]. The actual value of the absorptivity is of limited importance. Internally consistent results were obtained. Absorbance at 458 nm was found to be 75.4 ± 0.3% of that at 434 nm. This factor is useful for relating CS analyses with TLS where the pump wavelength used was 457.9 nm.

The buffer in the chromophore solution plays a role in ionic strength control as well as in that of pH control. To adequately constrain both of these parameters at predetermined values it was necessary to prepare buffers based on calculated concentrations of conjugate acid and base rather than by empirical means. To assure consistency, a stock of concentrated buffer was prepared.

The concentrated buffer solution was prepared by dissolving 28.17g of bis-tris (Bis(2-hydroxyethyl)imino-tris(hydroxymethyl) methane; Sigma; oven dried; pK_a=6.46

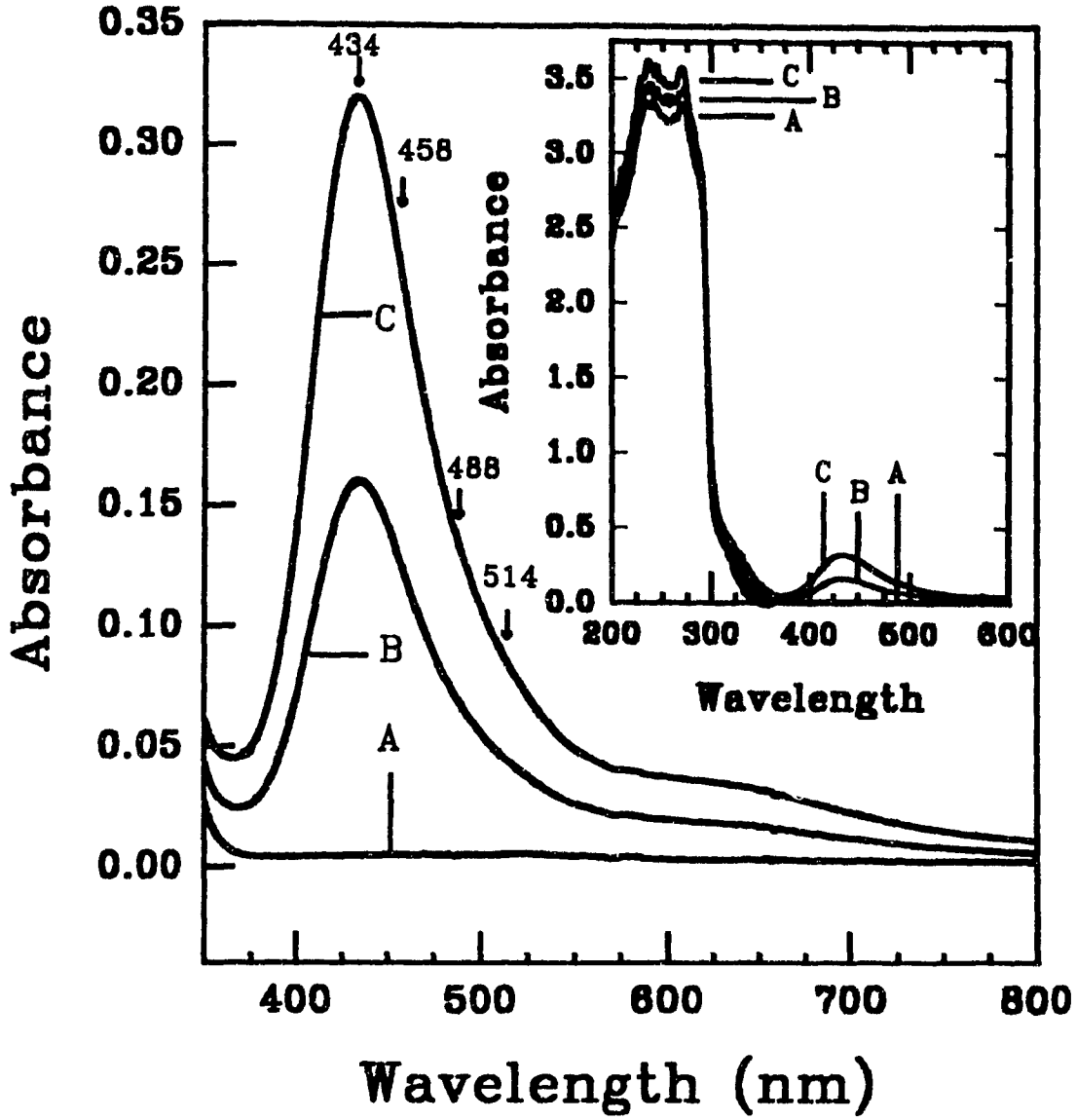

Figure 4-19: Visible absorption spectrum of $Cu(PHTTT)_3$ measured in a 1.00 cm QS cell. The following were mixed 1:1 (v:v) with chromophore solution: A) water; B) 2.42×10^{-5} M Cu^{2+}; C) 4.84×10^{-5} M Cu^{2+}. The labelled wavelengths show the absorption maximum and some of the potential pump lines emitted by an argon ion laser. Absorption by the chromophore in the UV region is seen in the inset.

at 25 °C) in 100.0 ml of 1.00 N HCl and diluting to 250.0 ml with water. PHTTT (0.149g) was dissolved in 50.0 ml of the concentrated buffer. This compound is not highly soluble in aqueous solution and significant agitation is necessary. The solution was diluted to 100.0 ml with water.

Measurements of pH were carried out at "room temperature". pH's of the bis-tris buffer solution = 5.77 ± 0.03 were observed. This variation is rather large and initially led to questioning the buffer stability and/or purity. The temperature sensitivity was investigated. It was determined that at 25.0°C the pH is 0.13 units lower than at 20.0°C. This explains day-to-day variations in measured pH and provides a more accurately known pH under the reaction conditions used.

Combination of equal volumes of chromophore/buffer solution with copper containing Fehox solution results in a mixture of 2.50×10^{-3} M PHTTT at 0.100 M ionic strength and buffered at pH 5.7 at 25.0°C. This pH was chosen due to its central location in the range of colloid pH's studied (4.5 to 7.0). This obviates too radical a change in pH of the Fehox solutions when mixing with chromophore/buffer.

The colloid containing solutions were not continuously stirred during kinetic analysis. The reason for this is graphically demonstrated in figure 4-20 which shows hydrous oxide solutions upon mixing with chromophore/buffer. The lower two curves are typical of Fehox which does not contain any copper. Note that in the absence of stirring absorbance change due to colloid settling is small and may be considered negligible for at least the first 30 minutes in the example shown. The upper curves show kinetic reaction of Fehox containing some copper. The Cu(II) is present at fairly low concentration resulting in a rather small but still distinct kinetic absorbance change.

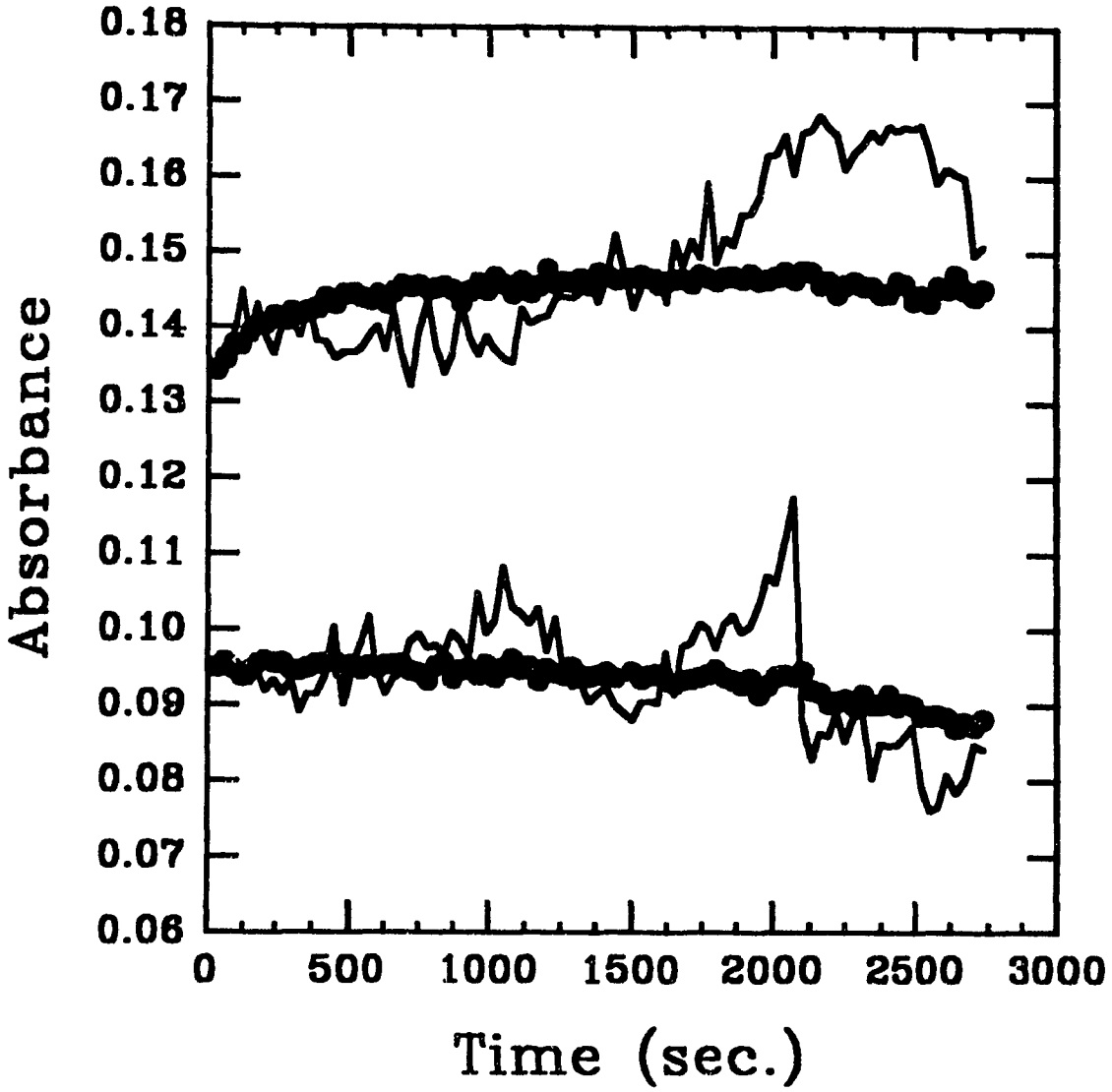

Figure 4-20: Kinetic profiles of Fehox with and without Cu^{2+} upon mixing with PHTTT solution. Colloids settle quite slowly during the acquisition period. Solid circles represent no stirring while lines are for continuous stirring during analysis. The effect of stirring in the cell is clearly detrimental to signal quality. In the upper curves Fe:Cu mol ratio is 25.

These distinct characteristics of both the Fehox blank and that with copper present become completely obscured under mixing conditions. For this reason continuous mixing was not used.

A time dependent variation in background signal can ideally be compensated for by digitally subtracting it from the kinetic signal. In the case of Fehox this is not optimal as the background signals are not well behaved. Replicate measurements frequently vary from a small decrease to no change in absorbance within the usual time scale of the experiment. Occasionally small increases were also observed [124]. Therefore the first few minutes of background measurements were averaged to obtain a single value which was used as background. It therefore becomes necessary to consider the effect of colloid settling on the resulting kinetic parameters.

The fastest of the kinetically measurable components reaches 99% completion in under 3 minutes. As such it is insensitive to the much slower changes in background signal. The second kinetically measurable component is somewhat slower requiring nearly 45 minutes to reach 95% completion. The effect of a decrease in background signal is to reduce both the apparent rate constant (k) and the component contribution (C). A further result of this will be a slight overestimate of the "non-recoverable" copper fraction. A small increase in background absorbance would have the opposite effects. It should be noted that the effect of background shown in figure 4-20 is a worst case. Absorbance change due to kinetically labile Cu(II) is normally somewhat larger, significantly decreasing the relative effect of background variation. The resulting errors in k and C should normally fall within experimental error.

A test was performed to evaluate the "shelf-life" of the chromophore/buffer stock.

Solutions which had been prepared freshly and 6, 13, 100 and 174 days earlier were mixed with equal volumes of a copper standard. Measured absorbance values of the five solutions agreed within 1% showing good reagent stability.

The reaction of free copper with the chromophore was immediate under the conditions used. The stability of the complex of copper with PHTTT was determined by monitoring the absorbance at 434 nm for up to 6 hours. Absorbance was observed to increase at a rate of c. 0.1% over the first hour and 0.15% over the second hour. This change then accelerated to about 0.5% per hour from 2 to 6 hours. Since kinetics of copper containing Fehox were typically monitored for 60 to 120 minutes, these changes are insignificant.

Colloids for kinetic speciation of copper were prepared at pH's 4.5, 5.5, 6.0, 6.7 and 7.0. Iron concentrations were c. $1x10^{-4}$, $2x10^{-4}$ or $3x10^{-4}$ M with iron:copper mole ratios ranging from about 2 to 30. The larger Fe:Cu ratio colloids were prepared at the higher concentrations of iron. This allowed copper concentrations to be maintained sufficiently hign as to permit resolution of changes in absorbance during kinetic analysis. A colloid with Fe:Cu of c. 10 was prepared with each set of four colloids to monitor consistency.

Two dilutions of the copper stock were independently prepared and analyzed along with each series of kinetics. Blank solutions of water mixed with chromophore solution were used to correct the standards and monitor the reagent water for Cu contamination. Tris solution was also analyzed for possible contamination.

For TLS analysis PHTTT/buffer solution was diluted 50-fold with water. Fehox solutions were handled in one of two ways. Some colloids were diluted 50-fold with tris

adjusted acid "blank" prior to mixing 1:1 with chromophore solution. In other cases 5.00 ml of diluted chromophore solution was mixed with 4.90 ml of water and 0.100 ml of "concentrated" colloid was added at kinetic time zero. An example of a TLS standard curve for $Cu(PHTTT)_3$ is shown in figure 4-21.

General data smoothing and speciation calculations by Laplace/nonlinear regression have been described in the introductory chapters. One point of some importance will be noted. Due to the relatively slow "manual" mixing of reagents in the spectrophotometer cell, typically the first two data points (time=0 and 3 seconds) were erroneous and were removed prior to analysis. Thus only data at times ≥6 seconds were treated. This had little effect on Laplace estimates. It was noted, however, that the NLR procedure had some difficulty with this lack of data at short times. NLR fitted parameters tended to over estimate the component 1 ("X"), largely at the expense of component 2.

Since the absorbance at time zero is due to a combination of background and component 1 (unknown), computation of what time zero absorbance should be was not possible. It was observed that the addition of data points at short times estimated by extrapolation of the experimental data improved the NLR results. Two difficulties were apparent. First, since the smoothing routines employ a logarithmic time base, data cannot be added at time zero. Second, each estimated data point added increases bias in the fitted parameters. A variety of techniques of "inserting" data were tested. The best results were obtained by adding a single estimated point A(t=0.5 s) at 0.5 seconds. This greatly improved NLR results while allowing them to remain reasonably insensitive to the estimate of A(t=0.5 s) used.

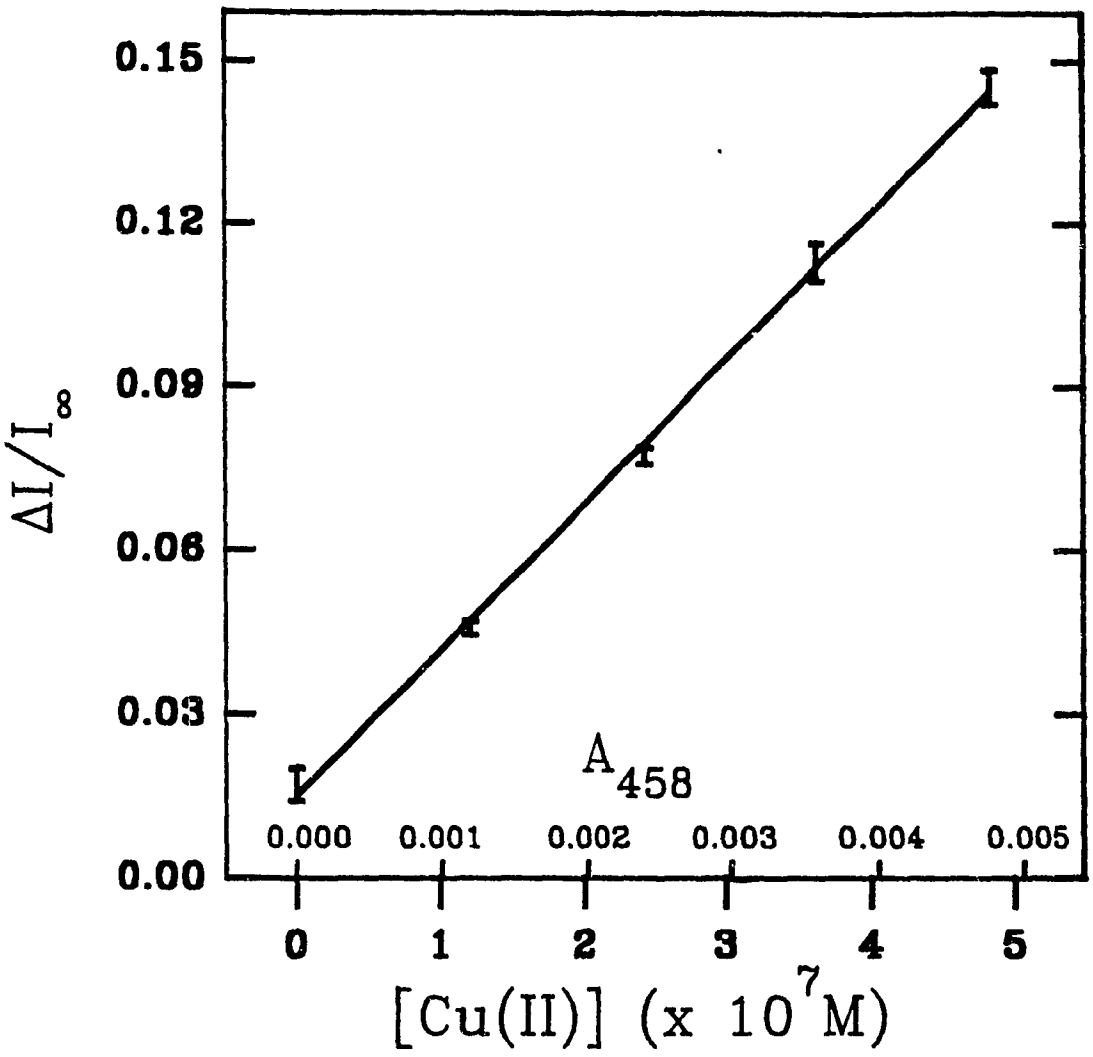

Figure 4-21: A standard curve for $Cu(PHTTT)_3$ obtained by thermal lensing analysis. Sensitivity in this case is 2.68×10^5 M^{-1} at 458 nm corresponding to an enhancement factor of 11.8. Linearity is good, the sample correlation coefficient being 0.9994. For comparison the equivalent absorbance values at this wavelength are also indicated on the abscissa. The thermal lensing conditions used were: DEVELOPMENT DELAY = 600 ms; DECAY DELAY = 2000 ms; INTERVAL = 6 s; MIXING DELAY = 60 s and P_0 = 65 mW at 458 nm. Points are the average of 150 acquisitions. Error bars show sample standard deviations of the acquisitions.

Chapter 5

RESULTS AND DISCUSSION

5.1 PROPERTIES OF COLLOIDAL MATERIALS

The ferric hydrous oxide used in this work was prepared by the slow hydrolysis of hexaaquairon(III). The formation and properties of Fehox have received considerable attention (see for example [96,125,126,127,128]). The hydrolytic method of preparation is relatively simple to institute in the laboratory. This has lead to its common use. It must be realized, however that Fehox prepared in this manner may differ significantly from the naturally occurring material. The morphological characteristics of natural Fehox may be more closely approximated by material prepared by the slow oxidation of hexaaquairon(II) [129]. This is not surprising as Fehox is thought to form from Fe^{2+} slowly diffusing upward from the anoxic to the oxic zone in natural water bodies. Laboratory preparation of consistent colloids by this oxidative method is significantly more difficult. Crystalline hematite (which has also been investigated by microscopy) is the eventual product of oxolation of bridging hydroxyl groups in the Fehox. Under natural conditions hematite formation is very slow [126,127,130].

A semi-quantitative evaluation of preparations of Fehox and its qualitative characterization by electron microscopy are presented in the following sections.

5.1.1 Observations of iron(III) hydrous oxide

The effect of copper on the aggregation properties of Fehox was evaluated in a

semi-quantitative manner. Colloids were kept for a period of weeks to several months after preparation. Two methods were used to monitor the colloidal stability of Fehox. The relative amounts of material which had settled in each solution was estimated visually. As well the relative intensity of yellow coloration of the solution (characteristic of Fehox) was also recorded. The results were averaged for colloids having the same mol ratios of Cu:Fe.

The averaged results for quantity of precipitate, determined from 44 colloids prepared in the presence of Cu^{2+}, appear in figure 5-1A. Aggregation and settling is enhanced by the presence of a small quantity of Cu^{2+}. Sufficiently large amounts of the metal ion (greater than about 0.1-0.2 Cu:Fe) actually lead to stabilization of the colloids. This observation is corroborated by the results found for coloration of the solutions (figure 5-1B). Data from 24 colloids were available in this case. The apparent limit which occurs for Cu:Fe > 0.2 is a result of the coarse scaling used for estimating. Darker discolourations were not distinguished. Complete precipitation of the Fehox was observed for Cu:Fe ratios of about 0.05. Insufficient data was available for the "post" Cu addition colloids to permit a similar "analysis".

5.1.2 Electron microscopy

Hematite particles having mean diameters of 107, 212 and 404 nm were examined by scanning electron microscopy (SEM) about one year after their receipt. This both allowed investigation of methods of sample preparation for SEM and permitted stability of the particles to be confirmed. Micrographs were compared to those appearing in [112].

As expected, the micrographs showed nearly spherical particles (with some

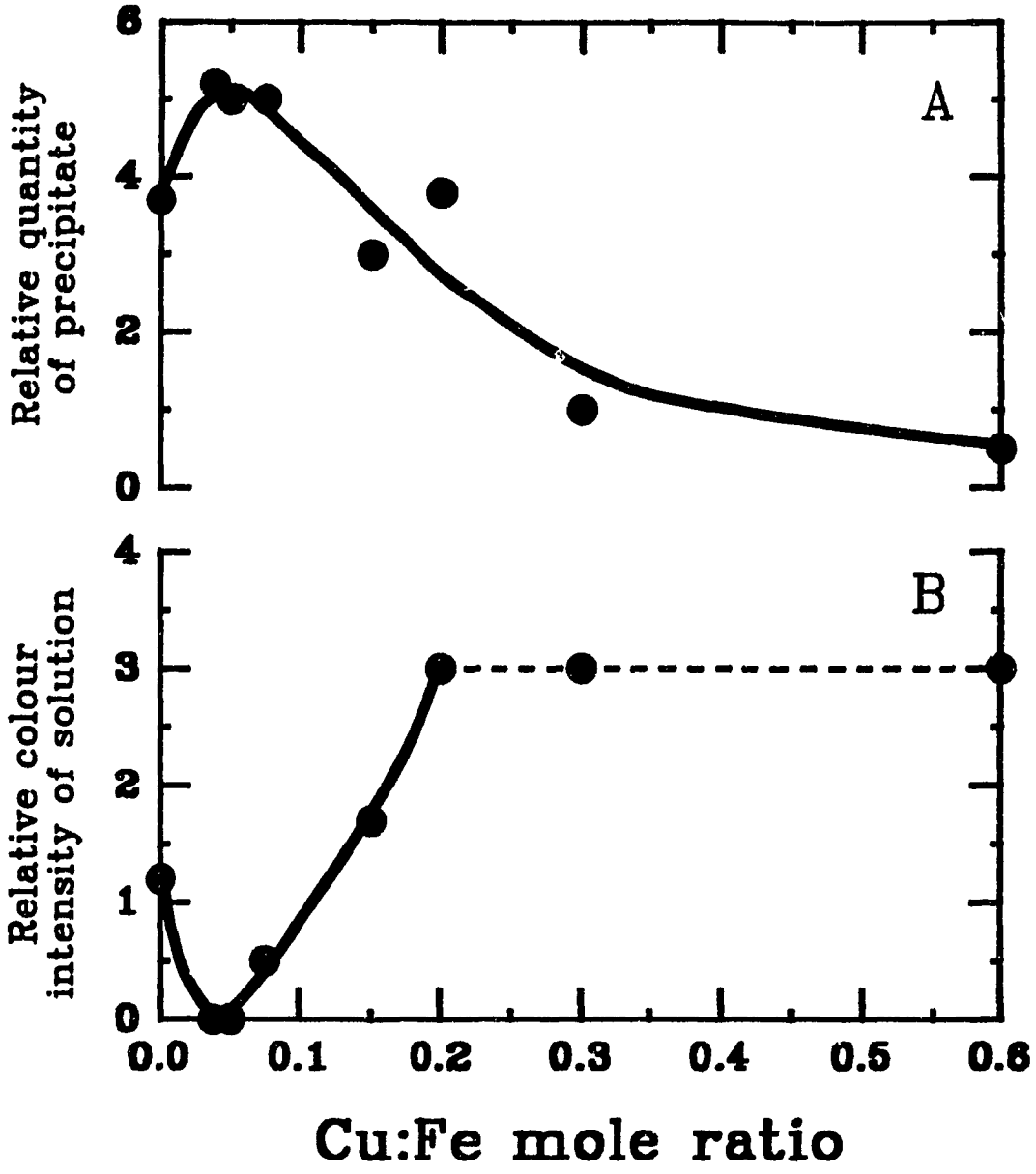

Figure 5-1: Stability of colloidal Fehox as a function of Cu:Fe mol ratio for colloids prepared in the presence of Cu^{2+}. These semi-quantitative results are based on visual estimates of the relative quantities of settled Fehox (A) and the relative intensities of yellow coloration of the overlying solution (B) for colloidal solutions which were left undisturbed for periods of weeks to months. The apparent plateau at larger Cu:Fe ratios in B is a manifestation of the course "scaling" used.

tendency toward a smoothed cubical shape) with very little variation in diameter for each size. The highly homodisperse character of the sols is demonstrated by the ratios of weight and number average particle sizes which is less than 1.03 [112]. Micrographs of the 107 nm sols show very close packing of the particles. This behaviour is similar to that observed for a thick layer of 80 nm sols obtained on a glass surface by successive deposition of small amounts of material [112]. The 212 and 404 nm samples show considerably looser packing of the particles. These materials seem to demonstrate a greater extent of "clumping" into loose aggregates. It is likely that the high degree of aggregation is a result of the relatively large amounts of material and the process of slow evaporation used in preparation of the SEM samples. Transmission electron micrographs for samples prepared by allowing particles to settle onto grids then rinsing off the excess show little aggregation of small (c. 100 nm) sols [112]. A higher degree of aggregation into "chains" is apparent for larger particles (c. 250 and 700 nm).

A series of six Fehox colloids which had been prepared at pH 5.5 with varying amounts of Cu^{2+} were also analyzed by SEM. The method of depositing the material on the sample stub by slow evaporation of the solvent under vacuum was again used. These samples were about 2000 times less concentrated than the hematite just discussed. As such the severe aggregation observed with hematite was not expected. The colloids were aged for 24 hours prior to sputtering then stored in a desiccator until analyzed by SEM.

The first series of SEM's were run after 7 days. All samples showed a high degree of polydispersity. Particle sizes ranging from < 100 nm to over 20 μm were observed (see figure 5-2A). This range of sizes is not atypical of natural Fehox. Laxen

Figure 5-2A: SEM of Fehox showing the large range of particle sizes observed. The small particles (most clearly seen at the bottom the photograph) are very spherical. Larger particles are not spherical but maintain smooth shapes.

[131] found iron hydrous oxides in several freshwater lakes to occur with a median particle size of about 1000 nm and a fairly normal distribution extending about an order of magnitude in either direction.

The largest particles (c. > 3 μm diameter) have an array of smooth shapes. All of the particles on the smaller side of this appear to be quite spherical. The absence of any fixed interfacial angles is demonstrative of the amorphous character of the hydrous oxide. In most cases particles are grouped in relatively small clusters. No clear differences in morphology could be established between pure Fehox, Fehox prepared in the presence of Cu^{2+} or Fehox with Cu^{2+} added to it.

Close inspection of some very large particles of one of the samples revealed that they actually have a detailed morphology. Round mounds 200-400 nm wide project slightly from their surfaces (figure 5-2B). The large spacing between mounds in some cases indicates that this is most likely a "growth" from the otherwise smooth surface rather than an agglomeration of small particles making up the larger ones. Larger particles for two of the other samples were checked for the presence of these mounds but none were found.

The same samples were reanalysed 19 days after their preparation using a different instrument. At this point most of the large particles showed the presence of mounds. The mounds were found to now project significantly from the particle surface and many had developed an elliptical shape. The size of the mounds was also less uniform than previously observed and their typical size had increased to about 1000 nm (figure 5-2C). Many of the large particles looked like they had partially broken away from the surface of the stub causing fractures in the sputtered coating. However, direction of the electron

Figure 5-2B: The particles at the bottom left of the micrograph show mounds which were apparent on some of the larger particles of one sample measured at 7 days.

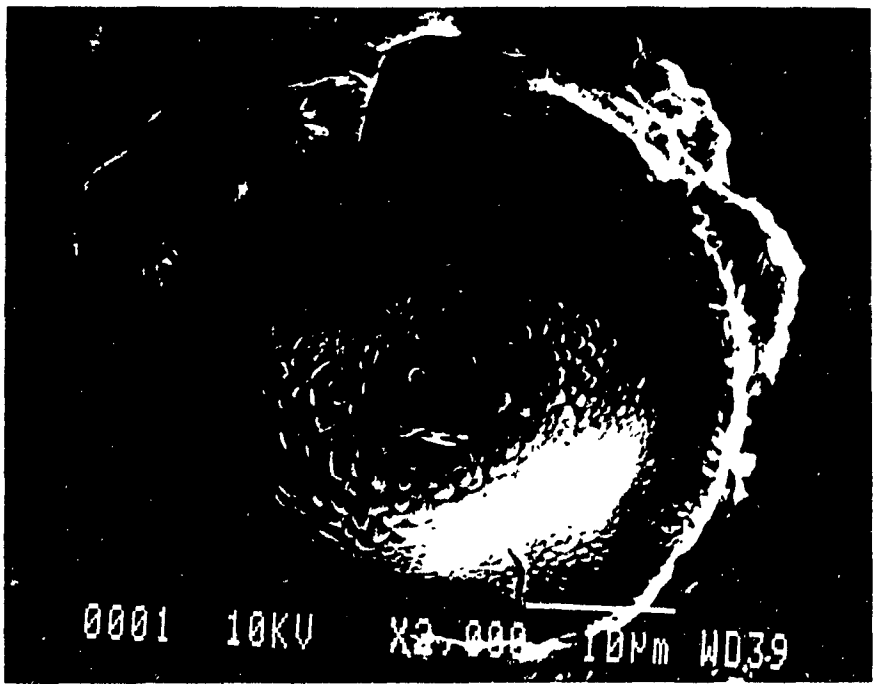

Figure 5-2C: Electron micrograph of a large particle taken 19 days after preparation of the SEM sample. Note the collapsed shape of the particle and the presence of numerous irregularly shaped mounds on its surface. The observed changes in morphology can not be unambiguously attributed to changes in the underlying Fehox.

beam into these fractures did not show any of the sparking associated with discharging even with the beam increased to 20 keV. The large masses also seemed to have flattened out to take on an annular shape. Many had lost their smooth shapes and developed sharp angles. Cracking of these large particles (sometimes severe) was also apparent.

While attempting to focus in on the mounds it was found that, over a period of 10 to 30 seconds they swelled and developed regions which appear as dark spots on the micrographs (see figure 5-2D). In some cases they appeared to burst. This only occurred when using higher magnification (c. ≥5000) although the darkened areas remained clearly visible at lower magnification. Focusing the beam onto surfaces which did not initially show the presence of mounds did not result in this decomposition even with the working distance (space between the sample and the electron beam source of the SEM) reduced from 39 to 15 mm. It is not known with any certainty that changes which occurred either between analyses or those observed during the latter measurements reflect actual changes in morphology of the underlying Fehox. As such any interpretation of the final micrographs must be viewed with caution.

Assuming that the SEM results are indicative of changes in Fehox, then it is probable that the phenomena observed result from dehydration of the hydrous oxide. Due to their gel like nature, a high sensitivity to moisture loss is not unlikely. The processes of sample preparation (solvent evaporation under vacuum), storage (desiccated) and analysis (heating by the electron beam) could all contribute to dehydration and changes in morphology. It has been speculated that bumps which develop on the large particles may be micro-crystallites [129]. This could be the incipient development of goethite or hematite. While normally very slow to form, the development of these crystalline

Figure 5-2D: Changes observed in the film when scanning at higher magnifications. Mounds were found to swell and develop regions which appear as dark spots on the micrograph.

materials may have been drastically accelerated by the conditions employed. It is pointed out that the environment in which the samples were analyzed by SEM differs tremendously from their normal solution conditions. Changes in morphology of SEM samples do not necessarily reflect changes which might occur in aqueous solution.

A more thorough investigation of the morphological properties of hydrous oxides by electron microscopy might profit from the use of a sample embedding preparation method. Prerequisite to most of these preparative techniques is solvent exchange to an organic matrix. This would undoubtedly alter the Fehox. There is, however, a water soluble melamine resin available (Nanoplast FB101) which allows hydrated samples to be embedded. Its use for the preparation of Fehox for transmission electron microscopy study is described by Perret et al. [132].

5.2 EFFECT OF LIGHT SCATTERING MATERIAL ON THERMAL LENSING ANALYSIS

It was pointed out in the introductory chapter that there are a number of types of metal complexants present in the natural environment. Among these are many based on colloidal suspensions such as dissolved organic matter and hydrous oxides. These light scattering materials can impede analysis by many optical methods. It is of utmost importance in speciation studies that natural samples be minimally perturbed prior to analysis. Pre-analysis filtration both removes the species associated with the colloids and may displace the equilibria of other species present. Problems associated with filtration itself are another factor. The results of speciation analyses after filtration may no longer

reflect the initial sample condition.

The presence of light scattering material presents some problem for sample analysis by conventional spectrophotometry. In CS the analytical signal is derived from the amount of light not transmitted through the sample. Any factor (such as scattering) which contributes to the loss of transmitted light will lead to erroneous experimental absorbance values. In thermal lensing spectrometry the analytical signal results from the amount of energy absorbed and redeposited into the solvent as heat. In this case the signal is due solely to the absorption of light energy by electronic excitation of the analyte. In theory the scatter of light does not contribute to the TLS signal. In dual beam TLS the probe beam is equally affected by light scattering matter both in the presence and in the absence of excitation. The attenuation of the pump beam power due to scattering results in a loss of sensitivity proportional to the amount of light scattered. It is a basic assumption of TLS that the exciting power remain constant over the path length of the cell. This necessitates that both scatter and absorption have a negligible effect in reducing the pump power. The effect of scatter is shown in the following [29]:

$$P_{abs} = \frac{P\alpha}{(\alpha+\alpha')} [1-e^{-(\alpha+\alpha')L}]$$

where P_{abs} is the actual amount of power absorbed by the analyte and converted to heat, P is the pump beam power, L the path length and α and α' the absorptivities for absorbance and scatter, respectively. Provided there is a minimal change in pump beam power as it traverses the sample, the scatter of light should not effect the TLS signal.

The following sections more thoroughly investigate the effect of scattering material on thermal lensing measurements. This discussion follows a progression from materials

which are pure scatterers[a] to those which both scatter and absorb light at the analytical wavelength. It is of particular importance for kinetic speciation by TLS that noise levels be low. High noise levels do not permit the resolution of minor components that is necessary.

5.2.1 Silica particles

The effect of one type of scattering material on the thermal lensing analysis of some natural organic matter has been evaluated [46,60]. Solutions of Armadale fulvic acid at pH 7.4 having absorbances of $1x10^{-4}$ to $5x10^{-3}$ were analyzed by TLS in the absence and presence of 0.01 - 0.025% SiO_2 (wt./wt. solution). The resulting curves were evaluated for linearity, detection limit and uniformity of response. It was observed that the signals remained unaffected by the presence of the SiO_2. It was concluded that TLS is insensitive to the presence of light scattering material in this region of particle concentration and that the pump beam (165 mW at 488 nm) was not measurably attenuated. This lack of susceptibility to scattering material was further supported by the observation that some of the relatively large SiO_2 particles settled during the analysis and that SiO_2 concentrations were not strictly controlled.

5.2.2 Polystyrene latex particles

To verify the silica results and to determine if particle size plays a role in the

[a] The term "pure" will be employed in the following discussion to describe two extremes. Matter which scatters light but does not absorb at the wavelength of the pump beam are termed "pure" scatterers. Those which absorb light but do not scatter it are "pure" absorbers.

effect of pure scatterers on the thermal lensing signal, spherical polystyrene latex particles were examined. Homodisperse particles having mean diameters of 176, 481 and 1090 nm were dispersed then matched by CS at 458 nm to have apparent "absorbances" of 0.050. The CS spectra appear in figure 5-3A. In spite of their apparent absorbance in the visible region, solutions of these particles are colourless demonstrating that they are pure scatterers. Solutions were further diluted and analyzed by TLS. The left side of figure 5-4 shows I_0 and I_∞ intensities and $\Delta I/I_\infty$ for these particles measured for 150 acquisitions. Although some in phase oscillation is observed, signal magnitude and noise levels appear similar for the 3 sizes of latex particles and a background solution (water). The pure absorber, $Cu(PHTTT)_3$ was measured for comparison. Although $\Delta I/I_\infty$ for this analyte is fairly large, its noise level is comparable to those of the blank and the purely scattering particles.

These results are quantified in table 5-1. The column labelled A_{458} refers to the expected apparent CS absorbance after the final dilution to the usual TLS domain. Minor differences in A_{458} were accounted for in calculations. The TLS analysis conditions for all curves in figure 5-4 and values in table 5-1 were: DEVELOPMENT DELAY = 600 ms; DECAY DELAY = 2000 ms; INTERVAL = 6 s; SCANS/ACQ. = 1000; MIXING DELAY 3.0 minutes; P_0 = 65 mW at 458 nm. Results were averaged over 150 acquisitions. Analyses were typically repeated 2-4 times. Values in the column "mean" under $\Delta I/I_\infty$ represent the average $\Delta I/I_\infty$ of the repetitions. The corresponding column "mean σ_{n-1}" contains values which are the sample standard deviations of the 150 acquisitions averaged over the number of repetitions. These values are most representative of the noise levels. Values of mean $\Delta I/I_\infty$ were compared to those

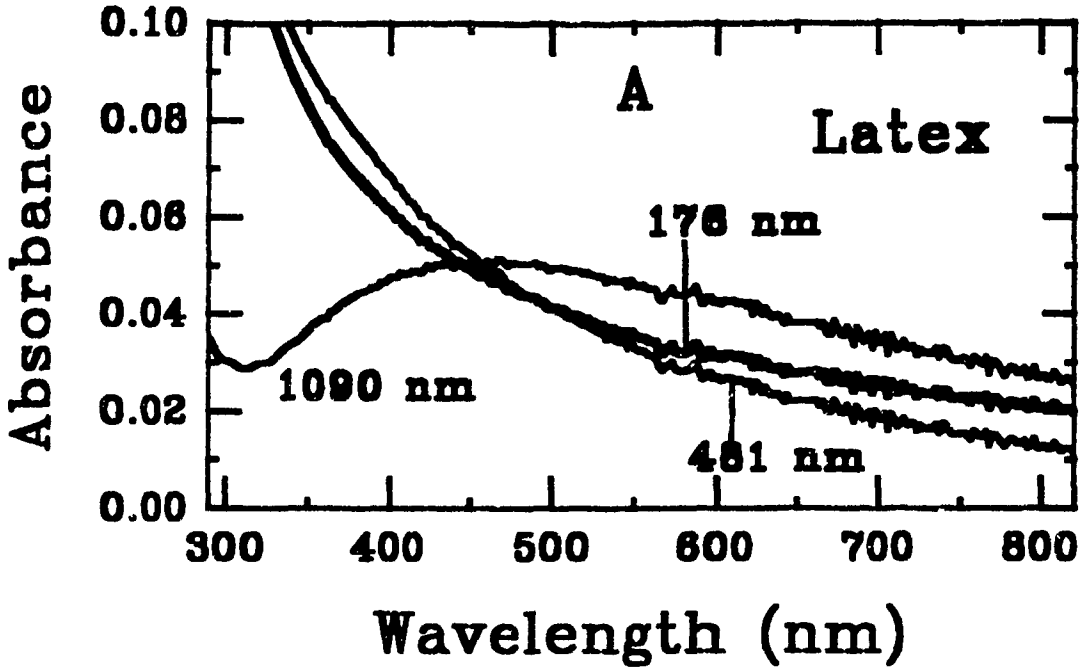

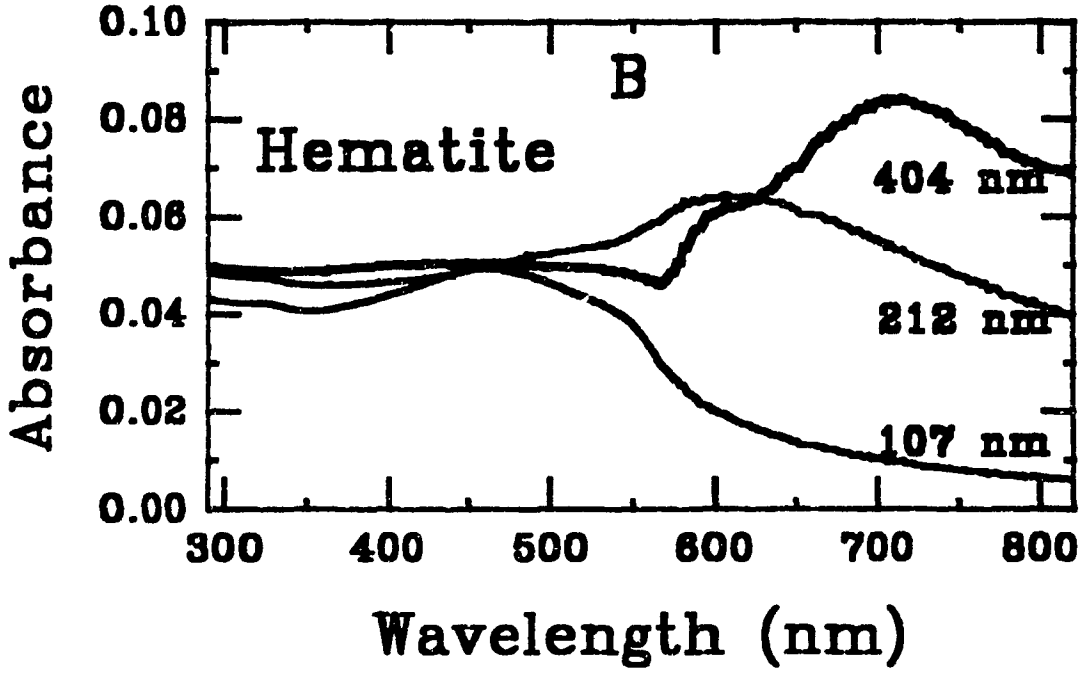

Figure 5-3: Visible spectra measured by conventional spectrophotometry for solutions of homodisperse particles. "A" shows spectra of purely scattering polystyrene latex particles. Spectra in "B" are for hematite particles which both absorb and scatter light. The mean diameters of the particles are labelled.

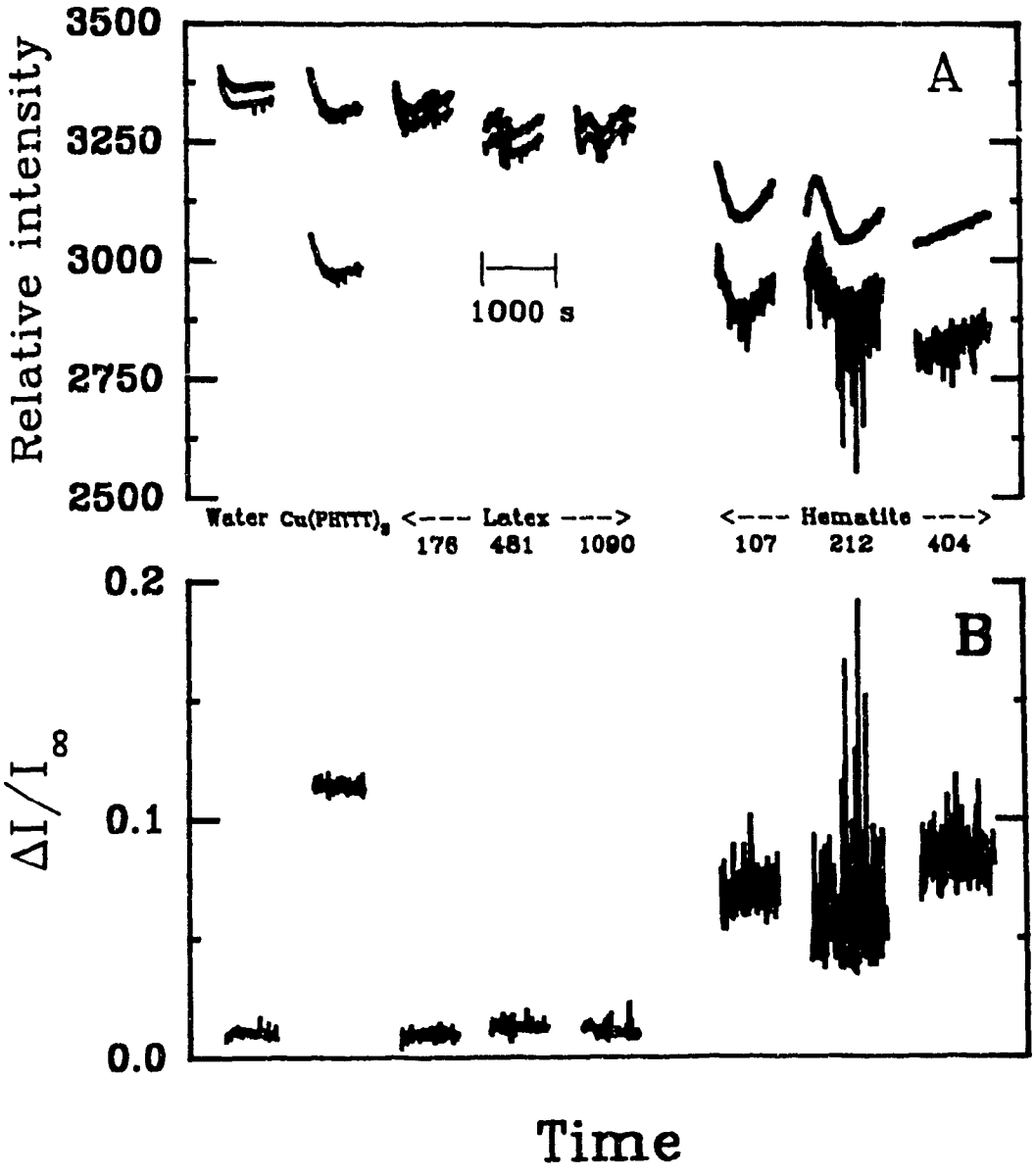

Figure 5-4: Thermal lensing results for solutions containing homodisperse particles of polystyrene and hematite. "A" shows relative intensities of I_0 and the lower intensity I_- measured over time. "B" shows the corresponding values of $\Delta I/I_-$. Note the much higher noise levels observed with the hematite, the source of which are the I_- intensities. A blank and a pure absorber are included for comparison. TLS conditions are given in the text.

Table 5-1: Noise levels observed in the laser thermal lensing analysis of colloidal suspensions of polystyrene latex and hematite.

	Concentration	Sonicated	A_{458}	$\Delta I/I_\infty$ mean	$\Delta I/I_\infty$ mean σ_{n-1}	% scattered
Latex:-176 nm	4.6×10^{8} n mL^{-1}	yes	0.0048	0.011	0.002	100 ± 10
-481 nm	3.7×10^{6} n mL^{-1}	yes	0.0049	0.013	0.002	98 ± 5
-1090 nm	2.8×10^{5} n mL^{-1}	yes	0.0050	0.012	0.002	99 ± 8
Water				0.010	0.002	---
$Cu(PHTTT)_3$	3.8×10^{-8} M		0.0050	0.117	0.002	0
Hematite-107 nm	2.0×10^{-6} M Fe	yes	0.0049	0.088	0.005	26 ± 2
-212 nm	8.4×10^{-5} M Fe	yes	0.0049	0.073	0.010	40 ± 3
-404 nm	8.0×10^{-6} M Fe	yes	0.0050	0.091	0.008	23 ± 7
Water				-0.010	0.001	---
$Cu(PHTTT)_3$	~3.4×10^{-7} M		~0.0044	0.095	0.002	0
Hematite-107 nm	2.5×10^{-6} M Fe	no	0.0049	0.071	0.007	30 ± 2
-212 nm	1.2×10^{-4} M Fe	no	0.0048	0.061	0.021	37 ± 3
-404 nm	8.5×10^{-6} M Fe	no	0.0051	0.085	0.009	21 ± 16

measured for the pure absorber. This allowed determination of the fraction of "absorbance" as measured by conventional means which is due to scattering rather than electronic excitation. This is shown in the column "% Scattered". Errors in this last column represent 95% confidence limits based on replicates.

From these results it is clear that latex particles having a significant range of sizes do not contribute to a TLS signal nor do they increase noise levels beyond those observed for non-scattering samples.

5.2.3 Homodisperse hematite

The results obtained in the previous section for a pure scatterer may be easily contrasted to those observed for a material which both scatters and absorbs in the analytical wavelength region. Approximately spherical homodisperse hematite particles having mean diameters of 107, 212 and 404 nm were again absorbance matched at 458 nm by dilution with water (figure 5-3B). These were further diluted and analyzed by TLS.

The hematite particles were studied on two occasions. In the first instance, the stock solutions of hematite were vigorously shaken prior to diluting for absorbance matching. Although the stock solutions were supposed to be of similar concentrations it was observed that the 3 particle sizes demonstrated quite different characteristics. The stock solution containing the intermediately sized 212 nm particles required an order of magnitude less dilution than those containing the larger and smaller sizes. Upon dilution, the 107 nm particles displayed an orange colour while the 404 nm particles appeared as redish-orange. The 212 nm size maintained the distinct brownish colour typical of the

concentrated stock solutions. In spite of the lesser dilution, the solution containing the 212 nm particles appeared significantly less "cloudy" than the others. These factors led to question of the efficiency of dispersion.

These results were repeated on another occasion after repeptizing the stock solutions by sonication. Results for both sets appear in table 5-1. This second set of results were measured at the same time and under the same conditions as the latex particles as reflected by the line dividing the table. The improved dispersion of the 212 nm particles results in a significant decrease in the associated noise level but has little if any effect on the other two particle sizes. The source of the anomalous behaviour of the 212 nm particles remains unclear.

For both sets, noise levels are significantly higher than those observed for water, a pure absorber or the purely scattering latex particles which, it is pointed out, are of similar particle diameter. Figure 5-4 shows the source of the noise to be large fluctuations in the I_- intensities. The major difference of the colloidal hematite from the other materials discussed here is that it is neither a pure absorber nor a pure scatterer. As shown in table 5-1 20-40% of the absorbance measured by CS is a result of light scatter.

5.2.4 Other chemical systems

Data derived from a number of experiments performed on other chemical systems are presented in table 5-2. This data was collected on different occasions (indicated by the lines separating experiments in the table) over a long period of time. This fact has several implications. First, day-to-day variations in sensitivity and noise levels occur.

Table 5-2: Noise levels observed in several chemical systems studied by thermal lensing. "% Scattered" is the fraction of A_{458} as measured by conventional spectrophotometry which results from light scatter by the absorbing species as opposed to electronic excitation. Values in parenthesis have been determined by extrapolation or comparison some of which may not be valid.

			$\Delta I/I_-$		
Notes	Solution analyzed	A_{458}	mean	mean σ_{n-1}	% Scattered
1	water		0.017	0.003	---
	$Cu(PHTTT)_3$ standards	0.0012	0.046	0.001	0
		to 0.0048	0.145	0.003	0
a,b,1	Cu-Fehox + PHTTT	(0.0009)	0.038	0.011	
		to(0.0029)	0.128	0.008	
a,c,1	Cu-Fehox(post) + PHTTT	(0.0016)	0.062	0.010	
		(0.0032)	0.137	0.007	
1	water		0.000	0.003	---
	SSA (blank)	0.0005	0.002	0.004	0
	$Fe(SSA)_3$ standards	0.0025	0.035	0.004	0
		to 0.0087	0.129	0.004	0
d,1	Fehox(pH 5.5) + HCl	(0.0021)	0.040	0.014	
	(pH 6.0)	(0.0036)	0.030	0.020	(<47)
	(pH 6.7)	(0.0037)	0.032	0.017	(<38)
d,1	Fehox(pH 5.5)+HCl+SSA	(0.0040)	0.058	0.027	
	(pH 6.0)	(0.0054)	0.038	0.027	
	(pH 6.7)	(0.0051)	0.040	0.022	

Table 5-2: - continued

Notes	Solution analyzed	A_{458}	$\Delta I/I_-$ mean	$\Delta I/I_-$ mean σ_{n-1}	% Scattered
e,2	water		-0.018	0.001	---
	blank + PHTTT		0.004	0.002	0
	Cu^{2+} + PHTTT	0.0040	0.108	0.003	0
e,2	Fehox (no Cu) + blank		0.032	0.041	
	Fehox (no Cu) + PHTTT		0.068	0.034	
3	water		-0.012	0.001	---
	stock PHTTT	0.0031	-0.002	0.002	0
	$Cu(PHTTT)_3$ standards	(0.0020)	0.012	0.002	0
		to 0.0099	0.088	0.004	0
f,3	HA + PHTTT	0.0059	0.037	0.004	(64 ± 24)
a,f,3	HA + Cu + PHTTT	0.0122	0.095	0.003	(61 ± 55)
a,4	cis-$[Co(en)_2Cl_2]^+$ + HCl	0.0032	0.058	0.001	0
1	water		-0.021	0.003	---
	Br_2 stds. in dil. H_2SO_4	0.0010	0.014	0.003	0
		to 0.0035	0.127	0.005	0

Table 5-2: continued

Notes:

a) Noise was measured after reaction had neared completion.

b) Fehox formed in the presence of various concentrations of Cu^{2+}.

c) Formation of Fehox followed by the addition of an aliquot of Cu^{2+}.

d) Noise was measured during initial part of reaction since Fehox is breaking down under the acidic conditions.

e) All solutions were handled in the same manner (mixed just prior to placing in the cell) expressly for comparison of noise levels.

f) HA refers to Laurentide humic acid.

Thermal lensing conditions:

1) DEVELOPMENT DELAY = 600 ms; DECAY DELAY = 2000 ms; INTERVAL = 6 s; SCANS/ACQ. = 1000; P_0 = 65 mW.

2) DEVELOPMENT DELAY = 500 ms; DECAY DELAY = 1200 ms; INTERVAL = 10 s; SCANS/ACQ. = 1000; P_0 = 65 mW.

3) DEVELOPMENT DELAY = 900 ms; DECAY DELAY = 3000 ms; INTERVAL = 15 s; SCANS/ACQ. = 900; P_0 = 68 mW (Spectra-Physics model 2020 Ar^+ laser).

4) DEVELOPMENT DELAY = 500 ms; DECAY DELAY = 1200 ms; INTERVAL = 6 s; SCANS/ACQ. = 1000; P_0 = 65 mW.

Sensitivity changes are largely due to slight differences in optical alignment. Noise levels may be influenced by such factors as fluctuations in source voltage and building vibration. It was clearly observed (though not quantified) that noise was significantly lower at night when the building was vacated and ventilation systems were shut down. (For a complete discussion of factors influencing noise levels in this system see chapter 4 of [46]).

A second implication is that there are some differences in TLS parameters used on various occasions as many of the experiments were conducted prior to "optimal" conditions being established. The parameters are, however, fairly consistent for all the data shown and are listed as numerical notes in table 5-2. No trends in behaviour related to the TLS conditions used are observed. All experiments shown (as well as those in table 5-1) were carried out using the fill-drain cell.

Finally, most of the experiments reported here were not designed and conducted specifically for the study of noise levels. As a result there are some gaps in the data. Where possible these missing pieces of information have been calculated by extrapolation or assumption. Such values (contained within parenthesis in the table) should be viewed with a degree of caution.

Some general observations may be made concerning the results in table 5-2. Although the magnitude of $\Delta I/I_\infty$ of the background (water) varies somewhat, the noise levels (mean σ_{n-1}) are relatively low and consistent, ranging from 0.001 to 0.003. Noise levels for solutions which do not scatter light tend to be slightly higher than background but do not exceed 0.004. Further, where analyses were performed over a range of concentrations (and hence of $\Delta I/I_\infty$) for a purely absorbing analyte, noise levels are only slightly higher for the larger signals. Unlike the hematite and latex particles, these

solutions were not absorbance matched by CS. As noted, for a pure absorber noise levels vary only slightly with concentration. Whether this relationship is also true for the partial absorbers is uncertain.

Since iron hydrous oxide is of considerable importance to this overall study it is worth commenting on TLS noise levels associated with its presence. It is seen from table 5-2 that noise levels for all solutions containing Fehox are considerably higher than those containing pure absorbers only. The average noise level for Fehox containing solutions is 0.020 with values ranging from 0.007 to 0.041. Analysis of I_0 and I_- intensities for these samples once again reveals the source of the noise to be negative intensity spikes of I_-. For pure absorbers noise levels are the same for I_0 and I_- and (with the exception of the occasional I_- data point) occur randomly in the negative and positive directions.

The other scattering material shown in table 5-2 is humic acid (HA). Extremely large out of phase oscillation of the I_0 and I_- intensities observed while monitoring this system (the first time oscillation was identified) largely precluded kinetic data analysis. However, ignoring the effect of the low frequency oscillation, noise levels measured with HA present are unusually low. "% scattered" values of about 60% were calculated for the HA. The nature of the calculation was such that error in the extrapolation may have caused these estimates to be high. This possibility is supported by the relation found between the fraction of light scattered and carbon content of dissolved organic matter (DOM) [46]. For samples of DOM containing 8% and 32% carbon, light scatter accounted for 78% and 4%, respectively of the absorbance measured at 600 nm by conventional means. Since the Laurentide humic acid used here contains 52% carbon [133] it may well be expected to scatter very little light. The low noise detected with HA

present may indicate that its scattering behaviour actually approaches that of a pure absorber.

5.2.5 Comparison and significance of results

Figure 5-5 compares measured noise levels to the calculated values of % scattered light. To account for day-to-day variations in system noise, figure 5-5 shows noise levels above a background level, defined to be that measured with water in the sample cell, which was measured daily. Noise is clearly lowest for the extreme cases of pure scatterers (latex particles) and pure absorbers. Noise level seems to rise fairly quickly with increasing scattering properties of the colloidal matter. As discussed, the HA may more correctly lie close to the pure absorber end. The HA-Cu-PHTTT system is not shown in the figure since the excessive magnitude of its 95% confidence interval makes it of little use. Unfortunately none of the materials tested clearly fall into the range of >50% light scatter. It is therefore unsure how the light scattering induced noise levels will behave in this domain. An argument from continuity would imply that at some level of scattering noise will again approach low values but it remains unclear where the maximum lies. Matter which scatters more light than it absorbs (>50% scattered) may not have as detrimental an effect on the thermal lensing signal.

It has been pointed out that scatter induced noise observed for hematite and Fehox is not random. Noise tends toward larger values of $\Delta I/I_{-}$. Data handling by averaging methods (including curve fitting in the case of kinetic data) will yield estimates which are larger than the true $\Delta I/I_{-}$ values. The extent of this overestimation will be a function of the extent of light scatter. The source of differences in light scatter include the amount

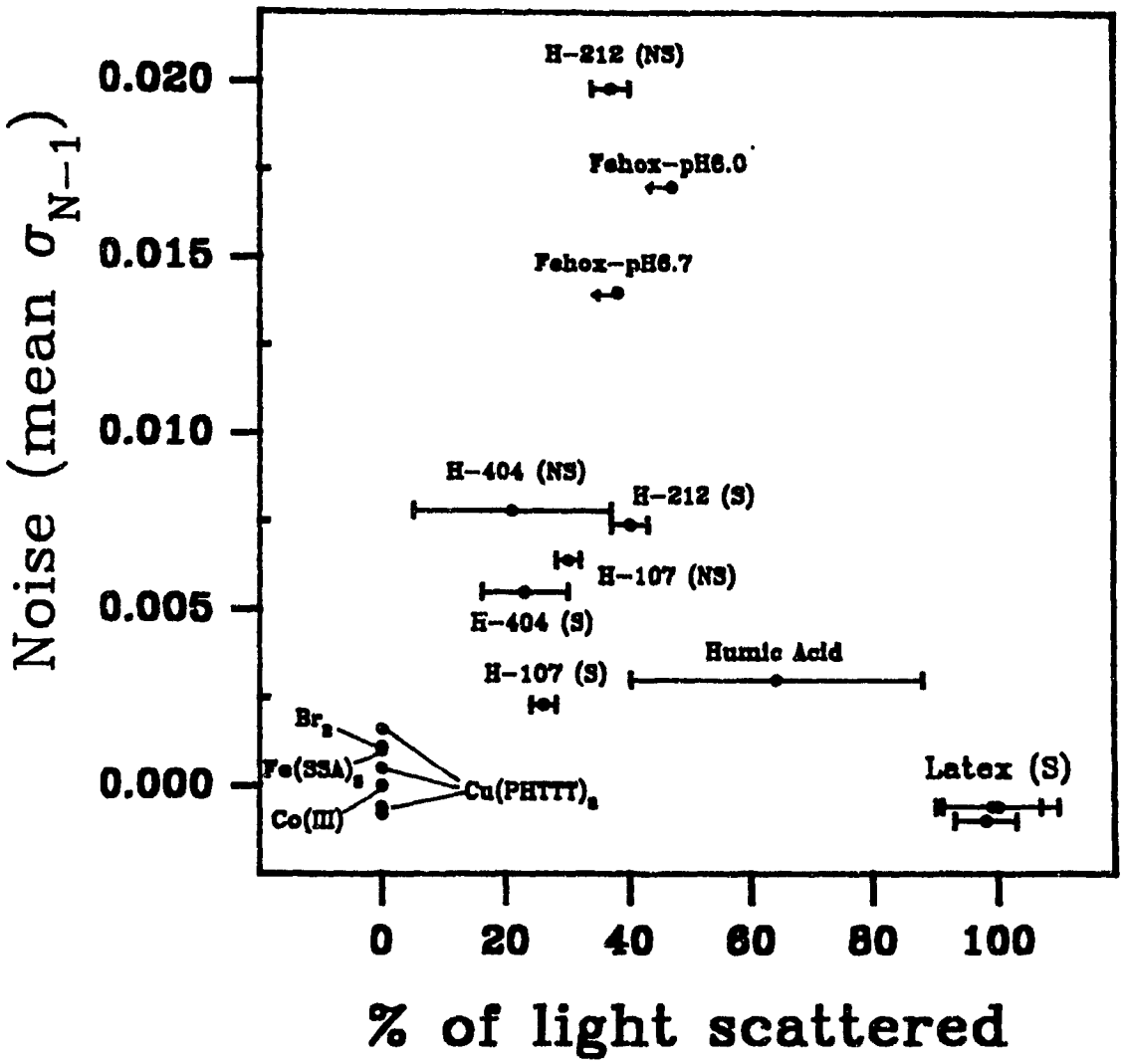

Figure 5-5: Average TLS noise levels observed for materials having a range of scattering properties. At one extreme are pure scatterers such as latex particles. At the other end are purely absorbing compounds. Intermediate are particles whose absorbance measured by CS is a combination of scattering and "true" absorbance (electronic excitation of the chromophore). Note that noise levels are significantly higher for this latter group. All values refer to measurement at 457.9 nm. Abbreviations used: H=hematite; S=sonicated; NS=not sonicated. Data are taken from tables 5-1 and 5-2.

of scattering material present and most likely the "% scatter" property related to the type of matter. This has important implications in the application of TLS analysis to samples containing matter which both absorbs and scatters light at the pump beam wavelength.

A systematic variation of noise level with "% scattered" could cause difficulty in the comparison of thermal lensing measurements made on samples having a range of scattering properties. An example of this type of application might include the determination of actual "electronic" absorbances of various dissolved organic matter (see for example references [46,60]). The relationship between the % scattered "property" and TLS noise levels warrants further investigation.

The sensitivity of noise level to light scatter also has ramifications for kinetic work. In situations where the amount of light scattered by a material does not remain constant, kinetic monitoring by conventional spectrophotometry will reflect these changes. In theory, the TLS signal is unaffected unless the true "electronic" absorbance also changes. However, since the magnitude of $\Delta I/I_-$ is a function of noise level, apparent kinetics will also be affected.

It is worth considering again the case of Fehox being mixed with 0.1 N HCl. In this situation the scattering material (Fehox) is itself being broken down. This results in a continual change in its scattering properties through the course of the reaction. In this type of case an analogy may be made between the effect of scattering on CS and TLS analyses. In the former, scattered and absorbed radiation can not be differentiated. In TLS the combined scatter/absorb properties of the Fehox lead to high noise levels. The nature of the noise is such that it leads to an average increase in the TLS signal. Since scattering decreases as the complex breaks down, noise decreases and therefore so does

the (averaged or fitted) TLS signal. It is clear that in this type of situation thermal lensing does not offer an advantage over CS absorbance monitoring. Indeed, the effect of scattering on conventional absorbance measurements has an established theoretical basis and hence is more predictable.

5.3 APPLICATION OF THERMAL LENSING TO KINETICS

A desirable expansion of the kinetic speciation work is the extension to concentrations more consistent with those found in natural systems. Thermal lensing is capable of measuring such low concentrations.

A number of studies by TLS have considered the kinetics of processes occurring on time scales shorter than the rate of lens formation. This has been accomplished by monitoring the time-resolved "profile" of thermal lens build-up. This in turn provides information on the rate of thermal energy deposition to the solvent which may be related to the rate of decay of meta-stable species. Note that the initiator of kinetics in this sense is excitation by the pump beam. Studies of this nature (which have extended into the sub-microsecond time domain) have included measurement of radical lifetimes from the photolysis of di-t-butyl peroxide [134]; quenching rates for photosensitized oxygenation of singlet oxygen acceptors [135]; gas phase vibration-vibration energy transfer in CO_2 [136] and triplet lifetimes of benzophenone [137].

One kinetic study has extended into longer time scales. Franko and Tran [138] looked at nucleophilic aromatic substitution of 1,2-dimethoxy-4-nitrobenzene for up to 40 seconds. Again the reaction was photoinitiated, the sample being continuously irradiated at 350 nm with a xenon lamp. They used a dual-beam system with modulation of the

pump beam. The rate of change of signal due to product formation in this case is still faster than lens formation and the suitable modifications to TLS theory to accommodate this are described in [139].

It appears that no studies have been reported based on the TLS monitoring of conventional kinetics with reaction initiated by the mixing of reagents.

A step-wise progression is used to demonstrate the potential and limitations for application of thermal lensing to kinetic analysis. The first step is to apply TLS monitoring in the kinetic study of a "clean" (non-scattering) chemical system.

5.3.1 Kinetics in non-scattering media (Bromination of acetone)

One of the most thoroughly studied of reaction kinetics is the halogenation of ketones. The generally accepted mechanism for the acid catalyzed reaction [140,141,142] is shown in the following scheme using acetone:

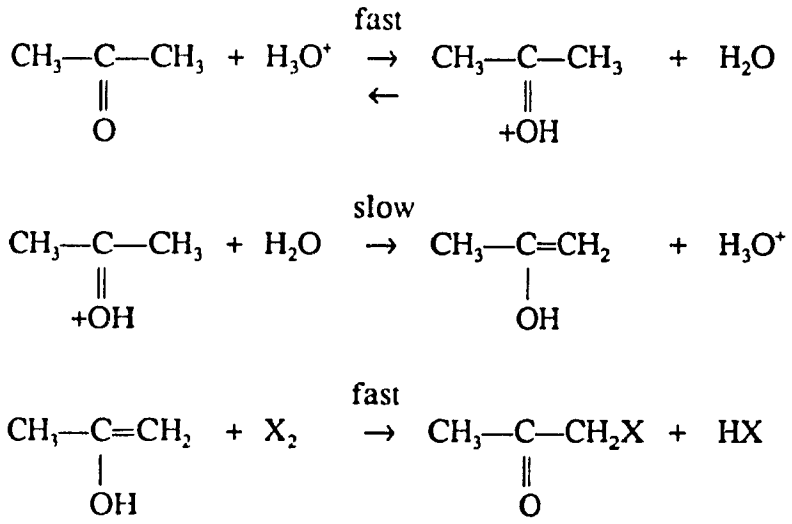

The initial step is rapid, reversible protonation of the carbonyl. This is followed

by the slow release of an α-hydrogen leading to the enol form. Final halogenation of the enol is again rapid. The rate determining step is enolization. This precedes the actual halogenation. As a result, the reaction is found to be first order in [H^+] and [ketone] but independent of halogen concentration. Further, the rate constant remains unchanged with the use of different halogens.

The rate of bromination of acetone was measured by both conventional spectrophotometry and thermal lensing. The decrease in bromine concentration was monitored at 458 nm by both methods as well as at 394 nm (the Br_2 absorption maximum) by CS. The molar absorptivity of Br_2 is 174 M^{-1} cm^{-1} at 394 nm and 90 M^{-1} cm^{-1} at 458 nm (determined as described in section 4.4.2.1). Reactions monitored by TLS were carried out using bromine and acetone at concentrations two orders of magnitude lower than those measured by CS. Acid concentration ([H^+] = 0.0602 M) was the same in all kinetic solutions.

To allow a more rigorous comparison of the two techniques, the concentration of acetone was varied allowing determination of its reaction order. Figures 5-6 and 5-7 show some of the results obtained by CS and TLS, respectively. A linear decrease in concentration of Br_2 is clearly observed consistent with its zero order dependence The dependence on acetone concentration is also clearly evident. The overall results are summarized in tables 5-3 (CS) and 5-4 (TLS). It may be noted that significant variation in initial concentrations of Br_2 occurred in solutions analyzed by both techniques as a result of the volatility of Br_2. Zero order [Br_2] dependence leaves the rates calculated for the disappearance of bromine unaffected.

Average rate constants of $5.3(\pm0.3)\times10^{-5}$ M^{-1} s^{-1} and $5.4(\pm0.2)\times10^{-5}$ M^{-1} s^{-1} found

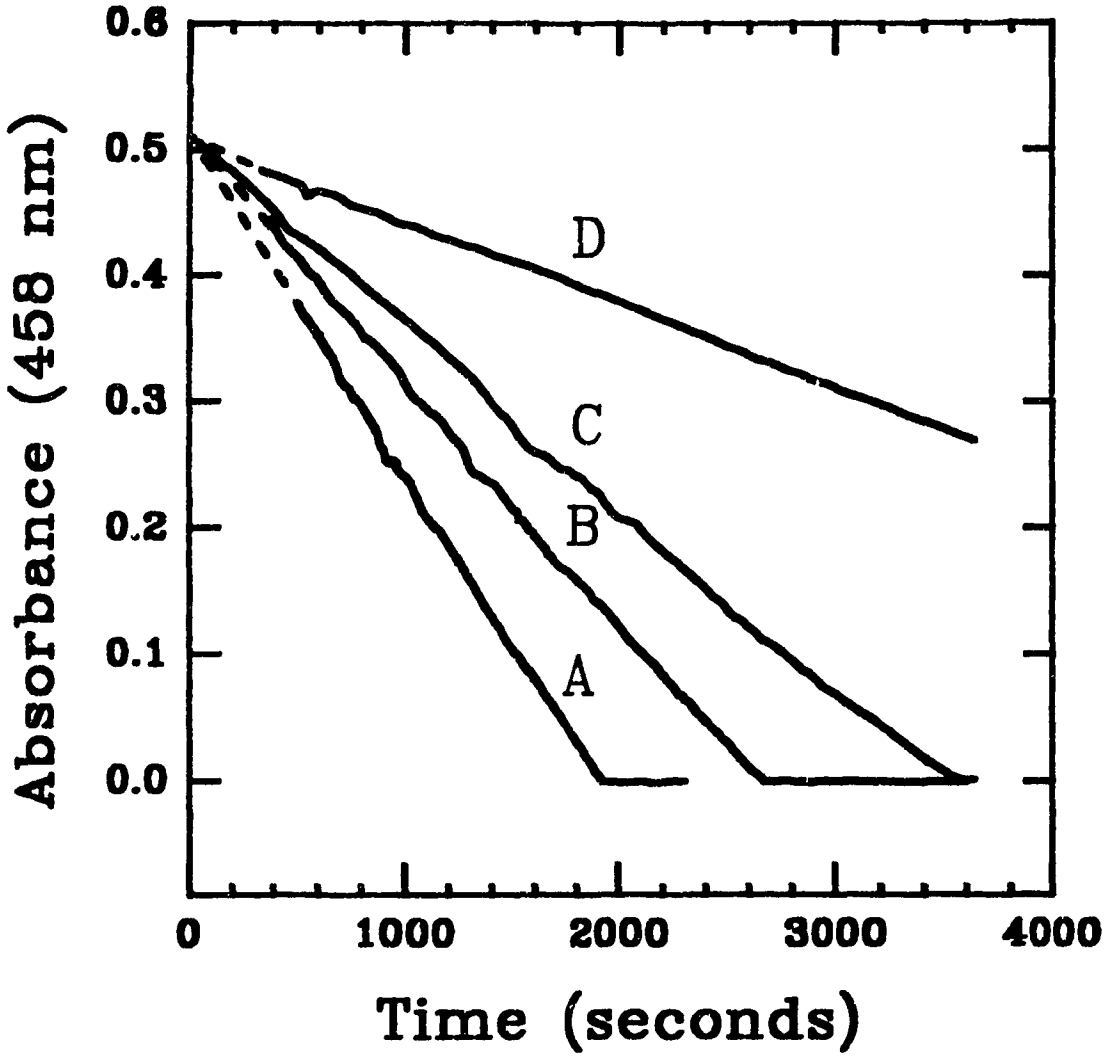

Figure 5-6: Bromination of acetone monitored at 458 nm by conventional spectrophotometry. The curves correspond to acetone concentrations of: A) 1.00 M; B) 0.700 M; C) 0.500 M and D) 0.200 M. Concentration of acid catalyst is 0.0602 M H^+ in all cases. Curves have been adjusted along the time axis to reflect a common initial concentration of Br_2. This more clearly shows the effect of acetone concentration on rate.

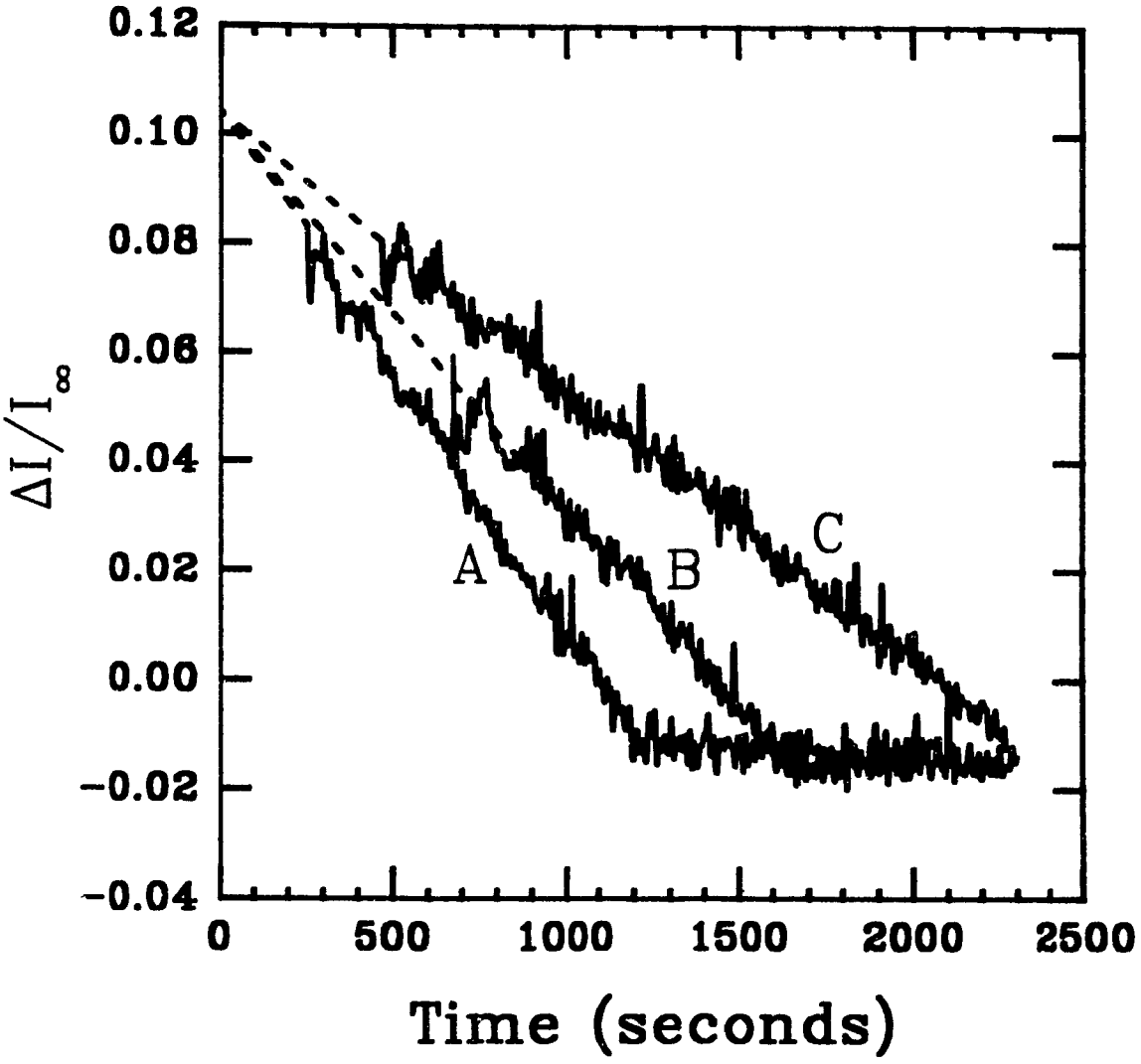

Figure 5-7: Some of the results obtained for the bromination of acetone measured by TLS. Acetone concentrations were: A) 10.0×10^{-3} M; B) 7.00×10^{-3} M and C) 5.00×10^{-3} M. Time scales of curves B and C have been adjusted to reflect a common initial concentration of bromine. Thermal lensing parameters were: DEVELOPMENT = 600 ms; DECAY = 2000 ms; INTERVAL = 6 s; SCANS/ACQ = 1000 and P_0 = 65 mW at 457.9 nm.

Table 5-3: Rate results obtained by conventional spectrophotometry for the bromination of acetone at $[H^+]$ = 0.0602 M. Reactions were monitored at both 394 nm (Br_2 absorption maximum) and 458 nm. Temperature was controlled at 25.0 ± 0.1 °C.

[acetone] (M)	$[Br_2]_{init}$[1] (M)	Wavelength (nm)	$A_{initial}$	Rate ($x10^8$ M s^{-1})	k ($x10^5$ M^{-1} s^{-1})
0.200	0.0054	394	0.937	66.1	5.49
		458	0.486	72.4	6.01
0.500	0.0057	394	1.005	164	5.45
		458	0.502	162	5.38
0.700	0.0058	394	1.049	224	5.32
		458	0.507	214	5.08
1.00	0.0042	394	0.753	302	5.02
		458	0.372	297	4.93
					5.3 ± 0.3

[1] Values calculated from initial absorbance (kinetic time zero).

Table 5-4: Thermal lensing results for the bromination of acetone with $[H^+] = 0.0602$ M. All results refer to 458 nm. Solutions were not thermostated but the ambient temperature in the enclosed area near the cell remained fairly constant at 25.3 ± 0.2 °C.

[acetone] ($x10^3$ M)	$[Br_2]_{init.}$[1] ($x10^5$ M)	equivalent[2] $A_{initial}$	Rate ($x10^8$ M s^{-1})	k ($x10^5$ M^{-1} s^{-1})
2.00	2.50	0.00225	0.634	5.26
	2.74	0.00247	0.659	5.47
5.00	2.99	0.00269	1.61	5.35
	3.99	0.00359	1.73	5.75
7.00	3.03	0.00273	2.06	4.89
	2.29	0.00206	2.15	5.10
	3.33	0.00300	2.49	5.91
10.0	2.98	0.00268	3.23	5.36
	4.37	0.00393	3.28	5.45
				5.4 ± 0.2

[1] Initial Br_2 concentrations calculated by extrapolation of kinetic date to time zero.
[2] Absorbance at 458 nm corresponding to the initial $[Br_2]$.

by CS and TLS analyses, respectively are in very good agreement. This is exemplified in figure 5-8 which shows the reaction order for acetone determined over nearly three orders of magnitude. As shown in the figure, reaction order was more accurately determined by thermal lensing than by conventional spectrophotometry. In both cases internal consistency is observed with sample correlation coefficients of >0.999 by CS and >0.995 by TLS. This may indicate lesser difficulty posed by volatile materials when working with dilute solutions.

It is impressive that continuity is observed in results obtained over such a wide range of concentration. As seen in table 5-4 total absorbance changes for most of the reactions measured by TLS were less than 0.003. Given the initial data lost due to the MIXING DELAY, absorbance changes of <0.002 were actually monitored in some cases. Indeed, with the use of a slightly higher pump beam power the concentration range covered could have been extended by another order of magnitude.

Initial attempts at the monitoring of kinetics in a non-scattering medium looked at the acid hydrolysis of some cobalt(III) complexes, particularly cis-dichlorobis(ethylenediamine)cobalt(III) perchlorate. A time dependent change in the observed signal was discernable. The difference, however, was quite small in comparison to the background signal and not readily amenable to quantitative characterization. Analysis by conventional spectrophotometry showed that the blue shift in the absorption band caused by replacement of chlorine by the stronger field ligand OH_2 was relatively small in the wavelength region accessible by the TLS pump beam. Other similar complexes were expected to suffer from the same difficulty. As a result, a more suitable

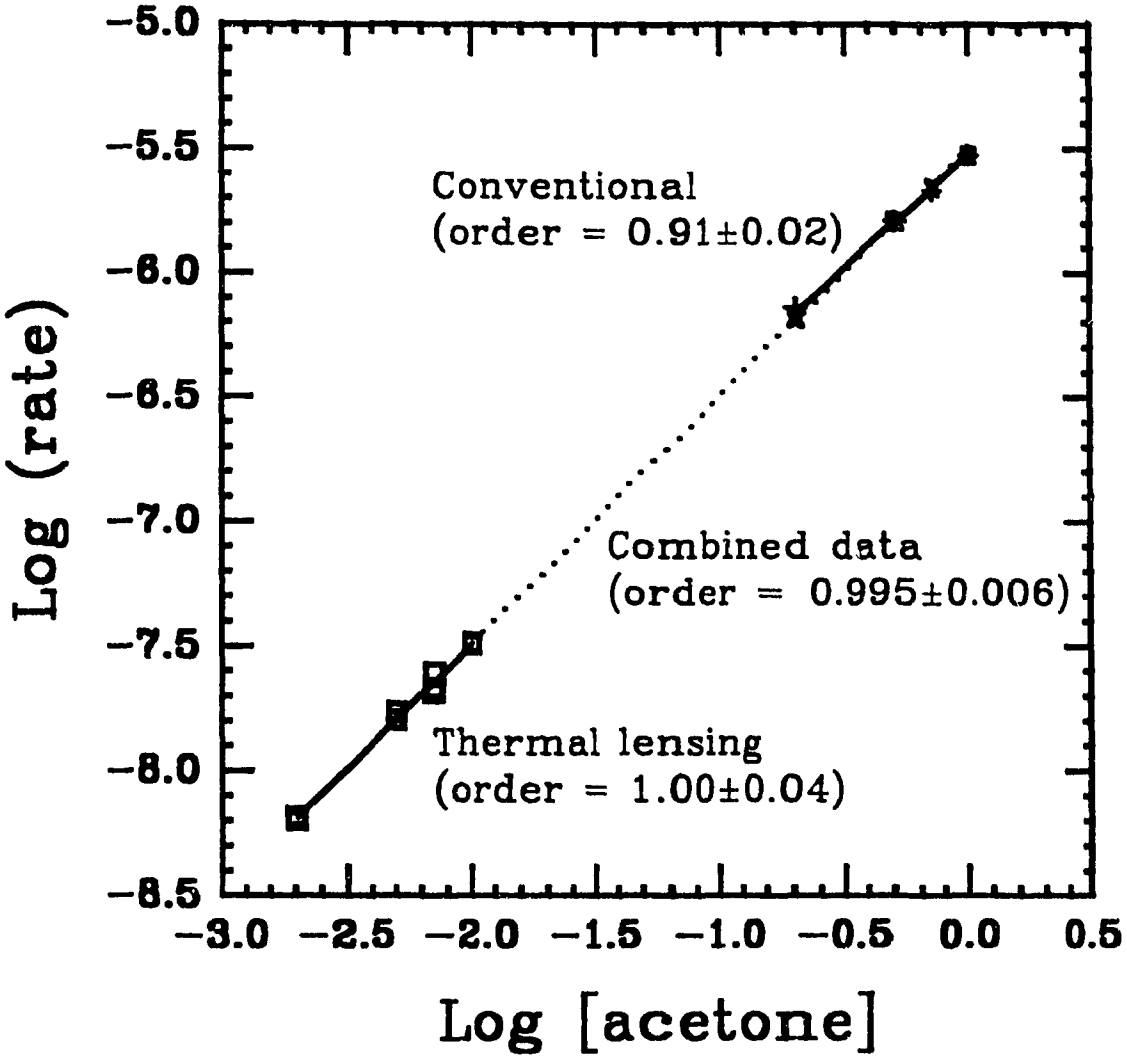

Figure 5-8: Effect of acetone variation on the rate of its bromination. The reaction was monitored at high concentrations by conventional absorbance measurement and at concentrations two orders of magnitude lower by thermal lensing. Measurements by CS were made at both 394 nm (X) and 458 nm (+). TLS conditions have been given in figure 5-7.

chemical system was sought. This example serves to exemplify the weakness of TLS in the monitoring of samples having a high background absorbance. Some studies of thermal lensing background correction using differential measurement have been reported [143,144].

5.3.2 Iron(III) hydrous oxide in an acid medium

The monitoring of kinetics using the thermal lens effect was also applied to the study of acid hydrolysis of Fehox. The liberated Fe(III) species were reacted with the chromophore SSA. As described in section 3.3.1 spectrophotometric study of this chemical system revealed three components in the initial solution. Monomeric Fe(III) had a rate constant (k_1) of 0.89 s^{-1}. A second component had $k_2 = 7.0 \times 10^{-4}$ s^{-1}. A final more slowly reacting component was related to larger (possibly crystalline) particles.

Monitoring of the reaction of Fehox with HCl with no chromophore present revealed some odd features. Absorbance measured by CS showed a rapid initial decrease, the duration of which may be loosely related to a period of very high noise levels and a decrease in I_0 and I_- intensities observed by TLS. The electronic transitions making up the absorption spectrum of Fehox are quite complex. The data collected here are insufficient to describe changes in it. It does, however, seem plausible that these observations may be explained by variations in scattering species and shifts in the energies of absorptions. Spectra of Fehox measured a long time after reaction with acid show bands which may be related to those quantified by Schugar and coworkers [145].

It is clear that processes occurring early in the reaction are rather complex and

lead to significantly elevated noise levels in signals measured by TLS. The kinetics of this system have already been thoroughly studied at higher concentration (see section 3.3.1). It is the goal of this work simply to extend this study to lower concentrations using TLS. With this objective in mind, noisy data observed at short times was omitted from kinetic data analysis. Further, variation of background absorbance was also omitted as this enhanced noise in the TLS results. This allows comparison of CS and TLS kinetic results without the unnecessary complication.

Of the three expected components in this system, only the middle one should be observed within the time constraints used in these experiments. The fastest component is only readily monitored by stop flow techniques. The third is extremely slow to react and therefore makes negligible contribution. Trial analysis of several data sets using the Laplace method gave no evidence of more than one component. On this basis the kinetic data were handled using first-order analysis methods.

Data obtained for this system by TLS monitoring were fairly noisy. Preparation of the data for fitting to a first-order rate law required smoothing as described in section 4.5.2.2. Briefly this involved manual removal of "spikes", application of a Blackman filter and polynomial fitting. Results were fit as first-order both before and after polynomial fitting.

Table 5-5 shows results of first-order analysis of data collected by CS. The differences in results between values at the two wavelengths is explained by misestimation of the background signal. This translates to a misestimation of A_∞. The higher rate constants obtained at 458 nm are associated with the larger background signal at this wavelength and are the less reliable.

Table 5-5: Results obtained from conventional absorbance data for the reaction of Fehox with the chromophore SSA in an acidic matrix. Absorbance data measured at both 458 and 502 nm have been analyzed by three first-order methods. In all cases the conditions during reaction were: [HCl] = 0.0500 M; [Fe(III)] = 7.80×10^{-5} M; [SSA] = 7.50×10^{-3} M; T= 25.0±0.01°C.

Colloid pH[1]	Colloid Age[2] (hours)	Observed rate constants ($\times 10^4$ s^{-1})					
		Kezdy-Swinbourne		First-order		Guggenhein	
		458	502	458	502	458	502
5.5	13	4.9	4.3	4.8	4.3	4.72	4.2
	39	5.0	4.4	5.0	4.4	4.8	4.1
	54	4.9	4.5	5.0	4.5	4.9	4.3
6.0	15	10.0	7.2	10.0	7.0	9.8	7.1
	42	8.2	6.2	8.1	6.2	8.3	6.2
	52	7.4	5.9	7.4	6.0	7.4	5.9
6.7	17	6.9	5.3	7.1	5.3	7.1	5.1
	45	6.8	5.4	6.8	5.4	6.8	5.9

1) Colloid pH during aging.
2) Time from end of colloid preparation to start of kinetic analysis.

The results from TLS analysis measured at 10-fold lower concentrations than by CS appear in table 5-6. Values which are considered of lower reliability are indicated in brackets. During data analysis these values were found to either vary somewhat with the fitting conditions used or exhibited poor linear correlation of the first-order plots.

The overall rate constants from both TLS and CS analyses are summarized in table 5-7. Internal consistency of TLS and CS results is reasonable. The difference between the two sets of results, however, appears to be significant and possibly indicates a change in the colloid characteristics on dilution to the TLS concentration domain. This is an important point. It illustrates the need to do model studies at "realistic" concentration levels.

5.4 EQUILIBRIUM SPECIATION OF COPPER(II)

Some of the ferric hydrous oxides prepared in the presence of Cu(II) were analyzed using a "separation" method. After having aged for 24 hours, part of the colloidal solutions were filtered through pores sufficiently small (0.45 μm) to retain the Fehox. The concentration of copper in the filtrate was used as a measure of the free copper in the initial solution. This is one of several equilibrium speciation methods frequently found in the literature. It was found that results obtained in this way adhere well to Langmuir isotherm. The Langmuir treatment is derived under the assumption of uniform, non-interacting adsorbing sites. Adherence to it provides no hint of site heterogeneity.

Table 5-6: Thermal lensing results for the reaction of Fehox with SSA in an acid medium. Data were smoothed two ways and fit by 3 first-order methods. Solution conditions during reaction: [HCl] = 0.0500 M; [SSA] = 7.50×10^{-4} M; T = 24.6 ±0.1°C. Thermal lensing monitoring conditions were: DEVELOPMENT DELAY = 600 ms; DECAY DELAY = 2000 ms; INTERVAL = 6 s; P_0 = 65 mW at 457.9 nm.

Colloid pH[1]	Colloid age[2] (hours)	$[Fe]_{Kin}$ ($\times 10^6$ M)	Observed rate constant ($\times 10^4$ s^{-1})					
			Blackman filtered			Blackman + poly. fit		
			K.-S.	1st	Gugg.	K.-S.	1st	Gugg.
5.5	45	7.80	4.2	4.2	4.0	3.7	3.8	(4.0)
	52	6.24	(3.0)	3.2	3.2	3.2	3.2	(3.2)
6.0	48	7.80	(5.3)	4.1	(3.4)	(3.7)	3.7	(3.3)
	56	6.24	4.6	4.1	(2.3)	(4.1)	3.9	(3.9)
6.7	54	6.24	2.4	2.6	--	2.3	2.4	(2.7)
	58	6.24	4.5	(4.2)	(4.0)	3.7	3.8	3.8

1) Colloid pH during aging.
2) Time from end of colloid preparation to start of kinetic analysis.

Table 5-7: Summary of rate constants determined from conventional absorbance and thermal lensing data for the reaction of Fehox with SSA in an acid medium. Detailed results are given in tables 5-5 and 5-6.

		Average rate constant ($x10^4$ s^{-1})		
		pH 5.5	pH 6.0	pH 6.7
Conventional:	-458 nm	4.9 ± 0.1	8.5 ± 0.8	6.9 ± 0.2
	-502 nm	4.3 ± 0.1	6.4 ± 0.4	5.4 ± 0.3
Thermal lens (457.9) nm:				
Blackman		3.6 ± 0.6	4.0 ± 1.1	3.5 ± 1.2
+ Polynomial fit		3.5 ± 0.4	3.8 ± 0.3	3.1 ± 0.8
+ Background removal			2.1 ± 0.8	2.8 ± 0.4

5.5 KINETIC SPECIATION OF Cu(II) BY CONVENTIONAL SPECTROPHOTOMETRY

Ferric hydrous oxide colloids were prepared under a wide range of conditions. The composition of the solutions had 5-fold variations of both copper and iron concentrations with Fe:Cu mole ratios ranging from 1.6 to 26. pH's ranged from 4.5 to 7.0 covering a region of varying adsorption properties. The reaction of Cu(II) in the solutions with the chromophore PHTTT under conditions of constant pH, ionic strength and temperature was monitored by CS. An example of the change in absorbance with time for a solution of Fehox prepared in the presence of Cu upon reaction with the chromophore/buffer solution is shown in figure 5-9. All results were analyzed using the Laplace transform method for determination of the number of components and initial estimation of their associated rate constants and component contributions followed by non-linear regression based on these estimates. The smoothing of noise in the measured absorbance-time profile using a least squares polynomial fit appears in figure 5-10. The result of Laplace analysis of this particular curve will be discussed in the next section.

In section 2.3 it was discussed that two criteria must be met in order to establish a chemical significance for the results obtained by kinetic speciation studies. The first of these was that the determined rate constants would reflect the constant chemical and physical conditions during reaction with the chromophore. This requires that rate constants remain stable over a range of equilibration conditions of the colloidal solutions. The second criterion is that the derived component contributions must vary in a way consistent with their chemical conditions prior to perturbation of the system.

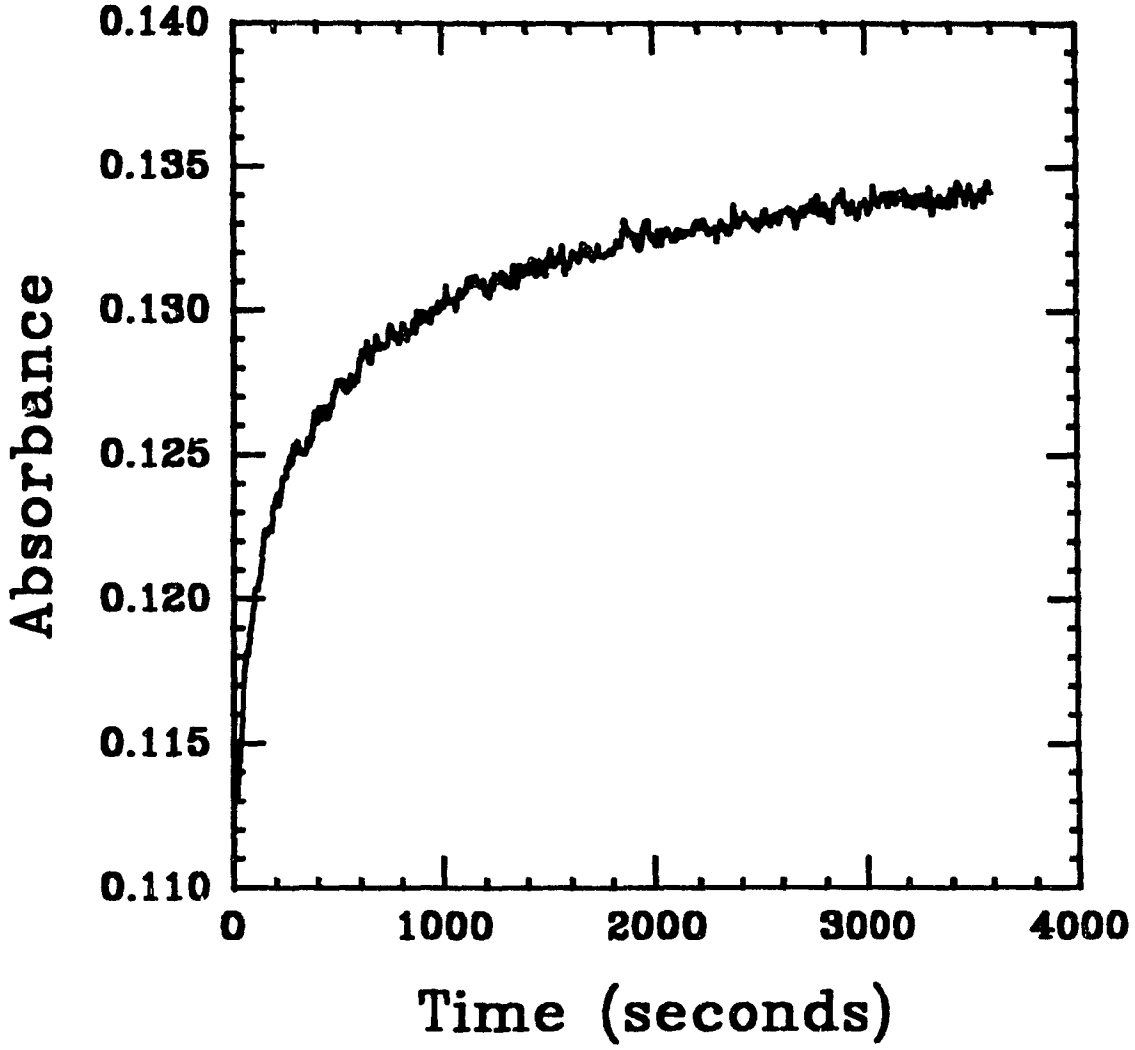

Figure 5-9: Conventional absorbance monitoring at 434 nm of the reaction between Cu(II) containing Fehox (Fe:Cu mole ratio = 19.3) prepared at pH 5.5 and the chromophore PHTTT. Although the kinetic change in absorbance is fairly small, the noise level is low.

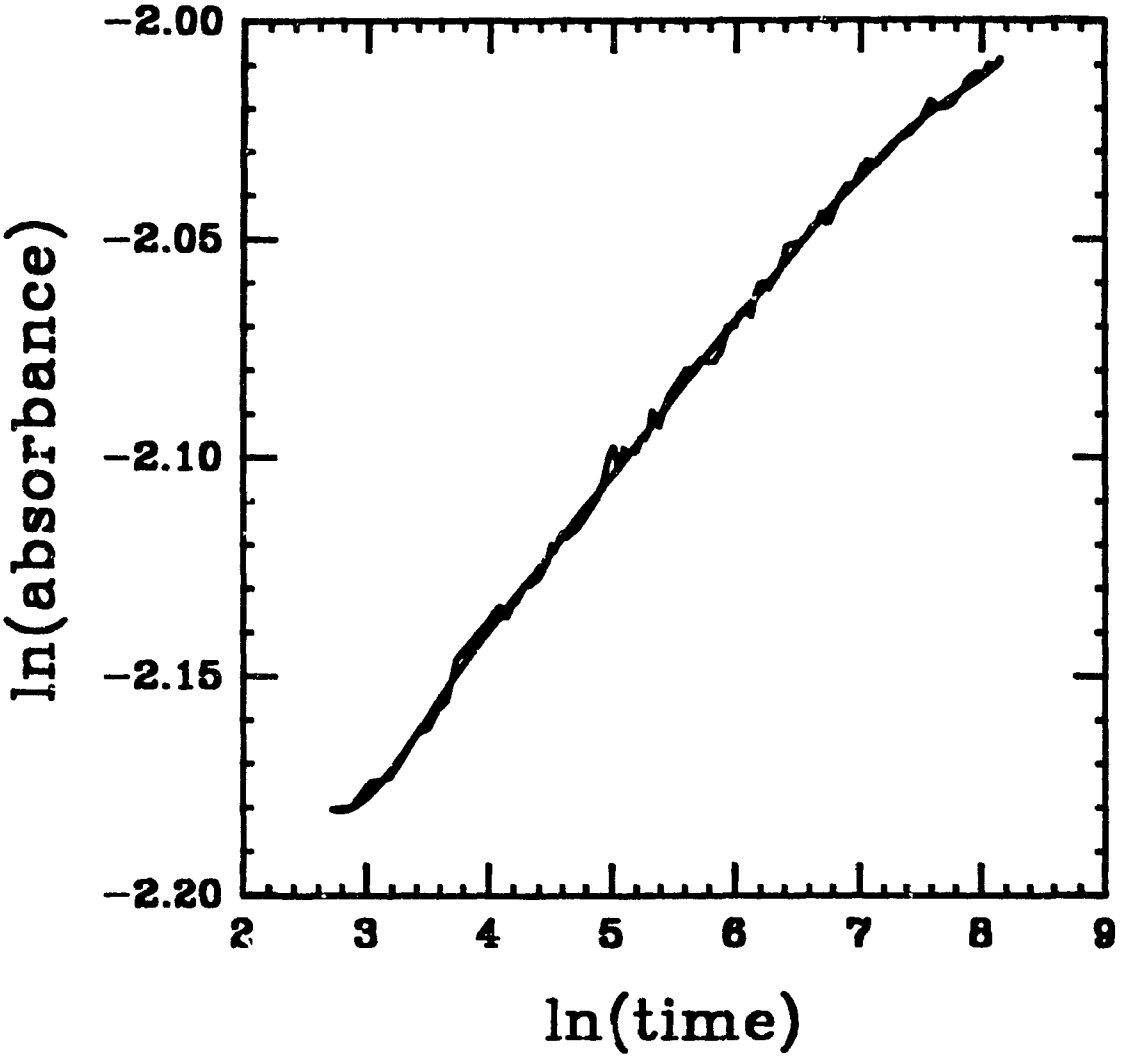

Figure 5-10: Smoothing applied to the absorbance-time data shown in the previous graph. Data has been fit as $\ln(A_{434})$ vs ln(t) using a 9^{th} degree polynomial. This is the lowest degree polynomial which faithfully followed the contours of the curve.

5.5.1 Stability of rate constants

The results shown in table 5-8 address the question of the stability of rate constants. There are two rate constants observed. These are shown for each pH from 4.5 to 7.0 and as averages of all the data. The fairly large variation of parameters was specifically employed to test the "ruggedness" of the rate constants. Both rate constants appear to be relatively stable over the range of conditions used with average values of $0.028 \pm 0.010\ s^{-1}$ and $0.0014 \pm 0.0006\ s^{-1}$. There is indication of a rather small change in k_3 with changing pH but this is within the error at the constant pH values. It is likely that this variation is due to better refinement of k_3 at the lower pH's. Generally noise levels were observed to improve with decreasing pH Not unexpectedly, deviations for k_2 are somewhat larger than for k_3. Noise in the absorbance-time profiles is generally worse at short times as the effects of turbulent mixing of reagents (such as bubbles in the cell) may remain.

On rare occasions for spectra having particularly low noise near the start, Laplace analysis hinted at the presence of three kinetic components. An example of this is shown in figure 5-11. If these three components are real it would in large part explain the fluctuations observed in k's. In particular k_2 was at times observed to have values in the region of $0.010\ s^{-1}$ and in other runs of c $0.04\ s^{-1}$. These are close to the values of 0.047 and $0.0075\ s^{-1}$ shown in figure 5-11. It appears that k_2 may be the average result of two different components which cannot normally be resolved. This is further supported by the observation that when only two kinetic components are resolved, ΣC_i is always lower than that predicted from the difference between estimates of A_0 and A_∞. Part of ΣC_i is distributed to the "X" and "not recovered" components. On the occasions when a third

Table 5-8: Rate constants for species of intermediate lability related to the kinetic speciation of copper(II) in iron(III) hydrous oxide. Results have been determined from data measured by conventional spectrophotometry.

System	Colloid pH	n^1	n^2	Rate constants (s^{-1}) k_2	k_3
Cu-Fe hox:					
-Pre-addition	4.5	1	5	0.024 ± 0.007	0.0012 ± 0.0002
	5.5	3	11	0.032 ± 0.010	0.0014 ± 0.0002
	6.0	4	13	0.028 ± 0.008	0.0013 ± 0.0002
	6.7	3	14	0.024 ± 0.011	0.0016 ± 0.0009
	7.0	1	4	0.032 ± 0.016	0.0016 ± 0.0005
	4.5 to 7.0	12	47	0.028 ± 0.010	0.0014 ± 0.0006
-Post-addition	4.5 to 6.7	7	9	0.032 ± 0.008	0.0018 ± 0.0010
Cu-hematite	6.0	1	2	0.0478 ± 0.0005	0.0018 ± 0.0005

1) n^1: number of colloid preparations.
2) n^2: number of successful Laplace/NLR results.

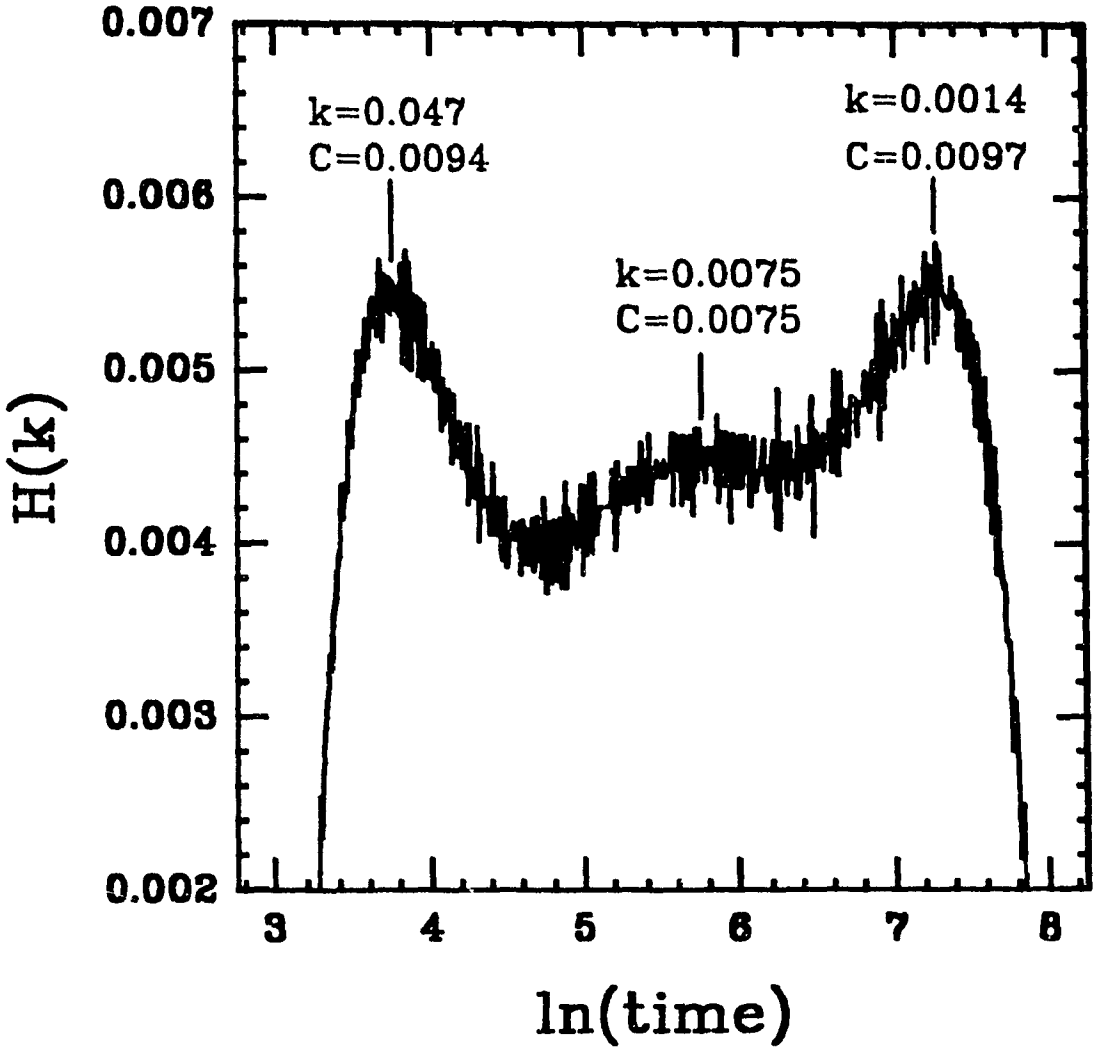

Figure 5-11: Laplace spectrum of data shown in figures 5-9 and 5-10. Normally Laplace analysis indicated the presence of only two kinetic components. When absorbance-time data was less noisy a third component could sometimes be found. It appears that the "k_2" normally measured may actually be a combination of two poorly resolved components.

component was observed ΣC_i was very close to the expected value. Improved refinement of k_3 at lower pH's (lower noise) also supports this possibility. It is useful to reiterate that results obtained from Laplace/NLR data analysis represent the **minimum** number of components required to describe the system.

One of the prime aims of this study has been to extend speciation analysis to lower metal concentrations. In most cases changes in absorbance resulting from kinetically observable components were about 0.01 absorbance units. Noise levels associated with these small changes are significant. This proves a formidable test of the Laplace/NLR method. It is quite possible that work with larger concentrations may have allowed more regular resolution of a third component but this would not necessarily reflect the behaviour of dilute Fehox colloids (see sections 5.3.2 and 5.6).

Absorbance measurement on solutions with the post-addition of copper were extremely noisy. Very few could be resolved by Laplace/NLR. Those which could, however, resulted in similar values of k_2 and k_3 to those determined for the colloids prepared in the presence of copper (table 5-8). This indicates that binding site strength or diffusion limitations which affect the kinetic lability of copper are similar in the two cases. (Post addition Cu(II) probably can diffuse into the colloids.)

Also shown in table 5-8 are rate constants determined from the kinetic speciation of Cu equilibrated at pH 6.0 for 24 hours with 212 nm diameter homodisperse hematite. The slower of the two constants is quite similar to k_3 of the Cu-Fehox system. The faster rate constant bears a striking resemblance to the fastest rate constant shown in figure 5-11. Some caution in this comparison is necessary. Noise levels in measured absorbance were quite severe for the first 500-1000 sec. Only two of the curves measured could be

resolved by Laplace/NLR.

It is interesting to mention at this point some kinetics measured for the release of copper which was ion exchanged with a sodium-A zeolite. This zeolite has an effective pore size of 4 Å. The formation of $Cu(PHTTT)_3$ was measured by both conventional and thermal lensing spectrometries. The results were fit to a first-order function in the same way described in section 4.4.2.2. A rate constant of 0.0026 s^{-1} was determined from CS data and 0.0025 s^{-1} from TLS data. Two further points of information are necessary before assigning a significance to these numbers. First, the zeolite particles were quite large, having been manually ground from pellets. As a result, most of the material quickly settled in the sample cell. Second, first order fitting is an over simplification of the processes occurring. The absorbance-time profiles measured by CS clearly showed an induction period during the first c. 200 s. Data from these early times were not used in the fitting.

What is of importance here is the similarity of rate constants determined from CS and TLS data. Since the zeolite is a crystalline structure its properties are concentration independent. Exactly the same processes are being monitored in both concentration regions. The similarity of results obtained using the two methods shows that CS and TLS are "parallel" monitoring techniques.

5.5.2 Chemical significance of components

The "master variable" used in studying the speciation of Cu(II) in the presence of Fehox has been pH. Figures 5-12 to 5-16 show results obtained at equilibration pH's of 4.5, 5.5, 6.0, 6.7 and 7.0, respectively. Error bars are shown for pH 6.0 and 6.7 at

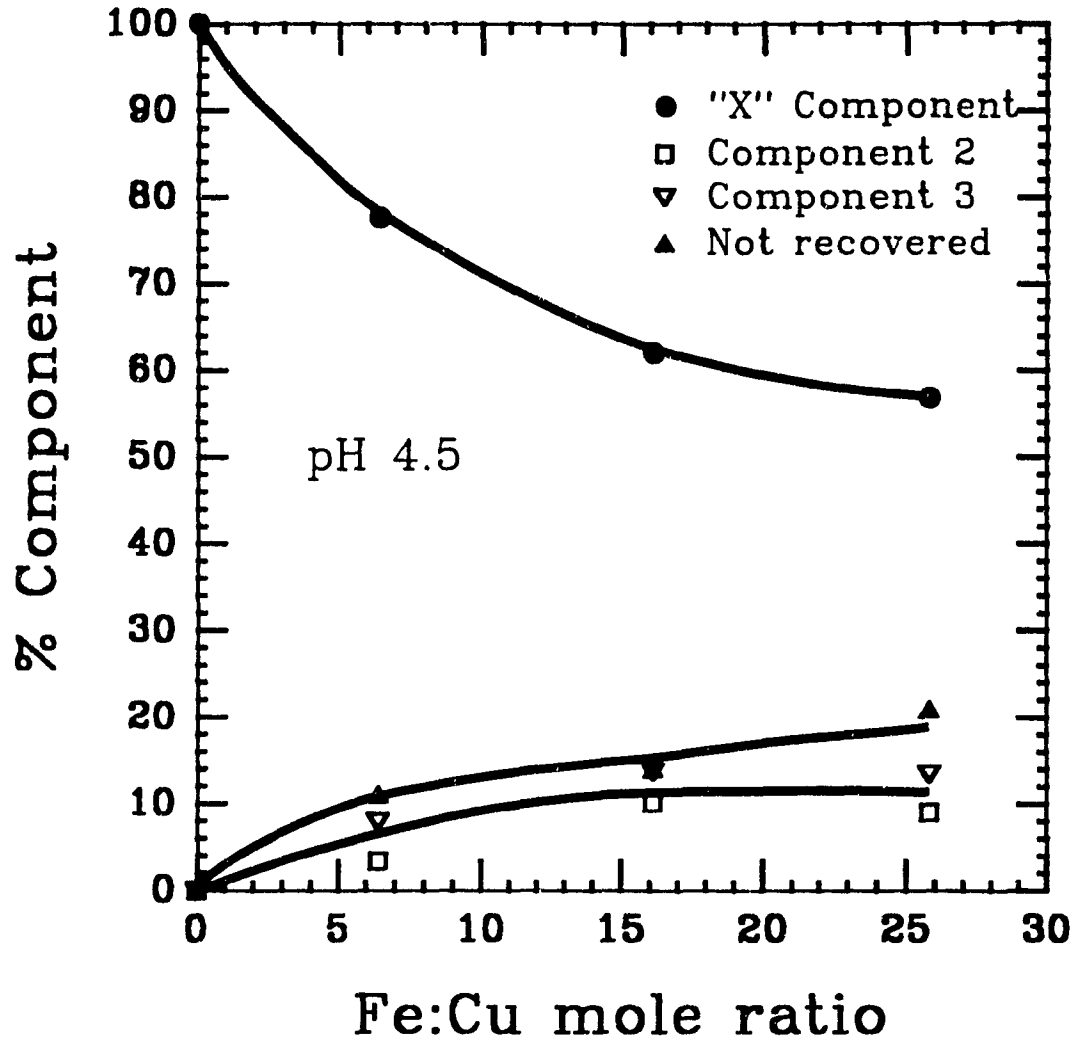

Figure 5-12: Component contributions for the kinetic speciation of copper(II) from ferric hydrous oxide at pH 4.5 determined from measurement of the absorbing complex $Cu(PHTTT)_3$ by conventional spectrophotometry. The majority of copper is in the highly labile "X" component even at larger Fe:Cu mole ratios.

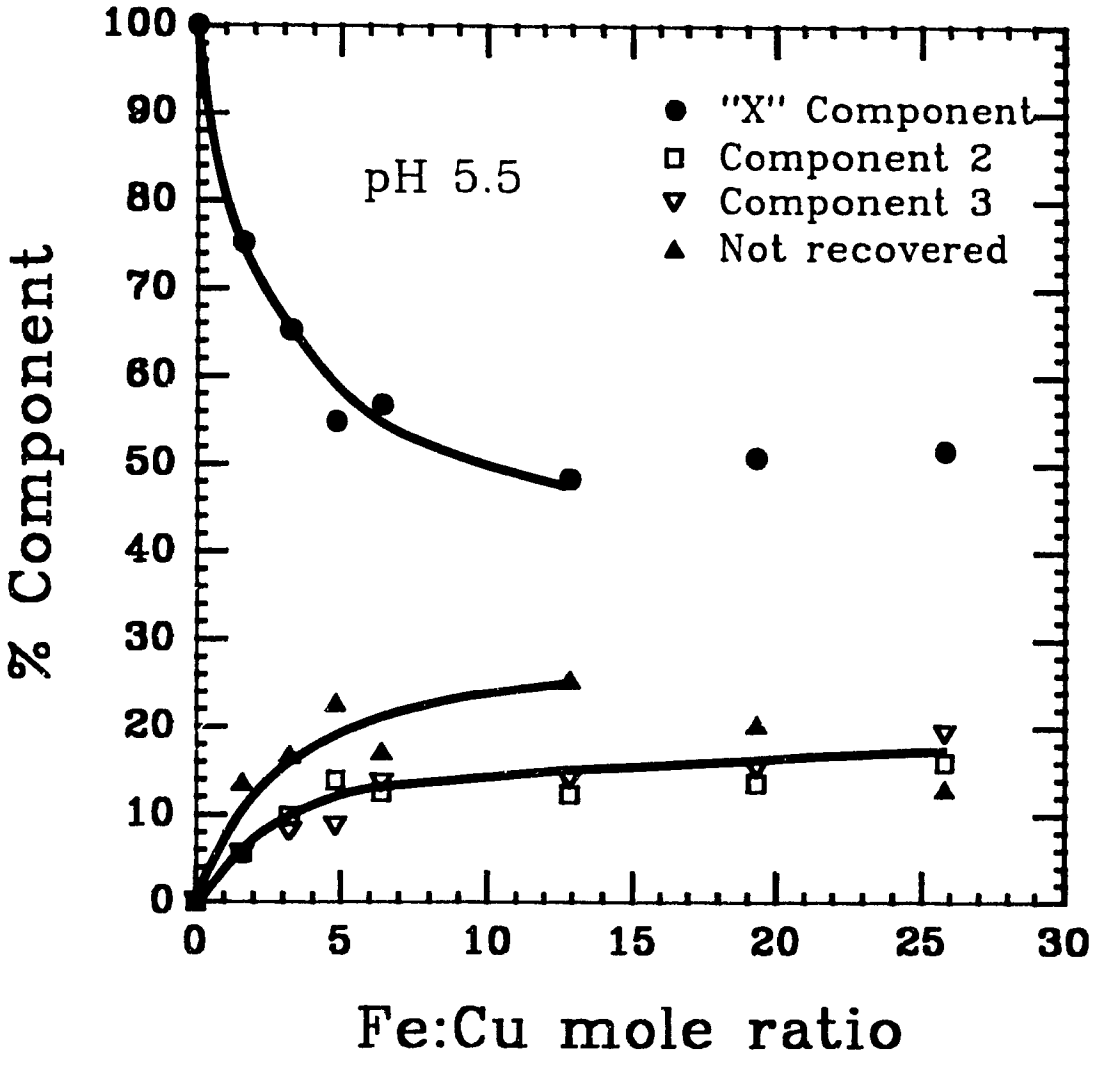

Figure 5-13: Component contributions for the kinetic speciation of copper(II) from ferric hydrous oxide at pH 5.5 determined from measurement of the absorbing complex $Cu(PHTTT)_3$ by conventional spectrophotometry. The noisier results are due to the adsorption edge for copper binding to Fehox which occurs near this pH.

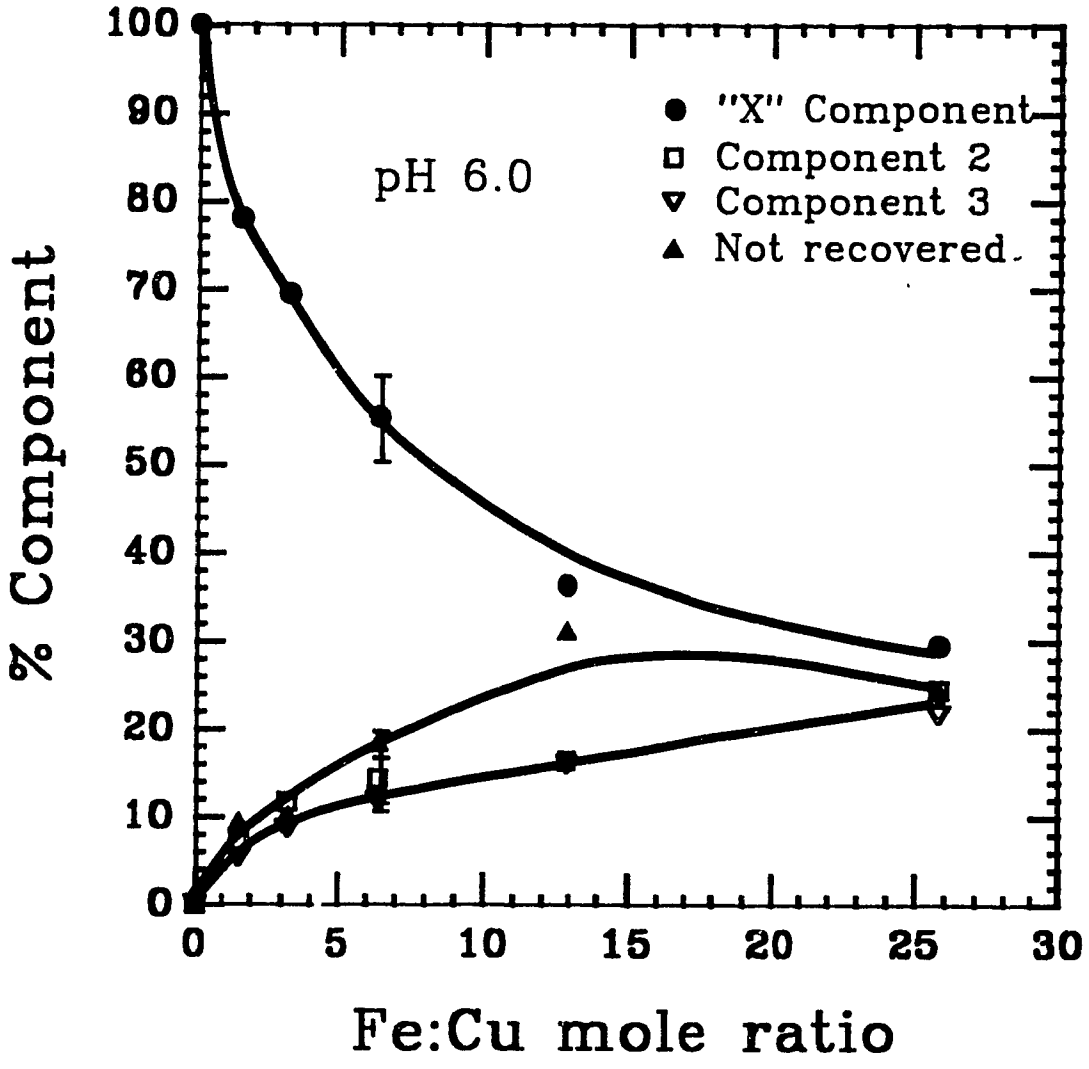

Figure 5-14: Component contributions for the kinetic speciation of copper(II) from ferric hydrous oxide at pH 6.0 determined from measurement of the absorbing complex $Cu(PHTTT)_3$ by conventional spectrophotometry. Data at this pH were measured at different times over a period of two years.

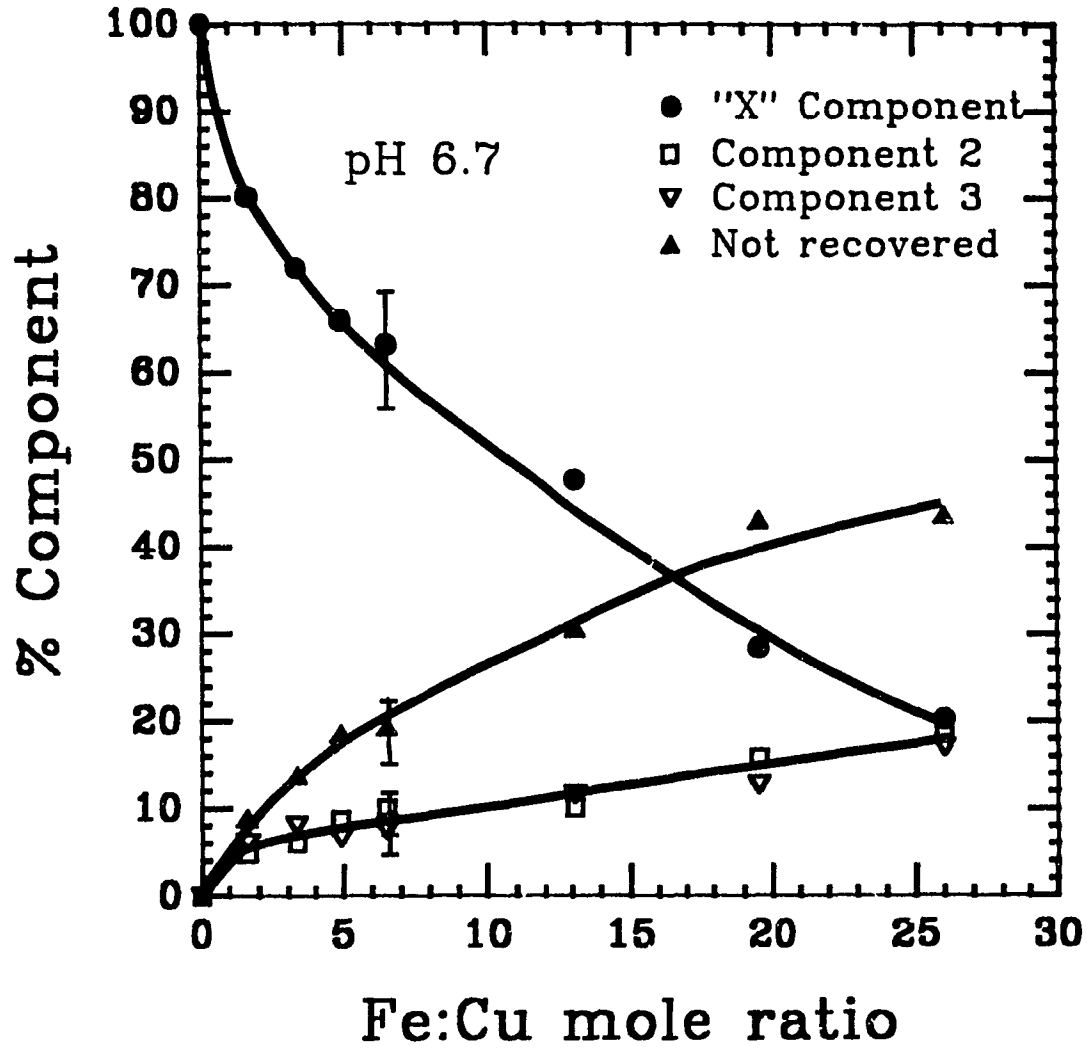

Figure 5-15: Component contributions for the kinetic speciation of copper(II) from ferric hydrous oxide at pH 6.7 determined from measurement of the absorbing complex $Cu(PHTTT)_3$ by conventional spectrophotometry.

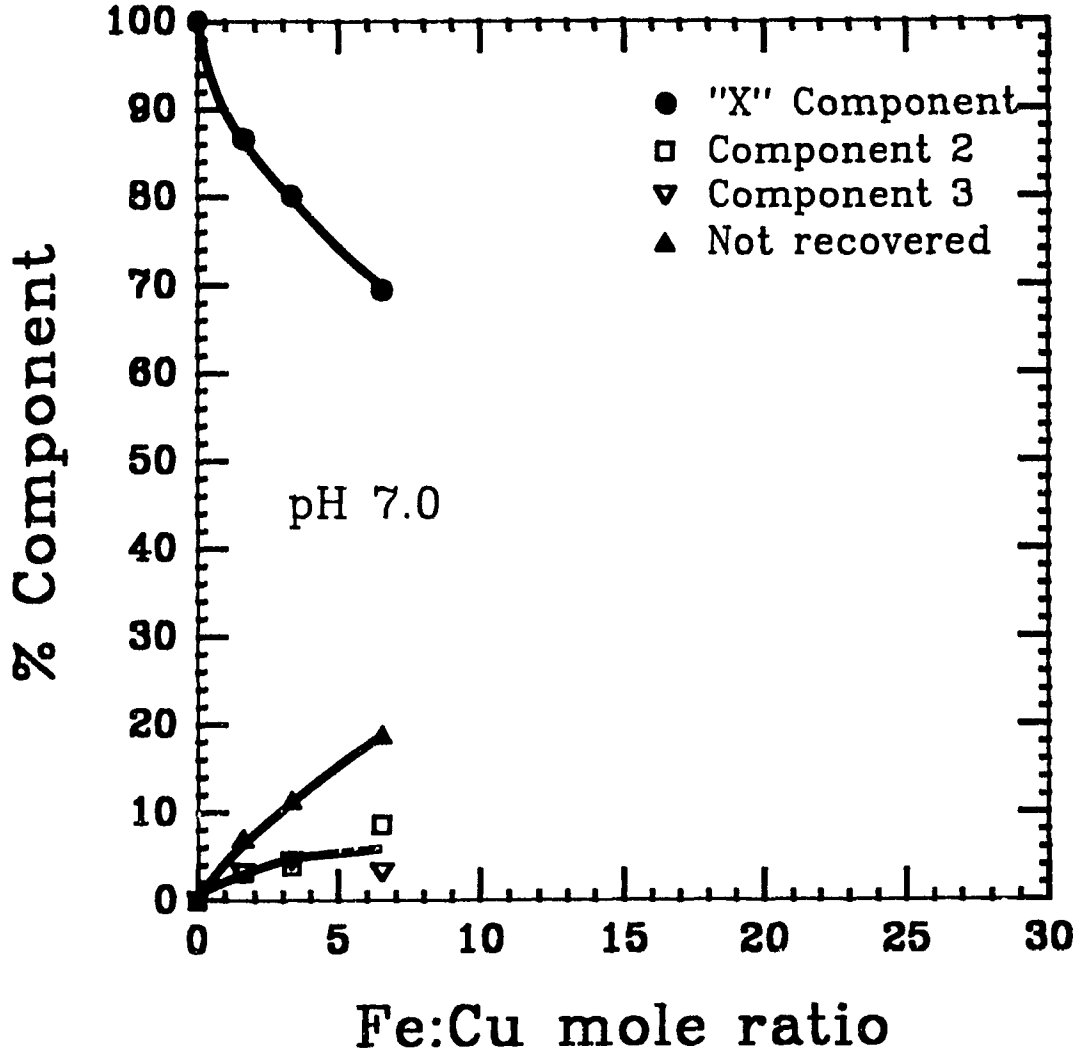

Figure 5-16: Component contributions for the kinetic speciation of copper(II) from ferric hydrous oxide at pH 7.0 determined from measurement of the absorbing complex $Cu(PHTTT)_3$ by conventional spectrophotometry. The results at Fe:Cu = 1.5 exceed the solubility limit of $Cu(OH)_2$.

Fe:Cu= 6.5 and represent standard deviations of 4 and 5 results, respectively, measured at different concentrations of iron and copper and with different "batches" of Fehox. For reasons to be explained, error bars for data at pH 5.5 may be somewhat larger. Only one set of Fehox was prepared at pH 7.0 as it was realized that the solubility limit of $Cu(OH)_2$ was being surpassed. In this case the value shown at Fe:Cu = 1.6 is influenced by $Cu(OH)_2$ precipitation. A single line is used to show the trends of components 2 and 3 as their relative contributions are similar.

Some of the data (particularly those at larger Fe:Cu ratios) may be less reliable due to difficulties in resolving species. It is believed that comparison of results obtained at pH's 4.5 and 6.7 (figures 5-12 and 5-15, respectively) provide the best indication of the processes actually occurring.

The variation in species distribution with Fe:Cu ratio is similar at each pH. As Fe:Cu increases the proportion of free (or kinetically very labile C_1 component) copper decreases while the amount of bound copper increases. This is readily predicted from equilibrium speciation. Kinetic speciation allows the bound copper to be characterized as different species. The largest of these is that which is not recovered within the time scale of the experiment. Two other components (C_2 and C_3) are present in very similar proportion and follow the same trend of increasing contribution at larger values of Fe:Cu.

Previous study and values found in the literature [11,146] show that the binding of copper to amorphous ferric hydrous oxide has an adsorption edge centred at about pH 5.5. The literature sources show copper adsorption changing from 10% to 90% adsorbed over a range of about one pH unit. In the systems they studied Fe:Cu mole ratios were very large (up to 2000) and Cu(II) was added after colloid formation. In the

current system Cu(II) adsorption was not found to exceed c. 70% nor decrease below about 20%. This upper limit may be explained by the relatively low values of Fe:Cu used. The lower limit is probably a result of different speciation for Fehox formed in the presence of copper.

The results obtained for pH 5.5 colloids were significantly more difficult to handle than those obtained at either higher or lower pH's. This is understandable given the precarious position of pH 5.5 colloids on the adsorption edge. Minor differences in pH may lead to large changes in component contribution. As explained in the experimental section, pH measurement in the colloidal solutions is problematic.

There are only minor differences in copper speciation in colloids at pH's 6.0 to 7.0. Results at pH 5.5 also appear similar if only the lower Fe:Cu ratios are considered indicating that they may lie on the higher side of the adsorption edge. Results at pH 4.5 show a significantly larger "X" component indicative of their position on the low side of the adsorption edge.

It has been mentioned that results obtained with post-addition of copper to Fehox are significantly more noisy and less likely to be analyzable by Laplace/NLR. This may relate to observations made in section 5.1.1 where it was discussed that the presence of copper has an effect on the stability of Fehox colloids. It appears that post-addition of copper has an even greater destabilizing effect on the colloids. Quantification of this process is impeded by the poor precision of results. For this reason no plots of % component versus Fe:Cu mole ratio are given. However, certain characteristics were common to the data which could be resolved. In all cases the % "X" component was significantly higher than with Fehox formed in the presence of copper at the same pH.

This seemed to occur largely at the expense of the non-recoverable fraction. The latter was sometimes not found at all even at fairly high Fe:Cu ratios. Components 2 and 3 appear to be relatively unaffected. These results disagree with those of Swallow et al. [111] who observed that only slightly less copper was carried down if it was added soon after precipitation than if it was present in the reactant solution during Fehox formation.

5.6 TLS ANALYSIS OF COPPER-HYDROUS FERRIC OXIDE

One application of thermal lensing to the study of "kinetics" remains to be discussed. Some efforts were directed to the kinetic speciation of copper(II) in Fehox using TLS monitoring. The copper containing colloids at pH 6.0 were diluted 50-fold with a matrix matched solution and mixed with the (50-fold diluted) chromophore/buffer at kinetic time zero. A MIXING DELAY of 120 seconds was used to allow the solutions to calm in the cell. The $\Delta I/I_{\infty}$ were rather noisy but did have one striking feature. They showed no sign of a change in signal with continuous monitoring for up to 60 minutes. Further, the signal indicated that almost all of the copper had already reacted before data acquisition began! These observations are quantified in table 5-9.

The column on the right was calculated from the rate constants k_2 and k_3 determined for speciation of copper in Fehox by CS. These values account for reaction which may have occurred during the MIXING DELAY and represent the % Cu recovered which should have been observed if speciation was the same in both cases. Even these values clearly exceed those determined by CS. The implication is that far more copper was in highly labile components in the system analyzed by thermal lensing. The only difference between the two systems was the concentration of Fehox and Cu(II). Fifty-fold

Table 5-9: Comparison of results obtained by CS and TLS for determination of the labile "X" component of copper(II) in iron(III) hydrous oxide colloid.

Fe:Cu mole ratio	CS % component		Time since dilution (minutes)	TLS % Cu recovered	
	"X"	Not recovered		Measured	Extrapolated
Fehox prepared with Cu(II) present:					
6.5	55 ± 5	18 ± 2	2	89 ± 4	75
			6	86 ± 4	72
			90	86 ± 4	72
			400	105 ± 5	91
12.9	36 ± 5	31 ± 2	2	74 ± 7	56
19.3	30 ± 5	30 ± 5	2	72 ± 9	52
Cu(II) added to Fehox:					
6.5	c. 80	c. 5	2	98 ± 4	> 84

dilution of the colloidal solution has resulted in a rapid change in speciation. Species of intermediate kinetic lability (components C_2 and C_3) appear to have been driven into a more quickly reacting state. The results indicate that only a percentage of copper similar to the "not recovered" fraction in CS work is not reacted although even this component seems to become available at long times after dilution (result measured at 400 seconds in table 5-9). In view of these results it is not unexpected that analysis of a dilute post-addition colloid showed complete recovery of copper.

All results, those on Fehox alone, Fehox reacting with SSA and Cu-Fehox reacting with PHTTT, confirm the importance of modelling colloidal hydrous oxide ligands at "realistic" concentrations. The nature of the colloidal ligand systems seems quite sensitive to total Fe concentration. That this is not an artifact of TLS is clearly shown by the result on zeolite particles where the ligand cannot be altered by dilution since it is a crystalline phase.

Chapter 6

CONCLUSION

The literature shows that equilibrium adsorption on metal oxide surfaces has almost always been successfully described by a single binding constant. The field has been dominated by the conception of a dominant binding site. In consequence it has been presumed that they are kinetically homogeneous. The CS results for the speciation of copper in iron(III) hydrous oxide show that this presumption is not correct. This does not, however, refute the conception that a single or small distribution of binding sites describes the equilibrium. It simply makes the point that binding sites may have differential accessibility.

The preparation of Cu-Fehox used here was designed to be similar to what may be expected to occur in most natural waters. Fehox was grown with copper present. This differs from most studies of binding to hydrous oxides where adsorbate metal is added to the already formed hox. Comparison of speciation in the two situations has shown that there does seem to be a higher degree of incorporation of copper in Fehox formed with Cu(II) present.

Several kinetic experiments compared thermal lensing detection to conventional spectrophotometry. In both the bromination of acetone and Cu exchanged zeolite studies agreement between CS and TLS results was very good. In both studies involving Fehox, CS and TLS results differed reflecting a variation in chemistry of the Fehox with total

iron concentration. The latter cases point out the need to model binding at concentrations of environmental relevance.

Since the thermal lensing process depends on the energy transformed and not too much on the net energy loss from the beam, scattering should be a minor factor. This had been supported by a partial test using silica. The study using polystyrene latex particles confirmed the expectation. A serious limitation was found with absorbing particles since they have a non-homogeneous distribution in solution. This has frustrated the attempt to study the same systems monitored by conventional spectrophotometry. This finding might not rule out the study of binding, for example by organic fractions. It requires finding a colorimetric system which is outside the spectral range of the particles. This is a considerable task. It is pointed out that although bothered by noise, TLS still provided useful insight in the speciation of the Cu-Fehox system.

1. Eichenberger, E., "The interrelation between essentiality and toxicity of metals in the aquatic ecosystem", in H. Sigel (ed.), "Concepts on metal ion toxicity", V20 of the series "Metal ions in biological systems", Marcel Dekker (1986) 67-100.

2. Sunda, W.G. and Hanson, A K., "Measurement of free cupric ion concentration in seawater by a ligand competition technique involving copper sorption onto C_{18} SEP-PAK cartridges", Limnol. Oceanogr., 32 (1987) 537-551.

3. Martin, R.B., "Bioinorganic chemistry of metal ion toxicity", in H. Sigel (ed.), "Concepts on metal ion toxicity", Vol. 20 of the series "Metal ions in biological systems", Marcel Dekker, (1986) 21-65.

4. Sunda, W. and Guillard, R.R.L., "The relationship between cupric ion activity and the toxicity of copper to phytoplankton", J. Mar. Res., 34 (1976) 511-529.

5. Sunda, W.G. and Lewis, J.A.M., "Effect of complexation by natural organic ligands on the toxicity of copper to a unicellular alga, *Monochrysis lutheri*", Limnol. Oceanogr., 23 (1978) 870-876.

6. Anderson, D.M., and Morel, F.M.M., "Copper sensitivity of *Gonyaulax tamarensis*", Limnol. Oceanogr., 23 (1978) 283-295.

7. Petersen, R., "Influence of copper and zinc on the growth of a freshwater alga, *Scenedesmus quadricauda*: The significance of chemical speciation", Environ. Sci. Technol., 16 (1982) 443-447.

8. Morrison, G.M.P., "Trace element speciation and its relationship to bioavailability and toxicity in natural waters", in G.E. Batley (ed.), "Trace element speciation: Analytical methods and problems", CRC Press, (1989) 25-41.

9. Lund, W., "Speciation analysis - why and how?", Fresenius J. Anal. Chem., 337 (1990) 557-564.

10. Laxen, D.P.H., "Adsorption of Pb, Cd, Cu and Ni onto hydrous iron oxides under realistic conditions", International Conference: Heavy Metals in the Environment, V2, Heidelberg, September 1983.

11. Davis, J.A., and Leckie, J.O., "Effect of adsorbed complexing ligands on trace metal uptake by hydrous oxides", Environ. Sci. Technol., 12 (1978) 1309-1315.

12. Lion, L.W., Altmann, R.S. and Leckie, J.O., "Trace-metal adsorption characteristics of estuarine particulate matter: Evaluation of contributions of Fe/Mn oxide and organic surface coatings", Environ. Sci. Technol., 16 (1982) 660 666.

13. Tipping, E., "Some aspects of the interactions between particulate oxides and aquatic humic substances", Mar. Chem., 18 (1986) 161-169 and references cited therein.

14. Morrison, G.M.P., Batley, G.E. and Florence, T.M., "Metal speciation and toxicity", Chem. Br., 25 (1989) 791-796.

15. Borg, H., "Metal fractions and complexing capacity of lake waters surrounding the Ronnskar smelters in northern Sweden", 70th Canadian Chemical Conference, Quebec, Canada, June 1987.

16. Buffle, J., "Complexation reactions in aquatic systems: An analytical approach", Ellis Horwood, Chinchester, (1988) 81-89.

17. Buffle, J., "Complexation reactions in aquatic systems: An analytical approach", Ellis Horwood, Chinchester, (1988) 195-200.

18. Olson, D.L. and Shuman, M.S., "Kinetic spectrum method for analysis of simultaneous, first-order reactions and application to copper(II) dissociation from aquatic macromolecules", Anal. Chem., 55 (1983) 1103-1107.

19. Dzombak, D.A., Fish, W. and Morel, F.M.M., "Metal-humate interactions. 1. Discrete ligand and continuous distribution models", Environ. Sci. Technol., 20 (1986) 669-675.

20. Buffle, J., Altmann, R.S., Filella, M. and Tessier, A., "Complexation by natural heterogeneous compounds: Site occupation distribution functions, a normalized description of metal complexation", Geochim. Cosmochim. Acta, 54 (1990) 1535-1553.

21. Buffle, J., "Complexation reactions in aquatic systems: An analytical approach", Ellis Horwood, Chinchester, (1988) 37-40.

22. Bowen, H.J.M., "Environmental Chemistry of the Elements", Academic Press, London, (1979).

23. Bowen, H.J.M., "Trace Elements in Biochemistry", Academic Press, London (1966).

24. Mattigod, S.V., Sposito, G. and Page, A.L., in "Chemistry in the Soil Environment", Soil Science Society America, Madison, Wis., (1981) 204.

25. Bruland, K.W., in J.P. Riley and R. Chester (eds.), "Chemical Oceanography", Vol. 8, Academic Press, London (1983).

26. Spear, P.A. and Pierce, R.C., "Copper in the aquatic environment: Chemistry, distribution and toxicology", NRCC pub. no. 16454, National Research Council Canada (1979).

27. Kliger, D.S., "Thermal lensing: A new spectroscopic tool", Acc. Chem. Res., 13 (1980) 129-134.

28. Miyaishi, K., Imaska, T. and Ishibashi, N., "Thermal lens spectrophotometry based on image detection of a probe laser beam", Anal. Chem., 54 (1982) 2039-2044.

29. Whinnery, J.R., "Laser measurement of optical absorption in liquids", Acc. Chem. Res , 7 (1974) 225-231.

30. Miyaishi, K., Imasaka, T. and Ishibashi, N., "Thermal lensing spectrophotometric analysis with ion-pair solvent extraction", Anal. Chim. Acta, 124 (1981) 381-389.

31. Dovichi, N.J., "Thermo-optical spectrophotometries in analytical chemistry", Crit. Rev. Anal. Chem., 17 (1987) 357-423

32. Thormahlen, I., Straub, J. and Grigull, U., "Refractive index of water and its dependence on wavelength, temperature, and density", J. Phys. Chem. Ref. Data, 14 (1985) 933-942.

33. Franko, M. and Tran, C.D., "Water as a unique medium for thermal lens measurements", Anal. Chem., 61 (1989) 1660-1666.

34. Gordon, J.P., Leite, R.C.C., Moore, R.S., Porto, S.P.S. and Whinnery, J.R., "Long-transient effects in lasers with inserted liquid samples", J. Appl. Phys., 36 (1965) 3-8.

35. Hu, C. and Whinnery, J.R., "New thermooptical measurement method and a comparison with other methods", Appl. Opt., 12 (1973) 72-79.

36. Swofford, R.L., Long, M.E. and Albrecht, A.C., "C-H vibrational states of benzene, naphthalene, and anthracene in the visible region by thermal lensing spectroscopy and the local mode model", J. Chem. Phys., 65 (1976) 179-190.

37. Swofford, R.L., and Morrell, J.A., "Analysis of the repetitively pulsed dual-beam thermo-optical absorption spectrometer", J. Appl. Phys. 49 (1978) 3667-3674.

38. Carter, C.A. and Harris, J.M., "Comparison of single- and dual-beam configurations for thermal lens spectrometry", Anal. Chem., 55 (1983) 1256-1261.

39. Fang, H.L. and Swofford, R.L., "The thermal lens in absorption spectroscopy" in D.S. Kliger (ed.), "Ultrasensitive laser spectroscopy", Academic Press, New York, (1983) 175-232.

40. Berthoud, T., Delorme, N. and Mauchien, P., "Beam geometry optimization in dual-beam thermal lensing spectrometry", Anal. Chem., 57 (1985) 1216-1219.

41. Tran, C.D., "Development of a double beam, dual wavelength thermal lens using a helium-neon laser", Analyst, 112 (1987) 1417-1420.

42. Pang, T-K.J. and Morris, M.D., "Pump/probe thermal lens spectroscopy with polarization-encoded laser beams", Appl. Spectros., 39 (1985) 90-93.

43. Yang, Y., "Rotoreflected laser beam thermal lens spectrometry", Anal. Chem., 58 (1986) 1420-1424.

44. Nakanishi, K., Imasaka, T. and Ishibashi, N., "Single-mode and multimode optical fibers for light introduction in thermal lens spectrophotometry", Anal. Chem., 59 (1987) 1550-1554.

45. Leite, R.C.C., Moore, R.S. and Whinnery, J.R., "Low absorption measurements by means of a thermal lens effect, using a He-Ne laser", Appl. Phys. Lett., 5 (1964) 141-143.

46. Power, J.F., "Laser studies of the photophysics of humic substances", PhD thesis, Concordia University, Montreal, Quebec 1986.

47. Power, J.F. and Salin, E.D., "Mode-mismatched laser induced thermal lens effect detection via spatial Fourier analysis of beam profiles", Anal. Chem., 60 (1988) 838-842.

48. Dovichi, N.J. and Harris, J.M., "Thermal lens calorimetry for flowing samples", Anal. Chem., 53 (1981) 689-692.

49. Skogerboe, K.J. and Yeung, E.S., "Single laser thermal lens detector for microbore liquid chromatography based on high-frequency modulation", Anal. Chem., 58 (1986) 1014-1018.

50. Georges, J. and Mermet, J-M., "Dual-beam thermal lens spectrophotometry in flowing samples with chopped continuous wave laser excitation", Analyst, 114 (1989) 541-546.

51. Weimer, W.A. and Dovichi, N.J., "Time-resolved thermal lens measurements in flowing samples", Anal. Chem., 57 (1985) 2436-2441.

52. Nickolaisen, S.L. and Bialkowski, S.E., "Pulsed laser thermal lens spectrophotometry for flowing liquid detection", Anal. Chem., 58 (1986) 215-220.

53. Vyas, R. and Gupta, R., "Photothermal lensing spectroscopy in a flowing medium: theory", Appl. Opt., 27 (1988) 4701-4711.

54. Buffett, C.E. and Morris, M.D., "Thermal lens detection for liquid chromatography", Anal. Chem , 54 (1982) 1824-1825.

55. Buffett, C.E. and Morris, M.D., "Microcell thermal lens detector for liquid chromatography", Anal. Chem., 55 (1983) 376-378.

56. Pang, T-K.J. and Morris, M.D., "Liquid chromatography absorbance detector with retroreflective array for aberration compensation and double pass operation", Anal. Chem., 57 (1985) 2700-2703.

57. Xu, M. and Tran, C.D., "Thermal lens-circular dichroism detector for high-performance liquid chromatography", Anal. Chem., 62 (1990) 2467-2471.

58. Sharma, D.K., Villamagna, F. and Langford, C.H., "Laser thermal lensing applied to the colorimetric detection of tris-1,10-phenanthroline iron(II) and sulfur dioxide", Can. J. Spectrosc., 28 (1983) 181-183.

59. Alfheim, J.A. and Langford, C.H., "Determination of formaldehyde with the thermal lens effect", Anal. Chem., 57 (1985) 861-864.

60. Power, J.F. and Langford, C.H., "Optical absorbance of dissolved organic matter in natural water studies using the thermal lens effect", Anal. Chem., 60 (1988) 842-846.

61. Lavigne, J.A., "Kinetic study of the speciation of nickel(II) bound to a fulvic acid", PhD. thesis, Concordia University, Montreal, Quebec, Canada, (1987).

62. Willis, B.G., Woodruff, W.H., Frysinger, J.R., Margerum, D.W. and Pardue, H.L., "Simultaneous kinetic determination of mixtures by on-line regression analysis", Anal. Chem., 42 (1970) 1350-1355 and references cited therein.

63. Margerum, D.W., Cayley, G.R., Weatherburn, D.C. and Pagenkopf, G.K., "Kinetics and mechanisms of complex formation and ligand exchange", in A.E. Martell (ed.), "Coordination Chemistry", Vol. 2, ACS Monograph 174, American Chemical Society, Washington (1978) 163-194.

64. Hering, J.G. and Morel, F.M.M., "Kinetics of trace metal complexation: Ligand-exchange reactions", Environ. Sci. Technol., 24 (1990) 242-252.

65. Schindler, P.W., "Surface complexation", in H. Sigel (ed.), "Circulation of metals in the environment", V18 of the series "Metal ions in biological systems", Marcel Dekker (1984) 111.

66. Gamble, D.S., Underdown, A.W. and Langford, C.H., "Copper(II) titration of fulvic acid ligand sites with theoretical, potentiometric, and spectrophotometric analysis", Anal. Chem., 52 (1980) 1901-1908.

67. Mak, M.K.S. and Langford, C.H., "Kinetic analysis applied to aluminum citrate complexing", Inorg. Chim. Acta, 70 (1983) 237-246.

68. Shuman, M.S., Collins, B.J., Fitzgerald, P.J. and Olson, D.L., "Distribution of stability constants and dissociation rate constants among binding sites on estuarine copper-organic complexes: Rotated disk electrode studies and an affinity spectrum analysis of ion-selective electrode and photometric data", in R.F. Christman and E.T. Gjessing (eds.), "Aquatic and Terrestrial Humic Materials", Ann Arbor Science, Ann Arbor, (1983) 349-370.

69. Mak, M.K.S., "Kinetic analysis of aluminum in environmentally and geochemically relevant problems", PhD thesis, Carleton University, Ottawa, Ontario (1980).

70. Marquardt, D.W., "An algorithm for least-squares estimation of nonlinear parameters", J. Soc. Indust. Appl. Math., 11 (1963) 431-441.

71. Cabaniss, S.E., "pH and ionic strength effects on nickel-fulvic acid dissociation kinetics", Environ. Sci. Technol., 24 (1990) 583-588.

72. Lavigne, J.A., Langford, C.H. and Mak, M.K.S., "Kinetic study of speciation of nickel(II) bound to a fulvic acid", Anal. Chem., 59 (1987) 2516-2620.

73. Provencher, S.W., "An eigenfunction expansion method for the analysis of exponential decay curves", J. Chem. Phys., 64 (1976) 2772-2777.

74. Provencher, S.W., "A constrained regularization method for inverting data represented by linear algebraic or integral equations", Comput. Phys. Commun., 27 (1982) 213-227.

75. Sojo, L.E. and De Haan, H., "Multicomponent kinetic analysis of iron speciation in humic lake Tjeukemeer: Comparison of fulvic acid from the drainage basin and lake water samples", Environ. Sci. Technol., 25 (1991) 935-939.

76. Figura, P. and McDuffie, B., "Determination of labilities of soluble trace metal species in aqueous environmental samples by anodic stripping voltammetry and chelex column and batch methods", Anal. Chem., 52 (1980) 1433-1439.

77. Campbell, P.G.C., Bisson, M., Bougie, R., Tessier, A. and Villeneuve, J.-P., "Speciation of aluminum in acidic freshwaters", Anal. Chem., 55 (1983) 2246-2252.

78. Muller, F L.L. and Kester, D.R., "Kinetic approach to trace metal complexation in seawater: Application to zinc and cadmium", Environ. Sci. Technol., 24 (1990) 234-242.

79. Bertsch, P.M., "Aluminum speciation: Methodology and applications", in S.A. Norton, S.E. Lindberg and A.L. Page (eds.), "Soils, aquatic processes, and lake acidification", Vol. 4 of the series D.C. Adriano and W. Salomons (eds.), "Acidic Precipitation", Springer-Verlag, New York, (1990) 66-70.

80. Turner, R.C., "Effect of aging on properties of polynuclear hydroxyaluminum cations", Can. J. Chem., 54 (1976) 1528-1534.

81. Lalande, H. and Hendershot, W.H., "Aluminum speciation in some synthetic systems: Comparison of the fast-oxine, pH 5.0 extraction and dialysis methods", Can. J. Fish. Aquat. Sci., 43 (1986) 231-234.

82. Jardine, P.M. and Zelazny, L.W., "Influence of inorganic anions on the speciation of mononuclear and polynuclear aluminum by ferron", Soil Sci. Soc. Am. J., 51 (1987) 889-892.

83. Duffy, S.J., Hay, G.W., Micklethwaite, R.K. and Vanloon, G.W., "A method for determining metal species in soil pore water", Sci. Total Environ., 76 (1988) 203-215.

84. Duquette, M. and Hendershot, W.H., "Copper and zinc sorption on some B horizons of Quebec soils", Commun. Soil Sci. Plant Anal., 21 (1990) 377-394.

85. Gamble, D.S. and Schnitzer, M., "The chemistry of fulvic acid and its reactions with metal ions", in P.C. Singer (ed.), "Trace Metals and Metal-Organic Interactions in Natural Waters", Ann Arbor Science, Ann Arbor, (1973) 266-273.

86. Bonifazi, M., "Kinetic study of the speciation of copper(II) bound to humic acid", MSc thesis, Concordia University, Montreal, (1990).

87. Wang, Z.-D., Gamble, D.S. and Langford, C.H., "Interaction of atrazine with Laurentian fulvic acid: Binding and hydrolysis", Anal. Chim. Acta, 232 (1990) 181-188.

88. Wang, Z.-D., Pant, B.C. and Langford, C.H., "Spectroscopic and structural characterization of a Laurentian fulvic acid: Notes on the origin of the color", Anal. Chim. Acta, 232 (1990) 43-49.

89. Eigen, M., "Proceedings of the seventh international conference on coordination chemistry", Butterworths, London, (1963).

90. Langford, C.H., "Complex formation and solvent-exchange kinetics: A dynamic approach to electrolyte solutions", in S. Petrucci (ed.), "Ionic interactions", Vol. 2, Academic press, New York, (1971) 16.

91. Turner, D.R., Varney, M.S., Whitfield, M., Mantoura, R.F.C. and Riley, J.P., "Electrochemical studies of copper and lead complexation by fulvic acid. 1. Potentiometric measurements and a critical comparison of metal binding models", Geochim. Cosmochim. Acta, 50 (1986) 289-297.

92. Buffle, J., "Natural organic matter and metal-organic interactions in aquatic systems", in H. Sigel (ed.), "Circulation of metals in the environment", Vol. 18 of the series "Metal Ions in Biological Systems", Marcel Dekker, New York, (1984) 202-207.

93. Olson, D.L. and Shuman, M.S., "Copper dissociation from estuarine humic materials", Geochim. Cosmochim. Acta, 49 (1985) 1371-1375.

94. Langford, C.H., Kay, R., Quance, G.W. and Khan, T.R., "Kinetic analysis applied to iron in a natural water model containing ions, organic complexes, colloids, and particles", Anal. Lett., 10 (1977) 1249-1260.

95. Langford, C.H. and Khan, T.R., "Kinetics and equilibrium of binding of Fe^{3+} by a fulvic acid: A study by stopped flow methods", Can. J. Chem., 53 (1975) 2979-2984.

96. Sommer, B.A., Margerum, D.W., Renner, J., Saltman, P. and Spiro, T.G., "Reactivity and aging in hydroxy-iron(III) polymers, analogs of ferritin cores", Bioinorg. Chem., 2 (1973) 295-309.

97. Langford, C.H. and Mak, M.K.S., "Kinetic studies of colloidal metal complex species relevant to natural waters", Comments Inorg. Chem., 2 (1983) 127-143.

98. Langford, C.H., Wong, S.M. and Underdown, A.W., "The interaction of a soil fulvic acid with precipitating hydrous ferric oxide at pH=6", Can. J. Chem., 59 (1981) 181-186.

99. Mak, M.K.S. and Langford, C.H., "A kinetic study of the interaction of hydrous aluminum oxide colloids with a well-characterized soil fulvic acid", Can. J. Chem., 60 (1982) 2025-2028.

100. Matijevic, E., Mathai, K.G., Ottewill, R.H. and Kerker, M., "Detection of metal ion hydrolysis by coagulation. III. Aluminum", J. Phys. Chem., 65 (1961) 826-830.

101. Matijevic, E., Janaur, G.E. and Kerker, M., "Reversal of charge of lyophobic colloids by hydrolyzed metal ions. I. $Al(NO_3)_3$", J. Colloid Sci., 19 (1964) 333-346.

102. Secco, F. and Venturini, M., "Mechanism of complex formation. Reaction between aluminum and salicylate ions", Inorg. Chem., 14 (1975) 1978-1981.

103. Tipping, E., Woof, C. and Ohnstad, M., "Forms of iron in the oxygenated waters of Esthwaite Water, U.K.", Hydrobiologia, 92 (1982) 383-393.

104. Catalogue "Optics guide 3", Melles Griot, Irvine, CA, (1985) p.60.

105. Anthore. R., Flament, P., Gouesbet, G., Rhazi, M. and Weill, M.E., "Interaction between a laser beam and some liquid media", Appl. Opt., 21 (1982) 2-4.

106. Livingston, P.M., "Thermally induced modifications of a high power CW laser beam", Appl. Opt., 10 (1971) 426-436.

107. Buffett, C.E. and Morris, M.D., "Convective effects in thermal lens spectroscopy", Appl. Spectros., 37 (1983) 455-458.

108. Alfonso, E.F.S., Revert, M.A.R., Alvarez-Coque, M.C.G. and Ramos, G.R., "Reduction of convective low-frequency noise in thermal lens spectrometry", Appl. Spectros., 44 (1990) 1501-1507.

109. Swinney, H.L. and Gollub, J.P., "The transition to turbulence", Physics Today, August (1978) 41-49.

110. Atomic absorption analyses of stock solutions and access to AAS instrumentation courtesy of the Science Industrial Research Unit, Concordia University.

111. Swallow, K.C., Hume, D.N. and Morel, F.M.M., "Sorption of copper and lead by hydrous ferric oxide", Environ. Sci. Technol., 14 (1980) 1326-1331.

112. Penners, N.H.G., "The preparation and stability of homodisperse colloidal haematite (α-Fe_2O_3)", PhD thesis, Wageningen Agricultural University, Netherlands (1985).

113. Pink, J.M., "Spectrophotometric determination of the hydrolysis constant of bromine at 25 °C", Can. J. Chem., 48 (1970) 1169-1171.

114. Blackman, R.B. and Tukey, J.W., "The measurement of power spectra", Dover (1958).

115. Ackroyd, M.H., "Digital filters", of the series "Computers in medicine", Butterworths, London.

116. Module 2 "Analysis" manual of "ASYST 2.0: A scientific system", ASYST software technologies, Rochester, New York, (1988) p. II-5-7.

117. Swinbourne, E.S., "Analysis of kinetic data", Thomas Nelson and sons, Don Mills, Ontario (1971) p. 80.

118. Dalton, L.K., "The preparation of thiazolidine-2-thiones from N-alkylglucosylamines" Aust. J. Chem., 19 (1966) 445-450.

119. Corbett, J.A., "Study of 3-methyl-5-hydroxy-5-(D-arabino-tetrahydroxybutyl)-thiazolidine-2-thione as a reagent for the spectrophotometric determination of copper", Talanta, 13 (1966) 1089-1096.

120. Stiff, M.J., "The chemical states of copper in polluted fresh water and a scheme of analysis to differentiate them", Water Res., 5 (1971) 585-599.

121. Chow, Y.M., Mak, K.S. and Lau, O.W., "Improved method for the synthesis of 3-propyl-5-hydroxy-5-D-*arabino*-tetrahydroxybutyl-3-thiazolidine-2-thione (PHTTT) and its homologues, Specific spectrophotometric reagents for copper", Analyst, 102 (1977) 139-140.

122. Stiff, M.J., "3-Propyl-5-hydroxy-5-D-arabinotetrahydroxybutyl-3-thiazolidine-2-thione, a specific colorimetric reagent for the determination of copper in water", Analyst, 97 (1972) 146-147.

123. Skoog, D.A. and West, D.M., "Principles of instrumental analysis", 2nd ed., Saunders, Philadelphia, (1980) p. 153.

124. It should be pointed out that an error was made in the preliminary results reported in Gutzman, D.W. and Langford, C.H., "Multicomponent kinetic analysis of trace metal binding sites on iron hydrous oxide colloids", Water Pollut. Res. J. Can., 23 (1988) 379-387. It was stated that part of the observed background absorbance was due to the formation of the iron(III)-chromophore complex. It is now understood that changes in the observed background were actually due to "fluctuations" of the type just described. It is also noted that Corbett [119] has reported that neither Fe(III) nor Fe(II) were found to complex with the methyl homologue of this chromophore.

125. Langmuir, D. and Whittemore, D.O., "Variations in the stability of precipitated ferric oxyhydroxides", in "Nonequilibrium systems in natural water chemistry", Advances in chemistry series 106, American Chemical Society, Washington, D.C., (1971).

126. Dousma, J. and de Bruyn, P.L., "Hydrolysis-precipitation studies of iron solutions: 1. Model for hydrolysis and precipitation from Fe(III) nitrate solutions", J. Colloid Int. Sci., 56 (1976) 527-539.

127. Byrne, R.H. and Kester, D.R., "Solubility of hydrous ferric oxide and iron speciation in seawater", Mar. Chem., 4 (1976) 255-274.

128. Buffle, J., "Complexation reactions in aquatic systems: An analytical approach", Ellis Horwood, Chinchester, (1988) 330-338 and references cited therein.

129. Personal communication, J. Buffle, University of Geneva, Switzerland.

130. Schwertmann, U., "Goethite and hematite formation in the presence of clay minerals and gibbsite at 25°C", Soil Sci. Soc. Am. J., 52 (1988) 288-291.

131. Laxen, D.P.H. and Chandler, I.M., "Size distribution of iron and manganese species in freshwaters", Geochim. Cosmochim. Acta, 47 (1983) 731-741.

132. Perret, D., Leppard, G.G., Müller, M., Belzile, N., De Vitre, R. and Buffle, J., "Electron microscopy of aquatic colloids: Non-perturbing preparation of specimens in the field", Water Res., 25 (1991) 1333-1343.

133. Wang, Z.-D., "Stoichiometric interactions of atrazine and hydroxyatrazine with chemically-characterized Laurentian soil and its key components", PhD thesis, Concordia University, Montreal, Quebec 1989.

134. Fuke, K., Hasegawa, A., Ueda, M. and Itoh, M., "A thermal lensing study of a photolysis of di-t-butyl peroxide", Chem. Phys. Lett., 84 (1981) 176-179.

135. Fuke, K., Ueda, M. and Itoh, M., "Thermal lensing study of singlet oxygen reactions", J. Am. Chem. Soc., 105 (1983) 1091-1096.

136. Bailey, R.T., Cruickshank, F.R., Pugh, D. and Middleton, K.M., "Vibration-vibration energy-transfer kinetics monitored by thermal lens", J. Chem. Soc., Faraday Trans. 2, 81 (1985) 255-265.

137. Isak, S.J., Komorowski, S.J., Merrow, C.N., Poston, P.E. and Eyring, E.M., "Thermal lens measurements in liquids on a submicrosecond time scale", Appl. Spectros., 43 (1989) 419-422.

138. Franko, M. and Tran, C.D., "Thermal lens technique for sensitive kinetic determination of fast chemical reactions: Part II - Experimental", Rev. Sci. Instrum., 62 (1991) 2438-2442.

139. Franko, M. and Tran, C.D., "Thermal lens technique for sensitive kinetic determinations of fast chemical reactions: Part I - Theory", Rev. Sci. Instrum., 62 (1991) 2430-2437.

140. Satchell, D.P.N., "The use of the acidity function H_0 as a tool for the study of reaction mechanism in mixed solvents", J. Chem. Soc., (1957) 2878-2882.

141. Laidler, K.J., "Chemical kinetics", 2nd ed., McGraw-Hill, New York, (1965) 514-517.

142. Morrison, R.T. and Boyd, R.N., "Organic chemistry", 3rd ed., Allyn and Bacon, Boston, (1973) 707-708.

143. Pang, T.-K.J. and Morris, M.D., "Differential thermal lens liquid chromatography detector", Anal. Chem., 57 (1985) 2153-2155.

144. Erskine, S.R. and Bobbitt, D.R., "Obliquely crossed, differential thermal lens measurements under conditions of high background absorbance", Appl. Spectros., 43 (1989) 668-674.

145. Schugar, H.J., Rossman, G.R., Barraclough, C.G. and Gray, H.B., "Electronic structure of oxo-bridged iron(III) dimers", J. Am. Chem. Soc., 94 (1972) 2683-2690.

146. Benjamin, M.M. and Leckie, J.O., "Multiple-site adsorption of Cd, Cu, Zn, and Pb on amorphous iron oxyhydroxide", J. Colloid Int. Sci., 79 (1981) 209-221.

Appendix A

THERMAL LENSING DATA ACQUISITION HARDWARE

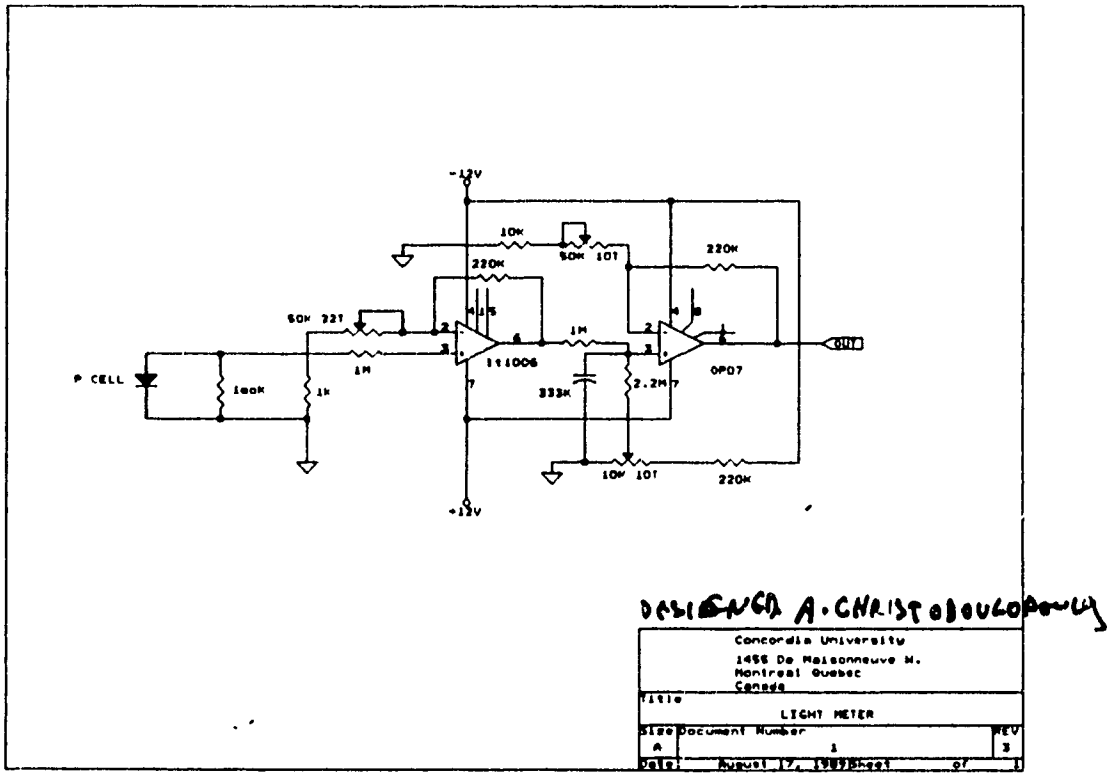

Figure A-1: Amplifier circuit for the photodiode used in combination with a pinhole as a detector in the thermal lensing apparatus. Potentiometers allow adjustment of baseline and gain. Voltage range full scale is -5V to +5V. (This unit was designed and constructed by the Science Technical Centre, Concordia University.)

Table A-1: Hardware settings of the TECMAR LABMASTER

Location	Pins	Operation
Mother board:		
J1		cable to daughter board
J2		unused
J3		unused parallel port
J4	1	D/A channel 0 output to shutter
	3	ground to shutter
J5	2-3	select I/O mapped option
	6-7	
J6	3-11	set D/A channel 0 for -10 to +10V
	9-10	
J7	(none)	interupts disabled
J8	1-2	select normal configuration of
	4-5	parallel port
J9		unused
SW1	($00)	
SW2	($04)	I/O address beginning at $0710
SW3	($C4)	
Daughter board (DT5712):		
JAD	5-6	factory set
	13-14	select unipolar input
JCD	4-16	normal and free run
	8-9	not external strobing
	19-20	not free run
JDD	9-10	
	11-23	
	12-24	bipolar 12-bit input
	13-14	(two's compliment output)
	19-20	
	21-22	
JFD		unused
JSD	1-2	
	3-4	select single ended input
	5-6	
P1D	20	channel 0 A/D in from photodiode
		(all other channels grounded)
P2D		cable to mother board
P3D		unused
P4D		unused
R_{ext}	(20kΩ)	set hardware programmable gain = 2
C_{ext}	(none)	(necessary for gain >10 only)

Note: Hyphen between pin nos. indicates jumper connection.

Legend: J Jumper SW Switch P Pin connector
R Resistor C Capacitor

Appendix B

THERMAL LENSING DATA ACQUISITION SOFTWARE

The data acquisition program is written in the Asyst language. Three programs must be present for Asyst operation: .COM (executable file); .OVL (overlay file containing defined operations); ASYST.MSG (error message file - must remain present during program execution). Asyst requires that the computer be equipped with a math coprocessor.

The source code for the most recent version (V 4.60) of the acquisition program is contained in the files LTL-460.ACQ and LTLA-460.ACQ[a]. A listing of the program is provided at the end of this appendix. The code was split to allow use of the Asyst V1.02 editor which has a 16 kB buffer. The files may also be edited using any ASCII compatible editor or word processor. Newer versions of Asyst allow the edit buffer to be expanded up to 64 kB. The Asyst language and the compiled programs have been combined and saved. They may be loaded by entering "LTL-V460" (corresponding to the .COM and .OVL files). This places the user in the Asyst environment.

The acquisition program is executed by entering "RUN". Figure B-1 contains a "map" of program use which is largely run using function keys. The first operation under the top menu is data acquisition. The acquisition menu allows relevant information to be entered (F1) and the various adjustable parameters to be set (F2-F8). The timing windows have several options. Normal operation is the use of "linear" windows <1>.

---

[a]Much thanks to Claude Arbour for writing the thermal lensing acquisition program version 1.0 for use with the photodiode array.

Provision has been made for the future addition of another type of window <2>. Alternatively timing windows may be loaded from a preexisting data file <3>. Data acquisition begins by pressing F9 in the acquisition menu. During acquisition a plot of I_∞ intensity versus time is displayed. Asyst "recognizes" a number of interface boards including the Tecmar Labmaster (system overlay file ACQLM.SOV in Asyst versions 2.0 and 3.0). This simplifies programming as all the details of communication are handled by Asyst. Asyst requires that the interface be I/O configured rather than memory mapped which does reduce acquisition frequency somewhat.

Analysis is the second option in the top menu. This includes saving (F1) and loading (F2) of raw data and saving data in formats suitable for Laplace analysis (F7-$\Delta I/I_\infty$ and true acquisition time) and general data handling software (F6-acquisition time, I_0, I_∞, and $\Delta I/I_\infty$). Changes in I_0 and I_∞ intensity and $\Delta I/I_\infty$ with time may be observed with plot data (F3). Segments of data may be expanded using the array readout functions described at the bottom of figure B-1. Plots may also be directed to the printer. Data or portions of it (range and every n^{th} step) may be printed using F4. Averages and standard deviations of I_0, I_∞ and $\Delta I/I_\infty$ can be calculated over a range of times (F5). This is suited to the analysis of standards or non-kinetic samples where the thermal lensing signal is not changing with time. F9 allows the data disk directory to be listed without having to exit the program.

A function key has been assigned to allow Laplace analysis routines to be added to the program (F3 in the top menu). Restrictions in memory allocation (such as for array size) will not permit both programs to be resident at the same time. However Asyst V3.0 permits user programs to be compiled into application overlays which may be accessed

very quickly. With limited modification to the existing programs both data acquisition and Laplace analysis routines could be accessed in a manner transparent to the user.

A routine to facilitate monitoring and debugging of timing has been included in the program. This allows various parameters important to timing synchronization to be printed out. The "check timing" routine (F4 in the top menu) should be executed after any changes are made to the acquisition sections of the program or any I/O hardware is altered. It may also be used to determine if a poor choice of adjustable parameters has resulted in timing faults during normal use. The printout lists the data point number (#.point) and a flag shows whether acquisition is fast (0) or normal (1). Synchro.delay is the interval between successive points while ramp.# is the cumulative interval (expected acquisition time). To reduce software overhead time during the actual acquisition these values are calculated at the beginning of the acquisition routine. The actual time between acquisition of each I_- and time zero is listed as "true.time". The true interval times are determined and appear as "difference". Errors in timing will appear most clearly as discrepancies between the calculated "synchro.delay" and the measured "difference". These errors in timing are relatively small and have been well defined for the current version of the acquisition program. They occur uniquely for the first point of a timing window. The largest error occurs in window 1 (start of acquisition). Tables B-1 and B-2 show how these discrepancies may be calculated. It should be pointed out that these "errors" are only differences between intervals requested by the user and those which actually occur. In no way do they reduce the accuracy of acquisition time in the final data. Indeed actual acquisition times are measured with a high degree of accuracy. An example of output from the check timing routine appears in table B-3.

The "alignment" option (F5 in the top menu) provides the user with an on screen continuous reading from the photodiode. This is useful in aligning optical components.

For more precise alignment of optics a second tool is available. "Fast acquisition" (F6) is a miniature acquisition routine. It uses the fixed parameters of 1000 scans/acquisition, 500 ms development delay and 1000 ms decay delay. On screen display of $\Delta I/I_{-}$ every c. 7 seconds (interval) facilitates maximizing sensitivity particularly in pinhole positioning and the coaxial alignment of pump and probe beams at the cell.

Figure B-1: Menu map of thermal lensing acquisition program

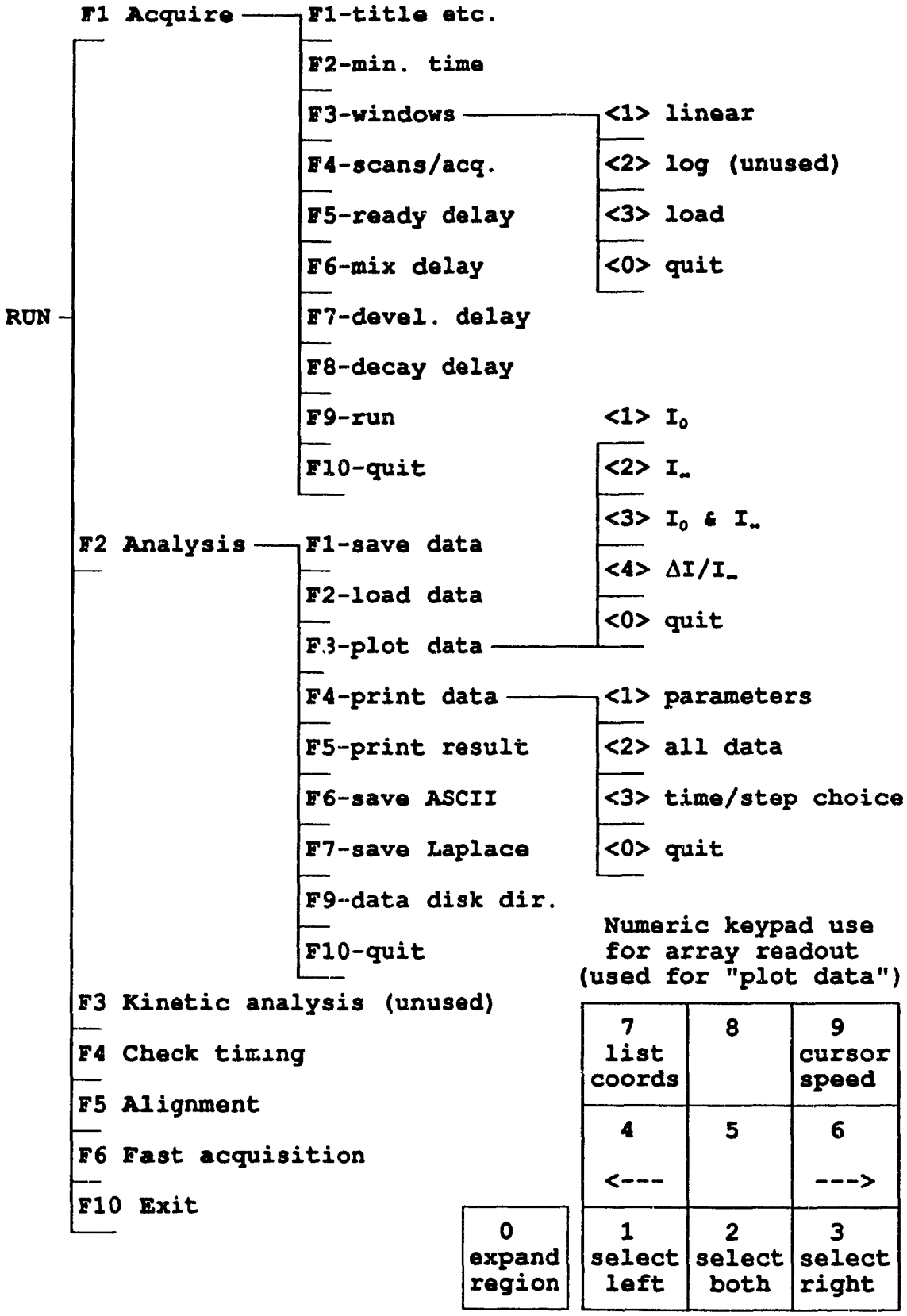

Table B-1
Calculation of discrepancies in timing by the acquisition software. These occur in the timing of the first I_{∞} acquisition in a window. In a "fast" acquisition window the shutter remains open.

Timing operation	Timing error (ms)
Fast acquisition window	(0.92 x SCANS/ACQ) + 150
Normal acquisition window	(0.92 x SCANS/ACQ) + 150 + DEVELOPMENT.DELAY

Table B-2:
Calculation of the actual time of the first I_{∞} acquisition relative to kinetic time zero. The calculated value (in ms) will correspond to the mid-point of the acquisition period.

first I_{∞} acq = MIX.DELAY +	DEVELOPMENT.DELAY (if window 1 = fast) **or** 2 x DEVELOPMENT.DELAY (if window 1 = normal)	+ (1.205 x SCANS/ACQ) + 20

Table B-3: Results of the timing check routine in LTL-V460. All times are in ms. A point is acquired at time zero. The windows are set to then acquire 5 more at each of 1000, 2000 and 5000 ms intervals. In this example the parameters have been poorly chosen. The window 1 interval time could not be met during actual operation (values of c. 1064 ms in "difference" column). The first value of "difference" in each of the 3 windows (marked by *) were calculated from table B-1 to be 2070, 3070 and 6470 ms, respectively. First acquisition was calculated from table B-2 to be 1625 ms.

#.point	flag	synchro.delay	ramp.#	true.time	difference
1	0	0.	0.	1628.	
2	0	1000.	1000.	3696.	2068. *
3	0	1000.	2000.	4760.	1064.
4	0	1000.	3000.	5824.	1064.
5	0	1000.	4000.	6892.	1068.
6	0	1000.	5000.	7956.	1064.
7	0	2000.	7000.	11024.	3068. *
8	0	2000.	9000.	13024.	2000.
9	0	2000.	11000.	15024.	2000.
10	0	2000.	13000.	17024.	2000.
11	0	2000.	15000.	19024.	2000.
12	1	5000.	20000.	25492.	6468. *
13	1	5000.	25000.	30492.	5000.
14	1	5000.	30000.	35492.	5000.
15	1	5000.	35000.	40492.	5000.
16	1	5000.	40000.	45492.	5000.

First acquisition = 1628 ms

Window no.=	1	win. type =	linear	no. times=	5
start time =	.ms	stop time =	5000.ms	interval=	1000.ms
Window no.=	2			no. times=	5
start time =	5000.ms	stop time =	15000.ms	interval=	2000.ms
Window no.=	3			no. times=	5
start time =	15000.ms	stop time =	40000.ms	interval =	5000.ms
scans/acq =	1000	min. time =	1000.ms	ready delay=	10000.ms
mix delay =	0.ms	dev. delay=	400.ms	decay delay=	700.ms

LASER THERMAL LENSING
DATA ACQUISITION AND ANALYSIS PROGRAM

*** LTLACQ V 4.60 ***
*** MAY 2/91 ***

```
\
\ DECLARATIONS AND INITIALIZATION
\ ********************************
```

```
INTEGER SCALAR CHOICE                \ user selection
      SCALAR CHOICE.1
      SCALAR PRINTER.CHOICE          \ output to printer/screen flag
      SCALAR #.SCAN                  \ scans/acquisition
      SCALAR POINTER                 \ array pointer
      SCALAR N.W                     \ number of windows set up
      SCALAR #.POINT                 \ total acquisition cycles
      SCALAR S.INDEX                 \ array pointer (start)
      SCALAR E.INDEX                 \   (end)
      SCALAR INDEX                   \ (located value)
      SCALAR INDEX.1
      SCALAR I.COUNT                 \ loop counter
      SCALAR LOOP.STEP               \ loop step (every nth point)
      SCALAR SHUTTER.?               \ fast/normal acquisition flag

      DIM[ 6 ] ARRAY N.TIME          \ number of cycles in each window
      DIM[ 2 ] ARRAY Y.D.PLOT        \ Y coordinates for data plot
      DIM[ 1 ] ARRAY #.SCAN.A        \ ".A" arrays are to allow save of scalar
      DIM[ 1 ] ARRAY #.POINT.A       \   variables (can not save scalars)
      DIM[ 1 ] ARRAY N.W.A
      DIM[ 1000 ] ARRAY IN.ARRAY     \ "buffer" for photodiode readings
      DIM[ 1000 ] ARRAY SHUT.FLAG    \ flag fast/normal acq. at each acq. time

REAL SCALAR DELAY.SYN                \ for calculation of delays
   SCALAR DECAY.DELAY
   SCALAR DEV.DELAY                  \ development delay
   SCALAR MIX.DELAY
   SCALAR READY.DELAY
   SCALAR TIME.ZERO                  \ computer clock time at kinetic time zero
   SCALAR TIME.START
   SCALAR FIRST.ACQ                  \ time of 1st I_ after kinetic time zero
   SCALAR TIME.SET                   \ for indexing time (ie. locating in array)
   SCALAR MIN.TIME                   \ determines if fast or normal acquisition
   SCALAR S.TIME                     \ start time (user selected interval)
   SCALAR E.TIME                     \ end time
   SCALAR I.ZERO.NO.SHUTTER          \ 1st I0 measured (used for fast acq.)
```

```
SCALAR BKG.DATA                          \ photodiode background reading
SCALAR FAST.I.ZERO                       \ used in FAST.DELTA.I (I0)
SCALAR FAST.I.INF                        \ alignment routine (I_)
SCALAR FAST.BKG.DATA

DIM[ 1000 ] ARRAY I.ZERO                 \ I0 (acquisition routine)
DIM[ 1000 ] ARRAY I.INF                  \ I_
DIM[ 1000 ] ARRAY DELTA.I                \ ΔI/I_
DIM[ 5 ] ARRAY START.TIME                \ window start time
DIM[ 5 ] ARRAY STOP.TIME                 \ (stop)
DIM[ 5 ] ARRAY TIME.FACTOR               \  (cycle time)
DIM[ 1000 ] ARRAY RAMP.#                 \ calculated time of each acquisition
DIM[ 4 ] ARRAY DELAYS.ARRAY              \ save
DIM[ 1 ] ARRAY FIRST.ACQ.A               \ save
DIM[ 2 ] ARRAY X.D.PLOT                  \ X coordinates for plotting
DIM[ 1 ] ARRAY MIN.TIME.A                \ save
DIM[ 1 ] ARRAY BKG.DATA.A                \ save
DIM[ 1000 ] ARRAY SYNCHRO.DELAYS         \ time until next acq. (precalculated)
DIM[ 1000 ] ARRAY TRUE.TIME              \ actual acquisition times

8 STRING SAVE.DATE                       \ experiment date (automatically recorded)
16 STRING OP.NAME                        \ operator
16 STRING TITLE                          \ experiment title
8 STRING EXP#                            \ experiment number
10 STRING W.TYPE                         \ type of window
5 STRING SAVE.TIME                       \ experiment time (automatically recorded)
16 STRING LASER                          \ pump laser type
5 STRING APERTURE                        \ pump laser aperture
13 STRING WAVELENGTH                     \ pump wavelength
35 STRING LASER.POWER                    \ pump power
14 STRING FILENAME
5 STRING VERSION                         \ acquisition software version

LAB.MASTER                               \ Configure A/D and D/A

0 0 A/D.TEMPLATE 0.CHNL.IN
IN.ARRAY TEMPLATE.BUFFER
A/D.INIT

0 0 D/A.TEMPLATE 0.CHNL.OUT
D/A.INIT

0 0 0 79 WINDOW {TOPLINE}                \ Define screen windows
1 0 19 79 WINDOW {SPECS}
20 0 20 79 WINDOW {SPLIT1}
23 0 24 79 WINDOW {SPLIT2}
19 0 24 79 WINDOW {PROLINE}
1 0 24 79 WINDOW {DEF-1}
21 0 22 79 WINDOW {SPLIT3}
```

```
: T.SC                                  \ Routines to clear screen windows
  {TOPLINE} SCREEN.CLEAR
;

: SS.SC                                 \ Note that routines are written as "colon
  {SPECS} SCREEN.CLEAR                  \ definitions". Each routine begins with a
;                                       \ colon and ends with a semi-colon. The
                                        \ word immediately following the colon is
: S1.SC                                 \ used to execute the routine.
  {SPLIT1} SCREEN.CLEAR
;

: S2.SC
  {SPLIT2} SCREEN.CLEAR
;

: P.SC                                  \ HINT: It is advisable to read this
  {PROLINE} SCREEN.CLEAR                \     program from the bottom up!
;

: D.SC
  {DEF-1} SCREEN.CLEAR
;

: S3.SC
  {SPLIT3} SCREEN.CLEAR
;

: DEF.FILE.TEMPLATE                     \ Define template for save/load routines
  FILE.TEMPLATE
   11 COMMENTS
   REAL DIM[ 1000 ] SUBFILE
   5 TIMES
   REAL DIM[ 4 ] SUBFILE
   INTEGER DIM[ 6 ] SUBFILE
   INTEGER DIM[ 1 ] SUBFILE
   3 TIMES
   REAL DIM[ 1 ] SUBFILE
   2 TIMES
   REAL DIM[ 5 ] SUBFILE
   3 TIMES
   REAL DIM[ 1 ] SUBFILE
   END
;

: GET.NUMBER
  CR ." Enter your choice = "
  #INPUT CHOICE :=
;
```

```
: BANNER
  T.SC
  5 SPACES
  ." *** LTL ACQUISITION PROGRAM " VERSION "TYPE
  ."  FOR PINHOLE/PHOTODIODE DETECTOR ***"
;

: MAIN.MENU                                   \ Display main menu
  S1.SC
  30 SPACES ." ** MAIN MENU **"
  S2.SC
  3 SPACES
  ." F1) ACQUISITION   F2) RAW ANALYSIS   F3) KINETIC ANALYSIS"
  CR 3 SPACES
  ." F4) CHECK TIMING   F5) ALIGNMENT      F6) FAST DELTA.I   F10) EXIT"
  CURSOR.OFF
;

\ SET UP PARAMETERS
\ **********************

: SHOW.PARA                                   \ Show parameter setting (screen or printer)
  SS.SC
  1 PRINTER.CHOICE = IF
   OUT>PRINTER
  THEN
  CR CR
  ." EXP. TITLE: " 16 TITLE "LEN "TYPE - SPACES
  ."  EXP. NO. : " 8 EXP# "LEN "TYPE - SPACES 5 SPACES
  ." FILE NAME  : " FILENAME "TYPE
  CR
  ." OPERATOR  : " 16 OP.NAME "LEN "TYPE - SPACES
  ."  EXP. DATE: " SAVE.DATE "TYPE 5 SPACES
  ." EXP. TIME  : " SAVE.TIME "TYPE 4 SPACES
  VERSION "TYPE
  CR CR
  ." LASER TYPE: " 16 LASER "LEN "TYPE - SPACES
  ."  APERTURE : " 5 APERTURE "LEN "TYPE - SPACES 8 SPACES
  ." WAVELENGTH : " WAVELENGTH "TYPE
  CR ." LASER POWER (mW) and measured position: " LASER.POWER "TYPE
  CR CR
  N.W 1 + 1 DO
   3 0 FIX.FORMAT
   ." WINDOW NO.=    " I .
   7 SPACES
   I 1 = IF
    ."  WINDOW TYPE =  " W.TYPE "TYPE
    ELSE 22 SPACES
   THEN
```

```
   5 SPACES
   4 0 FIX.FORMAT
   ." NO. TIMES  =" 4 SPACES N.TIME [ I ] .
   CR
   8 0 FIX.FORMAT
   ." START TIME=" START.TIME [ I ] . ." ms"
   ."     STOP TIME   = " STOP.TIME [ I ] . ." ms"
   ."  INTERVAL   = " TIME.FACTOR [ I ] . ." ms"
   CR
  LOOP
  CR
  4 0 FIX.FORMAT
  ." SCANS/ACQ.=   " #.SCAN . 8 SPACES
  8 0 FIX.FORMAT
  ." MINIMUM TIME= " MIN.TIME . ." ms"
  ."  READY DELAY= " READY.DELAY . ." ms"
  CR
  ." MIX DELAY =" MIX.DELAY . ." ms"
  ."    DEVEL. DELAY= " DEV.DELAY . ." ms"
  ."  DECAY DELAY= " DECAY.DELAY . ." ms"
  9 2 FIX.FORMAT
;

: ACQ.MENU                              \ Display data acquisition menu
  S3.SC
  S1.SC
  26 SPACES ." ** ACQUISITION MENU **"
  S2.SC
  ." F1) TITLE ETC. F3) WINDOWS   F5) READY DELAY F7) DEVEL DELAY"
  ."   F9) RUN" CR
  ." F2) MIN.TIME   F4) SCANS/ACQ F6) MIX DELAY   F8) DECAY DELAY  "

  ."  F10) EXIT"
  SHOW.PARA
;

: SET.TITLE                             \ Enter relevant data (F1 in acq. menu)
  S1.SC
   ." Space bar + Enter to retain previous value"
  S2.SC
   CR ." OPERATOR NAME (16 chars.): "
   "INPUT "DUP
   "  " "= IF
    "DROP
    ELSE OP.NAME ":=
   THEN
  S2.SC
   CR ." EXP. TITLE (16 chars.): "
   "INPUT "DUP
```

```
    " " "= IF
     "DROP
     ELSE TITLE ":=
    THEN
   S2.SC
    CR ." EXPERIMENT NO. (8 chars.): "
    "INPUT "DUP
    " " "= IF
     "DROP
     ELSE EXP# ":=
    THEN
   S2.SC
    CR ." LASER TYPE (16 chars.): "
    "INPUT "DUP
    " " "= IF
     "DROP
     ELSE LASER ":=
    THEN
   S2.SC
    CR ." LASER APERTURE (5 chars.): "
    "INPUT "DUP
    " " "= IF
     "DROP
     ELSE APERTURE ":=
    THEN
   S2.SC
    CR ." WAVELENGTH (13 chars.): "
    "INPUT "DUP
    " " "= IF
     "DROP
     ELSE WAVELENGTH ":=
    THEN
   S2.SC
    CR ." LASER POWER (mW) AND MEASURING POSITION (35 chars.): "
    "INPUT "DUP
    " " "= IF
     "DROP
     ELSE  LASER.POWER ":=
    THEN
   ACQ.MENU
;

: SET.MIN.TIME                          \ Parameter set by F2 in acq. menu
   S3.SC
   ." SHUTTER STAYS OPEN IF MINIMUM > [INTERVAL - DEVEL. - DECAY]"
   S2.SC
   CR ." Enter minimum time (ms): "     \ NOTE THAT ALL TIMING IN THIS
   #INPUT MIN.TIME :=                   \ PROGRAM IS IN MILLISECONDS
   S3.SC
```

```
  ACQ.MENU
;

: WINDOW.RAMP                          \ Set linear windows
  D.SC                                 \ (associated with SET.UP.WINDOW)
  CR
  1 POINTER :=
  1 N.TIME :=
  1 N.W :=
  0 RAMP.# :=                          \ Initialize to prevent RUN.ACQ crash
   CR 5 SPACES
   ." ** Since data is acquired at start time in window 1, number of times"
   CR 5 SPACES ."         is 1 greater than indicated"
   CR 5 SPACES
   ." ** For multiple windows start time is normally previous stop time"
   CR 5 SPACES ." ** Maximum of 5 windows allowed. Max of 998 data points"
   CR 5 SPACES
   ." ** Do NOT place a fast acq. window [ MIN > (INTERVAL-DEVEL-DECAY)]"
   CR 5 SPACES ."         after a normal one."
   CR 5 SPACES
   ." ** Window following a no-shuttering one should NOT have a long interval"
   CR CR 25 SPACES ." *** ENTER ALL ZEROS WHEN DONE ***"
  BEGIN
   CR CR ." WINDOW no. " N.W .
   CR ." Enter the starting time (ms)  = "
   #INPUT START.TIME [ N.W ] :=
   CR ." Enter the stopping time (ms)  = "
   #INPUT STOP.TIME [ N.W ] :=
   CR ." Enter the number of times (>2) = "
   #INPUT N.TIME [ N.W ] :=
   N.TIME [ N.W ] 0 = NOT IF
    STOP.TIME [ N.W ] START.TIME [ N.W ] - N.TIME [ N.W ] /
    TIME.FACTOR [ N.W ] :=
    N.TIME [ N.W ] 1 + 1 DO
     START.TIME [ N.W ] TIME.FACTOR [ N.W ] I * +
     RAMP.# [ POINTER I + ] :=
    LOOP
    N.TIME [ N.W ] POINTER + POINTER :=
    N.W 1 + N.W :=
   THEN
   6 N.W = IF
    0 N.TIME [ N.W ] :=
   THEN
   N.TIME [ N.W ] 0 =
  UNTIL
  POINTER #.POINT :=
  0 RAMP.# [ 1 ] :=
  N.W 1 - N.W :=
;
```

```
: LOAD.RAMP                          \ Load timing ramp from another data file
  D.SC
  CR ." Enter the data filename (specify drive): "
  "INPUT FILENAME ":=
  FILENAME DEFER> FILE.OPEN
  5 COMMENT> W.TYPE ":=
  4 SUBFILE RAMP.# FILE>ARRAY
  6 SUBFILE DELAYS.ARRAY FILE>ARRAY
  7 SUBFILE N.TIME FILE>ARRAY
  8 SUBFILE #.SCAN.A FILE>ARRAY
  9 SUBFILE #.POINT.A FILE>ARRAY
  10 SUBFILE N.W.A FILE>ARRAY
  12 SUBFILE MIN.TIME.A FILE>ARRAY
  13 SUBFILE START.TIME FILE>ARRAY
  14 SUBFILE STOP.TIME FILE>ARRAY
  15 SUBFILE TIME.FACTOR FILE>ARRAY
  FILE.CLOSE
  DELAYS.ARRAY [ 1 ] READY.DELAY :=
  DELAYS.ARRAY [ 2 ] MIX.DELAY :=
  DELAYS.ARRAY [ 3 ] DEV.DELAY :=
  DELAYS.ARRAY [ 4 ] DECAY.DELAY :=
  #.POINT.A [ 1 ] #.POINT :=
  #.SCAN.A [ 1 ] #.SCAN :=
  N.W.A [ 1 ] N.W :=
  MIN.TIME.A [ 1 ] MIN.TIME :=
;

: LOG.WINDOW                         \ Allows addition of another type of
  D.SC                               \   window ramping
  CR CR
  CR ." This program is not available yet !"
  CR ." Press any key to continue. "
  PCKEY ?DROP DROP
;

: SET.UP.WINDOW                      \ Parameters set by F3 in acq. menu
  D.SC
  CR CR
  CR ." 1) Linear Window    2) Log Window    3) Load Window    0) Quit"
  CR CR CR
  GET.NUMBER
  CHOICE 1 = IF
   " LINEAR" W.TYPE ":=
   WINDOW.RAMP
  ELSE
   CHOICE 2 = IF
    " LOG" W.TYPE ":=
    LOG.WINDOW
   ELSE
```

```
    CHOICE 3 = IF
     LOAD.RAMP
    THEN
   THEN
  THEN
  ACQ.MENU
;

: SET.#.SCAN                                    \ Parameter set by F4 in acq. menu
  S2.SC
  ." Integration=(0.591*#.SCANS)+3.8ms    Shutter open=(0.911*#.SCANS)+~22 ms"
  CR ." Enter the number of scans per acquisition (1000 max.) = "
  #INPUT #.SCAN :=
  ACQ.MENU
;

: SET.READY.DELAY                               \ Parameter set by F5 in acq. menu
  S2.SC
  CR ." Enter the ready delay (ms; >=5000) = "
  #INPUT READY.DELAY :=
  ACQ.MENU
;

: SET.MIX.DELAY                                 \ Parameter set by F6 in acq. menu
  S2.SC
  CR ." Enter the mixing delay (ms; >=0) = "
  #INPUT MIX.DELAY :=
  ACQ.MENU
;

: SET.DEV.DELAY                                 \ Parameter set by F7 in acq. menu
  S2.SC
  CR ." Enter the development delay (ms; >=0) = "
  #INPUT DEV.DELAY :=
  ACQ.MENU
;

: SET.DECAY.DELAY                               \ Parameter set by F8 in acq. menu
  S2.SC
  CR ." Enter the decay delay (ms; >=0) = "
  #INPUT DECAY.DELAY :=
  ACQ.MENU
;
```

```
\ ACQUISITION AND CONTROL
\ ****************************

: SET.SHUTTER.FLAGS                    \ Set flags to indicate in which windows
  1 POINTER :=                         \ shutter will operate (ie. normal or fast
  0 SHUT.FLAG :=                       \ acquisition)
  N.W 1 + 1 DO
   0 SHUTTER.? :=                      \ 0 = shutter remains open (fast acq.)
   TIME.FACTOR [ I ] DEV.DELAY - DECAY.DELAY - MIN.TIME > IF
    1 SHUTTER.? :=                     \ 1 = shutter operates (normal acquisition)
   THEN
   N.TIME [ I ] 1 + 1 DO
    SHUTTER.? SHUT.FLAG [ POINTER I + ] :=
   LOOP
   N.TIME [ I ] POINTER + POINTER :=
  LOOP
  SHUT.FLAG [ 2 ] SHUT.FLAG [ 1 ] :=
;


: SET.SYNCHRO.DELAYS                   \ Set delay for acq. timing synchronization
  .001 SYNCHRO.DELAYS [ 1 ] :=         \ Delay cannot = 0
  #.POINT 1 DO
   RAMP.# [ I 1 + ] RAMP.# [ I ] - DELAY.SYN :=
   DELAY.SYN SYNCHRO.DELAYS [ I 1 + ] :=
  LOOP
  SYNCHRO.DELAYS [ #.POINT ] SYNCHRO.DELAYS [ #.POINT 1 + ] :=
;

: VIDEO.SET                            \ Set screen to allow monitoring of L
  0 .4 VUPORT.ORIG                     \  intensity during acquisition
  1 .6 VUPORT.SIZE
  AXIS.DEFAULTS
  5 7 AXIS.DIVISIONS
  HORIZONTAL
   GRID.OFF
   0 1 LABEL.POINTS
   0 RAMP.# []MAX WORLD.SET
  VERTICAL
   GRID.OFF
   0 1 LABEL.POINTS
   0 4200 WORLD.SET
  XY.AXIS.PLOT
;
```

```
: CLOSE.SHUTTER                          \ D/A voltage low to close shutter
  0.CHNL.OUT
  D/A.INIT
  0 D/A.OUT
;

: OPEN.SHUTTER                           \ D/A voltage high to open shutter
  0.CHNL.OUT
  D/A.INIT
  1024 D/A.OUT
;

: ACQ.DATA                               \ Read the photodiode "scans/acq." times
  0.CHNL.IN                              \   and average the result
  A/D.INIT
  #.SCAN 1 + 1 DO
   A/D.IN>ARRAY
  LOOP
  IN.ARRAY SUB[ 1 , #.SCAN , 1 ] MEAN
;

: I.ZERO.IN                              \ Acquire I0 value
  0 SHUT.FLAG [ I ] = IF                 \ If fast acq. then use initial I0 value
   I.ZERO.NO.SHUTTER I.ZERO [ I ] :=
  ELSE                                   \ If normal acq. then close shutter and
   CLOSE.SHUTTER                         \   read I0
   DECAY.DELAY MSEC.DELAY
   ACQ.DATA
   BKG.DATA - I.ZERO [ I ] :=
  THEN
;

: I.INF.IN                               \ Acquire I∞ value
  0 SHUT.FLAG [ I ] = IF                 \ If fast acq. then read immediately
   REL.TIME                              \ (First acq. of I∞ allowing development
   ACQ.DATA                              \   is handled in RUN.ACQ routine)
   BKG.DATA - I.INF [ I ] :=
   TRUE.TIME [ I ] :=
  ELSE                                   \ If normal acq. then allow development
   OPEN.SHUTTER                          \   before reading I∞
   DEV.DELAY MSEC.DELAY
   REL.TIME
   ACQ.DATA
   BKG.DATA - I.INF [ I ] :=
   TRUE.TIME [ I ] :=
  THEN
;
```

```
: PLOT.POINT                          \ Plot I_ point on screen during acquisition
  0 Y.D.PLOT :=                       \   (Associated with RUN.ACQ)
  0 X.D.PLOT :=
  I.INF [ I ] Y.D.PLOT [ 2 ] :=
  RAMP.# [ I ] X.D.PLOT [ 2 ] :=
  DOTTED
  X.D.PLOT Y.D.PLOT XY.DATA.PLOT
;

: RUN.ACQ                             \ MAIN ACQUISITION ROUTINE
  " V4.60" VERSION ":=                \ Reset V. in case changed by loading data
  SET.SHUTTER.FLAGS
  SET.SYNCHRO.DELAYS
  "DATE SAVE.DATE ":=
  "TIME SAVE.TIME ":=
  GRAPHICS.DISPLAY
  P.SC
  ACQ.DATA                            \ Test for excessive photodiode gain
  ." INTENSITY READING = "
  9 2 FIX.FORMAT DUP 2048 + .
  1800 > IF
   CR ." ** A/D LIMIT IS 4095 ** REDUCE GAIN ** "
  THEN
  VIDEO.SET
  CR CR ." Close the He-Ne beam."
  CR ." Press any key to start."
  PCKEY ?DROP DROP
  #.SCAN #.SCAN.A [ 1 ] :=
  1000 #.SCAN :=
  ACQ.DATA
  BKG.DATA :=
  #.SCAN.A [ 1 ] #.SCAN :=
  BELL
  P.SC
  ." BACKGROUND = " BKG.DATA 2048 + .    \ A/D input is -2047 to 2048
  CR CR ." Open the He-Ne beam."         \ User sees 0 to 4095
  CR ." Press any key and mix at the second beep."
  PCKEY ?DROP DROP
  P.SC
  ." * DATA ACQUISITION IN PROGRESS *"
  SYNCHRO.DELAYS [ 1 ] SYNC.PERIOD
  READY.DELAY 5000 - MSEC.DELAY
  BELL
  5000 MSEC.DELAY
  BELL
  REL.TIME TIME.ZERO :=
  MIX.DELAY MSEC.DELAY
  ACQ.DATA
  BKG.DATA - I.ZERO.NO.SHUTTER :=
```

```
  SYNCHRONIZE
  OPEN.SHUTTER                          \ This is necessary to allow fast acq. but
  DEV.DELAY MSEC.DELAY                  \    causes excess development of first I_
  #.POINT 1 + 1 DO                      \    in normal acq.
   SYNCHRONIZE
   I.INF.IN
   PLOT.POINT
   SYNCHRO.DELAYS [ I 1 + ] SYNCHRO.DELAYS [ I ] = NOT IF
    SYNCHRO.DELAYS [ I 1 + ] SYNC.PERIOD
    SYNCHRONIZE
   THEN             \ The calculations below do:
   I.ZERO.IN        \ 1) Find timing delay of the first I_ acquisition relative to
  LOOP              \         the expected start time
  CLOSE.SHUTTER     \ 2) Correct all acq. times to centre of the I_ acquisition period
  BELL              \ 3) Calculate ΔI/I_ for all acquisitions
  P.SC
  CR CR ." * DATA ACQUISITION TERMINATED *"
  CR ." * RESULT CALCULATION IN PROGRESS *"
  TRUE.TIME [ 1 ] TIME.ZERO - FIRST.ACQ :=
  0.591 #.SCAN * 2 / FIRST.ACQ + FIRST.ACQ :=
  #.POINT 1 + 1 DO
   I.ZERO [ I ] I.INF [ I ] - I.INF [ I ] / DELTA.I [ I ] :=
   TRUE.TIME [ I ] TIME.ZERO - TRUE.TIME [ I ] :=
   0.591 #.SCAN * 2 / TRUE.TIME [ I ] + TRUE.TIME [ I ] :=
  LOOP
  BELL
  8 0 FIX.FORMAT
  P.SC CR ." * CALCULATION TERMINATED * FIRST ACQ. @ (ms): "
  FIRST.ACQ .
  CR CR ." Press any key to continue."
  PCKEY ?DROP DROP
  9 2 FIX.FORMAT
  SCREEN.CLEAR
  BANNER
  ACQ.MENU
;

: ACQ.KEYS                              \ Initialize F-keys for acq. menu
  F1 FUNCTION.KEY.DOES SET.TITLE
  F2 FUNCTION.KEY.DOES SET.MIN.TIME
  F3 FUNCTION.KEY.DOES SET.UP.WINDOW
  F4 FUNCTION.KEY.DOES SET.#.SCAN
  F5 FUNCTION.KEY.DOES SET.READY.DELAY
  F6 FUNCTION.KEY.DOES SET.MIX.DELAY
  F7 FUNCTION.KEY.DOES SET.DEV.DELAY
  F8 FUNCTION.KEY.DOES SET.DECAY.DELAY
  F9 FUNCTION.KEY.DOES RUN.ACQ
  F10 FUNCTION.KEY.DOES ESCAPE
;
```

```
: SET.ACQ.MENU                          \ F1 in main menu
  D.SC
  STORE.FUNCTION.KEYS
  ACQ.KEYS
  ACQ.MENU
  INTERPRET.KEYS
  ONESCAPE: RESTORE.FUNCTION.KEYS MAIN.MENU
;

: MAIN.QUIT                             \ Exit program
  D.SC
  S2.SC
  BELL
  ." Quit (Y/N) ?"
  PCKEY ?DROP 89 = IF BYE THEN
  MAIN.MENU
;
```

*** LTLA-ACQ V 4.60 ***

*** MAY 2/91 ***

```
\ DATA ANALYSIS AND I/O
\ ************************

: RAW.MENU                              \ Show analysis menu
  D.SC
  S1.SC
  30 SPACES ." ** RAW DATA MENU **"
  S2.SC
  ." F1)SAVE F2)LOAD F3)PLOT F4)PRINT F5)ANAL. F6)SAVE F7)SAVE      F9)DISK
F10)QUIT"
CR ."   DATA   DATA   DATA   DATA   RESULT  ASCII  LAPLACE  DIR"
;

: SAVE.DATA                             \ Save all necessary acq. parameters
  DEF.FILE.TEMPLATE                     \  (F1 in analysis menu)
  D.SC
  CR ." Enter the filename for save (specify drive): "
  "INPUT FILENAME ":=
  FILENAME DEFER> FILE.CREATE
  FILENAME DEFER> FILE.OPEN
  READY.DELAY DELAYS.ARRAY [ 1 ] := \ Place scalars in arrays to save
  MIX.DELAY DELAYS.ARRAY [ 2 ] :=
  DEV.DELAY DELAYS.ARRAY [ 3 ] :=
  DECAY.DELAY DELAYS.ARRAY [ 4 ] :=
  #.SCAN #.SCAN.A [ 1 ] :=
```

```
  #.POINT #.POINT.A [ 1 ] :=
  N.W N.W.A [ 1 ] :=
  FIRST.ACQ FIRST.ACQ.A [ 1 ] :=
  MIN.TIME MIN.TIME.A [ 1 ] :=
  BKG.DATA BKG.DATA.A [ 1 ] :=
  SAVE.DATE 1 >COMMENT
  OP.NAME 2 >COMMENT
  TITLE 3 >COMMENT
  EXP# 4 >COMMENT
  W.TYPE 5 >COMMENT
  SAVE.TIME 6 >COMMENT
  LASER 7 >COMMENT
  APERTURE 8 >COMMENT
  WAVELENGTH 9 >COMMENT
  LASER.POWER 10 >COMMENT
  VERSION 11 >COMMENT
  1 SUBFILE I.ZERO ARRAY>FILE
  2 SUBFILE I.INF ARRAY>FILE
  3 SUBFILE DELTA.I ARRAY>FILE
  4 SUBFILE RAMP.# ARRAY>FILE
  5 SUBFILE TRUE.TIME ARRAY>FILE
  6 SUBFILE DELAYS.ARRAY ARRAY>FILE
  7 SUBFILE N.TIME ARRAY>FILE
  8 SUBFILE #.SCAN.A ARRAY>FILE
  9 SUBFILE #.POINT.A ARRAY>FILE
  10 SUBFILE N.W.A ARRAY>FILE
  11 SUBFILE FIRST.ACQ.A ARRAY>FILE
  12 SUBFILE MIN.TIME.A ARRAY>FILE
  13 SUBFILE START.TIME ARRAY>FILE
  14 SUBFILE STOP.TIME ARRAY>FILE
  15 SUBFILE TIME.FACTOR ARRAY>FILE
  16 SUBFILE BKG.DATA.A ARRAY>FILE
  FILE.CLOSE
  RAW.MENU
;

: LOAD.DATA                          \ Load a data file (F2 in analysis menu)
  D.SC
  CR ." Enter the filename for load (specify drive): "
  "INPUT FILENAME ":=
  FILENAME DEFER> FILE.OPEN
  1 COMMENT> SAVE.DATE ":=
  2 COMMENT> OP.NAME ":=
  3 COMMENT> TITLE ":=
  4 COMMENT> EXP# ":=
  5 COMMENT> W.TYPE ":=
  6 COMMENT> SAVE.TIME ":=
  7 COMMENT> LASER ":=
  8 COMMENT> APERTURE ":=
```

```
  9 COMMENT> WAVELENGTH ":=
  10 COMMENT> LASER.POWER ":=
  11 COMMENT> VERSION ":=
  1 SUBFILE I.ZERO FILE>ARRAY
  2 SUBFILE I.INF FILE>ARRAY
  3 SUBFILE DELTA.I FILE>ARRAY
  4 SUBFILE RAMP.# FILE>ARRAY
  5 SUBFILE TRUE.TIME FILE>ARRAY
  6 SUBFILE DELAYS.ARRAY FILE>ARRAY
  7 SUBFILE N.TIME FILE>ARRAY
  8 SUBFILE #.SCAN.A FILE>ARRAY
  9 SUBFILE #.POINT.A FILE>ARRAY
  10 SUBFILE N.W.A FILE>ARRAY
  11 SUBFILE FIRST.ACQ.A FILE>ARRAY
  12 SUBFILE MIN.TIME.A FILE>ARRAY
  13 SUBFILE START.TIME FILE>ARRAY
  14 SUBFILE STOP.TIME FILE>ARRAY
  15 SUBFILE TIME.FACTOR FILE>ARRAY
  16 SUBFILE BKG.DATA.A FILE>ARRAY
  FILE.CLOSE
  DELAYS.ARRAY [ 1 ] READY.DELAY :=
  DELAYS.ARRAY [ 2 ] MIX.DELAY :=
  DELAYS.ARRAY [ 3 ] DEV.DELAY :=
  DELAYS.ARRAY [ 4 ] DECAY.DELAY :=
  #.SCAN.A [ 1 ] #.SCAN :=
  #.POINT.A [ 1 ] #.POINT :=
  N.W.A [ 1 ] N.W :=
  FIRST.ACQ.A [ 1 ] FIRST.ACQ :=
  MIN.TIME.A [ 1 ] MIN.TIME :=
  BKG.DATA.A [ 1 ] BKG.DATA :=
  SET.SHUTTER.FLAGS
  SET.SYNCHRO.DELAYS
  RAW.MENU
;

: SET.PLOT                                  \ (Associated with PLOT.DATA.A)
  GRAPHICS.DISPLAY
  0 .4 VUPORT.ORIG
  1 .6 VUPORT.SIZE
  AXIS.DEFAULTS
  8 9 AXIS.DIVISIONS
  HORIZONTAL
   GRID.OFF
   0 1 LABEL.POINTS
   0 RAMP.# [ #.POINT ] WORLD.SET
  VERTICAL
   GRID.OFF
   0 1 LABEL.POINTS
   4 CHOICE = IF
```

```
    -0.5 DELTA.I []MAX 0.5 + WORLD.SET
   ELSE
    0 4500 WORLD.SET
   THEN
  XY.AXIS.PLOT
;

: PLOT.DATA.A                          \ (Associated with PLOT.DATA)
  P.SC
  CR
  ." 1)I zero   2)I inf   3)I zero & I inf   4)DELTA I   0)Quit"
  CR
  GET.NUMBER
  0 CHOICE = NOT IF
   SET.PLOT
  THEN
  1 CHOICE = IF
   RAMP.# SUB[ 1 , #.POINT ]
   I.ZERO SUB[ 1 , #.POINT ]
   XY.DATA.PLOT
  ELSE
   2 CHOICE = IF
    RAMP.# SUB[ 1 , #.POINT ]
    I.INF SUB[ 1 , #.POINT ]
    XY.DATA.PLOT
   ELSE
    3 CHOICE = IF
     RAMP.# SUB[ 1 , #.POINT ]
     I.ZERO SUB[ 1 , #.POINT ]
     XY.DATA.PLOT
     RAMP.# SUB[ 1 , #.POINT ]
     I.INF SUB[ 1 , #.POINT ]
     XY.DATA.PLOT
    ELSE 4 CHOICE = IF
     RAMP.# SUB[ 1 , #.POINT ]
     DELTA.I SUB[ 1 , #.POINT ]
     XY.DATA.PLOT
     THEN
    THEN
   THEN
  THEN
  0 CHOICE = NOT IF
   NORMAL.COORDS
   .7 .9 READOUT>POSITION
   WORLD.COORDS
   ARRAY.READOUT
   S3.SC
   ." ENTER 1 TO PRINT SCREEN OR 0 TO CONTINUE: "
   #INPUT CHOICE :=
```

```
   1 CHOICE = IF
    SCREEN.PRINT
   THEN
   S3.SC
  THEN
;

: PLOT.DATA                          \ Plot the acquired or reloaded data
  D.SC                               \  (F3 in analysis menu)
  BEGIN
   PLOT.DATA.A                       \ Array.readout is engaged for all plots
   0 CHOICE =                        \  allowing X,Y coordinate readout
  UNTIL                              \  and expansion of selected segments
  BANNER                             \  of the plot
  D.SC
  RAW.MENU
;

: PRINT.PARA                         \ Parameters list out to screen or printer
  S2.SC
  ." PARAMETER OUTPUT TO SCREEN <0> OR PRINTER <1>?: "
  #INPUT PRINTER.CHOICE :=
  SHOW.PARA
  CR CR ." REAL START TIME =  "
  8 0 FIX.FORMAT
  FIRST.ACQ . ."  ms"
  9 2 FIX.FORMAT
  CR ." BACKGROUND USED = " BKG.DATA 2048 + . CR
  CONSOLE
;

: PRINT.TIME.DATA                    \ (Associated with PRINT.DATA)
   D.SC
   S2.SC
   ." DATA OUTPUT TO SCREEN <0> OR PRINTER <1>?: "
   #INPUT PRINTER.CHOICE :=
   S2.SC ." CTRL + NUM. LOCK TO PAUSE SCROLL"
   SS.SC
   1 PRINTER.CHOICE = IF
    OUT>PRINTER
   THEN
   CR CR CR 12 SPACES
   ." *** LTLACQ " VERSION "TYPE ."  ** PINHOLE/PHOTODIODE DATA REPORT
***"
   CR  ." STEP = " 3 0 FIX.FORMAT LOOP.STEP .
   10 SPACES ." FILE NAME: " FILENAME "TYPE CR
   ."     TIME        I.ZERO        I.INF        DELTA.I     TRUE.TIME"
   CR CR
   E.INDEX 1 + S.INDEX DO
```

```
    11 2 FIX.FORMAT
    RAMP.# [ I ] . 3 SPACES
    10 3 FIX.FORMAT
    I.ZERO [ I ] . 3 SPACES
    I.INF [ I ] . 3 SPACES
    10 5 FIX.FORMAT
    DELTA.I [ I ] . 3 SPACES
    11 2 FIX.FORMAT
    TRUE.TIME [ I ] .
    CR
   LOOP.STEP
   +LOOP
   11 5 FIX.FORMAT
   CR 2 SPACES ." MEAN DELTA I OF ALL DATA MEASURED = "
   DELTA.I SUB[ 1 , #.POINT ] MEAN DUP .
   CR 17 SPACES ." STANDARD DEVIATION = "
   DELTA.I SUB[ 1 , #.POINT ] SAMPLE.VARIANCE SQRT DUP .
   CR 17 SPACES ." RELATIVE DEVIATION = "
   SWAP / 100 * . ."  %"
   CR
   CONSOLE
   9 2 FIX.FORMAT
   CR 20 SPACES ." PRESS ANY KEY TO CONTINUE"
   PCKEY ?DROP DROP
;

: TIME.CHOICE                          \ Allows definition of a time period for
  S2.SC                                \  various uses.  Times entered by the
  ." ENTER THE STARTING TIME =  "      \  user should correspond to those
  #INPUT S.TIME :=                     \  defined by the timing windows
  CR ." ENTER THE FINAL TIME    =  "
  #INPUT E.TIME :=
  S2.SC
  ." ENTER THE STEP INCREMENT"
  CR ." EX.) 2 GIVES EVERY 2nd POINT: "
  #INPUT LOOP.STEP :=
;

: INDEX.TIME                           \ Locate array coordinate corresponding
  0 I.COUNT :=                         \  to a specified acquisition time
  BEGIN
   1 I.COUNT + I.COUNT :=
   TIME.SET RAMP.# [ I.COUNT ] =
  UNTIL
  I.COUNT INDEX :=
;
```

```
: PRINT.DATA                                    \ F4 in analysis menu
  BEGIN                                         \ Print all or part of data to video or printer
   D.SC                                         \ "Time" is defined by timing windows
   S2.SC                                        \ "True time" is actual time of I- acq.
   ." 1) PARAMETERS   2) ALL DATA   3) TIME & STEP CHOICE   0) QUIT"
   #INPUT CHOICE.1 :=
   1 CHOICE.1 = IF
    PRINT.PARA
    CR CR 20 SPACES ." PRESS ANY KEY TO CONTINUE"
    PCKEY ?DROP DROP
   ELSE
    2 CHOICE.1 = IF
     1 S.INDEX :=
     #.POINT E.INDEX :=
     1 LOOP.STEP :=
     PRINT.TIME.DATA
    ELSE
    3 CHOICE.1 = IF
     TIME.CHOICE
     S.TIME TIME.SET :=
     INDEX.TIME
     INDEX S.INDEX :=
     E.TIME TIME.SET :=
     INDEX.TIME
     INDEX E.INDEX :=
     PRINT.TIME.DATA
    THEN
   THEN
  THEN
  0 CHOICE.1 =
  UNTIL
  0 PRINTER.CHOICE :=
  D.SC
  RAW.MENU
;

: PRINT.RESULTS                                 \ Print averages and standard deviations of
  S2.SC                                         \ I0, I- & ΔI/I- for a chosen time period
  ." PRINT PARAMETERS <0> OR NOT <1>"  \ (F5 in analysis menu)
  GET.NUMBER
  0 CHOICE = IF
   PRINT.PARA
  THEN
  S2.SC
  15 SPACES ." RESULTS OUTPUT TO SCREEN <0> OR PRINTER <1>: "
  #INPUT PRINTER.CHOICE :=
  SS.SC
  1 PRINTER.CHOICE = IF
   OUT>PRINTER
```

```
  THEN
  CR 8 SPACES
  ." *** LTLACQ " VERSION "TYPE ."  **  PINHOLE/PHOTODIODE RESULTS
REPORT ***"
  CR
  BEGIN
   CONSOLE
   TIME.CHOICE
   S.TIME TIME.SET :=
   INDEX.TIME
   INDEX S.INDEX :=
   E.TIME TIME.SET :=
   INDEX.TIME
   INDEX E.INDEX :=
   D.SC
   1 PRINTER.CHOICE = IF
    OUT>PRINTER
   THEN
   11 2 FIX.FORMAT
   E.INDEX S.INDEX - 1 + LOOP.STEP / 0.3 + INDEX.1 :=
   CR ." FOR TIMES " S.TIME . ."  TO " E.TIME . ."  WITH STEP "
   4 0 FIX.FORMAT LOOP.STEP . ."   FOR FILE:  " FILENAME "TYPE CR
   ." I.ZERO  =  "
    10 5 FIX.FORMAT
    I.ZERO SUB[ S.INDEX , INDEX.1 , LOOP.STEP ] MEAN DUP .
    ."    +- "
    I.ZERO SUB[ S.INDEX , INDEX.1 , LOOP.STEP ] SAMPLE.VARIANCE
     SQRT DUP .
    ."    ("
    7 2 FIX.FORMAT
    SWAP / 100 * . ."  %)"
   CR
   10 5 FIX.FORMAT
   ." I.INF   =  "
    I.INF SUB[ S.INDEX , INDEX.1 , LOOP.STEP ] MEAN DUP .
    ."    +- "
    I.INF SUB[ S.INDEX , INDEX.1 , LOOP.STEP ] SAMPLE.VARIANCE
     SQRT DUP .
    ."    ("
    7 2 FIX.FORMAT
    SWAP / 100 * . ."  %)"
    8 0 FIX.FORMAT
    ."     START = "
    FIRST.ACQ . ."  ms"
   CR
   10 5 FIX.FORMAT
   ." DELTA.I =  "
    DELTA.I SUB[ S.INDEX , INDEX.1 , LOOP.STEP ] MEAN DUP .
    ."    +- "
```

```
    DELTA.I SUB[ S.INDEX , INDEX.1 , LOOP.STEP ]
    SAMPLE.VARIANCE SQRT DUP .
    ."    ("
    7 2 FIX.FORMAT
    SWAP / 100 * . ."  %)"
    9 2 FIX.FORMAT
    ."       BKG = "
    BKG.DATA 2048 + .
   CR CR
   CONSOLE
   S2.SC
   CR ." ENTER <0> TO QUIT OR <1> FOR ANOTHER SET: "
   #INPUT CHOICE.1 :=
   0 CHOICE.1 =
  UNTIL
  0 PRINTER.CHOICE :=
  9 2 FIX.FORMAT
  RAW.MENU
;

: SAVE.ASCII                          \ Save data in a format suitable for reading
  D.SC                                \   into a spreadsheet etc.
  CR                                  \   (F6 in analysis menu)
  ." Suitable data file must already be loaded. If it is <0> else <1>: "
  #INPUT CHOICE :=
  0 CHOICE = IF
   D.SC
   CR ." ENTER FILE NAME FOR SAVE (x:yyyyyyyy.PRN): "
   "INPUT FILENAME ":=
   CR CR ." Do NOT TOUCH KEYBOARD until save is complete"
   CR CR 20 SPACES ." ** SAVE IN PROGRESS **
   1500 MSEC.DELAY
   D.SC
   FILENAME DEFER> OUT>FILE
   CR ."      TIME          I.ZERO        I.INF        DELTA.I"
   CR
   #.POINT 1 + 1 DO
    11 2 FIX.FORMAT
    RAMP.# [ I ] . 2 SPACES ." ,"
    I.ZERO [ I ] . 2 SPACES ." ,"
    I.INF [ I ] . 2 SPACES ." ,"
    10 5 FIX.FORMAT
    DELTA.I [ I ] .
    CR
   LOOP
   OUT>FILE.CLOSE
  THEN
  RAW.MENU
;
```

```
: SAVE.LAPLACE                          \ Save data in format suitable for Laplace
  D.SC                                  \  or nonlinear regression analysis
  CR                                    \  (F7 in analysis menu)
  ." ENTER FILE NAME FOR SAVE (SPECIFY DRIVE): "
  "INPUT FILENAME ":=
  CR CR ." DO NOT TOUCH KEYBOARD until save is complete"
  CR CR 20 SPACES ." ** SAVE IN PROGRESS **"
  CR CR CR
  ." Times being saved are already corrected for real start time"
  3000 MSEC.DELAY
  14 5 FIX.FORMAT
  D.SC
  FILENAME DEFER> OUT>FILE
  #.POINT 1 + 1 DO
   DELTA.I [ I ] . CR
   TRUE.TIME [ I ] . CR
  LOOP
  OUT>FILE.CLOSE
  9 4 FIX.FORMAT
  RAW.MENU
;

: CHECK.DIRECTORY                       \ Display data disk directory (currently=B:)
  SS.SC
  ." DIRECTORY OF B:"
  DIR B:
  CR CR CR
  ." PRESS ANY KEY TO CONTINUE"
  PCKEY ?DROP DROP
  SS.SC
;

\ "MAIN" PROGRAMS
\ *********************

: CLEAR.FKEYS
  133 0 DO
   I FUNCTION.KEY.DOES NOP
  LOOP
;

: RAW.KEYS                              \ Initialize F-keys for analysis menu
  CLEAR.FKEYS
  F1 FUNCTION.KEY.DOES SAVE.DATA
  F2 FUNCTION.KEY.DOES LOAD.DATA
  F3 FUNCTION.KEY.DOES PLOT.DATA
  F4 FUNCTION.KEY.DOES PRINT.DATA
  F5 FUNCTION.KEY.DOES PRINT.RESULTS
  F6 FUNCTION.KEY.DOES SAVE.ASCII
```

```
   F7 FUNCTION.KEY.DOES SAVE.LAPLACE
   F8 FUNCTION.KEY.DOES NOP
   F9 FUNCTION.KEY.DOES CHECK.DIRECTORY
   F10 FUNCTION.KEY.DOES ESCAPE
   120 FUNCTION.KEY.DOES NOP          \ ALT-1
   121 FUNCTION.KEY.DOES NOP          \ ALT-2
   122 FUNCTION.KEY.DOES NOP          \ ALT-3
   123 FUNCTION.KEY.DOES NOP          \ ALT-4
   124 FUNCTION.KEY.DOES NOP          \ ALT-5     Alt keys currently unused
   125 FUNCTION.KEY.DOES NOP          \ ALT-6
   126 FUNCTION.KEY.DOES NOP          \ ALT-7
   127 FUNCTION.KEY.DOES NOP          \ ALT-8
    1 FUNCTION.KEY.DOES NOP           \ ALT-0
;

: RAW.ANAL                            \ Enter data analysis and I/O menu
   D.SC                               \  (F2 in main menu)
   STORE.FUNCTION.KEYS
   RAW.KEYS
   RAW.MENU
   INTERPRET.KEYS
   ONESCAPE: RESTORE.FUNCTION.KEYS MAIN.MENU
;

: KINETIC.ANAL                        \ To allow expansion to include Laplace
   S1.SC                              \  (F3 in main menu)
   30 SPACES ." ** KINETIC ANALYSIS **"
   S2.SC
   3 SPACES
   ." This program is not available yet !"
   CR ." Press any key to continue."
   PCKEY ?DROP DROP
   MAIN.MENU
;

: TIMING.CHECK                        \ Displays information pertinent to acq.
   D.SC                               \  timing.  Should be run after any
   CR                                 \  modifications are made to timing
   ." SCREEN <0> OR PRINTER <1>: "    \  or acquisition routines or the
   #INPUT PRINTER.CHOICE :=           \  A/D D/A interface
   D.SC                               \  (F4 in main menu)
   ." CTRL + NUM LOCK TO PAUSE " CR
   1 PRINTER.CHOICE = IF
    OUT>PRINTER
   THEN
   CR 10 SPACES
   ." *** LTLACQ " VERSION "T    E ."  ** SYNCHRONIZATION AND TIMING CHECK
***"
   CR 10 SPACES ." FILE NAME:  " FILENAME "TYPE CR CR
```

```
  ." #.POINT FLAG  SYNCHRO.DELAY   RAMP.#    TRUE.TIME  DIFFERENCE"
  CR CR
  #.POINT 1 + 1 DO
   3 0 FIX.FORMAT
   I .
   5 SPACES
   SHUT.FLAG [ I ] .
   3 SPACES
   10 2 FIX.FORMAT
   SYNCHRO.DELAYS [ I ] .
   4 SPACES
   11 2 FIX.FORMAT
   RAMP.# [ I ] .
   2 SPACES
   TRUE.TIME [ I ] .
   2 SPACES
   10 2 FIX.FORMAT
   TRUE.TIME [ I 1 + ] TRUE.TIME [ I ] - .
   CR
  LOOP
  CR
  ." FIRST.ACQ = "
  15 2 FIX.FORMAT
  FIRST.ACQ .
  CR
  CONSOLE
  CR 20 SPACES
  ." PRESS ANY KEY TO CONTINUE"
  PCKEY ?DROP DROP
  9 2 FIX.FORMAT
  SCREEN.CLEAR
  BANNER
  D.SC
  MAIN.MENU
;

: ALIGN.DIODE                    \ Displays photodiode intensity readings
  D.SC                           \   in real time.  Useful for alignment
  #.SCAN #.SCAN.A [ 1 ] :=       \   or optical components
  ." Limits of reading are 0 to 4095"   \   (F5 in main menu)
  CR CR
  ." Press any key to stop acquisition" CR CR
  ." ENTER SCANS/ACQ. (1-1000) :  " CR
  #INPUT #.SCAN :=
  6 0 FIX.FORMAT
  BEGIN
   CR 35 SPACES
   ACQ.DATA 2048 + .
   350 MSEC.DELAY
```

```
  ?KEY
  UNTIL
  9 2 FIX.FORMAT
  #.SCAN.A [ 1 ] #.SCAN :=
  SCREEN.CLEAR
  BANNER
  D.SC
  MAIN.MENU
;

: CHECK.DELTA.I                          \ Displays ΔI/I_ values using a fixed
  #.SCAN #.SCAN.A [ 1 ] :=               \  parameter format. Even more useful
  1000 #.SCAN :=                         \  for alignment of optics!
  D.SC                                   \  (F6 in main menu)
  28 SPACES ." ** FAST TEST OF SIGNAL **" CR CR
  ." This routine does NOT alter normal acquisition parameters or data" CR
  ." Parameters used: DEV=500, DECAY=1000, S/A=1000, cycle c. 5000 ms" CR CR
  ."     CLOSE He/Ne BEAM AND PRESS A KEY TO START" CR CR
  PCKEY ?DROP DROP
  ACQ.DATA
  FAST.BKG.DATA :=
  BELL
  ."     OPEN BEAM AND PRESS A KEY TO CONTINUE" CR
  PCKEY ?DROP DROP
  ."     Press any key to stop" CR CR
  10 5 FIX.FORMAT
  BEGIN
   OPEN.SHUTTER
   500 MSEC.DELAY
   ACQ.DATA
   FAST.BKG.DATA - FAST.I.INF :=
   CLOSE.SHUTTER
   1000 MSEC.DELAY
   ACQ.DATA
   FAST.BKG.DATA - FAST.I.ZERO :=
   FAST.I.ZERO FAST.I.INF - FAST.I.INF /
   35 SPACES ." DELTA.I/I.INF = " . CR
   3000 MSEC.DELAY
   ?KEY
  UNTIL
  9 2 FIX.FORMAT
  #.SCAN.A [ 1 ] #.SCAN :=
  SCREEN.CLEAR
  BANNER
  D.SC
  MAIN.MENU
;
```

```
: MAIN.KEYS                                  \ Initialize main menu F-keys
  F1 FUNCTION.KEY.DOES SET.ACQ.MENU
  F2 FUNCTION.KEY.DOES RAW.ANAL
  F3 FUNCTION.KEY.DOES KINETIC.ANAL
  F4 FUNCTION.KEY.DOES TIMING.CHECK
  F5 FUNCTION.KEY.DOES ALIGN.DIODE
  F6 FUNCTION.KEY.DOES CHECK.DELTA.I
  F7 FUNCTION.KEY.DOES NOP
  F8 FUNCTION.KEY.DOES NOP
  F9 FUNCTION.KEY.DOES NOP
  F10 FUNCTION.KEY.DOES MAIN.QUIT
;

: OPENING.COMMENTS
  D.SC
  ."     *** LTL PINHOLE/PHOTODIODE ACQUISITION & ANALYSIS PROGRAM
***" CR
  ."                        *** VERSION " VERSION "TYPE ." ***" CR CR CR
  ." * COMMENTS:" CR CR
  ."   - Acquisition times are adjusted at the end of acquisition to " CR
  ."     reflect the CENTER of the I.inf acquisition period (based on" CR
  ."     0.591 ms/scan). Data collected using versions prior to V4.50" CR
  ."     ARE NOT CORRECTED for the duration of the acquisition period." CR CR
  ."   - For highest precision, the first couple of points should be" CR
  ."     ignored during raw data analysis"
  CR CR CR CR
  ."                  Press any key to continue"
  PCKEY ?DROP DROP
;

: MAIN.PROGRAM
  LAB.MASTER
  MAIN.KEYS
  MAIN.MENU
  INTERPRET.KEYS
;

: RUN                                        \ Program is executed by entering "run"
  " V4.60" VERSION ":=
  CLEAR.FKEYS
  GRAPHICS.DISPLAY
  0.CHNL.IN A/D.INIT
  0.CHNL.OUT D/A.INIT
  OPENING.COMMENTS
  BANNER
  9 2 FIX.FORMAT
  D.SC
  MAIN.PROGRAM
;
```

Appendix C

DATA HANDLING SOFTWARE

The following program translates data from the HP 8452A spectrophotometer (operating under "HP89530A MS-DOS UV/VIS Operating software V1.0") to a file format suitable for Laplace analysis under Asyst. Entitled PRELAP, it is written in interpreter basic (MS-DOS 5.0 QBASIC; Microsoft).

Kinetic data files from the HP 8452A start with 7 lines of descriptive parameters. These are followed by absorbance values measured over the specified period. Each absorbance value uses a separate line. (Where kinetic analysis has been performed using multiple or a range of wavelengths, all absorbance values measured at one time appear on the same line of the file. These files must be reduced to single wavelength values using the HP software prior to analysis by PRELAP.)

PRELAP first allows the user to enter the names of up to 100 files to be processed. A file is read, the first 7 lines are removed and times corresponding to absorbance values calculated. The first 15 recorded points are displayed allowing the user to select the initial time to be kept. Further data is displayed and the user selects the final point to be preserved. The selected data range is then saved in the format $[A(t_i), t_i, A(t_{i+1}), t_{i+1}, \ldots A(t_f), t_f]$ which is compatable with the Laplace analysis procedures. A hardcopy containing file name, initial and final times and number of points is produced as a record. PRELAP is currently written to read data from drive A: (*filename*.TIM) and save to drive B: (*filename*.DAT). This choice may be altered by editing the READOUT and SAVEDATA subroutines.

```
'                                        PRELAP.BAS
'                                        **********


'       Declarations and initialization
'       -------------------------------------

DECLARE SUB LASTPOINT ()
DECLARE SUB SAVEDATA ()
DECLARE SUB TIMEPOINT ()
DECLARE SUB SHOWFIRSTPOINT ()
DECLARE SUB PRINTFILE ()
DIM SHARED INFO(26), FILE$(100), FI, ABSORBANCE(2500), POINTS, COUNT,
TIME(2500)
DIM SHARED START
DECLARE SUB READDATA ()
DECLARE SUB BATCHFILE ()


'       Main program
'       ------------------

BATCHFILE
FOR COUNT = 1 TO FI
  PRINT : PRINT : PRINT "PROCESSING FILE "; FILE$(COUNT)
  READDATA
  TIMEPOINT
  SHOWFIRSTPOINT
  LASTPOINT
  LPRINT FILE$(COUNT);                    :' Make hardcopy of pertinent data
  SAVEDATA
  LPRINT " NEW NAME => "; FILE$(COUNT)
  LPRINT "             "; "INITIAL TIME     "; TIME(START)
  LPRINT "             "; "FINAL TIME       "; TIME(POINTS)
  LPRINT "             "; "NUMBER OF POINTS "; POINTS - START + 1
NEXT
SYSTEM
END
```

```
'       Subroutines
'       ---------------

SUB BATCHFILE                          :' Read names of files to be processed
CLS : LOCATE 1, 1
INPUT "HOW MANY FILES TO BE PROCESSED"; FI
FOR I = 1 TO FI
PRINT "#"; I; : INPUT "NAME OF FILE"; FILE$(I)
NEXT
PRINTFILE
INPUT "DO YOU WANT TO MODIFY ANY FILE NAME? (Y/N)", EDIT$
IF EDIT$ = "n" THEN EDIT$ = "N"
DO UNTIL EDIT$ = "N"
  INPUT "WHICH FILE NAME DO YOU WANT TO ALTER"; CHANGE
  INPUT "TYPE NEW FILE NAME"; FILE$(CHANGE)
  PRINTFILE
  INPUT "DO YOU WANT TO MODIFY ANY FILE NAME? (Y/N)", EDIT$
  IF EDIT$ = "n" THEN EDIT$ = "N"
LOOP
END SUB


SUB PRINTFILE                          :' Display list of file names
CLS
LOCATE 1, 1
FOR I = 1 TO FI
PRINT I; " => "; FILE$(I)
NEXT
END SUB


SUB READDATA                           :' Read HP data file
NOM$ = "A:\" + FILE$(COUNT) + ".TIM"
OPEN NOM$ FOR INPUT AS #1
FOR J = 1 TO 26
   INPUT #1, INFO(J)
NEXT
POINTS = 0
DO UNTIL EOF(1)
   POINTS = POINTS + 1
   INPUT #1, ABSORBANCE(POINTS)
LOOP
CLOSE #1
END SUB
```

```
SUB TIMEPOINT                          :' Calculate times corresponding to
absorbances
TIME(0) = -INFO(25)
FOR I = 1 TO POINTS
  TIME(I) = TIME(I - 1) + INFO(25)
NEXT
END SUB


SUB SHOWFIRSTPOINT                     :' Show initial data.  Set first time to use.
FIRST$ = "N"
DO WHILE FIRST$ = "N"
 CLS : LOCATE 1, 1
 PRINT "POINT NUMBER", "TIME", "ABSORBANCE"
 FOR I = 1 TO 15
  PRINT I, TIME(I), ABSORBANCE(I)
 NEXT
 INPUT "WHICH POINT WILL BE THE FIRST POINT? (POINT NUMBER)";
START
 PRINT "CONFIRME BY Y/N THAT THE FIRST POINT WILL BE "
 PRINT START, "TIME "; TIME(START), "ABSORBANCE ";
ABSORBANCE(START);
 INPUT " "; FIRST$
 IF FIRST$ = "n" THEN FIRST$ = "N"
LOOP
END SUB


SUB LASTPOINT                          :' Display data.  Set last time to be used.
SEE$ = "Y"
DO WHILE SEE$ = "Y"
 INPUT "FROM WHICH POINT WOULD YOU LIKE TO SEE THE DATA"; DUM
 CLS : LOCATE 1, 1
 K = 0
 FOR J = DUM TO POINTS - 1 STEP 2
   PRINT J; " "; TIME(J); " "; ABSORBANCE(J); "       "; J + 1; " "; TIME(J + 1); "
"; ABSORBANCE(J + 1)
   K = K + 1
   IF K = 23 THEN
       INPUT "PRESS ENTER TO SEE NEXT SCREEN", DUM$
       K = 0
   END IF
 NEXT
 INPUT "WOULD YOU LIKE TO SEE THEM AGAIN?(Y/N)", SEE$
 IF SEE$ = "y" THEN SEE$ = "Y"
LOOP
```

```
LAST$ = "N"
LAST = POINTS
DO WHILE LAST$ = "N"
   INPUT "WHAT IS THE LAST POINT OF THE DATA SET"; LAST
   PRINT "CONFIRM THAT "; LAST; "   TIME  "; TIME(LAST); " IS THE LAST
POINT BY Y/N";
   INPUT " "; LAST$
   IF LAST$ = "n" THEN LAST$ = "N"
LOOP
POINTS = LAST
END SUB


SUB SAVEDATA                          :' Save selected data to new file
FILE$(COUNT) = "B:\" + FILE$(COUNT) + ".DAT"
OPEN FILE$(COUNT) FOR OUTPUT AS #2
FOR I = START TO POINTS
 WRITE #2, ABSORBANCE(I)
 WRITE #2, TIME(I)
NEXT
CLOSE #2
END SUB
```